QA4EO
Atmospheric Composition Uncertainty Field Studies

Final Report

(D5 as defined in SoW, including D5e, D5f, D5 g as defined in CCN1)
Final version

Lead author:
Anca Nemuc
anca@inoe.ro
National Institute of Research and Development for Optoelectronics
INOE, Romania

Co-Authors:
Anja Schönhardt, schoenhardt@iup.physik.uni-bremen.de, IUP-UB
Kezia Lange, lange@iup.physik.uni-bremen.de, IUP-UB
Andreas Richter, richter@iup.physik.uni-bremen.de, IUP-UB
Thomas Ruhtz, thomas.ruhtz@fu-berlin.de, FUB
Frank Hase, frank.hase@kit.edu, KIT
Maheh Kumar Sha, mahesh.sha@aeronomie.be, BIRA
Francesco D'Amato, francesco.damato@ino.cnr.it, CNR - National Institute of Optics
Frederik Tack frederik.tack@aeronomie.be, BIRA
Stefan Sebastian Iancu Sebastian.iancu@incas.ro, INCAS

ESA Contract No.	4000128426/19/NL/FF/ab
Project coordinator:	Anca Nemuc National Institute of R&D for Optoelectronics INOE anca@inoe.ro
Technical officer:	Dirk Schuettemeyer ESA/ESTEC Dirk.Schuettemeyer@esa.int

Document Version	Date	Status	Reason for change	Originator
Doc, v00	20.10.2023	Submitted to partners	New document	Anca Nemuc, INOE
Doc, v01	09.08.2024	Final version	Submitted to ESA after input from partners	Anca Nemuc, INOE

Contributors to the document:

Name	Section
Anca Nemuc, INOE	Draft document, integration, overview, Campaign in Romania
Alexandru Dandocsi, INOE	S5p data, PANDORA, FTIR -campaign in Romania
Livio Belegante, INOE	Lidar data--campaign in Romania
Stefan Iancu INCAS	Airborne measurements, campaign in Romania
Anja Schönhardt, IUP Bremen	Ruhr campaign
Kezia Lange, Andreas Richter, André Seyler, IUP Bremen	IUP Bremen mobile (airborne and car) and IUP Bremen ground-based measurements, Pandora ground-based measurements
Thomas Wagner, Vinod Kumar, MPIC Mainz	MPIC car MAX-DOAS measurements
Alexis Merlaud, BIRA	BIRA car and BIRA ground-based MAX-DOAS measurements
Thomas Ruhtz Jeremy Gordon	Airborne campaign planning and measurements, navigation data processing
Frank Hase, KIT Maheh Kumar Sha, BIRA	COCCON activities
Francesco D'Amato, CNR-INO	ACCLIP All sections
Silvia Viciani, Giovanni Bianchini, CNR-INO	ACCLIP airborne measurements, Instrument set-up and calibration, Data analysis, Data validation
Marco Barucci, CNR-INO	ACCLIP Instrument set-up and calibration, Data validation
Cyril Crevosier, CNRS	Magic campaign 2019

Table of Contents

List of Figures 1

LIST OF TABLES

1 Introduction

1.1 Purpose of Document

The main technical objective of QA4EO is the assessment of the uncertainties of the operational level 2 atmospheric composition products derived especially (but not exclusively) from the TROPOMI instrument on board of the Sentinel 5 Precursor (S5p) satellite. This was achieved by performing collocated airborne and ground based measurements of the respective products during dedicated field studies.
The field studies proposed are:

- Airborne and ground-based campaign 1 and 2 in the German Ruhr area (1.4.1)
- Airborne and ground-based campaign in Romania (2.2)
- COCCON ground based FTIR deployments (2.3)
- Support to the MAGIC campaign
- Support for ACCLIP campaign (D5f-- a summary of the measurements performed during the campaign) 2.5
- Support for HYTES campaign (D5g) 2.6

The purpose of this Final Report is to provide a full description of the field studies and the results from the comparison with S5p data. This includes full documentation of the processing steps followed and results of the analysis
The final report contains also a comprehensive introduction of the context, a description of the programme of work and report on the activities performed and the main results achieved.

1.2 Definitions, acronyms and abbreviations

ACTRIS	Aerosol, Clouds and Trace Gases Research Infrastructure
AERONET	Aerosol Robotic Network
AERSS	Atmospheric Environmental Remote Sensing Society
AirMAP	Airborne Imaging DOAS instrument for measurements of atmospheric pollution
AMF	Air Mass Factor
AOD	Aerosol Optical Depth
AOT	Aerosol Optical Thickness
AROMAPEX	campaign in April 2016
AROMAT	Airborne ROmanian Measurements of Aerosols and Trace gases
BDRF	Bidirectional Reflectance Function
BIRA	Royal Belgian Institute for Space Aeronomy
CAMS	Copernicus Atmosphere Monitoring Service
Cal/Val	Calibration/ Validation
CCD	Charge Coupled Device
COCCON	Collaborative Carbon Column Observing Network
CIP	Campaign Implementation Plan
DAR	Data Acquisition Report
DC	Intensity offset of an interferogram (typically measured in electrical units)

DOAS	Differential Optical Absorption Spectroscopy
dSCD	differential Slant Column Density
EARLINET	European Aerosol Research Lidar Network
ECMWF	European Centre for Medium-Range Weather Forecasts
ERA5	ECMWF Reanalysis Version 5
EVDC	ESA EO Validation Data Centre
FTIR	Fourier Transform InfraRed
FTS	Fourier Transform Spectrometer
FUB	Free University of Berlin
dSCD	differential Slant Column Density
FZJ	Forschungszentrum Jülich
GEOMS	Gene GHG Greenhouse Gase
HDF	Hierarchical Data Format
ILS	Instrumental Line Shape
INOE	National Institute of R&D for Optoelectronics INOE 2000
IUP-UB	Institute of Environmental Physics – University of Bremen
JPL	Jet Propulsion Laboratory, California, USA
KIT	Karlsruhe Institute of Technology, Karlsruhe, Germany
LER	Lambertian Equivalent Reflectivity
LT	Local Time
MAX-DOAS	Multi-Axis Differential Optical Absorption Spectroscopy
MPD	Maximum Path difference (of an interferogram)
MPIC	Max-Planck Institute for Chemistry Mainz
NDACC	Network for Detection of Atmospheric Composition Change
NIR	Near InfraRed
OPD	Optical Path Difference (abscissa value of an interferogram)
PGN	PANDONIA Global Network
SCD	Slant Column Density
S-5p	Sentinel-5 Precursor, mission in the framework of Copernicus Programme, dedicated to monitor air pollution
SRON	Netherlands Institute for Space Research
TCCON	Total Carbon Column Observing Network
SZA	Solar Zenith Angle
TROPOMI	TROPOspheric Monitoring Instrument: UV/VIS/NIR/SWIR spectrometer payload on Sentinel-5P mission
TUM	Technical University of Munich, Munich, Germany
UTC	Coordinated Universal Time
VCD	Vertical Column Density
VZA	Viewing Zenith Angle
XGAS	Column-averaged dry air molar fraction of an atmospheric trace gas
WRF	Weather Research and Forecasting Model

1.3 Applicable Documents

- ESA contract no. 4000128426/19/NL/FF/ab
- CCN1/03.08.2020 to ESA contract no. 4000128426/19/NL/FF/ab
- CCN2/ 11.11.2021 to ESA contract no. 4000128426/19/NL/FF/ab

1.4 Structure of the document

This document is describing the field studies performed, divided into several sections, presenting the Objectives, Instrument set-up, the timing, campaigns execution, data analysis, studies and main results, dissemination and publications. These sections are framed with introduction of the context and ends with summary and lessons learnt.

2 Campaigns final reports

2.1 Airborne and ground-based campaign 1 and 2 in the German Ruhr area

2.1.1 Objectives

The Ruhr campaign focuses on industrial and urban emissions of NO_x, as well as assumptions made on a priori data in the retrieval of the S-5p NO_2 level-2 product. Emphasis is given to the a priori parameters NO_2 model profiles, aerosols and surface reflectance. For this purpose, it was planned to deploy similar instruments as was done during the AROMAT-2 (Merlaud et al 2020) and AROMAPEX campaigns consisting of an airborne as well as a ground-based component. The airborne activities are designed to comply with the characteristics of the central instrument, AirMAP, measuring NO_2 vertical column densities in the air column below the aircraft. However, the focus of the campaign and of this report lies on the evaluation of the NO_2 observations.
With regards to QA4EO, the main objective of this activity is to create a campaign data set applicable for studies of the uncertainties of satellite atmospheric trace gas products. The results of the Ruhr activity will contribute to the validation of the tropospheric NO_2 vertical column density retrieved from S-5p observations.

2.1.2 Comprehensive introduction of the context

The Ruhr area is a polluted area in Western Germany with strong anthropogenic emission sources and related large variability of pollutant abundances. Observations of NO_2 by the S-5p satellite instrument are affected by uncertainties related to a list of influencing factors, the strong spatial variability being one of them. In addition, amongst others, influences from clouds, aerosol abundances, the NO_2 profile and surface reflectance on the retrieved satellite products are relevant.
In order to examine the impact of these influences on the uncertainty of the satellite data, a suite of alternative measurements is setup and used for detailed comparison of the trace gas results.
The Ruhr campaign combines a focus on mobile – airborne and car-based – measurements with a suite of ground-based short term as well as long term, partly year-round measurements. Dedicated to the assessment of the uncertainty of S-5p NO_2 tropospheric products, campaign preparation and implementation were aligned with S-5p overpass times and characteristics (such as viewing angles). Weather conditions for feasible satellite data comparison were carefully checked, and flight patterns chosen accordingly.

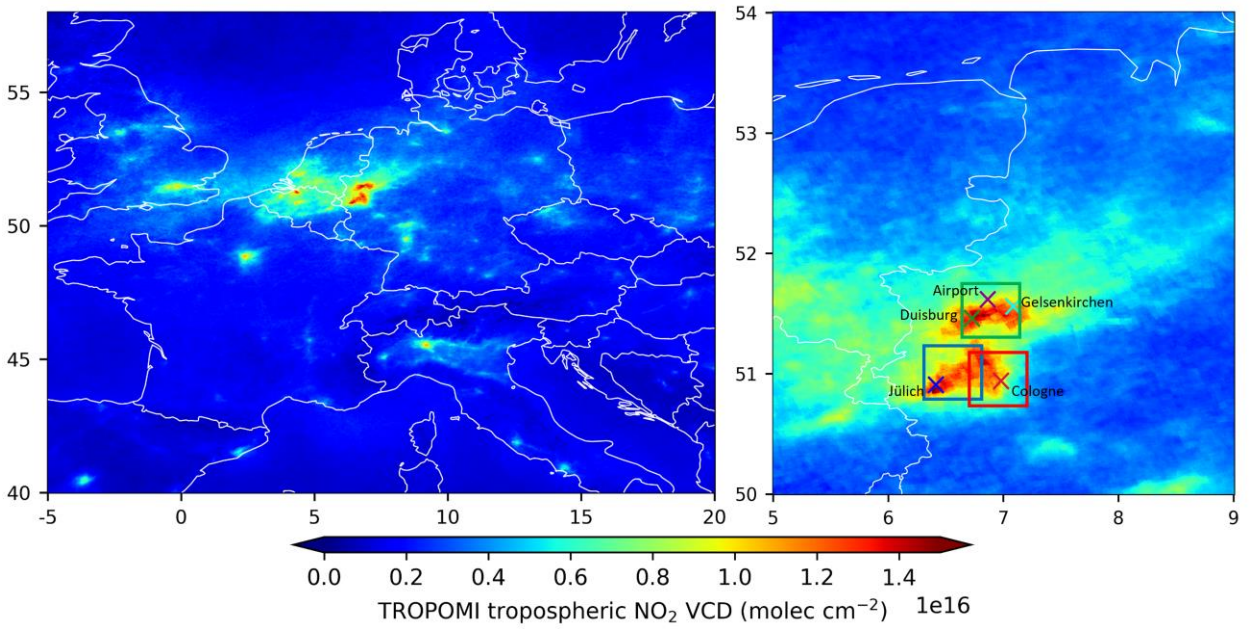

Figure 1: Satellite S-5p image of central Europe showing the tropospheric NO_2 VCD from the PAL V02.03.01 product as an average over the entire campaign month September 2020 (left). Closer view on the target area with the flight boxes and marked locations of the stationary instruments (right). Figure from Lange et al., 2023.

2.1.3 Description of timeline and instruments

The Ruhr campaign activities were conducted in the years 2019 and 2020. Due to unfavourable weather conditions during the main campaign time window in 2019, the aircraft measurements were postponed to a second time period in September 2020. In this time window, the regional weather forecast was much better, with a stable high-pressure period over Germany, and seven golden days were included. The seven golden days with one aircraft mission per day were September 12th –18th in 2020. Mobile car DOAS measurements were performed in the same time period.

The ground-based component was active for a longer period of time, mostly covering the golden days and partly several months before and/or after the main campaign period. Details of the timeline of each instrument, as well as instrument descriptions, are summarized below in this section. Details on the timing and location of each measurement flight, as well as collocation information with satellite overpasses, are given in the following section 2.1.4.

Table 1 lists the instruments that participated in the mobile component of the Ruhr activity, including instruments based on the aircraft as well as on cars. The general availability of instruments for each of the seven flight periods is shown as an overview in Table 2.

Table 1: Overview of the mobile campaign instruments and respective main variables/species measured during the present campaign

Instrument	Owner organisation	Contact person	Measured variables	Platform	Platform operator	Uncertainty
AirMAP	IUP-UB	Anja Schönhardt	NO_2 column, Surface reflectance	Cessna T207A	FUB	< 30%
Nadir Avantes	IUP-UB	Andreas Richter	NO_2 (SO_2) column	Cessna T207A	FUB	< 30%
FUB Attitude (Inertial Navigation System, INS)	FUB	Thomas Ruhtz	Aircraft position, velocity and altitude	Cessna T207A	FUB	<0.5 m
Aerial Imagery Cameras (48MPix & 16MPix)	FUB	Thomas Ruhtz	Aerial Images incl. Geo Tagging, 16MPix: in oblique projection	Cessna T207A	FUB	n/a
IUP-UB mobile car DOAS	IUP-UB	Kezia Lange	NO_2 (and SO_2) columns	car	IUP-UB	< 25 %
MPIC mobile car DOAS	MPIC Mainz	Thomas Wagner	NO_2 columns	car	MPIC Mainz	< 25 %

Table 2: Overview of the instrument performance of mobile instruments (Cessna or car) during the flight periods of the seven research flights in 2020. Green: Nominal operation, Yellow: Operation with some restrictions as explained below, Red: No data

Instrument	12 Sep	13 Sep	14 Sep	15 Sep	16 Sep	17 Sep	18 Sep
AirMAP							
Nadir Avantes							
Aerial Cameras							
IUP-UB car							
MPIC car							
BIRA car							

Before the campaign period in September 2019, some ground-based instruments were installed in the Ruhr area, partly on a campaign basis and partly for longer term measurements. The instruments took measurements for different time periods between September 2019 and October 2020, and were partly still active in 2021. Table 3 gives an overview of the measurement periods of these ground-based instruments in the Ruhr area. Considering support of the flight activity, the availability of data from the ground-based instruments on the seven flight days of the Ruhr campaign in 2020, is indicated in Table 4.

Except for the Avantes instrument in Wuppertal, which was only active in 2019, all other six instruments took measurements on the seven golden days.

The Pandora instrument in Jülich also recorded data on all days between 12th and 18th of September. From the raw data on the 12th September, only NO_2 total columns are

available. In addition to the total column densities, the tropospheric NO_2 VCD and surface concentrations are derived from 13th to 18th of September for this station.

Table 3: List of instruments installed in the Ruhr area for a long-term period

Site	Instrument	Operator	Period	Number of days with data	Comments
Cologne	Pandora	IUP-UB	24.10.19 – 17.11.19 and 29.06.20 – 01.11.21	25 days in 2019, 186 days in 2020, 280 days in 2021	
Jülich	Pandora	IUP-UB	23.10.19 – 13.10.21	70 days in 2019, 339 days in 2020, 272 days in 2021	
Jülich	Avantes	IUP-UB	19.08.19 – 21.08.21	125 days in 2019, 359 days in 2020, 230 days in 2021	
Gelsenkirchen	Avantes	IUP-UB	12.09.19 – 01.11.19 and 24.07.20 – 27.11.20	41 days in 2019, and 121 days in 2020	
Wuppertal	Avantes	IUP-UB	18.08.19 – 03.11.19	63 days in 2019	The instrument was dismounted in November 2019, so there is no data in 2020.
Duisburg	Max-DOAS	IUP-UB	20.09.19 – 26.09.19 and 04.09.20 – 19.09.20	7 days in 2019 and 14 days in 2020	
Dinslaken	Max-DOAS	BIRA	30.09.19 – 23.10.19 and 03.08.20 – 29.09.20	24 days in 2019 and 54 days in 2020	KinAero in 2019, Skyspec-mini (Airyx) in 2020

Table 4: Availability of data from the ground-based instruments on the seven flight days in 2020, Green: Nominal operation, Yellow: Operation with some restrictions explained in the text, Red: No data.

Site/Instrument	12 Sep	13 Sep	14 Sep	15 Sep	16 Sep	17 Sep	18 Sep
Cologne Pandora							
Jülich Pandora							
Jülich Avantes							
Gelsenkirchen Avantes							
Duisburg Max-DOAS							
Dinslaken Max-DOAS							

Description of the main instruments used for the purpose of the present project

The AirMAP instrument

The Airborne imaging Differential Optical Absorption Spectroscopy (DOAS) instrument for Measurements of Atmospheric Pollution (AirMAP) has been developed for the purpose of trace gas measurements and pollution mapping at the Institute of Environmental Physics of the University of Bremen (IUP-UB). AirMAP is a push-broom UV/vis imager with a wide field-of-view of around 52° across track, leading to a swath width of about the same size as the flight altitude. Due to its large swath and the use of a frame transfer charge coupled device (FT-CCD) detector, gapless maps of horizontal trace gas distributions can be acquired within a relatively short time.

AirMAP collects scattered Sunlight from below the aircraft with a wide field of view objective in nadir geometry. The light is coupled into an imaging grating spectrograph via a sorted fibre bundle, retaining the spatial information. The dispersed light is imaged onto a FT-CCD. The CCD images are stored on a PC. From a maximum of 35 individual viewing directions, created by 35 single fibres, the number of viewing directions used can be adapted to each situation by averaging according to signal-to-noise or spatial resolution requirements. The single fibres are stacked vertically at the spectrometer entrance slit and are oriented across flight direction in the focal point of the telescope. The spectrometer is an Acton 300i imaging spectrograph with a focal length of 300 mm and an f-number of f/3.9. The spectrometer is temperature stabilised at 35°C. The wavelength region can be chosen according to the chemical species of interest, with a spectral coverage of around 64 nm, using a 400 g/mm grating blazed at 400 nm. Table 5 lists some relevant experimental properties.

Table 5: General properties of the AirMAP instrument. For the present campaign only the VIS-setup is relevant, the UV-setup is included for information only.

Property	UV-setup	VIS-setup
Spectral range	303 – 367 nm	429 - 493 nm
Spectral resolution	0.8 – 1.5 nm	0.8 – 1.5 nm
Typical integration time	0.5 sec	0.5 sec
Field of View	44°	51.7°

The instrument is further equipped with an optional camera for scene photography. These photographic images are triggered by the spectroscopic measurements and can be used, e.g., for position control and interpretation of the observed scene. The AirMAP instrument, as well as the aircraft, is equipped with an Attitude and Heading Reference System (AHRS) and GPS sensor. AirMAP measures spectra of scattered sunlight. The spectra are analysed using Differential Optical Absorption Spectroscopy (DOAS) in order to derive column densities of trace gases. In addition, the effective surface reflectance is derived for each ground scene. A detailed description of the instrumental setup, its performance, the viewing geometry and the georeferencing is described in Schönhardt et al. (2015). The retrieval of vertical column densities, considering a variable surface reflectance, and an explicit aerosol correction, is described in Meier et al. (2017). The latest description with instrument overview and explanation of measurements and retrieval method is contained in Lange et al. (2023) and Lange (2023).

IUP Bremen mobile car DOAS instrument

The main part of the IUP Bremen car DOAS device is an Avantes spectrometer with a wavelength range between 290 and 550 nm, cf. Lange (2023). Together with a measurement notebook and a GPS receiver, the instrument is located within the car. The spectrometer receives light through a light fibre, which is fixed by a light fibre holder mounted in the car window. The fibre views into one fixed elevation angle, which was directed to the zenith for the present campaign. To protect the instrument from direct sunlight, a cylinder-shaped tube is placed at the light fibre entrance. Power for the spectrometer is received from the notebook's USB connection, and the notebook is powered by the car's cigarette lighter.
Averaging time of individual spectra to a mean spectrum was set to 10s. Depending on the speed of the car, the resulting spatial resolution typically lies between 80 and 300m. The IUP mobile car DOAS instrument was successfully operated at several previous measurement campaigns, e.g., during CINDI-2 in the Netherlands.

BIRA mobile car DOAS system

The BIRA double channel mobile-DOAS instrument is based on a double channel Avantes spectrometer installed on a car. The entry slit is 50 µm, the focal length 75 mm and the grating is a 600l/mm, blazed at 300 nm. The spectral range is 200-750 nm with a 1.2 nm resolution (FWHM). The CCD detector is a Sony2048 linear array with a Deep-UV coating for signal enhancement below 350 nm. An optical head, mounted on the car window, holds the two telescopes achieving a 2.5° field-of-view with fused silica collimating lenses. One telescope points zenith while the other is directed 30° above the horizon. Two 400 µm chrome plated brass optical fibres connects the telescopes to the spectrometer. Individual spectra are co-added and the analysis is performed on measurements averaged over (typically) 30 seconds in the case of the QA4EO campaign. A GPS antenna is used for georeferencing the measurement, the whole set-up is powered by the car 12V through an inverter. While measuring, the instrument records spectra continuously and simultaneously from the two directions (Piters et al., 2012; Merlaud, 2013). The mobile system was successfully operated at several previous measurement campaigns, e.g., AROMAT-2, AROMAPEX, CINDI-2.

MPIC mobile car DOAS instrument

The MPIC MAX-DOAS (so-called Tube MAX-DOAS) is a self-built MAX-DOAS, which covers the UV and part of the visible spectral range (300 – 460 nm) using an Avantes spectrometer. The instrument is separated into a telescope unit and a spectrometer unit. Both are connected via a 12 m long fibre bundle. The spectrometer is thermally stabilised by a combined cooling/heating unit. Measurements can be taken at 90° elevation and at a second low elevation angle (between 20 and 30°, 22° in the case of the QA4EO campaign). During transfer from Mainz to the Ruhr measurement site, the instrument measured alternatingly in 22° and 90° (zenith) elevation from the horizon. During the central round-trip routes in the flight area, only zenith measurements were done. From the measured spectra the column densities of NO_2 are retrieved. Because the instrument measures at two elevation angles, the absolute tropospheric trace gas VCDs can be directly determined from the measurements (see also Wagner et al., 2010; Ibrahim et al., 2010). The MPIC mobile MAX-DOAS was successfully operated at several measurement campaigns, e.g., AROMAT-2, AROMAPEX, CINDI-2.

Zenith-DOAS instruments
The two instruments were deployed at the Jülich research centre and at a local residence in Gelsenkirchen (in the Northern Duisburg flight area). The instruments use an experimental setup, which comprises an Avantes spectrometer (290–550 nm) and a light fibre with a fixed viewing direction to the zenith measuring scattered sunlight in the UV-Vis spectral range (similar as in Schreier et al., 2019). More details can be found in Lange et al. (2023).

MAX-DOAS measurement truck
From 7 to 19 September 2020, the IUP Bremen measurement truck performed MAX-DOAS measurements in the harbour area of Duisburg, close to the Rhine River. This MAX-DOAS instrument uses a UV spectrometer (282–412 nm) with a light fibre connected to a telescope on a pan-tilt head and was scanning in multiple elevation angles. The tropospheric NO_2 VCDs are estimated from the dSCD measurements in 30° elevation angle with a sequential zenith-sky reference spectrum (interpolated from the zenith-sky measurements shortly before and after the off-axis measurement).

BIRA Sky-Spec Max-DOAS
A further MAX-DOAS instrument was set up at the airport Schwarze Heide in Dinslaken from 3 August to 29 September 2020. The instrument, deployed by BIRA, was an Airyx Compact SkySpec MAX-DOAS, based on an Avantes spectrometer (300–463 nm). A scanning prism in elevation direction can rotate 180°, enabling elevation scan measurements in two azimuthal directions (Airyx GmbH, 2022; Kreher et al., 2020). At the airport, the instrument was scanning in azimuths of 132° and 312° and at multiple elevation angles. In this study, only measurements in a northwesterly direction (312°) are used for the analysis.

Pandora instruments
The Pandora instrument is a ground-based UV-Vis spectrometer that provides direct sun total column and sky scan MAX-DOAS tropospheric column observations, comprising an Avantes spectrometer (270–520 nm) (e.g., Herman et al., 2009; Kreher et al., 2020; Verhoelst et al., 2021). Two Pandora instruments are deployed and operated in the campaign area to provide long-term measurements. They were installed in August 2019

and were still in operation in 2022. One Pandora is located at the Jülich research centre and a second one in Cologne, district Deutz. All data are processed as part of the Pandonia Global Network (2023).

2.1.4 Report on the activities performed

For the Ruhr campaign, flights in the German industrial Ruhr area were planned, including soundings on weekdays as well as weekend. Seven research flights were performed on seven consecutive days. Flight patterns and schedules are presented below in the following subsection. In the subsequent subsection, the stationary activities are explained in more detail.

Report on the mobile measurement activities

Within the Ruhr area, three regions of interest (flight boxes) had been determined (see Figure 2), as stated in the CIP. All planned flights have been conducted, including flights in each of the chosen flight boxes. The deployed aircraft was the FUB Cessna T207A, the same as in the preceding campaigns (AROMAT-1/-2 and AROMAPEX).

Overall, seven research flights were performed in three different areas on seven consecutive days, i.e., with one flight per day, on the 12th to 18th of September 2020. All flights started and ended at the airport “Schwarze Heide” close to Dinslaken. The three predefined flight boxes are areas around Jülich (A), Cologne (B), and Duisburg (C), respectively. Example flight tracks for all three flight boxes of the FUB Cessna flights are displayed in Figure 2 with different colours for the three different areas - blue for Jülich, red for Cologne and green for Duisburg. Repeated flight tracks are essentially the same as the depicted tracks. The number of flights per flight box is three in the Duisburg box, and two each above Jülich and Cologne. The number of flight tracks per survey depends on the area and is 13 for Cologne, 14 for Jülich and 15 for Duisburg.

In general, the flights were planned in dependency of the weather and cloud conditions above the three target areas, and decision which route to fly was made accordingly.
In addition, flights were coordinated with S-5P overpasses in order to achieve a maximum number of collocations between satellite and aircraft measurements, and hence optimal conditions for validation purposes. An overview of S-5p overpass times during the main campaign period is displayed in Table 6. In the case of two satellite overpasses per day, focus was laid on the overpass with smaller Viewing Zenith Angle (VZA).

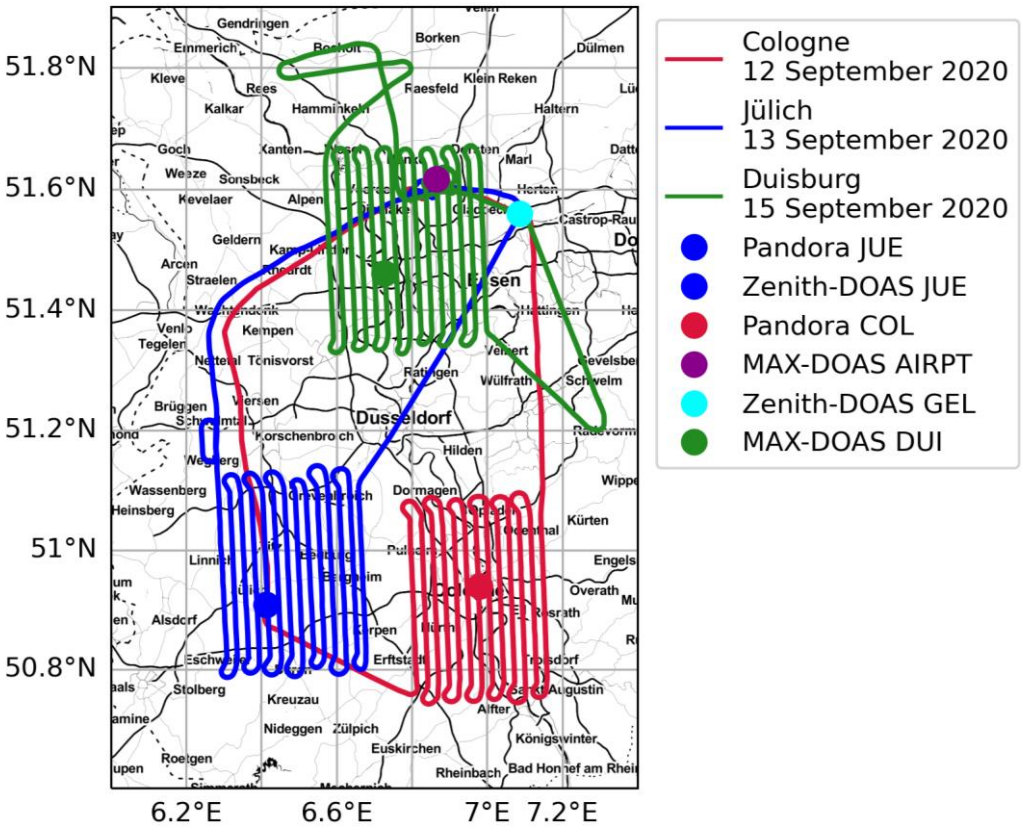

Figure 2: Flight tracks performed by the FUB Cessna aircraft carrying the AirMAP instrument, the nadir Avantes as well as the Aerial Cameras in the three flight areas. Example flights are marked by individual colours as shown in the legend. The mobile car DOAS instruments performed measurements at the same time in the area covered by the aircraft tracks. In addition, the locations of the ground-based instruments are indicated. Figure from Lange et al., 2023.

Table 6: Overview of S5p overpasses for latitude=51.0° and longitude=7.0° for all days of mobile measurements between the 12th and 18th of September, 2020.

Date	Time [UTC]	Viewing Zenith Angle [°]	Solar Zenith Angle [°]
2020-09-12	10:51:20	67.38	47.53
2020-09-12	12:31:03	15.94	48.78
2020-09-13	12:12:12	8.75	48.24
2020-09-14	11:53:24	30.71	48.01
2020-09-14	13:33:59	64.93	54.64
2020-09-15	11:34:39	46.69	48.10
2020-09-15	13:14:58	55.40	53.20
2020-09-16	11:15:57	57.72	48.50
2020-09-16	12:56:00	41.87	52.04
2020-09-17	10:57:18	65.53	49.21
2020-09-17	12:37:05	22.62	51.11

2020-09-18	12:18:13	1.57	50.48

The car DOAS routes were planned as circles within the area covered by the airborne measurements. The routes of the up to three instruments share common segments in the centre of the imaged area. This strategy ensures coincidences between airborne and car measurements across the whole pattern. Repetition of the routes enables the investigation of temporal variability. The common car segments allow a comparison between the car instruments themselves. If applicable, the car routes bypass the stationary ground-based instruments. To enable many repetition cycles, it was planned to use mainly highways. An overview of the car DOAS driving routes on all seven days is given in Figure 3.

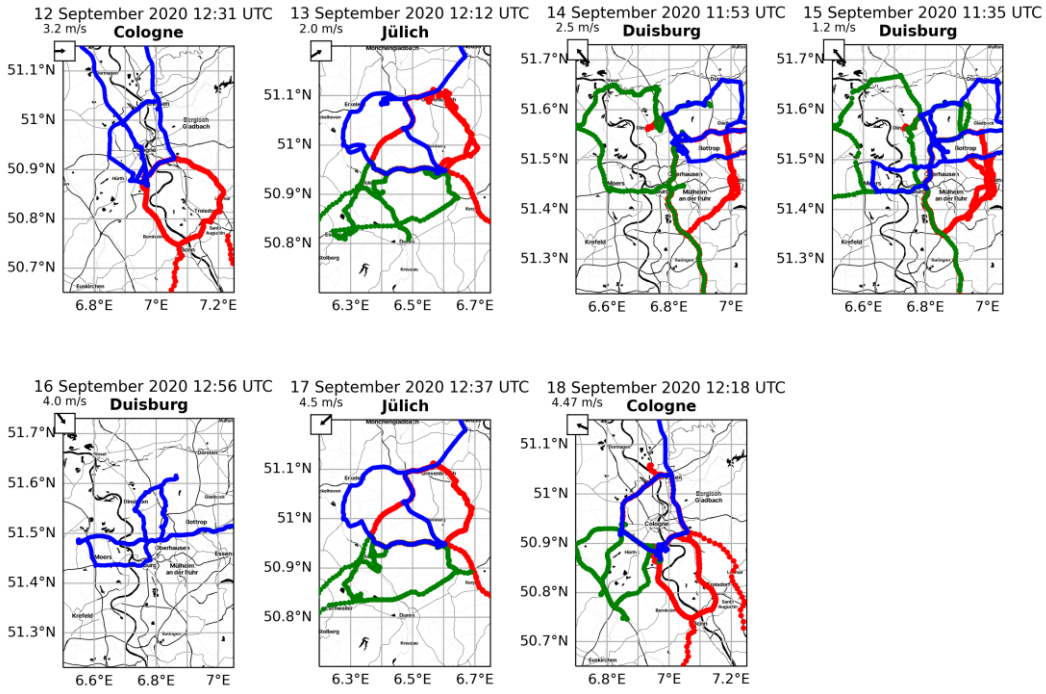

Figure 3: Driving routes of the three car DOAS mobile instruments during the QA4EO measurement campaign between Sep 12 and Sep 18, 2020, including the IUP Bremen (blue), the MPIC (red) and the BIRA (green) car DOAS systems. In the central parts of the driving routes, overlaps of the routes was achieved for collocation and comparability between the instruments.

Flight on 2020-09-12 (Saturday), Cologne:

On the first day of mobile measurements, a southern region (flight box B above Cologne) was chosen due to higher risk for cloud cover in the North. There were two S-5p overpasses, cf. Table 6**Error! Reference source not found.**. The mobile measurements focused on the second overpass with smaller VZA of S-5P at 12:31 UTC.

A graphical summary of the planned measurements is displayed in Figure 4 giving an impression of the typical flight pattern and collocation with the additional measurements. The flight pattern and its timing were optimized for a nadir overpass over the Cologne Pandora instrument close to S-5p overpass time. Location of the Pandora instrument is marked by the orange star. The figure shows the three car routes in red, black and blue.

The three routes in the centre belong to the Cologne box B, while the routes visible in the West of the flight box are located in box A (Jülich). The routes had a duration of about one hour each, and they were repeated during the central measurement period.
The flight was completed with no technical issues and at clear sky.

Flight report:	
Takeoff	10:17 UTC
First track above target area	10:58 UTC
End of final track	13:12 UTC
Landing	13:37 UTC
Duration total/above target area	3h20 / 2h14

Flight on 2020-09-13 (Sunday), Jülich:
On this day, there was only one S-5p overpass at 12:12 UTC. With clear sky above Jülich, flight box A was chosen for this day. Slight influence from Cirrus clouds might have been present temporarily.

Flight report:	
Takeoff	10:20 UTC
First track above target area	10:50 UTC
End of final track	13:11 UTC
Landing	13:36 UTC
Duration total/above target area	3h16 / 2h21

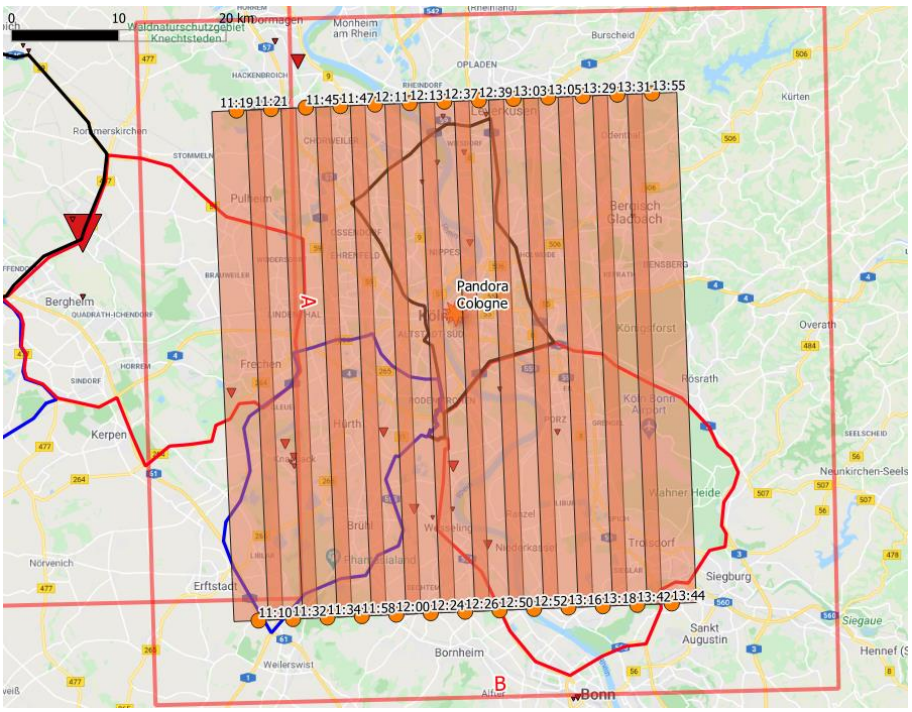

Figure 4: Graphical summary of planned measurements in Cologne on 2020-09-12. The red rectangle shows the area registered at Air Traffic Control for research flights. The semi-transparent polygons show the area covered by the AirMAP instrument during each flight track. The labelled circle markers show the estimated overpass time (LT, here UTC+1h) of the FUB Cessna at start and end time of the respective track. Blue, red and black lines show the planned routes for mobile car-

DOAS measurements. The location of the stationary Pandora instrument in Cologne is displayed as a labelled star marker approximately in the centre of the pattern.

Flight on 2020-09-14 (Monday), Duisburg:
From two S-5p overpasses on this day, the overpass with smaller VZA of 30.7° at 11:53 UTC was chosen to synchronize with flight time. For the first of three consecutive days, a flight pattern within the Duisburg Northern flight Box C was performed. The flight included overpasses over the MAX-DOAS instruments in Duisburg and at the Dinslaken airport, as well as the Avantes zenith-sky DOAS instrument in Gelsenkirchen. Some Cirrus clouds were present above the target area.

Flight report:

Takeoff	10:14 UTC
First track above target area	10:46 UTC
End of final track	13:22 UTC
Landing	13:47 UTC
Duration total/above target area	3h33 / 2h36

Flight on 2020-09-15 (Tuesday), Duisburg:
On this day, the pattern above flight box C from the day before was repeated due to favourable wind and weather conditions. Timing was chosen such that collocation with the second S-5p overpass was achieved at 11:35.

Flight report:

Takeoff	09:15 UTC
First track above target area	09:48 UTC
End of final track	12:16 UTC
Landing	12:44 UTC
Duration total/above target area	3h28 / 2h28

Flight on 2020-09-16 (Wednesday), Duisburg:
The third flight above the Duisburg flight box C with the same tracks as the two days before was synchronized with the second S-5p overpass at 12:56. The first overpass at 11:16 was also during aircraft operation above the target area. Both overpasses had relatively large VZA.
While there was clear sky during the flight, there was temporarily some haze visible. In addition, some darker haze was visible from the mobile car routes above the measurement area, potentially caused by enhanced aerosol load from the industrial areas.

Flight report:

Takeoff	10:37 UTC
First track above target area	11:06 UTC
End of final track	13:34 UTC
Landing	14:05 UTC
Duration total/above target area	3h28 / 2h28

Flight on 2020-09-17 (Thursday), Jülich:
On this day, the same pattern as on Sunday 13th Sep was flown above the Jülich Box A. Timing was chosen to overlap with the second overpass of S-5p at 12:37.
Strong wind was present on this campaign day, while sky was mostly clear.

Flight report:	
Takeoff	10:45 UTC
First track above target area	11:17 UTC
End of final track	13:34 UTC
Landing	14:16 UTC
Duration total/above target area	3h32 / 2h17

Flight on 2020-09-18 (Friday), Cologne:
Also for flight box B, a second flight was possible. On this day, the pattern above Cologne from Saturday 12th Sep was repeated under clear sky conditions. S-5p overpass was at 12:18 with a very small VZA of 1.6°.

Flight report:	
Takeoff	10:48 UTC
First track above target area	11:30 UTC
End of final track	13:36 UTC
Landing	14:08 UTC
Duration total/above target area	3h19 / 2h14

Report on the stationary measurement activities

The time line of the stationary measurements is summarized in Table 3 and Table 4 in Section 2.1.3. The instruments usually performed measurements from shortly before sunrise until shortly after sunset.

2.1.5 Data analysis

The data analysis applied to the data of the QA4EO project greatly follows previous evaluations. The description given here is based on the CIP and on Lange et al., (2023).

2.1.5.1 *Data acquisition and DOAS retrieval for AirMAP*

For the NO_2 retrieval, the DOAS method is applied to the measured spectra in a fitting window of 438–490 nm. The NO_2 differential SCDs (dSCDs) are retrieved relative to inflight-measured reference background spectra, which were measured over a region with small NO_2 concentrations during the same flight. The dSCD is converted into a tropospheric SCD (SCD_{trop}) by correcting for the amount of NO_2 in the reference background measurement (SCD_{ref}):

$$SCD_{trop} = dSCD + SCD_{ref}$$
$$= dSCD + VCD_{trop,ref} \times AMF_{trop,ref} \quad (1)$$

Determination of vertical column densities

For the conversion to the desired tropospheric VCD (VCD_{trop}), the SCD_{trop} is divided by the tropospheric air mass factor (AMF_{trop}):

$$VCD_{trop} = SCD_{trop} / AMF_{trop}$$
$$= (dSCD + VCD_{trop,ref} \times AMF_{trop,ref}) / AMF_{trop} \quad (2)$$

Since the AMF of the actual measurement (AMF_{trop}) and of the reference background measurement ($AMF_{trop,ref}$) are usually not the same, simply adding the $VCD_{trop,ref}$ would introduce additional uncertainties. To correct for the NO_2 in the reference spectrum (SCD_{ref}), we assume a tropospheric VCD of $1x10^{15}$molec/cm² over the reference background region, which is a typical value during summer in Europe (Popp et al., 2012; Huijnen et al., 2010). This assumption can be supported by the car DOAS measurements, see Section 2.1.7. All measurements of the campaign were performed around noon close to the S-5P overpass. The maximum difference between the time of the reference background and the actual measurement is of around 3 h, which is the total measurement time. We assume that the effect of the changing solar zenith angle (SZA) and the diurnal variation of the stratospheric NO_2 concentration are small (Schreier et al., 2019), and a stratospheric correction of the data is therefore not necessary.

Determination of the Air Mass Factor

The AMF calculated using SCIATRAN estimates the relative light path length through the absorbing layer by accounting for the effects of sun and viewing geometry, surface reflectance, aerosols, and the NO_2 profile assuming cloud-free conditions. As only limited information about the NO_2 profile is available in the campaign area and the profile shape is expected to vary strongly within each flight region every day, we assume a typical urban NO_2 profile, which is based on an old WRF-Chem (Weather Research and Forecasting model coupled with Chemistry) run and scaled to a height of 1 km. This assumption is supported by typical boundary layer heights in the measurement area and time of approximately 1 km (ERA5 reanalysis; Hersbach et al., 2018).

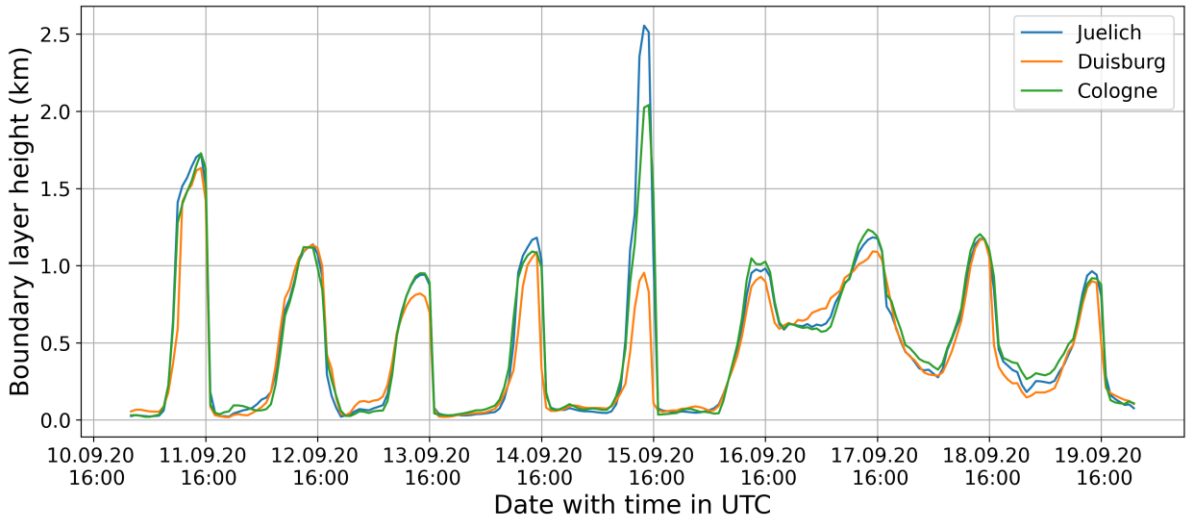

Figure 5: Time series of the ERA5 boundary layer height extracted for the respective target areas in the campaign period in September 2020. On day 2020-09-15 with strong regional differences, a survey flight was performed over Duisburg.

Input parameters related to aerosols (single-scattering albedo, asymmetry factor, and aerosol optical thickness) were extracted from the AERONET station FZJ-JOYCE at the Jülich research centre (Löhnert et al., 2015), which is the only known source providing local ground-based aerosol information in the campaign area. During the campaign measurement days, the daily averages of aerosol optical thickness (AOT) at 440 nm measured at FZJ-JOYCE ranged between 0.235 and 0.398 with a mean value of 0.285. This information is spatially constrained, and the situation can differ during the flights in the Duisburg and Cologne area. A sensitivity study using AMFs for a range of AOTs between 0.003 and 0.6 for the AirMAP NO_2 VCD retrieval demonstrated that the influence on the AirMAP tropospheric NO_2 VCD data set is small (<1 %, comparing AirMAP tropospheric NO_2 VCDs assuming AOTs of 0.003 and 0.6). Considering the mean AOT of 0.285 from the AERONET station and the results from the sensitivity study, the AirMAP data set was retrieved using an AOT of 0.3 for all measurement days. We also considered the pre-operational TROPOMI AOT product (de Graaf, 2022), which can provide a larger picture of the aerosol. In general, it shows AOT values in the same range as investigated within the sensitivity study.

Bright surfaces enhance the relative contribution of light reflected from the surface to the signal received by the airborne instrument, increasing the sensitivity to NO_2 near the ground. Therefore, areas of high surface reflectance in the fitting window generally show larger dSCDs for the same amount of NO_2. Thus, differences in the surface reflectivity must be accounted for in the AMF calculations. As far as we are aware, reflectance data that have a sufficient spatial resolution are not available for the region of our flight campaign. Therefore, we use the individual AirMAP-recorded intensities together with a method based on a reference area with a known surface reflectance taken from the ADAM database (a surface reflectance database for ESA's Earth observation mission; Prunet et al., 2013) and a look-up table of AirMAP radiances. Detailed information about

the derivation of the surface reflectance and also about the general conversion from dSCDs to tropospheric NO_2 VCDs can be found in Meier et al. (2017).

Post-processing step for destriping
The original retrieved VCDtrop results show some slight systematical dependency on the viewing direction, which originates from slightly different instrumental properties for the different geometries. These differences are not related to real atmospheric conditions. Therefore, a moderate destriping procedure is applied, which is considered to result in an NO_2 field closer to reality as the original retrieved NO_2 field according to the above retrieval steps only. For this purpose, the data for each viewing direction is regarded as a time series, and specifically chosen retrieval parameters for each measurement (Ring fit factor, intensity offset correction, spectral shift with respect to the reference measurement) are tested for systematic dependencies on the viewing direction during a time of 5 s (11 measurements as sliding window over the data set). Deviations from the mean between one viewing direction and the two neighbouring directions to both sides are taken into account, and the deviating pattern is subtracted from the original measurement.

2.1.5.2 *Data acquisition and DOAS retrieval for the mobile car DOAS instruments*

IUP-Bremen mobile car DOAS
The tropospheric NO_2 VCD is determined similarly as done for the AirMAP measurements by the following equation:

$$VCD_{trop} = (dSCD + SCD_{ref} - VCD_{strat} \cdot AMF_{strat}) / AMF_{trop} \quad (3)$$

using

$$SCD_{ref} = VCD_{trop,\,ref} \cdot AMF_{trop,\,ref} + VCD_{strat,\,ref} \cdot AMF_{strat,\,ref}. \quad (4)$$

The dSCD are retrieved relative to reference background spectra, measured in a region with small NO_2 concentrations on 13 September around noon. The SCD_{ref} cannot be measured directly. Similar to the AirMAP VCD determination, the NO_2 in the reference background spectrum is corrected for by assuming a tropospheric NO_2 VCD of $1x10^{15}$ molec/cm^2 over the reference background region. The other car DOAS instruments do not rely on this value as they use dedicated measurements taken at lower elevation angle to directly estimate the tropospheric column in the reference measurement.
The assumption of a $VCD_{trop,ref}$ of $1x10^{15}$ molec/cm^2 can be supported by a comparison of co-located car DOAS measurements of the three instruments, which shows a very good agreement. Since we used a fixed reference background measurement for all car DOAS measurement days, a stratospheric correction is applied to the car DOAS data. The correction is based on the Bremen 3D chemistry transport model (B3dCTM; Hilboll et al., 2013), providing a daily diurnal cycle of the stratospheric NO_2 VCDs and scaled to TROPOMI stratospheric VCDs in the measurement area. Stratospheric AMFs are calculated with the radiative transfer model SCIATRAN (Rozanov et al., 2014). For the conversion of tropospheric SCDs to tropospheric NO_2 VCDs, a constant tropospheric AMF of 1.3 was used. The AMF of 1.3 for an elevation angle of 90° is closer to the true

AMF (derived from radiative transfer simulations) than the geometric approximation for the tropospheric AMF of 1 (Shaiganfar et al., 2011; Merlaud, 2013; Schreier et al., 2019).

MPIC mobile car DOAS

Before and after the validation measurements, the elevation angles alternate between 22° elevation and zenith-sky (90°). The combination of both angles allows the determination of the absorption in the reference spectrum SCD_{ref}, as well as the absorption in the stratosphere.

The DOAS analysis is performed in a wavelength interval of 400–460 nm using a daily fixed reference background at 90° elevation and at low SZA in a region with small NO_2 concentrations.

NO_2 dSCDs retrieved from the DOAS analysis are converted to tropospheric NO2 VCDs by using Eq. (3) (see also Wagner et al., 2010; Ibrahim et al., 2010). Radiative transfer model calculations for NO_2 box profiles of 500 or 1000m and moderate aerosol loads provide on average tropospheric AMFs of 3 and 1.3 with an assumed uncertainty of 20% for the 22° and 90° elevation angle measurements, respectively (Shaiganfar et al., 2011; Merlaud, 2013).

BIRA mobile car DOAS

The DOAS analysis is performed in a wavelength interval of 450–515 nm on spectra averaged every 30 s using a single pair of time-coincident low SZA zenith reference spectra for all measurement days. The measurements on both channels being simultaneous, the retrieval of tropospheric NO_2 VCDs follows the MAX-DOAS principle (see Eq. 3), using the differences in dSCDs and AMFs for two elevation angles. For the AMFs, a sun-position dependent look-up table (LUT) is used. This LUT was calculated using DISORT and provides AMFs of 2.5 and 1.3 for the 30 and 90° elevation angle measurements, respectively (Merlaud, 2013). Notably, most of the spectra were recorded in cloud-free conditions. An additional zenith-DOAS instrument was operated for SO_2 measurements, results are not shown in this report.

2.1.5.3 *Data acquisition and DOAS retrieval for the ground-based instruments*

The ground-based instruments deployed during QA4EO in the Ruhr area belong to one of three different general types of instruments – individual MAX-DOAS instruments, zenith-sky instruments based on an Avantes spectrometer or Pandora instruments.

Zenith DOAS instruments

The tropospheric NO_2 VCDs are estimated from the dSCDs resulting from the DOAS fit using Eq. (3). For the reference background spectra in the DOAS fit, we use a fixed spectrum taken in summer on a clean day around noon. The amount of NO_2 in the reference background spectrum, SCD_{ref}, is determined from the long time series using the lowest measured NO_2. For the measurements made by the Zenith-DOAS in Gelsenkrichen, this is a SCD_{ref} of 1.7×10^{16} molec/cm^2. For the Zenith-DOAS in Jülich, the SCD_{ref} is determined as 1.0×10^{16} molec/cm^2 using the same approach. The SCD_{sref} given here include the stratospheric and tropospheric NO_2 in the reference background

spectrum. The VCD_{strat} is estimated from twilight Langley fits (e.g., Constantin et al., 2013) with an uncertainty of $2x10^{14}$ molec/cm², and the stratospheric AMFs are obtained from SCIATRAN calculations. For the tropospheric AMF we use the same value of 1.3 as for the car DOAS.

MAX-DOAS measurement truck

The tropospheric NO_2 VCDs are estimated from the dSCD measurements in 30° elevation angle with a sequential zenith-sky reference spectrum (interpolated from the zenith sky measurements shortly before and after the off-axis measurement):

$$VCDtrop = dSCD(30°) / (AMF_{trop}(30°) - AMF_{trop}.(90°)) \quad (5)$$

Based on SCIATRAN AMF calculations for a wavelength of 350 nm, adjusted to the ground-based and AirMAP comparison times around noon regarding SZA and with typical albedo and AOT values found during the campaign measurement days, AMFs of 2.5 and 1.4 are used for elevation angles of 30 and 90°, respectively. The total uncertainty of the tropospheric NO_2 VCD originates from uncertainties in the retrieved dSCD, which results mainly as the error of the DOAS fit, and uncertainties from the AMF for which we assume 20%.

BIRA Sky-Spec Max-DOAS

The tropospheric NO_2 VCDs are retrieved by applying the Mexican MAX-DOAS Fit (MMF; Friedrich et al., 2019) inversion algorithm using dSCDs retrieved with the spectral fitting software QDOAS (Danckaert et al., 2017) using the FRM4DOAS settings and setup (Hendrick et al., 2016). The tropospheric NO_2 VCD error is calculated from the covariance smoothing error matrix, the covariance measurement noise error matrix and a systematic error as a fixed fraction of the VCD, based on the systematic uncertainty of the cross section.

Pandora instruments

All data from the Pandora instruments during the Ruhr campaign are processed as part of the Pandonia Global Network (2023). Tropospheric NO_2 VCDs are retrieved using coincident sky scan MAXDOAS and direct-sun observations and are calculated based on the Spinei et al. (2014) approach (Cede et al., 2022). NO_2 values are given, together with the respective uncertainty, as tropospheric NO_2 VCD. The analysed data are labelled with quality flags, which indicate whether the data quality is high, medium, or low and whether the data are quality assured and usable or not. Only data with a quality flag accounting for high and medium quality (assured as well as not assured) are used.

2.1.6 Data format

AirMAP data is produced in a constant ascii format for many campaigns in the past, the same format is retained for the QA4EO data set as described below.
First of all, the files follow a certain naming convention, including information on data, viewing direction and further indicators for the instrument and applied retrieval, in the following way:

YYMMDD[VD]II.EXTENSION
YY=year

MM=month
DD=day
[VD]=viewing direction (01 until 35)
II=indicator for the spectrometer used (for internal information)
EXTENSION= file name extension (indicating, e.g., trace gas in focus)

Example file name and explanation: 20091201II.NO2VIS

This file will contain data from date 2020-09-12, of the 1st viewing direction. The extension is NO2VIS indicates that the main product in the file is the column density of NO_2 and that the DOAS retrieval is performed in the visible spectral range.

In these files, the respective data from the flight is provided as tables in ASCII format. The data is preceded by a text header, where the data content in the columns is described. In addition, the most important DOAS retrieval settings are given, such as the fitting window, the applied cross sections, the reference spectrum and similar.

Following the header, the data is listed with 58 data columns in total, ordered by time as decimal day-of-year. The data columns include information on time, viewing geometry, location of the aircraft, aircraft angles, flight altitude, slant column results of all included trace gases, respective fitting errors, retrieval RMS, iterations needed, intensity, integration time, latitude/longitude coordinates of all 4 ground pixel corners, post-processed slant column result of NO_2, correction terms from post-processing, stratospheric slant column of NO_2 applied in the conversion, albedo and AOT applied for AMF computation, resulting vertical column of NO_2 and respective uncertainty.

2.1.7 Main results achieved, including comparison with S5p data

During the course of the campaign, mobile and stationary observations were successfully performed on the seven golden days between Sep 12th and Sep 18th, 2022. The results from these measurements are suitable for the assessment of satellite data uncertainties, validation of satellite products and intercomparison studies between the instruments.

In the following, an overview of the main AirMAP observations is given. For each of the seven flight days, the AirMAP results of NO_2 VCDs are shown day by day, as well as the map of the retrieved surface reflectance at the same resolution as the NO_2 data. The displayed albedo data is directly used in the AMF determination required for the retrieval of the NO_2 VCD maps and is therefore considered a valuable side product of the AirMAP measurements.
The AirMAP data are themselves validated with ground-based instruments at fixed locations as well as three mobile car DOAS instruments. These results are combined for all seven days.
Then the validation of the S5p satellite products is discussed and the influence of the most relevant parameters determining the AMF is analysed, because the AMF is a main source of uncertainties when using trace gas column results from DOAS analyses.

AirMAP NO_2 results day by day

AirMAP observed NO_2 vertical columns on all seven golden days. The average over all 35 viewing directions together with the standard deviation is shown in Figure 6 as time line for a first overview.

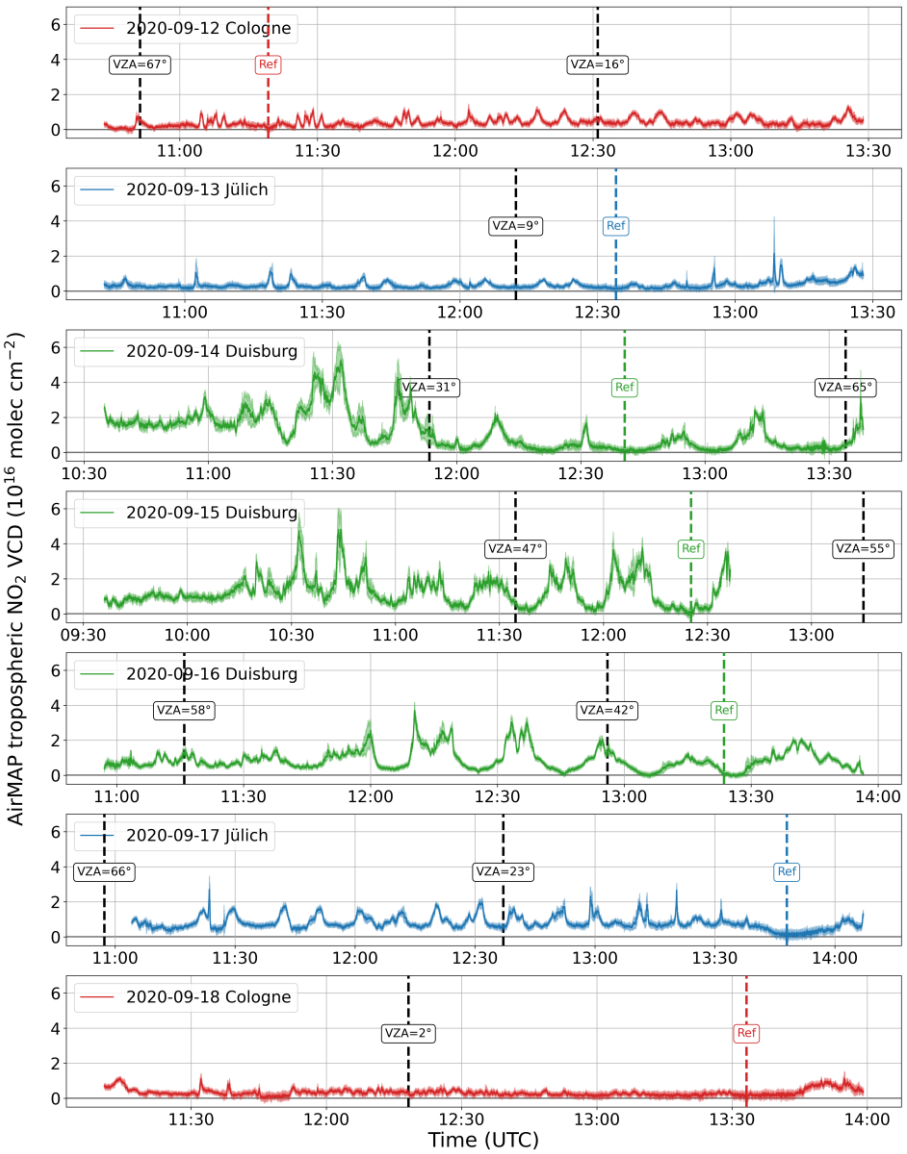

Figure 6: Timeseries of AirMAP NO_2 from all seven flight days showing the average NO_2 VCD from all 35 viewing directions (main dark line) as well as the standard deviation (shaded area around the line). The line colour represents the flight area according to Figure 2. Vertical dashed lines in black mark the S5P overpasses also stating the respective VZA, vertical dashed lines in line colour mark the times when the AirMAP reference measurement is taken. Strong variability is clearly visible between the different measurements, with strong differences between weekday and weekend, as well as between different flight areas. Figure from Lange et al., 2023.

Flight on 2020-09-12 (Saturday), Cologne:
The clear-sky flight on this day was performed between 10:17 and 13:37 UTC. On this day, moderate wind conditions of about 3.2 m/s westerly winds caused plumes extending roughly in easterly directions. The wind condition is always indicated as a small arrow in the top left corners of the maps, and is received from ERA5 wind data (Hersbach et al., 2018) at 10m altitude for the location of the respective flight area and for the middle of the flight time (cf. Figure 7).
Rather moderate pollution with NO_2 was observed with maximum NO_2 VCD values in the plumes below 1.5 x10^{16} molec/cm² and widespread NO_2 VCD amounts below 1.0 x10^{16} molec/cm².

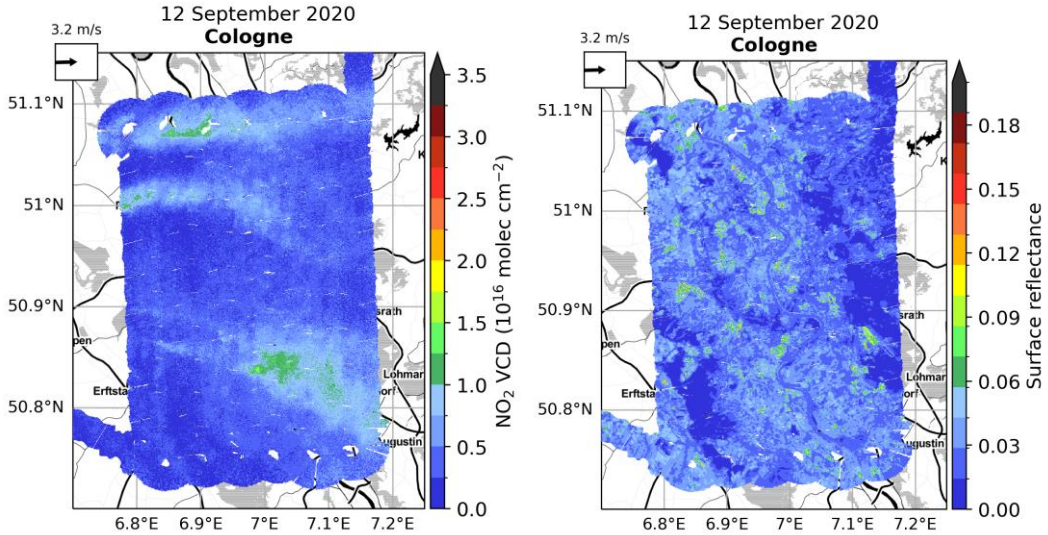

Figure 7: AirMAP results from the flight on Saturday, 2020-09-12, showing the retrieved NO_2 VCD (left) and retrieved surface reflectance (right) above the Cologne flight area colour coded according to the legend next to the respective map. Moderate wind conditions are indicated by the wind arrow in the top left corners.

Flight on 2020-09-13 (Sunday), Jülich:
The flight above Jülich was performed between 10:20 and 13:36 UTC mainly at clear sky with potential slight influence from Cirrus clouds temporarily.
Mild wind was coming from the Southwest with a wind speed of about 2.0 m/s. While most of the surroundings were affected only by background NO_2 VCD amounts clearly below 1.0 x10^{16} molec/cm², three small but clear plumes from three power plants in the survey area are observed with largest NO_2 amounts in the far West of the flight area in the westernmost flight track with values exceeding 3 x10^{16} molec/cm² (see Figure 8).

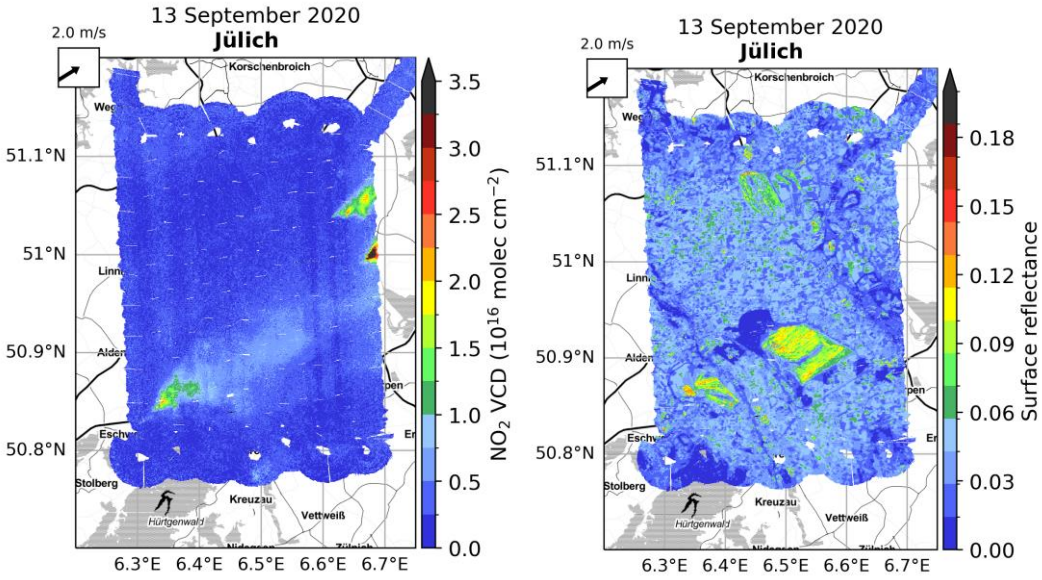

Figure 8: AirMAP results from the flight on Sunday, 2020-09-13, showing the retrieved NO_2 VCD (left) and retrieved surface reflectance (right) above the Jülich flight area colour coded according to the legend next to the respective map. Mild wind conditions are indicated by the wind arrow in the top left corners.

Flight on 2020-09-14 (Monday), Duisburg:
This flight was synchronized with the first overpass of S-5p and took place between 10:14 and 13:47 UTC with some influence of cirrus clouds above the target area.
Wind was coming from the Southeast at moderate speeds around 2.5 m/s. In comparison to the former two areas, the Duisburg area is affected by much stronger and more widespread NO_x emissions, that cause more than half of the survey area to be covered in enhanced NO_2 amounts clearly above background values (cf. Figure 9). Largest NO_2 VCDs reach up to about 5 x10^{16} molec/cm² on this day. Areas towards the Northwest of the emission sources are covered by strong NO_2 plumes.

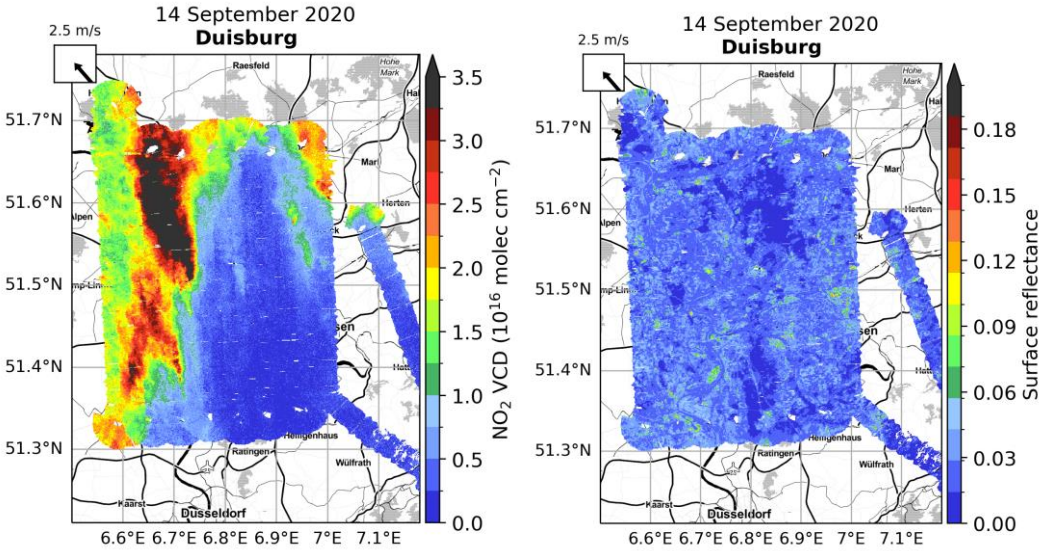

Figure 9: AirMAP results from the flight on Monday, 2020-09-14, showing the retrieved NO_2 VCD (left) and retrieved surface reflectance (right) above the Duisburg flight area colour coded according to the legend next to the respective map. Mild wind conditions are indicated by the wind arrow in the top left corners.

Flight on 2020-09-15 (Tuesday), Duisburg:
This flight repeats the pattern from the day before at favourable wind and weather conditions taking place between 9:15 and 12:44 UTC. In comparison to the day before, wind was coming from a similar direction but was much weaker, so that plumes are less widespread, and maximum NO_2 columns are still large (see Figure 10). Again, more than half of the area is affected by strong NO_2 pollution and only a small part in the Southeast shows background NO_2 amounts (in bright blue colour).

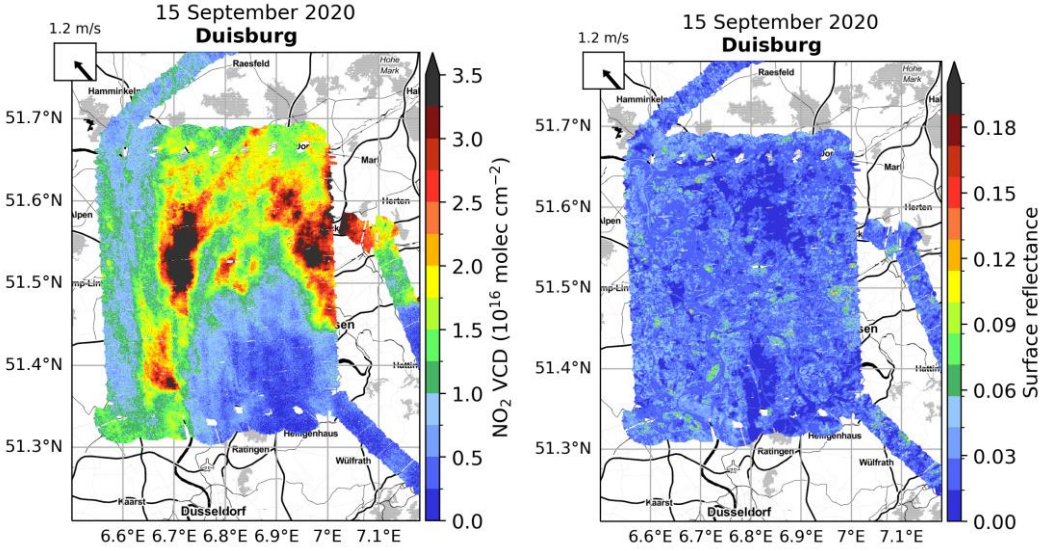

Figure 10: AirMAP results from the flight on Tuesday, 2020-09-15, showing the retrieved NO_2 VCD (left) and retrieved surface reflectance (right) above the Duisburg flight area colour coded according

to the legend next to the respective map. The wind condition is indicated by the wind arrow in the top left corners.

Flight on 2020-09-16 (Wednesday), Duisburg:
Again, the same tracks as the two days before were flown, this time between 10:37 and 14:05 UTC with some haze visible at times, darker haze being visible from the mobile car routes. This might have an influence on the quality of the observational results. In comparison to the two days before, the wind direction has changed, wind is coming from the Northwest at a higher speed of 4.0 m/s. Therefore, the NO_2 pattern in the area has completely changed as can be seen in Figure 11. The Northern part, especially the Northeast is fairly clean of NO_2 pollution, partly only showing background NO_2 amounts, while the emission plumes transport NO_2 to the South and Southeast of the area.

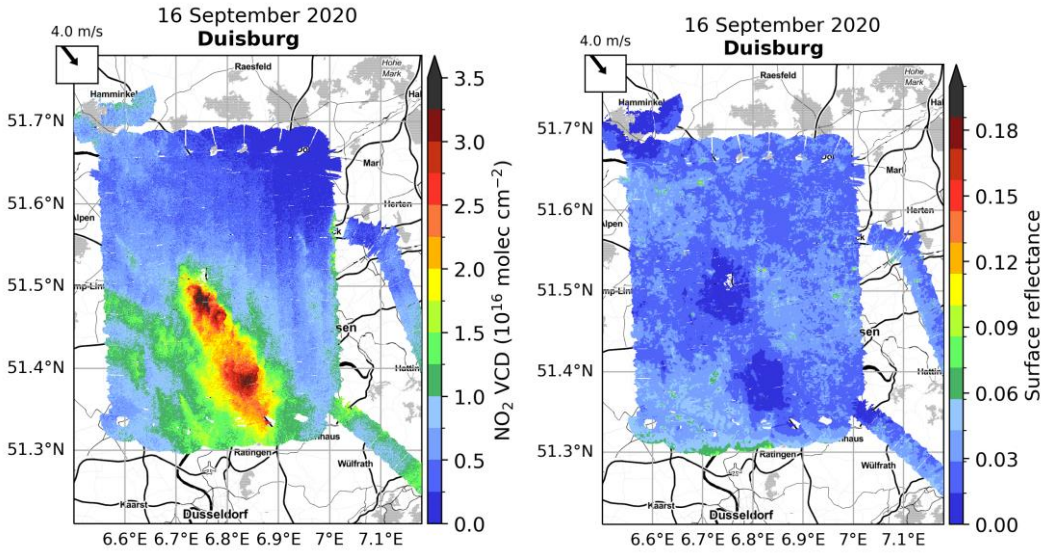

Figure 11: AirMAP results from the flight on Wednesday, 2020-09-16, showing the retrieved NO_2 VCD (left) and retrieved surface reflectance (right) above the Duisburg flight area colour coded according to the legend next to the respective map. The wind condition is indicated by the wind arrow in the top left corners.

Flight on 2020-09-17 (Thursday), Jülich:
The same pattern as on Sunday 13th Sep was flown above the Jülich flight area between 10:45 and 14:16 UTC with strong wind and clear sky. In comparison to the first survey above Jülich, the wind has turned by about 180° and is much stronger on this day, so that the emission plumes are transported faster and in the other direction. The two emitters on the Eastern side of the area now cause NO_2 pollution in the middle of the flight area, with NO_2 VCD values going up to 2.5 $x10^{16}$ molec/cm² in the centre of the plumes (cf. Figure 12). In addition to different wind conditions, also a weekend effect may cause some of the differences between this survey and the one on 2020-09-13.

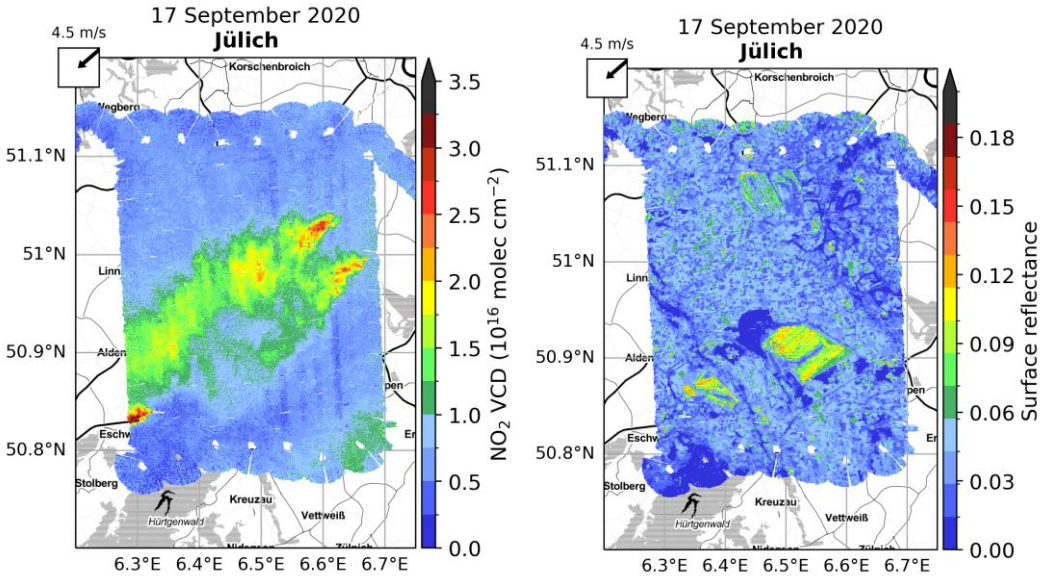

Figure 12: AirMAP results from the flight on Thursday, 2020-09-17, showing the retrieved NO_2 VCD (left) and retrieved surface reflectance (right) above the Jülich flight area colour coded according to the legend next to the respective map. The wind condition is indicated by the wind arrow in the top left corners.

Flight on 2020-09-18 (Friday), Cologne:

This flight repeats the pattern above Cologne from Saturday 12th Sep and was performed between 10:48 and 14:08 UTC. Similar to the first flight, the NO_2 values are low to moderate and only weak emission plumes are visible. Nevertheless, the plumes can clearly be distinguished from the background and are transported from the sources in North-westerly directions according to the wind coming from the Southeast at 4.47m/s. Great parts of the survey area show clean air with only background NO_2 amounts, and NO_2 amounts within the plumes reach about 1.5 $x10^{16}$ molec/cm^2.

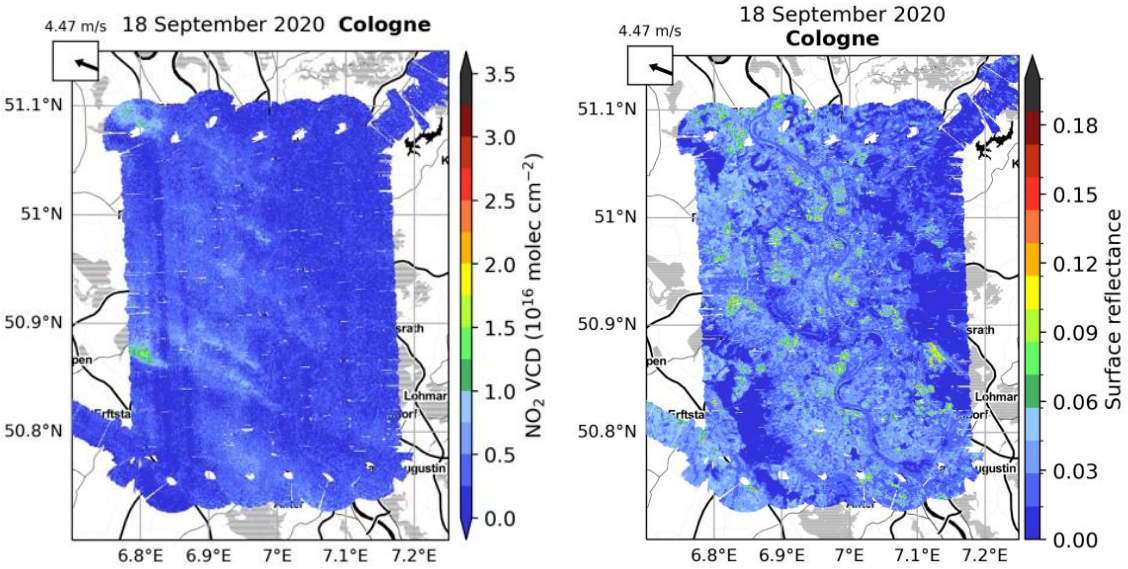

Figure 13: AirMAP results from the flight on Friday, 2020-09-18, showing the retrieved NO_2 VCD (left) and retrieved surface reflectance (right) above the Duisburg flight area colour coded according to the legend next to the respective map. The wind condition is indicated by the wind arrow in the top left corners.

Validation of the AirMAP data with stationary DOAS and mobile DOAS data

Before the AirMAP data is used for validation of satellite data and assessment of their uncertainties, the AirMAP data is compared to other independent observations. Ground-based observations from six stationary DOAS instruments of different types (zenith-sky Avantes, Max-DOAS and Pandora instruments) have been deployed for a longer period of time before and after the main campaign period in September 2020. **Error! Reference source not found.** gives an overview of the timeseries of the ground-based data from the stationary instruments during September 2020. Again, these data sets clearly demonstrate the strong temporal and spatial variability of NO_2 in the respective areas. Especially in the Duisburg data, but also under certain conditions in Jülich, the NO_2 tropospheric VCD rise to large values above 5 x10^{16} molec/cm².

The second part of the comparison is based on the mobile car DOAS instruments from IUP Bremen, MPIC Mainz and BIRA. The driving routes are displayed above in Figure 3 and retrieval results of tropospheric NO_2 VCDs are shown in Figure 15. There are clear differences between the different campaign days also in the car DOAS data, with the Cologne area showing rather low NO_2 values and largest column amounts in the Duisburg area, exceeding 3 x10^{16} molec/cm² for substantial parts of the routes.

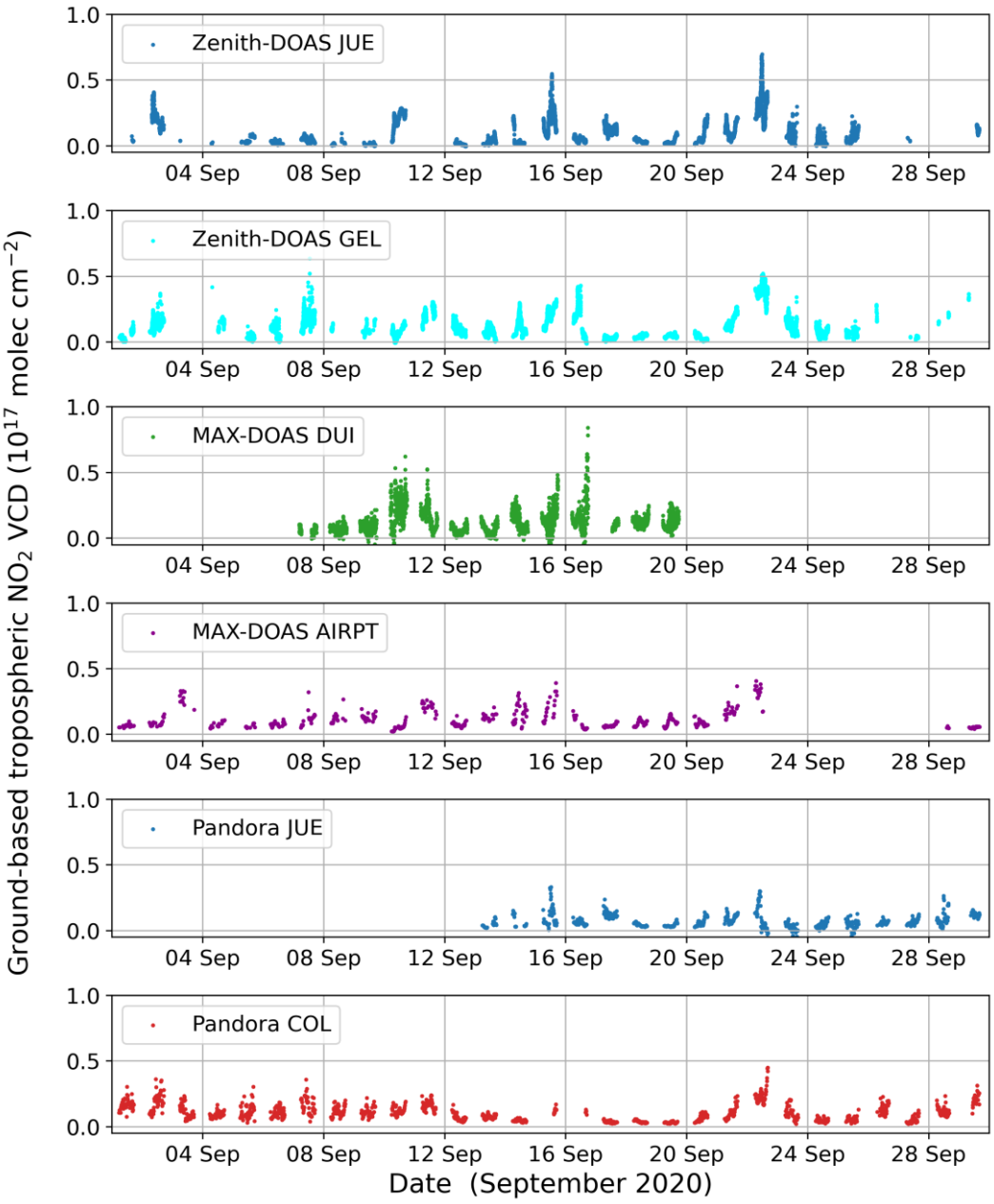

Figure 14: Timeseries of tropospheric NO_2 VCDs from the six stationary ground-based instruments in September 2020 covering the main campaign period from 12th-18th September, 2020, including two zenith-sky Avantes in Jülich and Gelsenkirchen (row 1 and 2), two Max-DOAS instruments in Duisburg and at the Airport Schwarze Heide (row 3 and 4) as well as two Pandora instruments in Jülich and Cologne (row 5 and 6). Figure from Appendix in Lange et al., 2023.

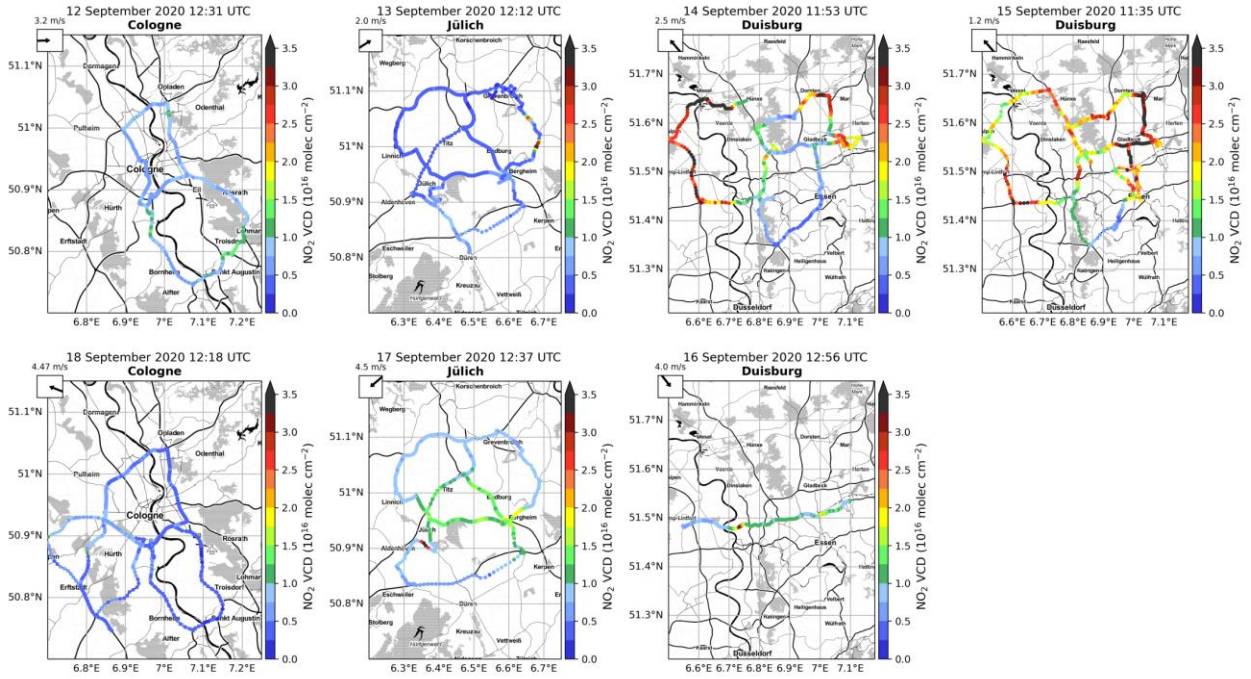

Figure 15: Maps of the mobile car DOAS results of tropospheric NO_2 VCDs on all seven flight days used for validation of the AirMAP data. Figure from Lange et al., 2023.

For both ground-based data sources, stationary as well as mobile car DOAS instruments, collocation criteria are applied to the data to make sure, instruments from the ground are observing sufficiently similar air masses as the airborne AirMAP device to enable a reasonable comparison.
For the stations, data from a time interval of 20 minutes around the AirMAP overpass was used and averaged before the analysis. For the comparison, AirMAP data were averaged within a 500m x 500m spatial area around the station location. From this procedure, 25 collocated measurements are achieved during the course of the campaign above the station locations.
For the car DOAS measurements, the collocation criteria allow data to deviate in time ±15 minutes around the aircraft overpass. In addition, both data sets are gridded in 500m x 500m boxes, and for the scatter plots, both data sets are averaged in 15 min time intervals. The data base comprises 572 collocated data points.

For the collocated data sets, orthogonal distance regression analyses are performed. The analysis of the collocated AirMAP to stationary DOAS data results in a slope of 0.92 and an offset of 0.75×10^{15} molec/cm² (cf. Figure 16, left).
The regression analysis for the collocated AirMAP and car DOAS data yields a slope of 0.98 close to unity and an offset of -1.77×10^{15} molec/cm² (cf. Figure 16, right).
Differences in the offset can be caused by different assumptions on the background measurement, as well as differences in the retrieval and AMF settings. The car DOAS data sets are completely independent as the data is analysed by three different groups without harmonized retrieval of AMF settings. Consequently, the resulting regression shows good quality of the AirMAP data in comparison to the mobile car DOAS results.

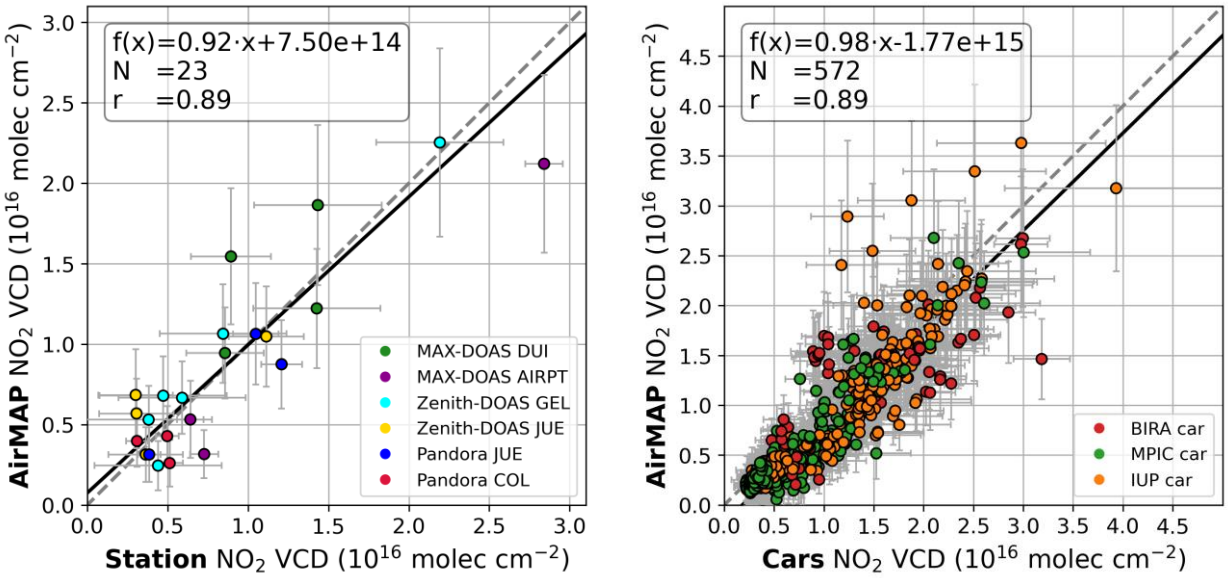

Figure 16: Scatter plots for AirMAP NO_2 tropospheric VCD results compared to the results from stationary instruments (left) as well as mobile car DOAS instruments (right). Data from different instruments are shown in different colour according to the legends in the bottom right. Results from the orthogonal distance regression are given in the top left. For the analysis, only data according to selected collocation criteria are used. Figure from Lange et al., 2023.

The present validation study comparing AirMAP data during QA4EO with ground-based independent measurements supports previous analyses, that the AirMAP tropospheric NO_2 VCD data is a reliable data source suitable to be used for satellite validation (see also Meier et al., 2017; Merlaud et al., 2020; Lange et al., 2023).

Validation with S-5p satellite products

For the validation of TROPOMI satellite data, different products of NO_2 are used. The main basic versions are the offline OFFL V01.03.02. data and the PAL V02.03.01 data as well as the IUP V02.03.01 version. For these basic products, several variants are taken into account, for which different input information is applied regarding the NO_2 profile, cloud correction, and surface reflectance.

In order to compare the AirMAP data with the satellite products, some processing steps, especially suitable gridding and applying collocation criteria, are required. These steps are illustrated by Figure 17.

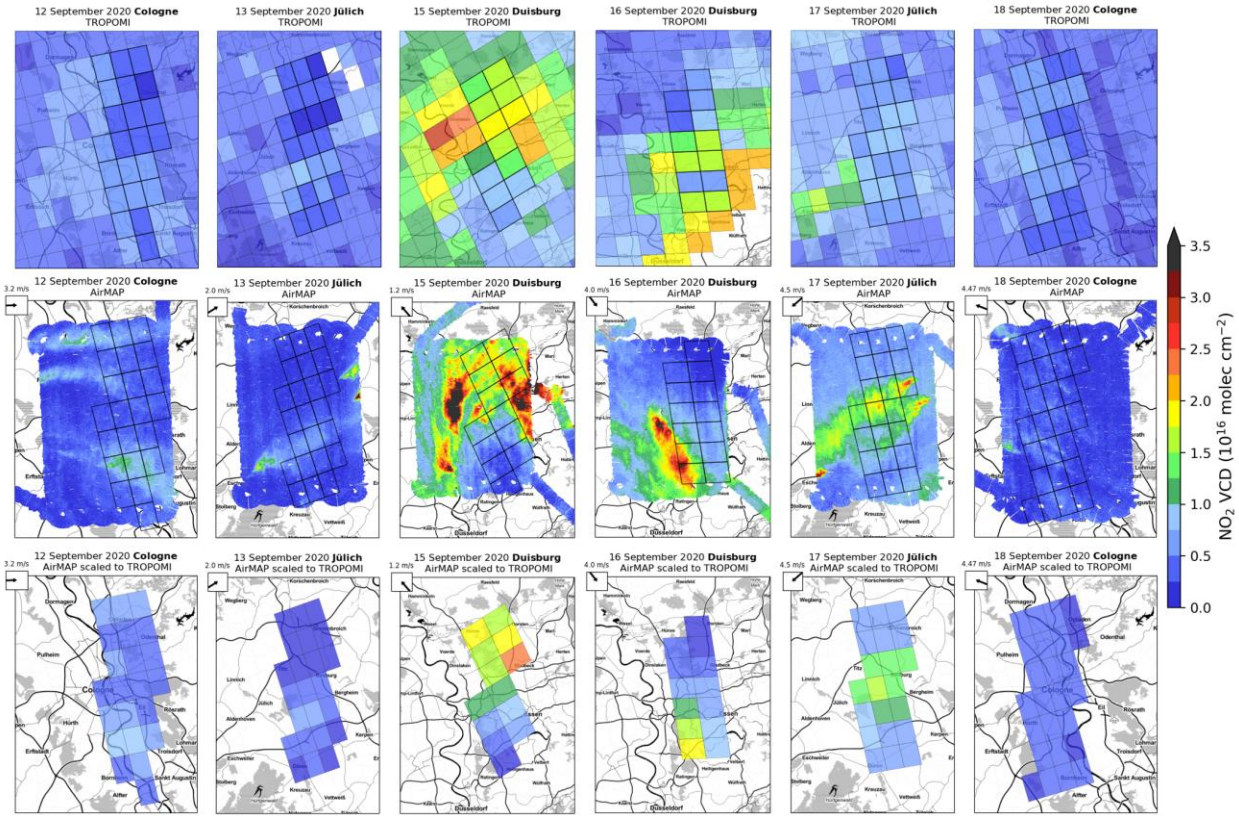

Figure 17: Data preparation for comparison of AirMAP aircraft data to satellite products. Top row: TROPOMI satellite tropospheric NO_2 data from the PAL V02.03.01 data version for six campaign days. Second row: AirMAP data with overlayed grid in black indicating pixels with sufficient overlap between satellite and aircraft data (>75%). Bottom row: Averaged AirMAP results in the selected grid boxes, prepared for direct comparison with the satellite product. Figure from Lange et al., 2023.

Briefly, TROPOMI pixels are only considered if at least 75 % of their area is mapped by AirMAP pixels (Figure 17, top row). AirMAP data are used when they match the temporal coincidence criteria of 30 min around the S-5P overpass time (Figure 17, second row). These spatial and temporal coincidence criteria are following the suggestion by Judd et al. (2020). During the seven flight days (for which TROPOMI data are only available on 6 days), AirMAP measurements coincide with 117 TROPOMI pixels. For the comparison of the two data sets, all AirMAP measurements are averaged within the respective TROPOMI pixel (Figure 17, third row).

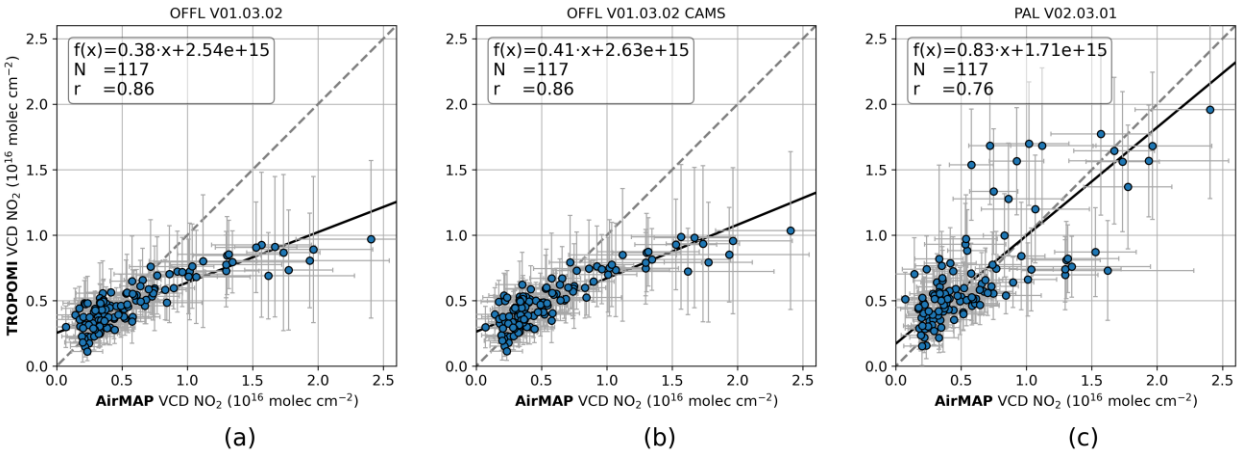

Figure 18: Scatter plots comparing the tropospheric NO_2 VCDs of three different TROPOMI products with the AirMAP observations. The different versions are the pure OFFL V01.03.02 product (left), the OFFL V01.03.02 product with using CAMS NO_2 profiles (middle) and the PAL V02.03.01 based on the reprocessed TROPOMI data (right). Figure from Lange et al., 2023.

In Figure 18, the averaged AirMAP tropospheric NO_2 VCDs are compared to the coincident satellite data for the three TROPOMI NO_2 data versions mentioned above. The scatter plots and orthogonal distance regression analysis show comparison of the TROPOMI and AirMAP NO_2 VCDs for (i) the TROPOMI operational OFFL V01.03.02 data, (ii) the adapted scientific TROPOMI V01.03.02 CAMS data using CAMS-based NO_2 profiles, and (iii) the reprocessed data version PAL V02.03.01.
The horizontal error bars in the figures correspond to the 10^{th} and 90^{th} percentiles of all airborne measurements within the respective TROPOMI pixel. Vertical error bars represent the reported precision of the TROPOMI tropospheric NO_2 VCD. The comparison of the different TROPOMI NO_2 data versions to the AirMAP data gives insight into the influence of different a priori assumptions made within each of the retrievals.

Figure 18(a) shows coincidences between AirMAP and the TROPOMI operational OFFL V01.03.02 data, with a high correlation coefficient of 0.86, a slope of 0.38 ± 0.02, an offset of 2.54 ± 0.15 × 10^{15} molec/cm^2, and a median relative difference of −9 % with an interquartile range of −28 % to 16 %. The regression parameters and their standard errors are calculated for the plotted data points. Taking the uncertainties of the data points into account and considering the parameters of the orthogonal distance regression over the complete range of these uncertainties yields a standard deviation of 0.14 for the slope and 0.39x10^{15} molec/cm^2 for the offset. The slope of 0.38 is significantly lower than the value of 0.68 found in comparisons of TROPOMI NO2 OFFL V01.03.02 data and aircraft measurements in the New York City and Long Island Sound region reported by Judd et al. (2020) and the 0.82 reported for comparisons of TROPOMI and APEX measurements over Brussels and Antwerp by Tack et al. (2021).

The second TROPOMI data set shown in Figure 18(b), the scientific TROPOMI data V01.03.02 CAMS based on the OFFL data V01.03.02, has the objective to investigate the influence of the a priori NO_2 profile information used by replacing the 1°x1° TM5 NO_2

profiles with the spatially better resolved 0.1°x0.1° CAMS-regional based profiles. The resulting scatter plot shows a correlation coefficient of 0.86 and a slope of 0.41±0.02 and the median relative difference improves from 9 % to 5 %. The correlation has not changed compared to the original data version and the slope increased only slightly, demonstrating that the replacement of the NO_2 profile has only a small impact on this data set. In general, using the CAMS regional NO_2 profile increases the dynamical range of NO_2 VCDs, with the largest impact (5 % - 30 %) over emission hot spots, but varying with the location and conditions (Douros et al., 2023). Tack et al. (2021) observed an increase of the slope from 0.82 to 0.93 when switching from the original data version to that using the CAMS regional a priori over Belgium. Thus, the relative difference (improvement) in slope between the original V01.03.02 and the V01.03.02 CAMS data is similar, i.e., 13 % in Tack et al. (2021) and 8 % in this study.

Since already earlier validation studies reported that the NO_2 data V01.02–01.03 are biased low, a complete mission reprocessing was performed with an updated TROPOMI NO_2 version V02.03.01 on the PAL system. The comparison of this TROPOMI product with the AirMAP data in Figure 18(**Error! Reference source not found.**c) shows much more scatter, with a correlation coefficient that is significantly poorer than for the OFFL V01.03.02 product, changing from 0.86 to 0.76. The slope, however, increased by more than a factor of 2 from 0.38±0.02 to 0.83±0.06, demonstrating that the updates in the new TROPOMI NO_2 data version have a large impact on the analysed data set from the Rhine-Ruhr region. Due to the large scatter and driven by the large number of measurements with tropospheric NO_2 VCDs of less than about $7.00 \pm 0.15 \times 10^{15}$ molec/cm^2, the PALV02.03.01 product has a positive median relative difference of 20 % with an interquartile range of 14 % to 66 %.
The main change from V01.03 to V02.03.01 is the switch to the FRESCO-wide product, which provides higher and therefore more realistic cloud altitudes for measurements with cloud fractions larger than zero. Only 1 out of the 117 TROPOMI pixels used in this study has a cloud fraction of zero. Higher cloud altitudes result in decreased tropospheric AMFs and therefore higher tropospheric NO_2 VCDs. With the update many of the 117 data points show increased TROPOMI VCDs and are now closer or even above the 1:1 line, increasing the slope and the median relative difference. However, there is also a lower branch of data points (with low TROPOMI NO_2, but large AirMAP NO_2 VCDs) that is not much affected by the modifications in the new data version and still matches the pattern of the OFFL V01.03.02 comparison. This lower branch is dominated by observations from 17 September, and is linked to cloud pressures close to the surface even after the change from FRESCO-S to FRESCO-wide. In the OFFL V01.03.02 product, 110 out of 117 pixels and thus 97 % of the TROPOMI observations were found to have cloud heights very close to the surface (within 50 hPa), which is not realistic, especially not for such a large number of observations. In the new PAL V02.03.01 product, the cloud retrieval yields a cloud height close to the surface for 28 out of 117 pixels, resulting in a better slope of the regression line. However, since some scenes remain problematic, it results in more scatter. Previous studies showed that for scenes with low clouds, i.e., close to the surface, a height that is even closer to the surface was retrieved by the original FRESCO implementation. Since the cloud algorithm does not discriminate between clouds and aerosols, this also holds for low aerosol layers. In many cases, FRESCO then retrieves the surface height, which is incorrect (Compernolle et al., 2021; van Geffen et al., 2022). Observations during the flights and VIIRS images of the campaign measurement days

revealed nearly perfectly cloud-free conditions during the measurements over the target areas. Thus, the high cloud pressures are suspected to be caused by a larger aerosol load, which is mis-identified as cloud.

Additional sensitivity tests were performed on the impact of using the CAMS regional a priori NO_2 profiles and different versions of the TROPOMI surface reflectivity climatology in the TROPOMI data retrieval. In order to perform such tests, the PAL V02.03.01 product was replicated with the IUP Bremen data processor, resulting in very close agreement (see Figure 19, top left, which is very similar to the previous Figure 18(c)).

As a first test, the TM5 NO_2 a priori data was again replaced by the CAMS regional ensemble data. The results are shown in Figure 19, top right. Using the spatially better resolved NO_2 profiles increases the slope from 0.88 ± 0.06 (IUP V02.03.01) to 1.00 ± 0.07 (IUP V02.03.01 REG), while maintaining nearly the same correlation of 0.75 as compared to 0.76. With a relative difference in slope of 14 %, the profile replacement has a slightly larger impact than the 8 % we found for changing the a priori NO_2 profile information from TM5 to CAMS-regional for the OFFL V01.03.02 data set. Using the spatially better resolved profile information has the effect that the profile shape over source regions has more NO_2 near the ground, which decreases the AMF and thus increases the tropospheric NO_2 VCD, compensating the reduced sensitivity of TROPOMI to trace gases close to the surface. This correction has a larger effect in the case of the more realistic lower cloud pressures of the PAL V02.03.01 data.

The second test replaced the OMI LER (Lambertian equivalent reflectance) used in the PAL V02.03.01 product by the TROPOMI LER V1.0, in addition to using the CAMS regional NO_2 a priori profiles. As demonstrated in Figure 19**Error! Reference source not found.**, bottom left, the effect is very limited for the data evaluated here. The slope increases slightly from 1.00±0.07 to 1.02±0.07, and the correlation hardly changes (from 0.75 to 0.74). The median relative difference decreased from 31 % to 24 %. This comparison shows that replacing the OMI LER with the TROPOMI LER data has only a small impact on the TROPOMI NO_2 VCD retrieval for our data set. Differences between the OMI LER and TROPOMI LER are rather small in the campaign region and in the NO_2 fit window, but can be larger in other regions of the world, and a change would thus have a greater impact there.

As a last test, the TROPOMI LER was replaced by its directionally dependent version DLER (Tilstra et al., 2022), now properly accounting for the difference in surface reflectivity when observing it under different viewing angles. As shown in **Error! Reference source not found.**, bottom right, also this test led to only small changes in the correlation results. A slope of 0.95±0.07 and a median relative difference of 21 % with a correlation of 0.75 was found. Thus, the directional aspect of the surface reflectivity only plays a small role in the tropospheric NO_2 retrieval in the campaign region with nearly cloud-free conditions (mean cloud radiance fraction 0.21 ±0.10) during the measurement days. As for the comparison between OMI LER and TROPOMI LER, it should be pointed out that this result is specific to the area, month, and cloud conditions, as the reflectivity influences the cloud height retrieval and thus also the AMF. Larger differences could, for example, be expected for snow-covered surfaces with high reflectivity.

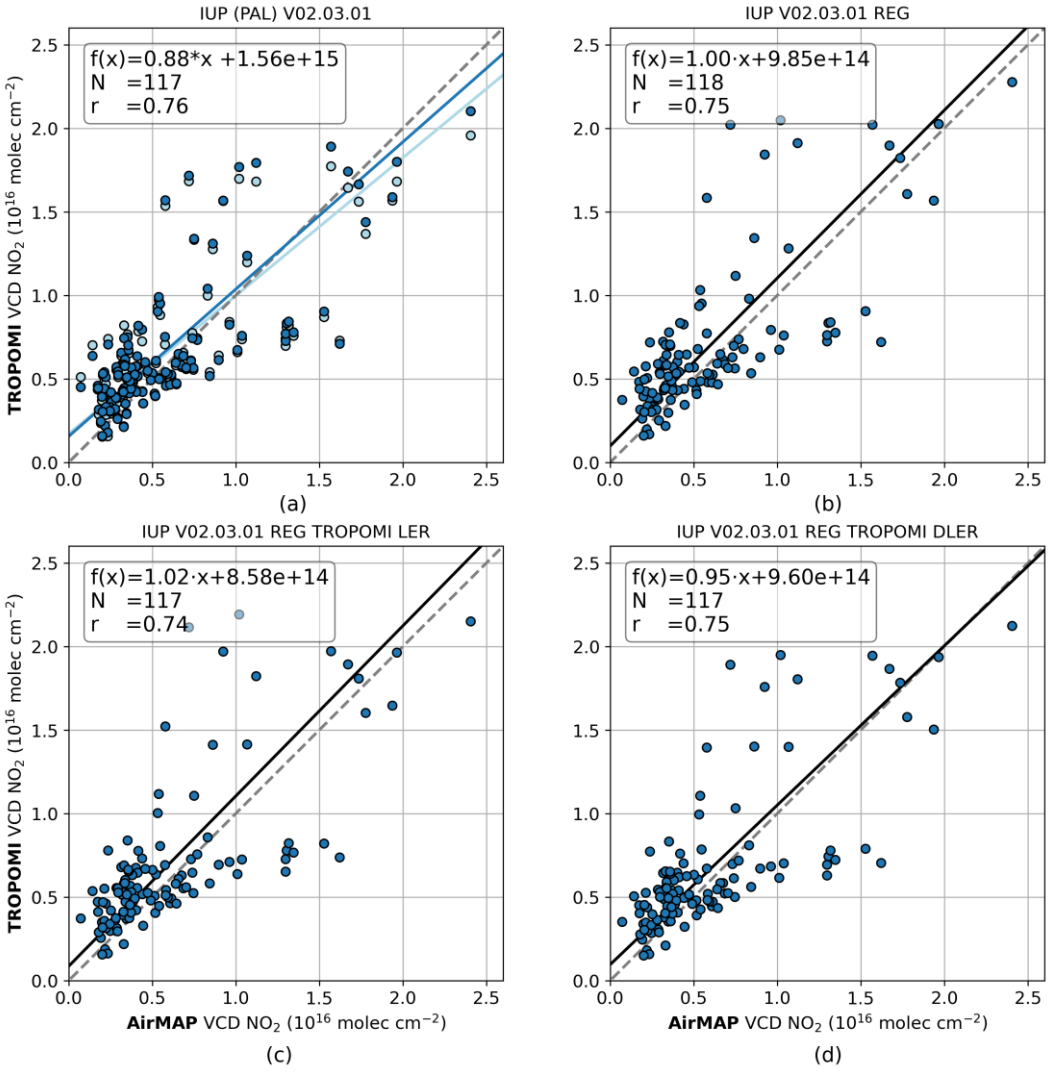

Figure 19: Scatter plots comparing four different TROPOMI data versions to the AirMAP data. The four versions are all based on the IUP data retrieval using the IUP V02.03.01 data with different auxiliary data input as indicated in the titles. Figure from Lange et al. 2023.

An overview on the validation results for all the different versions of the TROPOMI retrieval evaluated here and three additional tests runs using different cloud retrieval flagging (see Lange et al., 2023 for details) is given in Figure 20. For the data set evaluated here, the smallest deviations are found for the OFFL V01.03.02 data after replacing the TM5 NO_2 a priori by the CAMS-regional profiles. However, as discussed above, the PAL V02.03.01 and its variations show a better slope in the validation comparisons.

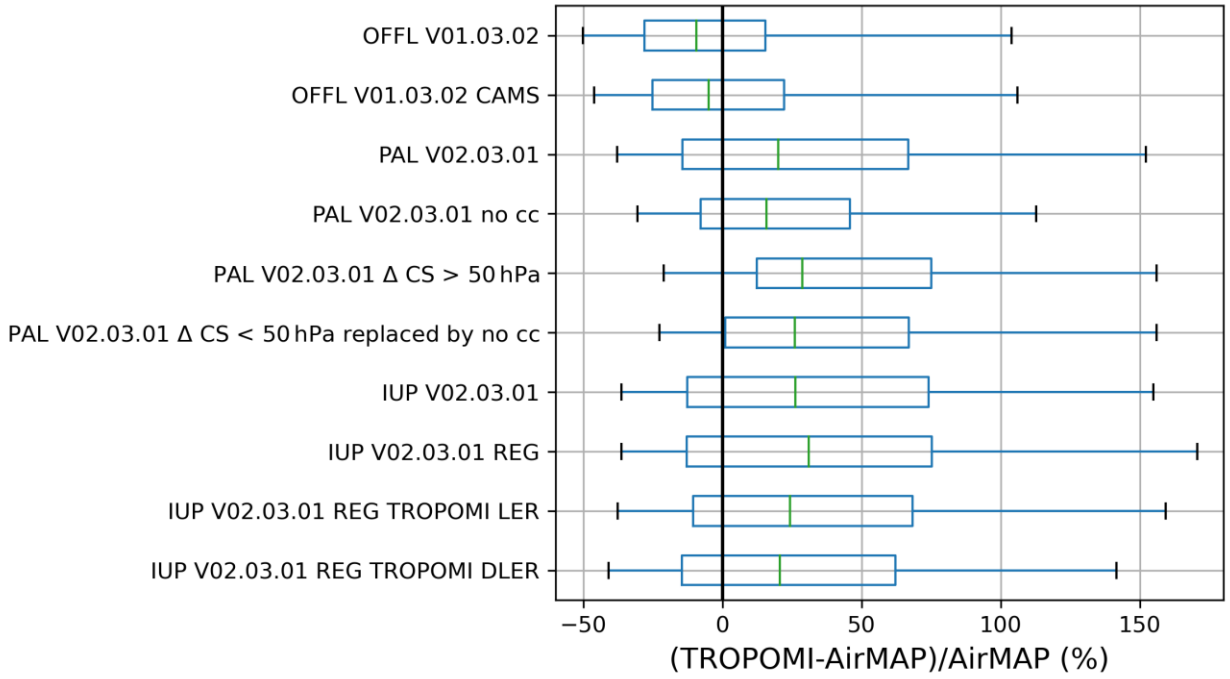

Figure 20: Box-and-whisker plots summarizing the bias and spread of the difference between the different TROPOMI versions and AirMAP tropospheric NO_2 VCDs. The green line inside the box represents the median relative difference. Box bounds mark the 25th and 75th percentiles, while the whiskers represent the 5th and 95th percentiles. Figure from Lange et al., 2023.

2.1.8 Dissemination and outreach activities (conference participation, articles, dissertations,etc)

The data sets recorded during the Ruhr 2020 campaign and the related analyses were shown and discussed on several conferences and meetings, and results where summarised especially into one central research article (Lange et al., 2023). In addition, they were used as an important part of a PhD Thesis by Kezia Lange in 2023.

Dissertation

Lange, Kezia: Investigating NO_2 distributions from satellite, airborne and ground-based measurements: spatiotemporal variability of NO_x emissions and validation of the TROPOMI NO_2 product, PhD Thesis, University of Bremen, 2023.

Research Article

Lange, K., Richter, A., Schönhardt, A., Meier, A. C., Bösch, T., Seyler, A., Krause, K., Behrens, L. K., Wittrock, F., Merlaud, A., Tack, F., Fayt, C., Friedrich, M. M., Dimitropoulou, E., Van Roozendael, M., Kumar, V., Donner, S., Dörner, S., Lauster, B., Razi, M., Borger, C., Uhlmannsiek, K., Wagner, T., Ruhtz, T., Eskes, H., Bohn, B., Santana Diaz, D., Abuhassan, N., Schüttemeyer, D., and Burrows, J. P.: Validation of Sentinel-5P TROPOMI tropospheric NO2 products by comparison with NO2 measurements from airborne imaging DOAS, ground-based stationary DOAS, and

mobile car DOAS measurements during the S5P-VAL-DE-Ruhr campaign, Atmos. Meas. Tech., 16, 1357–1389, https://doi.org/10.5194/amt-16-1357-2023, 2023.

Conference contributions

- Lange, K., et al., Comparison of TROPOMI tropospheric NO_2 observations with airborne, stationary ground-based and car DOAS measurements during the S5Pval-DE-Ruhr campaign, Sentinel-5P 5 years anniversary meeting, Taormina, Italy, October 11, 2022.
- Schönhardt, A., et al., S5Pval-DE-Ruhr campaign - Quick report on current status, SVANTE / QA4EO progress meeting, online, June 17th, 2021.
- Lange, K., et al., Representativeness and variability of the ground-based measurements from the S5P-VAL-DE-Ruhr campaign, MAX-DOAS Workshop, online, May 12, 2021.
- Lange, K., et al., Validation of Sentinel-5P TROPOMI tropospheric NO_2 with airborne imaging, ground-based stationary, and mobile DOAS measurements from the S5P-VAL-DE-Ruhr campaign, EGU21-10637, EGU General Assembly 2021, online, April 28, 2021.
- Lange, K., et al., First results from the Sentinel-5P-VAL-DE-Ruhr campaign in 2020, IUP-AWI-Blockseminar, online, February 22, 2021.
- Lange, K., et al., First results from the Sentinel-5P-VAL-DE-Ruhr campaign in 2020, Sentinel-5P Validation Team Meeting, online, October 20, 2020.
- Meier, A. C., et al: First results from the S5PVAL-Ruhr campaign, OMI-TROPOMI Workshop, online, October 2020.
- Meier, A. C., et al., German campaign activities for the uncertainty characterization of trace gas products from Sentinel-5p, *Poster contribution to Copernicus Sentinel-5 Precursor Validation Team Workshop, Frascati, Italy,* November 2019.

2.1.9 Conclusions

The Ruhr campaign 2020 combined airborne AirMAP measurements with stationary ground-based data and car-DOAS observations. The approach was to use ground-based and car-DOAS measurements to check and validate the airborne data and then to apply the verified AirMAP data for the validation of TROPOMI tropospheric NO_2 data. The good spatial resolution and continuous coverage of the AirMAP measurements make them particularly useful for satellite validation, as complete coverage of several TROPOMI ground-pixels can be achieved within 30 minutes of S-5P overpass. However, this type of validation is only possible under favourable weather conditions, and the first attempt of a Ruhr validation campaign in 2019 failed because of a long stretch of cloudy weather.

For the validation, several different TROPOMI NO_2 data products were used, including the operational OFFL V1.03.02 and pre-operational PAL V02.03.01 data as well as additional scientific data versions varying different input parameters in an attempt to identify critical factors in the data retrieval. The main conclusions of the validation exercise are

1. OFFL V1.03.02 data show good correlation with AirMAP measurements (0.86), but a low slope of 0.38 in the regression results.

2. PAL V02.03.01 results in a clearly improved slope of 0.83 in the regression results, but increased scatter and a reduced correlation coefficient (0.76).
3. The problems in both versions appear to be linked to scenes for which unrealistically low cloud heights are retrieved. Excluding these scenes or not applying cloud correction in such cases improves the correlation and regression slope.
4. Using the spatially better resolved CAMS-regional NO_2 profiles as input improves the slope of the regression but does not increase the correlation coefficient.
5. Switch from OMI to TROPOMI LER or DLER has relatively small effects on the comparison between TROPOMI and AirMAP data.

It is important to note that while many TROPOMI measurements were validated during the Ruhr campaign, they all were taken under similar conditions (nearly cloud free September observations in the polluted Ruhr area), and the conclusions can not necessarily be generalised to other seasons, regions and pollution levels.

2.2 Airborne and ground based campaign in Romania

2.2.1 Objectives

The field study in Romania (Bucharest area) focusses on industrial and urban emissions of NO_x, as well as assumptions made on a priori data in the retrieval of the S-5p NO_2 level-2 product. Emphasis is given to the a-priori parameters aerosols and surface reflectance.
For this purpose, we have deployed similar instruments as was done during the AROMAT-2 (Merlaud et al 2020) and RAMOS campaigns consisting of an airborne as well as a ground-based component.
The airborne activities are designed to comply with characteristics of the central instrument, AirMAP, measuring NO_2 vertical column densities in the air column below the aircraft.
The main objective of this activity is to create a campaign data set applicable for studies of the uncertainties of satellite atmospheric trace gas products.
The results of the activity in Romania will contribute to the validation of the tropospheric NO_2 vertical column density retrieved from S-5p observations.

2.2.2 Comprehensive introduction of the context

This campaign deployment focuses on urban and industrial emissions of tropospheric reactive gases and aerosols in the Bucharest area (Romania).
The largest and capital city of Romania, Bucharest, is home to around two million people. It is a substantial source of NO_2, mostly from emissions from vehicles but also from a few power plants inside the Bucharest perimeter. The region experiences hot, sunny summers, which enhance the release of volatile organic compounds (VOCs) from both man-made and natural (vegetation) sources within the city.
With two consecutive AROMAT campaigns in September 2014 and August 2015, as well as the AROMAPEX campaign in 2016, this field study seeks to fully capitalize on the experience gained from these events. We have used the infrastructure created throughout the RAMOS project (2017–2023).

The Sentinel-5P satellite provides coverage of the Bucharest area at least once per day, excluding nighttime overpasses. Additionally, every five days, there are two daytime overpasses, albeit at the edge of the swath, providing limited pixel coverage for the region of interest. With the area of interest being larger than 20 x 20 km, there's ample coverage to sample multiple pixels and address the project objectives effectively.

Given these satellite overpass patterns, it's feasible to compare data from Sentinel-5P on a daily basis, but it's important to consider the timing of airborne measurements to coincide with these overpasses. Close overpasses occur with a periodicity of 5 or 10 days, with Bucharest being close to nadir during these passes. This information can help schedule airborne measurements strategically to maximize synergy between satellite and ground-based observations.

Overall, the setup and measurements planned for the Bucharest campaign aim to enhance our understanding of atmospheric conditions, particularly regarding aerosols and NO_2, and contribute to improving the accuracy and reliability of satellite-based measurements.

2.2.3 Description of timeline and instruments

During the campaign, ground-based measurements (PANDORA 2S, aerosol lidar, F-TIR, in-situ gases samplers, sun photometer) were performed. The airborne operations (BN-2A 27 platform) have been scheduled during clear-sky conditions. The sites layout can be seen in Figure 21. The research flights for the aerosol campaign have been conducted across the Bucharest metropolitan area, aiming to capture the city's plume comprehensively and encompass a broader surface area relative to the ground resolution of Sentinel-5P. Several points of interest have been delineated within this study area, facilitating strategic flight planning and execution. These points of interest are detailed in the accompanying table of Figure 21.

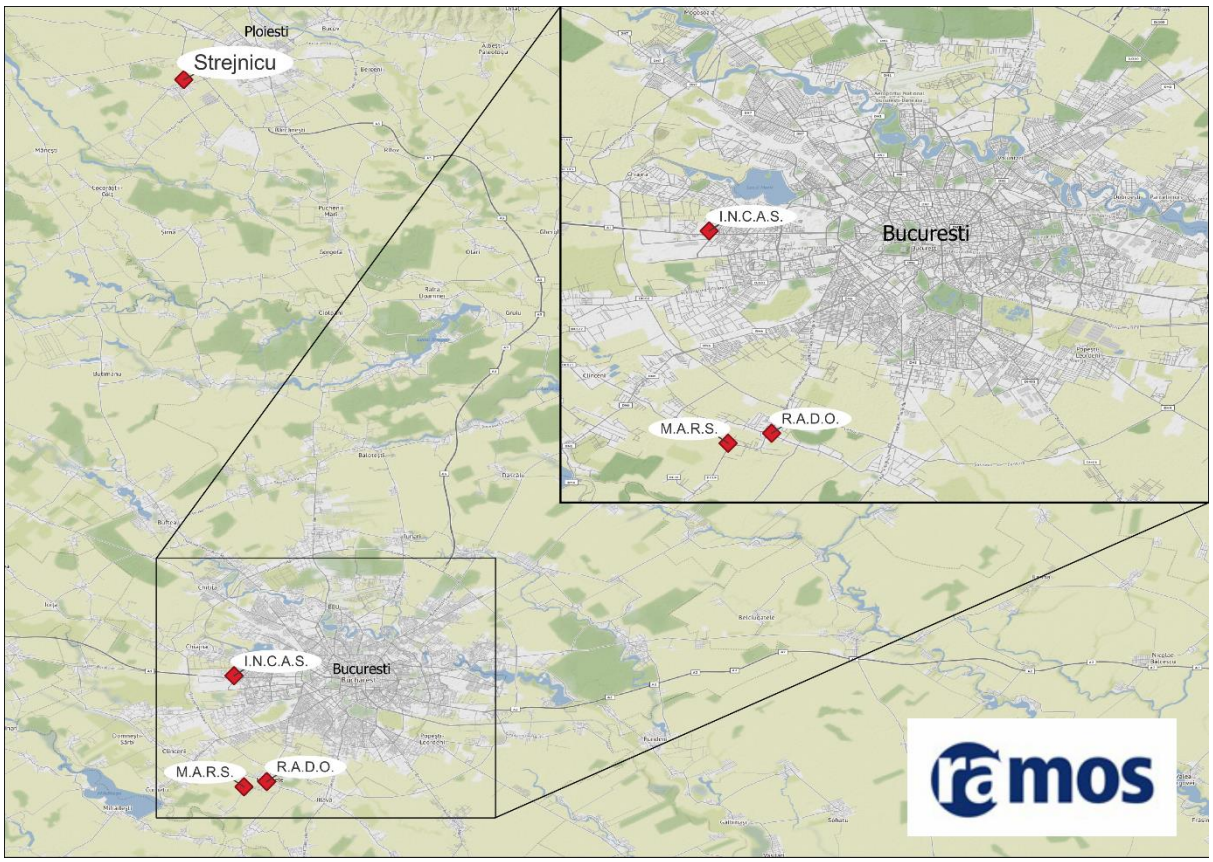

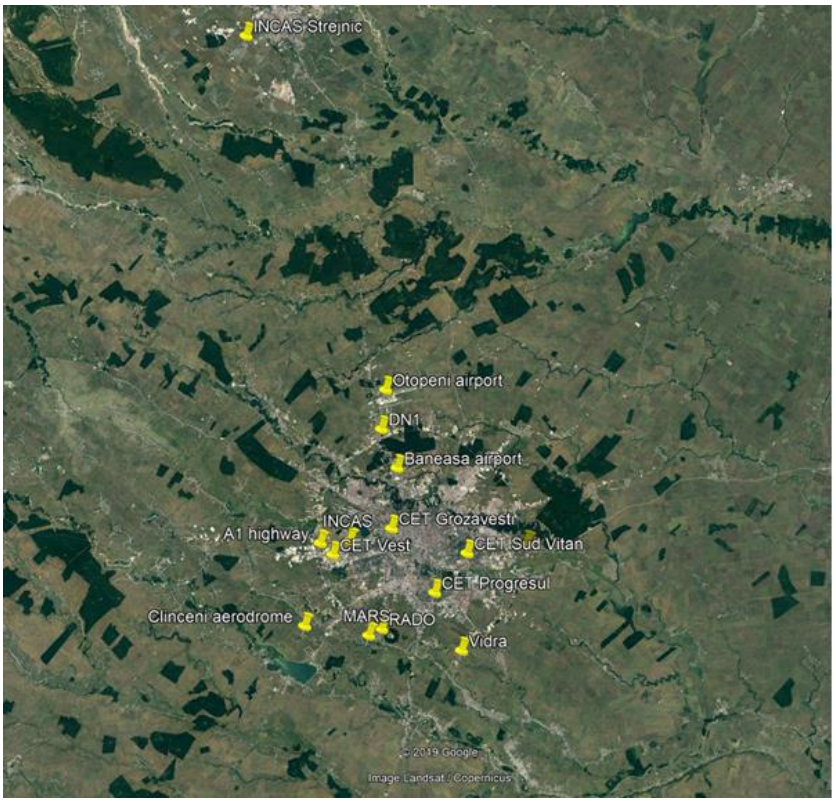

Point of interest	Latitude	Longitude
CET Vest	44°25'26.78"N	25°58'51.96"E
CET Sud Vitan	44°24'26.08"N	26° 9'23.68"E
CET Grozăvești	44°26'26.36"N	26° 3'45.92"E
CET Progresul	44°22'29.82"N	26° 6'24.26"E
A1 / Bucharest ring road	44°26'11.81"N	25°58'0.92"E
A2 / Bucharest ring road	44°24'28.29"N	26°14'9.42"E
Vidra landfill	44°19'2.08"N	26° 7'50.61"E
DN1/ Bucharest ring road	44°32'4.84"N	26° 4'6.50"E
RADO	44°20'53.55"N	26° 1'51.46"E
MARS	44°20'38.26"N	26° 0'46.06"E
INCAS	44°26'08.2"N	26°00'20.7"E
INCAS Strejnicu	44°55'16.24"N	25°57'55.77"E
Baneasa airport	44°29'46.37"N	26° 4'53.74"E
Otopeni airport	44°34'14.79"N	26° 4'53.54"E
Clinceni airfield	44°21'41.25"N	25°55'51.54"E

Figure 21 a) upper graph: Sites layout for QA4EO campaign (same as during RAMOS) b) lower graph: Points of interest for the Bucharest campaign

Timeline of the measurements performed is detailed in Table 7. Green: Nominal operation, Yellow, red: no data; Blue: two S5p overpasses.

Table 7 Overview of the ground based and airborne measurements performed during the QA4EO campaign in Romania

Ground based

no.	date	HORIBA	FTIR	PANDORA	LIDAR	sunphotometer	S5p
1	8/30/2022						
2	9/26/2022						
3	9/30/2022						
4	11/2/2022						
5	9/22/2023						
6	9/25/2023						
7	9/26/2023						
8	9/27/2023						
9	9/28/2023						
10	9/29/2023						

Airborne

no.	date	SWING+	Picarro G2401-m	Picarro G2107	Envea AS32M	APS	Nephelometer	IMU
1	08/30/2022							
2	09/26/2022							
3	09/30/2022							
4	11/02/2022							
5	09/22/2023							
6	09/25/2023							
7	09/26/2023							
8	09/27/2023							
9	09/28/2023							
10	09/29/2023							

2.2.3.1 *Fixed ground-based measurements*

Magurele Centre for Atmosphere and Radiation Studies (**MARS**) is a state-of-the-art infrastructure located in south-east Romania, hosting and operating a wide variety of instruments and laboratories for atmospheric research. MARS is a ground-based platform established in 2020 and located 8 km southwest of Bucharest in a pre-urban environment, but close to the rig-road of the capital of Romania (Figure 46,Figure 22). MARS it is a regional station WMO-GAW station, inheriting some of the instrumentation from the initial site RADO (Romanian Atmospheric 3D Observatory) (Nicolae D. et al., 2010) and it is close to RADO (about 2 km).

Figure 22 Aerial view of the MARS site, in Magurele

PANDORA 2S

The instrument is installed in Magurele, RADO site, and it measured continuously. It is part of PANDONIA Global Network PGN. The data can be visualised and are available only almost in real time: http://blickv.pandonia-global-network.org/; site Bucharest instrument #111. Data can be downloaded from: http://data.pandonia-global-network.org/Bucharest/.

The Pandora – 2S system (Figure 23) is capable of measuring the O_3 and NO_2 vertical column concentrations in Dobson Units (1 DU ≈ 2.7×10^{16} molecules cm^{-2}). The system has two spectrometers, first ranging from 290 nm to 500 nm with a 0.6 nm resolution and the second one with a range from 400 nm to 900 nm with a resolution of 1 nm. With a field of view of 1.5^0 , an elevation range from -10^0 to $+90^0$ and azimuth range of 360^0, the system is capable of pointing anywhere in the sky in order to perform direct sun, zenith sky, principal plane, or almucantar observations. Complimentary control software allows automated measurements and virtual monitoring and data transfer over the internet.

Figure 23 Pandora - 2S left side, near the sunphotometer -right side of the picture on the rooftop of RADO in Magurele

Data products: The output parameters are the concentrations (in Dobson units) of different trace gases, like O_3, NO_2, O_2O_2, SO_2, CH_4, etc. but the products validated for this system are only the NO_2 and the O_3 concentrations. The measurements are using the procedures implemented by PGN and the data products are retrieved using the standard PGN algorithms.

Known issues

Limitations:

Pandora – 2S observation cannot be usable in the presence of clouds, because of their high albedo. Uncertainties during cloudy sky and precipitation are large.

Calibration and quality assurance:

Regularly sun calibrations are made automatically during Pandora – 2S operation. Also, manual correction for the sun searches is made at a frequency determined by the principal investigator of the system.

Uncertainties:

Main uncertainties of the gas concentrations come from the temperature – dependent cross sections of the measured species (A.M. Bass and R.J. Paur, 1985, Burrows, et.al., 1999), from the Ring spectrum fit or from applying different corrections (dark, non-linearity, latency, temperature, stray light).

Fourier transform infrared spectrometer (FTIR)

The Bruker EM27/SUN is a robust and portable FTIR spectrometer, which has been developed by KIT in collaboration with Bruker Optics GmbH (Gisi et al., 2012; Hase et al., 2016). The EM27/SUN FTIR spectrometer has a solar tracker directly attached to it (which

uses a camera-controlled feedback for optimally aligning the spectrometer's line-of-sight with the solar position in the sky, a concept also developed by KIT (Gisi et al. 2011) for collecting solar spectra in the near infrared spectral range with 0.5 cm^{-1} spectral resolution (1.8 cm maximum optical path difference). Column-averaged abundances of CO_2, CH_4, and CO can be deduced from these observations with excellent precision and accuracy. The instrument is installed in Magurele, MARS site, and it measured on days with clear sky conditions.
The EM27/SUN is operated in accordance with COCCON (COllaborative Carbon Column Observing Network) requirements (Frey 130 et al., 2019; Alberti et al., 2022). This guarantees strict common methods for ensuring the quality of measurements (evaluation of the optical alignment and instrumental line shape), proper calibration of all COCCON spectrometers with respect to the TCCON site Karlsruhe and the COCCON reference EM27/SUN spectrometer operated permanently at KIT, and adherence to the COCCON data analysis scheme ensures the generation of precise and accurate data products.

Figure 24 EM27/SUN spectrometer taking measurements at MARS, in Magurele

Measurement principle: a compact system with a solar cam tracker, with two mirrors, rotating automatically to follow the sun position and a spectrometer, used to analyse solar radiation. It requires clear sky condition for optimal operation, with no clouds between the optical path from FTIR and sun.
Known issues: it cannot operate under high humidity conditions or precipitation.
Species measured: greenhouse gases.
Parameters delivered: column concentrations of CO_2, CH_4, CO; mixing ratio volume

Sunphotometer
The AERONET-integrated Cimel CE318 radiometer is utilized for both direct solar and diffuse sky observations in Magurele, Romania (Figure 23). For each direct solar/lunar measurement, a four-quadrant sensor mounted in the radiometer's head is used, together with a two-axis robot to automatically orient toward the sun. With a field of view of around 1.3 to 140 degrees, solar/lunar and sky measurements are often obtained every 15 minutes or at specified air mass intervals (Holben et al., 1998; Torres et al., 2013). Nine narrow band-pass filters with silicon and indium gallium arsenide detectors enable the

recording of wavelengths of 340, 380, 440, 500, 675, 870, 940, 1020, and 1640 nm. Full-width-at-half-maximum (FWHM) measurements of the bandwidth show that it spans from 2-4 nm (340-380 nm) in the ultraviolet to 10 nm. AOD, with its spectral variations, can be calculated from the direct solar/lunar measurements, and the aerosol's microphysical properties can be retrieved from multi-angular observations using operational inversion algorithms (Holben et al., 1998; Giles et al., 2019; Dubovik and King, 2000)
The data available now is the level 1.5 and 2.0, version 3 AOD products from the AERONET database, which provides cloud screened and quality-controlled AOD data.
Data products: AOD
The data can be accessed via the AERONET website:
https://aeronet.gsfc.nasa.gov/cgi-bin/data_display_aod_v3?site=Magurele_Inoe&nachal=2&level=1&place_code=10

In-situ gas monitors
The monitors are permanently installed in INOE's van and measured in Magurele, at MARS site (as shown below in **Figure 25**) October 2022-October 2023 and on August 30, 2022 at INCAS site in Bucharest (see Figure 21 for geographical locations).

Figure 25 Van with HORIBA monitors measuring during QA4EO campaign at MARS site in Magurele

Measurement principle: In situ gas analysers mounted inside the mobile laboratory monitor the atmospheric concentration several gases. Output values are instantaneous, integrated or averaged data. Standard deviation, instrument's linearity and span drifts are the errors of the instruments.
Known issues: Periodic zero/span calibrations to ensure the quality of the data. Different respond times for the different monitors: CO monitor: 50s, SO_2 monitor 120s, the NO_x monitor: 90s, THC monitor: 60s, and for O_3 monitor is 75s.
Species measured: concentration of in situ gases.
Parameters delivered: in situ concentrations NO_x (0-1ppm), SO_2 (0-0.5ppm), O_3 (0-1ppm), CH_4, NMHC and THC (0-50ppmC), CO (0-100ppm), CO_2 (0-100ppm). The output results are averaged, integration values and rolling average concentration with an integrating time of 3 or 30 minutes.

Multiwavelength Raman lidar (RALI)

The instrument is installed in Magurele, MARS site, and it measured one hour (or more) before and one hour (or more) after S5P overpass times.

Figure 26 RALI measuring during QA4EO campaign

Measurement principle: A multiwavelength Raman with laser emission wavelengths at 1064 nm, 532 nm, and 355 nm and the detection channels at 1064, 532 cross, 532 parallel, 355 nm (elastic wavelengths), and 607, 387 and 408 nm (Raman channels, operable night-time). The optimal dynamic range cover 0.8-15 km depending on atmosphere transmission, with a 3.75 m spatial resolution.

Known issues: Lidar measurements are not usable in the presence of clouds with altitudes lower than 4km. Fog and precipitation is also a major constrain for lidar measurements. During these periods, lidar measurements cannot be performed.

- the overlap of the lidar is above 800m; layers near to the ground cannot be quantitatively assessed;

Calibration and quality assurance: The multi-wavelength Raman depolarization Lidar is part of ACTRIS and complies to all quality assurance procedures available at the network level. During the last years, a considerable amount of effort was dedicated to assure the quality of the lidar products within CARS- Centre for Aerosol Remote Sensing.

Uncertainties: The uncertainties related to the backscatter profiles are mainly the result of the assumptions required to perform the Klett inversions (especially during daytime) (Kovalev and Eichinger, 2004).

According to (Freudenthaler et al., 2009), the backscatter coefficient is derived from the total signal using Fernald-Klett inversion, for which a calibration value at a reference range is needed. The range dependent lidar ratio is also needed for this inversion. E.g., for the daytime measurements performed using the RALI lidar system we used a 20% uncertainty for the calibration value and 10 sr for the lidar ratio (which was usually considered to be 55 sr if no additional aerosol type data is assumed). Although the

statistical noise is usually small compared with the systematic, the error introduced by the noise can add up during daytime measurements, when the background light is high. For data provided during the QA4EO campaign, the uncertainties related to these errors are added to the total systematic error.
Species measured: Profiles of the aerosol optical properties: backscatter coefficient, the extinction coefficient (during night time), water vapor mixing ratio (for 407 nm), and particle depolarization ratio (for 532 nm).
Parameters delivered: 1-h averaged backscatter vertical profiles at 355, 532nm and 1064nm, 1-h averaged vertical profiles particle depolarization ratio (for 532 nm).

2.2.3.2 *Airborne measurements*

Table 8 shows the instruments that participated in the airborne campaign of the Bucharest activity.

Table 8. Overview of the airborne campaign instruments and respective measured variables/species

Instrument	Measured variables	Uncertainty
SWING+	NO_2 (SO_2, HCHO) column	1.7 * 10^{15} molecules/cm^2
Picarro G2401-m	CO, CO_2, CH_4, H_2O	CO: <15ppb/1.5ppb CO2: <50ppb/20ppb CH4: <1ppb/0.5ppb H2O: <30ppm/5ppm
Picarro G2107	HCHO, H_2O	100 ppb/15 ppb
Envea AS32M	NO_2 (in-situ)	Detection limit (2 δ); 0.1 ppb
Aerodynamic Particle Sizer	Aerosol concentration	0.02 µm at 1.0 µm, 0.03 µm at 10 µm
Nephelometer	Total and backscatter signals of aerosols at three wavelengths: 450 nm (blue), 550 nm (green) and 700 nm (red)	
IMU	Aircraft position, velocity and attitude	

2.2.3.3 *Britten-Norman BN2A-27 Islander*

All instruments presented are installed onboard the Britten-Norman 2 Islander (BN2A), operated by INCAS (**Figure 27**).

The INCAS Britten Norman Islander BN2 B-27 aircraft (**Figure 27**), registered YR-BNR, has a propulsion of 2 piston engine, model Lycoming O-540-E4C5, that allows a climb rate of 295 m/min with a cruise speed of 257 km/h and a maximum speed of 273 km/h. The range during flight is of 1400 km. It has a length of 10.86 m, height of 4.18 m and wingspan of 14.94 m. During research flights the BN2 aircraft could reach a minimum altitude of 300 m and a maximum altitude of 4024 m. The maximum take-off weight is of 2994 kg (where 1667 kg is the empty weight), with a maximum scientific payload of 200 kg).

Figure 27. Britten-Norman 2 Islander (BN2A), operated by INCAS

2.2.3.1 *SWING+*

The SWING+ (**Figure 28**) payload is a compact DOAS whiskbroom imaging system developed at BIRA specifically designed to be operated onboard the BN2A-27 and is based on an AVANTES compact ultra-violet visible spectrometer (75 mm focal length, 50 microns slit, 1200l/mm) and a scanner to achieve whiskbroom imaging of the trace gases fields (NO_2 and SO_2). Including the housing and the electronics (based on a PC-104 and an Arduino), the weight, size, and power consumption of the SWING payload are respectively 3800 g, 45x19x15cm, and 25 W.

Figure 28. The SWING+ instrument

Measurement principle: Atmospheric composition imager based on the Differential Optical Absorption Spectroscopy (DOAS) technique. It relies on an Avantes UV-Vis spectrometer to record scattered light from the nadir direction.
Known issues: The performance of the spectrometer in the UV range is not suited for UV absorbing trace gases.

Uncertainties: The total error on the vertical column originates from (i) error on the DSCDs (ii) error on the AMFs and (iii) error on the reference column. At the time of writing the DAR, the first one is well characterized and respectively accounts for $2e^{15}$ molec/cm^2 and 1.5e16 molec/cm^2 of the NO_2 and SO_2 DSCDs. This corresponds for the typical NO_2 and SO_2 columns inside the plume to signal-to-noise ratios of respectively 40 and 20.
Species measured: Column densities of NO_2.
Parameters delivered: NO_2 vertical column density (VCD).
Data products: SWING records spectra of the backscattered radiation on the ground or in the atmosphere below the aircraft (Level 0). These spectra are analyzed with the DOAS method (Platt and Stutz) to retrieve both the NO2 and SO2 differential slant columns densities (DSCDs). This is done for the BIRA instrument using the QDOAS software (Danckaert et al., 2014). These DSCDs are the integrated concentration along the optical path, with respect to the same quantity in a reference spectrum (Level 1). These slant columns are first georeferenced with the IMU and GPS data recorded onboard the Cessna, and then converted to vertical columns (concentration integrated vertically) with air mass factors (AMFs) which are calculated with a radiative transfer model such as Lidort (Spurr, 2006). The AMFs accounts for the effective light path of a measurement, which depend on the geometry of each measurement (solar position, viewing angle) and the geophysical and atmospheric state (ground albedo, aerosol load, trace gases profiles). The georeferenced vertical columns are the level 2 products.

2.2.3.2 *Picarro G2401-m*

The Picarro gas analyzer, model G2401-m, provides simultaneous and continuous measurements of four most common greenhouse gases: water vapours, carbon monoxide, carbon dioxide and methane. Based on near–infrared cavity ring down spectroscopy technology, the analyzer has implemented a highly stable temperature and sample pressure control and a patented wavelength monitor which provides a good control of laser's wavelength, and thus very accurate measurements of targeted species. By tuning the laser with a known wavelength (generally the specific absorption wavelength of the targeted gas) for quantifying the spectral features of gas phase molecules in an optical cavity (including three mirrors of 99.9% reflexivity) and by using a sophisticated algorithm, the voltage decay in time is recorded and by employing improved electronics, the concentration profiles are displayed in real time. Therefore, sensitivities down to parts-per-billion (ppb) with negligible drift are reached.
Measurement principle: In situ gas analyzer based on the Cavity Ring-Down Spectroscopy (CRDS) principle.
Known issues: none.
Species measured: Concentrations of in situ greenhouse gases.
Parameters delivered: In situ concentration of CO (ppm), CO_2 (ppm), CH_4 (ppm), H_2O (%).

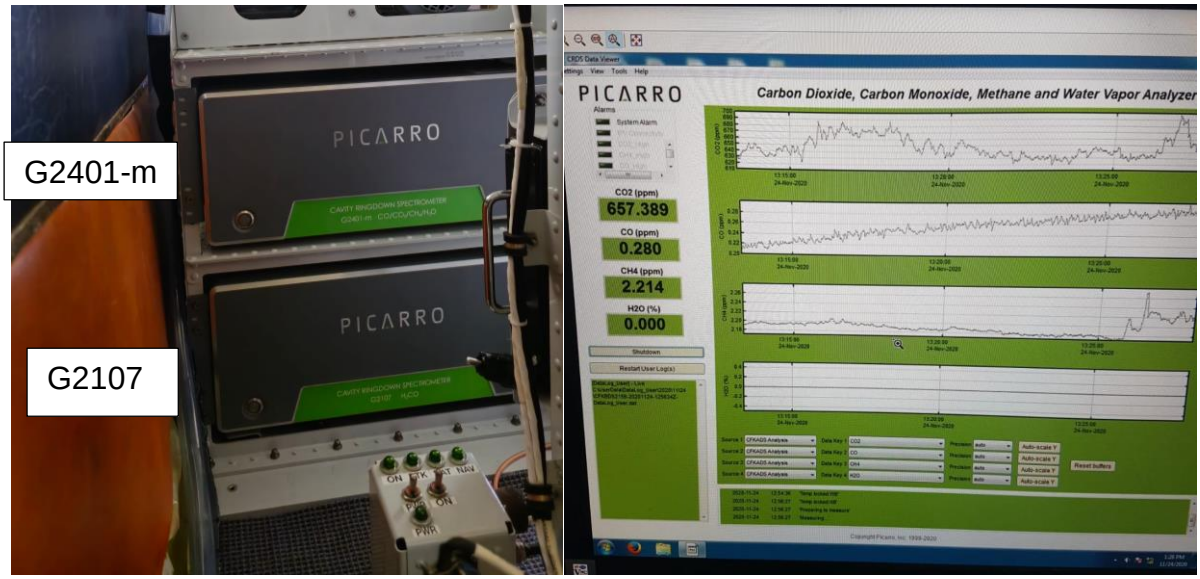

Figure 29. Real time monitoring of greenhouse gases using the Picarro analyser during a research flight

2.2.3.3 ***Picarro G2107***

The Picarro gas analyzer, model G2107, provides simultaneous and continuous measurements of water vapors and formaldehyde. Based on near–infrared cavity ring down spectroscopy technology, the analyzer has implemented a highly stable temperature and sample pressure control and a patented wavelength monitor which provides a good control of laser's wavelength, and thus very accurate measurements of targeted species. By tuning the laser with a known wavelength (generally the specific absorption wavelength of the targeted gas) for quantifying the spectral features of gas phase molecules in an optical cavity (including three mirrors of 99.9% reflexivity) and by using a sophisticated algorithm, the voltage decay in time is recorded and by employing improved electronics, the concentration profiles are displayed in real time. Therefore, sensitivities down to parts-per-billion (ppb) with negligible drift are reached.

Measurement principle: In situ gas analyzer based on the Cavity Ring-Down Spectroscopy (CRDS) principle.

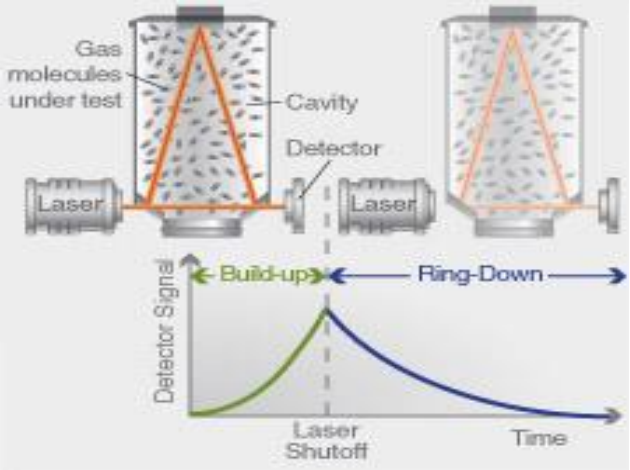

Figure 30. Picarro G2401-m onboard BN2A-27 (left) and the working principle (right)

Known issues: Sensitivity not high enough for in-flight H_2CO concentration measurements.
Species measured*:* Concentrations of in situ formaldehyde.
Parameters delivered: In situ concentration of H_2CO (ppm).

2.2.3.4 *Envea AS32M*

The Cavity Attenuated Phase Shift nitrogen dioxide (NO_2) type AS32M monitor manufactured by Envea S.A. deployed during the RAMOS campaign, operates as an optical absorption spectrometer (**Error! Reference source not found.**). It is capable of measuring direct NO2 with high precision and sensitivity using a blue light-emitting diode (LED) as a light source, a near-co focal arrangement of two high reflectivity (R~0.9999) mirrors in tandem with an enclosed sample cell of 26 centimetres in length and a vacuum phototube detector. Its efficiency is based on the fact that NO2 is a broadband absorber of light in the visible region of the spectrum. The wavelength and spectral band pass of the measurement are defined by the use of an interference filter centred at 450±10 nanometer. The monitor is enclosed within a standard 19 inch rack-mounted instrumentation box, weighs 12.5 kilogram, and uses 225 Watts of electrical power including the vacuum pump.
Measurement principle: In situ gas analyzer based on the Visible (450 nm) absorption measurement using the Cavity Attenuated Phase Shift (CAPS) technology.

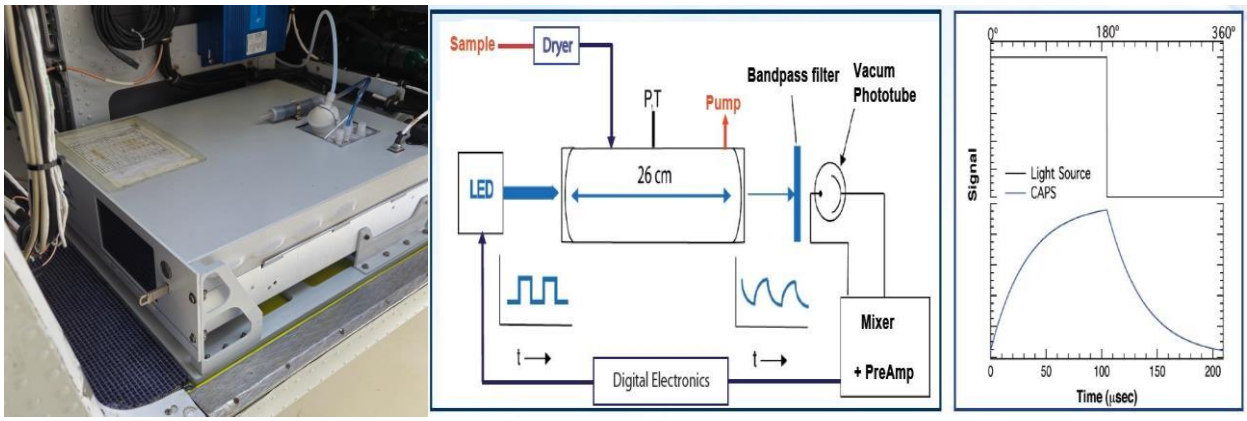

Figure 31. The Envea S.A. AS32M optical absorption NO_2 (CAPS) analyser as used during the QA4EO campaign (left) and the schematic and working principle (right)

***Known issues*:** may present unpredictable behaviour due to the zero-calibration that the instrument performs automatically.
Uncertainties: Apart from the optical temperature and pressure dependence for which the NO_2 signal is automatically corrected, a negligible water dependence remains of < 2 ppb / 20000 ppm H_2O. Also, a fractional additional temperature dependence remains of 0.1 % per °C which can be manually corrected for.
Species measured*:* Concentrations of in situ NO_2.
Parameters delivered: In situ concentration of NO_2 (0 – 1000 ppb).

2.2.3.5 *Aerodynamic Particle Sizer*

The Aerodynamic Particle Sizer provides the diameter of particles using time-of-flight technique on 0.5-20 µm particles, measured in an accelerating flow field with a single high speed timing processor. Simultaneously, a light scattering technique is used to detect particles between 0.37 and 20 µm. The Aerodynamic Particle Sizer Spectrometer can measure from 0.5 to 20 µm by aerodynamic sizing and 0.37 to 20 um by optical detection. The instrument was installed on the INCAS BN2 for airborne in-situ measurements around Bucharest.

Figure 32. Aerodynamic Particle Sizer (left) and its installation aboard INCAS BN2A-27

***Measurement principle**:* Time-of-flight of individual particles measured in an accelerating flow field with a single, high-speed timing processor, coincidence detection achieved using a double-crest optical system, particle size binning based on internally stored calibration curve

***Known issues**:* The airplane inlet could affect the measurements since large particles could be obstructed by the sampling. According to the preliminary analysis, the particle loss due to sampling was negligible.

Uncertainties:_The instrument undergoes periodic maintenance an inter-calibration procedures using ground based gravimetric measurements within RADO. The data quality is assured by continuous monitoring of internal parameters like the inlet flow, laser diode energy, inlet temperature and pressure.

***Species measured**:* Aerosol concentration.

Parameters delivered: PM_1, $PM_{2.5}$, PM_{10} number concentration, total concentration.
The output parameters are particle size raw counts from 52 channels, number, diameter, surface, volume and mass particle size calculated with the aid of its software program.

2.2.3.6 *Sentinel-5 Precursor (S5p) data*

The Sentinel-5 Precursor (S5p) is the first atmospheric Sentinel mission focusing on global observations of the atmospheric composition for air quality and climate monitoring. Launched on Oct. 13 2017 with a 7 years design lifetime. The TROPOspheric Monitoring Instrument (TROPOMI) is the payload of the S5P mission. It has global coverage within 1 day (swath of 2600 km) and ground-pixel spatial resolution of 7 x 3.5 km. Open data access is following the Copernicus Data Policy. We have used portal https://evdc.esa.int overpass predictor and Orbit Tool to generate the overpass times and plan the flights within Romania campaign (Table 9)

Table 9 Overview of S5p overpasses for latitude=44.426° and longitude=26.102° for all days of airborne measurements between the 30th of August 2022 and 29th of September 2023.

no.	date	S5p overpass times UTC		S5p second overpass time UTC	
1	8/30/2022	10:00:59	10:09:47	11:40:08	11:50:32
2	9/26/2022	11:33:45	11:44:19		
3	9/30/2022	10:19:05	10:28:53		
4	11/2/2022	10:00:46	10:09:33	11:39:54	11:50:19
5	9/22/2023	10:26:04	10:36:08	12:06:47	12:16:04
6	9/25/2023	11:09:26	11:20:17		
7	9/26/2023	10:50:44	11:01:27		
8	9/27/2023	10:32:15	10:42:32	12:13:23	12:22:14
9	9/28/2023	10:13:58	10:23:30	11:53:55	12:03:51
10	9/29/2023	11:34:44	11:45:17		

2.2.4 Report on the activities performed

This report contains information on flight objectives, flight patterns, instrument status and data acquisition for individual flights.

2.2.4.1 *The flight objectives and flight patterns*

For the Bucharest campaign, flights in the Bucharest metropolitan area were planned. For this, 10 flights were performed. Two flight strategies were used, detailed bellow.

All the planned flight hours have been spent with a total of **22:49** of flight time. The deployed aircraft was the Britten-Norman BN2A-27 Islander, operated by INCAS. The flights were performed between Summer 2022 – Autumn 2023.

A. Strategy 1 – remote sensing

The first flight strategy for the campaign over Bucharest involves overflying the metropolitan area at an altitude of 3000m, with consideration given to wind direction patterns for the execution of flight legs. The plan includes executing one loop in the east or south of the study area and a touch-and-go maneuver at Băneasa airport (LRBS). However, it's noted that the touch-and-go action at Băneasa airport may be subject to potential restrictions from air traffic control authorities.

Two potential flight patterns are presented in **Figure 33.** Flight strategy for E-W wind direction, including a touch and go at LRBS before executing the raster pattern (3000m) **Figure 33** and **Figure 34**, each corresponding to different wind directions (E-W and S-N). If there are no additional restrictions from authorities, it's proposed to widen the flight legs in the downwind direction. However, for S-N wind direction, widening the flight legs may not be approved due to daily aerial operations at LROP (Henri Coandă International Airport).

This strategy is designed to optimize the collection of airborne measurements while considering safety, regulatory compliance, and operational constraints. It's essential to liaise with air traffic control authorities to ensure coordination and adherence to any restrictions or guidelines during flight operations.

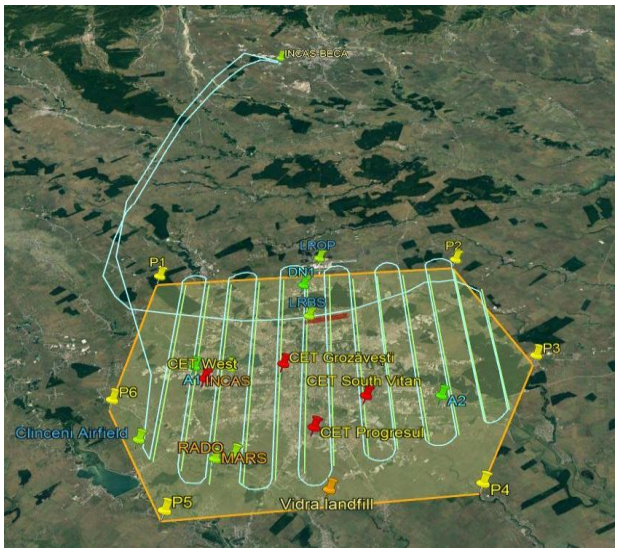

Figure 33. Flight strategy for E-W wind direction, including a touch and go at LRBS before executing the raster pattern (3000m)

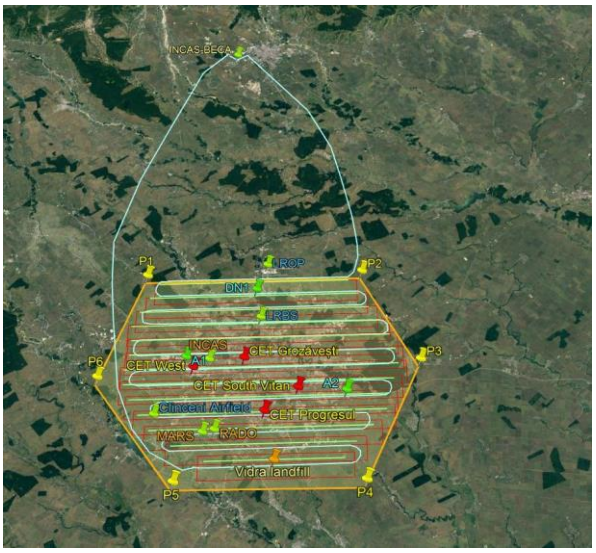

Figure 34. Flight strategy for S-N wind direction, including a loop in the south before executing the raster pattern (3000m)

B. *Strategy 2 – in situ*

The second flight strategy used involves conducting low-altitude flights above Bucharest, preferably at 500m, 1000m, or 1500m. These flights will utilize airborne in-situ instrumentation to measure aerosols and trace gases, with a focus on NO2, CH4, and H2CO. The flight plan includes around 10 flight legs at two altitude levels, with Figure 3 presenting the proposed flight plan for NE-W wind direction.

Before executing the raster pattern, two vertical profiles will be conducted for each exit of the A1 and A2 highways. These profiles will span from 300/500m up to 2000m altitude. This approach allows for a comprehensive sampling of the atmospheric composition at different altitudes and geographic locations within the Bucharest metropolitan area.

By conducting low-altitude flights with specialized instrumentation, this strategy aims to provide detailed insights into the distribution and concentration of pollutants in the lower atmosphere. It's crucial to ensure safety and compliance with airspace regulations during these low-altitude operations, especially given the proximity to populated areas and potential air traffic. Coordination with relevant authorities and stakeholders will be essential to facilitate smooth execution of the flight plan.

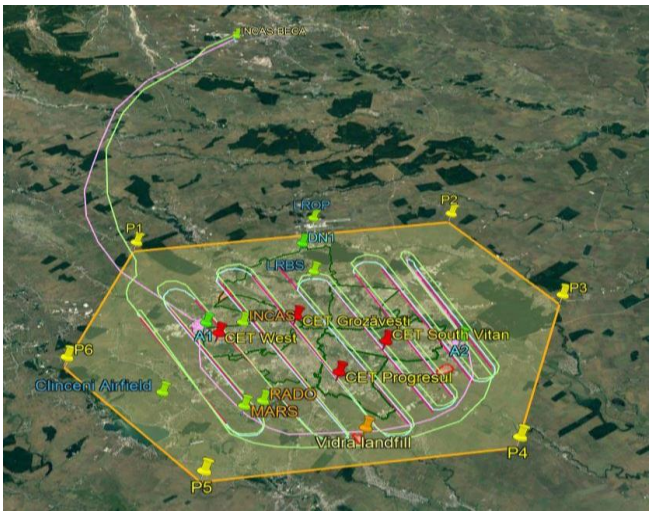

Figure 35. Flight strategy for NE-W wind direction, including 2 vertical soundings in the proximity of exits A1 and A2 highways; raster pattern for two altitude levels 500 m and 1000 m

2.2.4.2 *Individual flights*

The flight planning process for the Bucharest campaign is comprehensive and considers various factors to optimize data collection. Weather and cloud conditions above the target areas play a crucial role in determining flight routes, with particular attention given to wind direction. Flight tracks are chosen perpendicular to the wind direction to minimize any potential interference or distortion of the collected data.

Additionally, coordination with Sentinel-5P (S-5P) satellite overpasses is a key aspect of the planning process. When there are two satellite overpasses per day, priority is given to the overpass with a smaller Viewing Zenith Angle (VZA). This prioritization helps ensure optimal alignment between satellite measurements and airborne observations, enhancing the synergy between different data sources.

By integrating weather conditions, wind direction, and satellite overpass timings into the flight planning process, the campaign can maximize the quality and utility of the collected data for achieving its scientific objectives.

A statistic of all the flights is presented in **Table 10**.

Table 10. Overview of the individual flight reports

Flight reports	30 Aug 2022	26 Sept 2022	30 Sept 2022	2 Nov 2022	22 Sept 2023	25 Sept 2023	26 Sept 2023	27 Sept 2023	28 Sept 2023	29 Sept 2023
Take-off	8:55	9:53	9:02	9:00	9:25	10:34	9:53	9:39	9:47	9:55
First track above target area	9:05	10:35	10:07	9:40	9:55	10:57	10:15	10:04	10:11	10:24

End of final track	10:22	11:57	11:34	11:15	10:45	12:34	11:31	11:14	11:44	12:00
Landing	10:43	12:05	12:15	11:35	11:13	13:03	11:55	11:38	12:04	12:21
Duration total/above target area	1:48/ 1:17	2:12/ 1:22	3:13/ 1:27	2:35/ 1:35	1:48/ 0:50	2:29/ 1:37	2:02/ 1:16	1:59/ 1:10	2:17/ 1:33	2:26/ 1:36

2.2.4.3 *Issues and other notes regarding the activities performed*

During the Bucharest activities, there have been observed some issues with the data quality collected with the APS (Aerodynamic Particle Sizer) and CAPS-NO_2 instruments during specific flights, characterized by negative values in CAPS-NO_2 data, high noise levels, and low particle counts in APS data. To identify the root causes of these issues, several tests and checks will be conducted:

Dismantling and Ground Tests: Requests have been made to the technical department to dismantle the instruments from the research aircraft and relocate them to the Strejnicu base for ground tests. This will involve examining the instruments in a controlled environment to assess their functionality and performance.
Vibration Tests: Tests will be conducted using a vibrating table to assess if vibrations are a contributing factor to the data quality issues. If vibrations are found to be problematic, vibration sensors will be mounted in the instrument rack during the first test flight to monitor the level of vibrations and their potential impact on data quality.
Air Inlet Inspection: The air inlet connected to the instruments will be checked on the ground to ensure that the pipes are not blocked or obstructed. Blocked air inlets could affect the flow of air to the instruments, leading to inaccurate measurements.

These steps are essential for troubleshooting and identifying any potential issues with the instruments that may be affecting data quality. By conducting thorough tests and checks, the team can address the root causes and ensure reliable data collection in future flights.

2.2.4.4 *Synoptic Context for Bucharest*

For each of the day of the flights a forecast has been performed following the procedure described below. Every Monday, the forecast charts provided by ECMWF (HRES) (https://www.ecmwf.int/en/forecasts/charts) and GFS, ICON-EU, ARPEGE NWP models (https://www.wxcharts.com/) were analysed in order to identify the most suitable days (with clear sky and light winds) for carrying out the proper environmental measurements as required in QA4EO campaign. Based on the analysis of medium range synoptic charts and, vertical profiles and meteograms for Bucharest, a message of stand-by for a certain day or time interval was provided (via WhatsApp) in order to give time for flight preparations Prior the scheduled flight, a forecast update was made, that includes 00UTC NWP model runs and Eumetsat RGB satellite products (https://view.eumetsat.int/productviewer?v=default). Based on this last set of information focused on a time interval which includes also the TROPOMI overpass, the final decision (take-off/no take-off) was applied.

The subsequent data analyses which involve data acquired during the flight were performed considering the meteorological context using ERA5 Reanalysis - hourly data on single and pressure levels (Hersbach et al., 2020). Schematic overviews of the representative synoptic charts and satellite images for the days (and time interval) when flights over Bucharest were scheduled during QA4EO implementation are available for all days

A sample of the synoptic charts one day of the flights within QA4EO (25.09.2023):

25.09.2023 (11UTC) was characterised by High pressure regime over the lower levels with an upper level cut-off low centred over the eastern Mediterranean basin, cirrocumulus clouds over Bucharest (at approx. 10-12 km altitude), good conditions for lower level measurements.

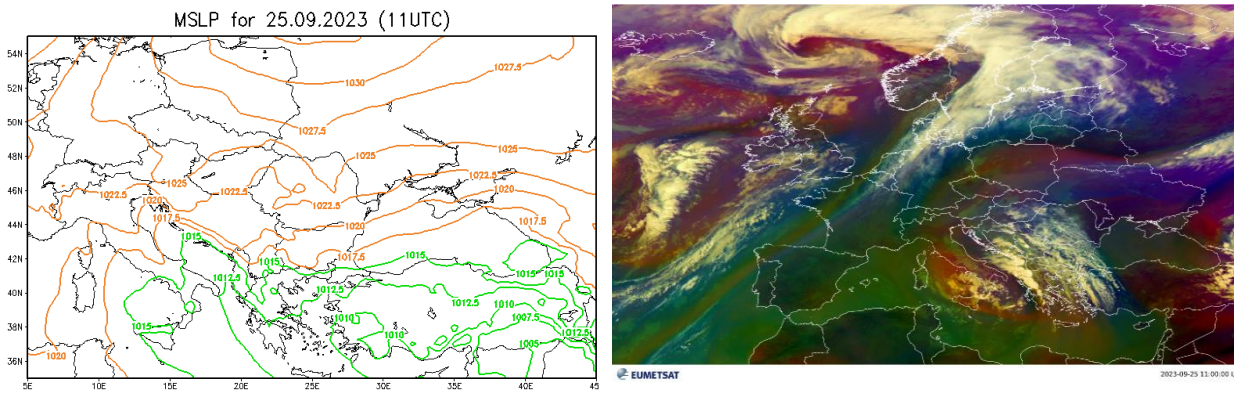

Figure 36 (left) Mean Sea Level Pressure derived ERA5 Reanalysis, (right) Eumetsat Airmass RGB statellite image for 25.09.2023 (11UTC)

2.2.4.5 *Ground based instruments*

Report on the stationary measurement activities

The time line of the stationary measurements is summarized in Table 7 in Section 2.1.3. PANDORA, FTIR, sunphotometer usually performed measurements from shortly after sunrise until shortly before sunset only during clouds free atmosphere. HORIBA gas analyzers measured continuously while lidar measurements usually started an hour before the S5p overpasses and continued one more hour.

2.2.5 Data analysis and data format of ground-based measurements

Products uncertainties are available in the table below:

Instrument	Measured Species	Accuracy / errors / precision
Mobile laboratory		
	backscatter coef @ 355	Accuracy ~15% @ 12km (daytime)

Multiwavelength Raman lidar		Accuracy ~10% @ 3km (daytime)
Bruker EM27/SUN FTIR	column concentrations of O_2	N/A
	column concentrations of xCO_2	Precision > 99.04 %
	column concentrations of xCH_4	Precision > 98.82 %
	column concentrations of H_2O	Precision > 97.98 %
Pandora 2S	column density of NO_2	RMS < 0.05 DU
	column density of O_3	RMS < 5 DU
Gas analysers	in situ concentrations NO_x	0.5 ppb for values < 0.2 ppm 0.5% for values > 0.2 ppm
	in situ concentrations SO_2	0.5 ppb for values < 0.2 ppm 0.5% for values > 0.2 ppm
	in situ concentrations O_3	0.5 ppb for values < 0.2 ppm 0.5% for values > 0.2 ppm
	in situ concentrations THC	0.05 ppmC for values < 5 ppmC 0.5% for values > 5 ppmC
	in situ concentrations CO	0.05 ppm for values < 10 ppm 0.5% for values > 10 ppm

2.2.5.1 ***Lidar***

One of the most important global archives for atmospheric aerosol profile data is the ACTRIS/EARLINET database (https://data.earlinet.org), that stores data from the regional GAW network EARLINET.
The multiwavelength Raman Lidar- RALI is part of EARLINET since 2005, and have been also going through the labelling process of ACTRIS, being one of the main instruments of INOE in CARS-Central for Aerosol Remote Sensing (https://www.actris.eu/topical-centre/cars), AHL-INOE.
ACTRIS/EARLINET developed standard operating procedures, terminology, and vocabulary for aerosol lidar data and products in cooperation with the other GALION - GAW regional networks. Standard formats and data products are defined in a Level structure by ACTRIS. Level 1 data are calibrated and quality assured data with minimum

level of quality control, while Level 2 data are approved and fully quality controlled ACTRIS data product or geophysical variable. Namely Level 1 optical passed all Technical quality controls, while Level 2 data passed both technical and advanced + if feasible multiproduct quality controls. The multi-product quality controls check that different backscatter profiles are consistent each other, lidar ratio and Angstrom exponent that result from different data files are consistent within 3 standard deviations with physically meaningful range of values.
Data are accessible through both human and machine to machine interface (through API system).

All Quality Assurance tests of the lidar hardware have been fulfilled. Data have been processed using SCC-Single Calculus Chain: https://docs.scc.imaa.cnr.it/en/latest/data_processing.html

The data is provided in NC-NetCDF format, CF compliant, ELDA- Earlinet Lidar Data Analyzer output. ELDA applies to the pre-processed signals, produced by the pre-processor module, the algorithms for the retrieval of aerosol optical parameters. The analysis can be done in a flexible way choosing from a set of possible pre-defined analysis procedures. ELDA implements retrieval of elastic aerosol backscatter profile, iterative algorithm. An automatic vertical-smoothing and time averaging technique selects the optimal smoothing level as a function of altitude on the base of different thresholds on product uncertainties fixed in the SCC database for each product. The final optical products are written in a NetCDF file with a structure according to the EARLINET rules.

Filenames follow also the rules implemented by EARLINET/ACTRIS:
<station_code>_<product_type_ID>_<wavelength>_<productID>_<starttime>_<stoptime>_<measurementID>_<SCC_module>_<SCC_version>.nc

where:

<station_code>	3 digits code INO- in our case
<product_type_ID>	numeric 3 digits (003 in our case)
<wavelength>	4 digits reporting the wavelength in nm (for example 0532)
<productID>	numeric 7 digits (0001803)
<starttime>	YYYYMMDDHHMM (for example 202102031832)
<stoptime>	YYYYMMDDHHMM (for example 202102031944)
<measurementID>	measurementID string (15 characters)
<SCC_module>	SCC module (hirelpp,cloudscreen,elpp,eldec,**elda**,elic)
<SCC_version>	SCC version (**v5.2.8**)

The field <product_type_ID> is codified as it follows:

Product_type_ID	Description
0	Raman Bacskcatter
1	Extinction only
2	Lidar Ration and Extinction
3	**Elastic Backscatter**
6	Linear Polarization Calibration
7	Raman Backscatter and Linear Depolarization Ratio
8	Elastic Backscatter and Linear Depolarization Ratio
9	High Resolution Pre-Processed data

Filename example:
ino_003_0355_0001803_202309251131_202309251159_20230925ino1104_elda_v5.2.8

All data is accompanied by data plots: quick looks files presented as time series of the Lidar backscattered profiles. The quick looks data is the temporal variation of aerosol layering at 532nm, providing information about the dynamics of aerosol layers in the troposphere. The maximum height of the data is given by the signal SNR. For RALI the height of the profiles can reach 12km.

2.2.5.2 *Pandora*

The data format is a text file having the following name and format:
Filename: ssNNNs1_LLL_L2tot_xx_ s1p1-7.txt
where:
- ss → system (eg. Pandora)
- NNN → system number (eg. In our case is111)
-S1
-Tot or tropo-
- LLLL → location name (eg. In our case is Bucharest)
- xxx →code for the type of gas (eg. For NO2 in rnv, out is the code for ozone)
- s1p1-7

The file contains a 23 lines header where are explained each and every column of the file.
For example, the file for total NO2 is named:
Pandora111s1_Bucharest_L2Tot_rnvs1p1-7.txt
Data integration – in the context of satellite validation: The products provided by the Pandora – 2S system are going to be compared with the similar products from the satellite data, the NO_2 and O_3 concentrations provided by S5P and the Ozone Monitoring Instrument, AURA mission.

2.2.5.3 *Gas monitors*

Filename:

A) av2-yyyymmddhhmm.xls (csv type)
yyyy - year
mm - month
dd - day
hh - hour
mm - minute
The 30 min averaged concentration file contains:
Time - date and time (UTC)
O_3 – min, mean, max, stddev concentration (ppb) ---
SO_2 - min, mean, max, stddev concentration (ppb) ---
NO - min, mean, max, stddev concentration (ppb) ---
NO_2 - min, mean, max, stddev concentration (ppb) ---
NOx - min, mean, max, stddev concentration (ppb) ---
CO – not provided
CH_4 - min, mean, max, stddev concentration (ppm) ---
NMHC - min, mean, max, stddev concentration (ppm) ---
THC - min, mean, max, stddev concentration (ppm) ---
B) av1- yyyymmddhhmm.xls (csv type)
yyyy - year
mm - month
dd - day
hh - hour
mm - minute
The 3 min concentration files:
Time - date and time (UTC)
O_3 – min, mean, max, stddev concentration (ppb) ---
SO_2 - min, mean, max, stddev concentration (ppb) ---
NO - min, mean, max, stddev concentration (ppb)
NO_2 - min, mean, max, stddev concentration (ppb)
NOx - min, mean, max, stddev concentration (ppb)
CO – not provided
CH_4 - min, mean, max, stddev concentration (ppm)
NMHC - min, mean, max, stddev concentration (ppm)
THC - min, mean, max, stddev concentration (ppm)

2.2.5.4 *FTIR*

Data Format: The raw data are collected on the computer operating the spectrometer. The data format is the proprietary data format used by the software OPUS, provided by the manufacturer Bruker for operating the spectrometer and for data collection. We are storing measured data, and performing regular backups on external hard disk drives. The OPUS data format contains all information (date + time, measurement settings, raw interferogram data) needed for the subsequent data processing.

The COCCON gas data processing and analysis tools are freely available at the COCCON website (https://www.imk-asf.kit.edu/english/COCCON.

Data of this campaign was submitted to COCCON. COCCON provides column-averaged trace gas abundances (more specifically: column-averaged dry air molar fractions) of water vapour, carbon dioxide, methane and carbon monoxide (carbon monoxide is available if a dual-channel spectrometer is operated). These abundances are derived from direct solar absorption spectra covering the near-infrared spectral range.
Data was submitted to EVDC and is also available at: https://www.imk-asf.kit.edu/english/3884.php.

2.2.6 Data analysis airborne measurements

2.2.6.1 *SWING+*

SWING records spectra of the backscattered radiation on the ground or in the atmosphere below the aircraft (Level 0). These spectra are analyzed with the DOAS method (Platt and Stutz) to retrieve both the NO_2 and SO_2 differential slant columns densities (DSCDs). This is done for the BIRA instrument using the QDOAS software (Danckaert et al., 2014). These DSCDs are the integrated concentration along the optical path, with respect to the same quantity in a reference spectrum (Level 1). These slant columns are first georeferenced with the IMU and GPS data recorded onboard the Cessna, and then converted to vertical columns (concentration integrated vertically) with air mass factors (AMFs) which are calculated with a radiative transfer model such as Lidort (Spurr, 2006). The AMFs accounts for the effective light path of a measurement, which depend on the geometry of each measurement (solar position, viewing angle) and the geophysical and atmospheric state (ground albedo, aerosol load, trace gases profiles). The georeferenced vertical columns are the level 2 products.

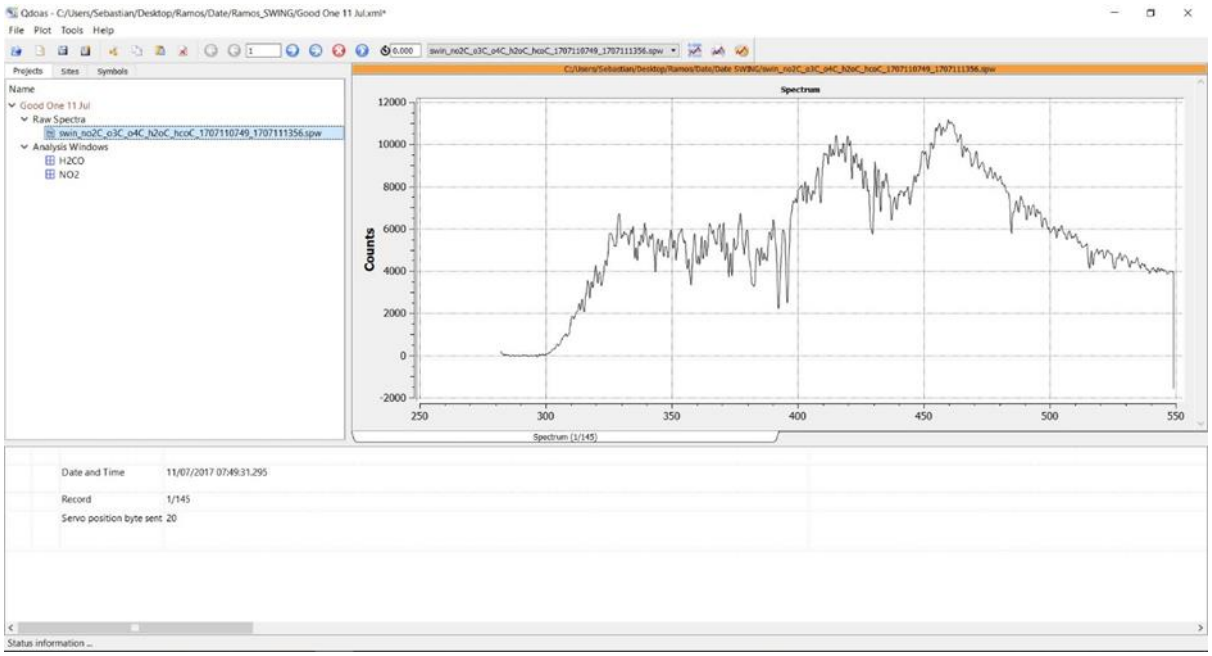

Figure 37. Example of recorded spectrum viewed in QDOAS

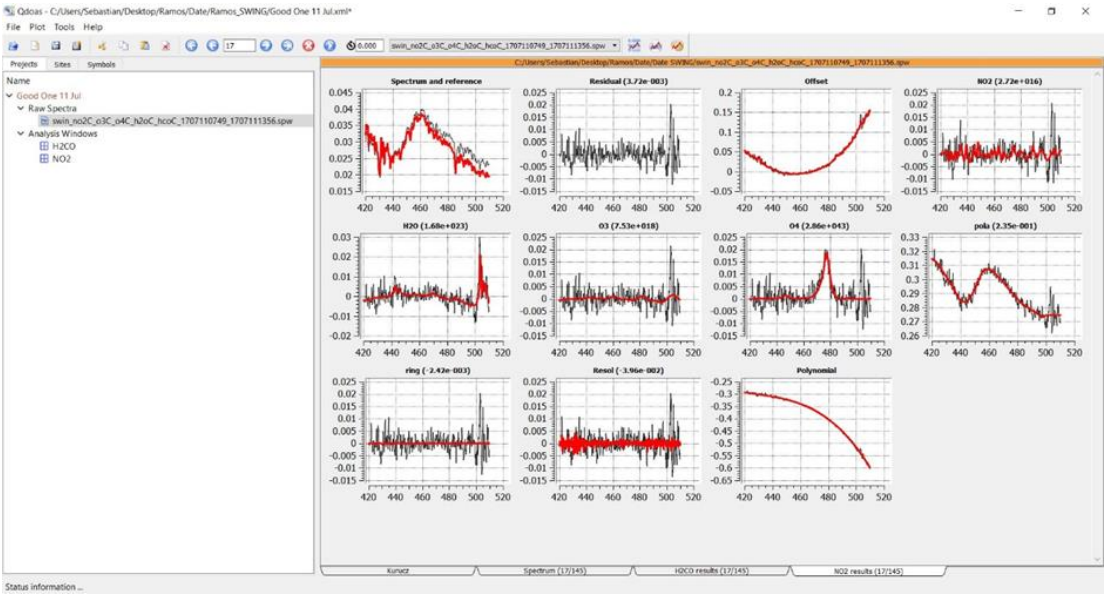

Figure 38. Example of results from the DOAS fit in QDOAS

2.2.6.2 *Aerodynamic Particle Sizer (APS)*

The APS processing procedure starts with calculating the number concentrations for PM1, PM2.5 and PM10. The data can be arranged in two formats when it is exported from the instrument: rows or columns. For the rows format, each new sample and its measured parameters are stored on a new row, while the opposite is valid for the columns format, where each new sample and its measured parameters are saved in a new column. For calculating PM1, PM2.5 and PM10 number concentrations, all the columns containing the measurements for each aerodynamic diameter up to 1, 2.5 and 10 µm are summed. Additionally, for the columns format, all the data are transposed. After these calculations, the data is georeferenced using data from the IMU unit. After the georeferencing is performed, all the data is graphically represented in time series format and in map format using MATLAB.

2.2.6.3 *Picarro (both)*

The first step in the processing procedure for the data provided by the Picarro analyzers is to average all the measurements in order to achieve a frequency of 1 measurement/second. Initially, the frequency of measurements is around 3Hz and in order to perform the georeferencing of the data the averaging procedure is needed. After the averaging, the georeferencing is done using the data provided by the IMU unit installed in the aircraft. The IMU has a 1Hz measurement frequency. After the georeferencing is performed, all the data is graphically represented in time series format and in map format using MATLAB.

2.2.6.4 *Envea AS32M*

The first step in the processing procedure for the data provided by the AS32M analyzer is to perform the georeferencing, which is done using the data provided by the IMU unit installed in the aircraft. The IMU has a 1Hz measurement frequency, same as the AS32M. After the georeferencing is performed, all the data is graphically represented in time series format and in map format using MATLAB.

2.2.6.5 *Nephelometer*

For data processing, 2 programs developed in Python are used. In the first program, the following steps are carried out:

- the data collected with the nephelometer is imported
- the data is scanned to be able to arrange them in columns
- Angstrom coefficients are calculated
- the time series of scattering, backscattering and Angstrom coefficients are graphical represented.

The second program is used to export data arranged in columns.

2.2.7 Data format of airborne measurements

2.2.7.1 *SWING+*

The raw data generated by the instrument is in .spw format and contains information about the recorded spectra. This file is analysed in QDOAS and the output is represented by an ASCII file that contains the results of the DOAS analysis. The columns of interest for further processing are Time (hh:mm:ss), Fractional tome, UAV servo sent position byte, NO2.RMS, NO2.SlCol(NO2), NO2SlErr(NO2). After the georeferencing, columns for the location of the aircraft are added and the approximated vertical column for NO2.

2.2.7.2 *Aerodynamic Particle Sizer (APS)*

filenames:
SSyymmddhhmm.pppp.PPPP
SS - station name
yy - year
mm - month
dd - day
hh - hour
mm - minute
pppp - data type: mass, volume, number
PPPP - data product: sdis - size distribution
The size distribution files contain:

- header with additional data
- columns of: date, time, size distribution [micro-g/m^3] for 0.523 0.542 0.583 0.626 0.673 0.723 0.777 0.835 0.898 0.965 1.037 1.114 1.197 1.286 1.382 1.486 1.596 1.715 1.843 1.981 2.129 2.288 2.458 2.642 2.839 3.051 3.278 3.523 3.786 4.068 4.371 4.698 5.048 5.425 5.829 6.264 6.732 7.234 7.774 8.354 8.977 9.647 10.370 11.140 11.970 12.860 13.820 14.860 15.960 17.150 18.430 19.810
- size distribution units [micro-m]

2.2.7.3 *Picarro G2401-m*

The data generated by this instrument is in various ASCII-format text output files. As it was mentioned before, the raw data, continuous read out from the analyzer, can be visualized in real time by using Graphical User Interface – GUI [RD-29]. This data is stored in C:\Userdata\DataLog_User \YYYY\MM\DD, where Y=year, M=month, D=day.
The output file is named:

CKFBDS##-yyyymmddhhmm-DataLog_User.dat

CKFBDS## - instrument serial number
yyyy – year
mm – month
dd – day
hh – hour
mm – minute

In this way, chronological evidence is maintained. Data files are created every 15 minutes and stored for 90 days before they are automatically deleted, with the possibility to modify the deletion frequency.

2.2.7.4 *Picarro G2107*

The data generated by this instrument is in various ASCII-format text output files. As it was mentioned before, the raw data, continuous read out from the analyzer, can be visualized in real time by using Graphical User Interface – GUI [RD-29]. This data is stored in C:\Userdata\DataLog_User \YYYY\MM\DD, where Y=year, M=month, D=day.
The output file is named:
LADS####-yyyymmddhhmmZ-DataLog_User.dat

LADS#### - instrument serial number
yyyy – year
mm – month
dd – day
hh – hour
mm – minute

In this way, chronological evidence is maintained. Data files are created every 15 minutes and stored for 90 days before they are automatically deleted, with the possibility to modify the deletion frequency.

2.2.7.5 *Envea AS32M*

Data files are generated presenting the data in the format of comma separated values containing all 17 parameters recorded, namely: date and time, NO2 concentration (ppb), analysers' internal T, T of optical chamber, T of analysed gas, raw NO2 signal, relative humidity (unused!), P inside of optical cavity, light intensity emitted by blue LED, optical loss of the cavity, gas permeation, auxiliary P and T (both unused!), light intensity received by the phototube, phase difference of received signal w.r.t. LED signal, reference voltage from analogue/digital converter, and analogue ground.

2.2.8 Main results achieved, including comparison with S5p data

2.2.8.1 *Ground based measurements*

Sunphotometer

Data visualization ("Quicklooks") has been available in almost real time on the AERONET site:
https://aeronet.gsfc.nasa.gov/cgi-bin/data_display_aod_v3?site=Magurele_Inoe&nachal=2&level=1&place_code=10 site

Looking at the daily averages AOD values at 550 nm (Figure 39) during 2023 we can conclude that during QA4EO campaign in 2023 the AOD values are within the annual averages charactering Magurele region. Sunphotometer measurements are taken in Magurele since 2015. Comparing each year's AOD during 22-29 of September (Figure 40) we can observe that during 2023 the values measured are close to the mean of previously measured.

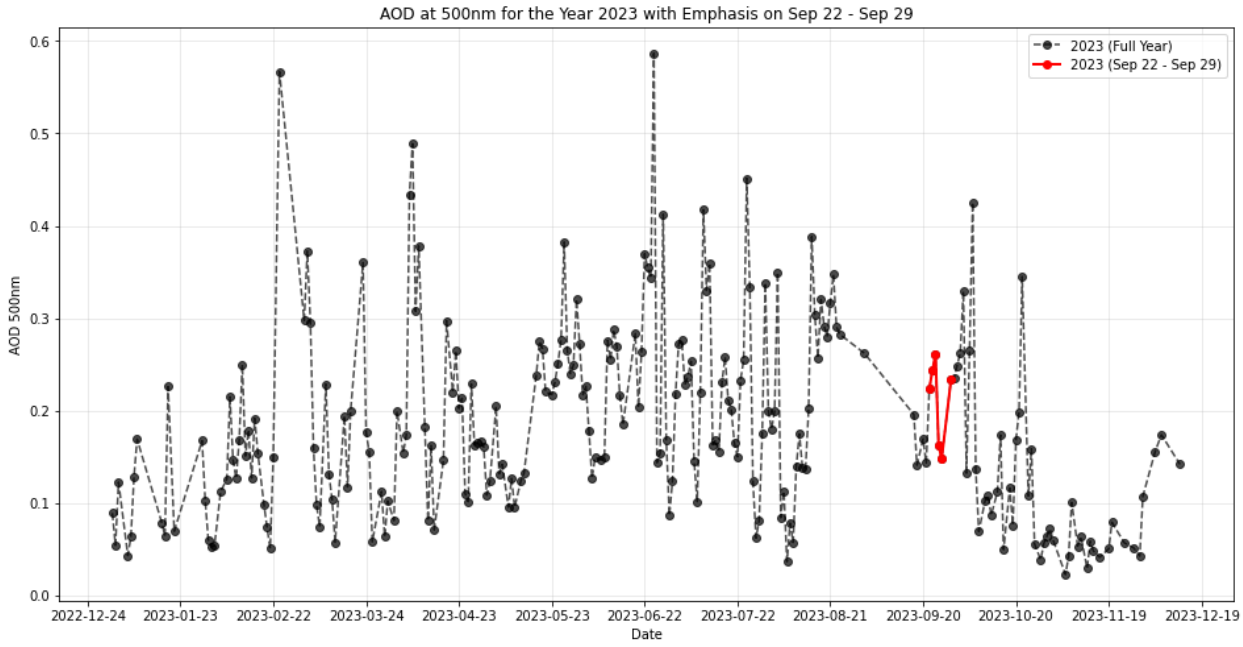

Figure 39 Daily averages of AOD at 550nm during 2023; in red values measured during QA4EO campaign days during September 22-29, 2023

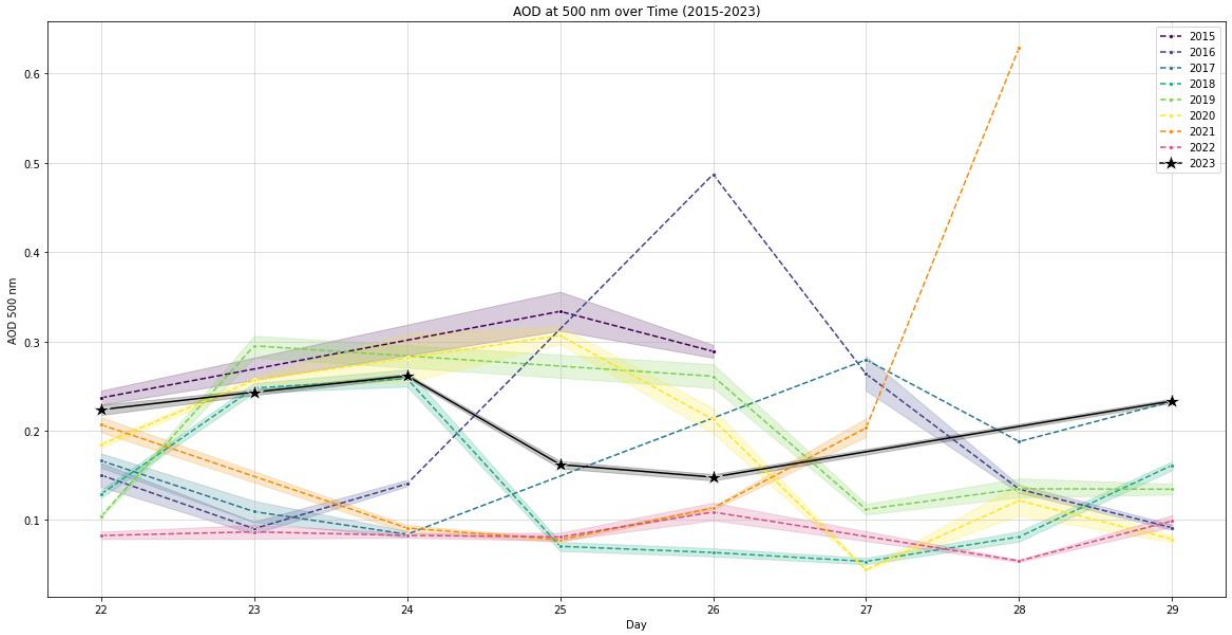

Figure 40 Daily Averaged AOD at 550nm measured in Magurele during 22-29 of September of each year during 2015-2023

Pandora

Data visualization (“Quicklooks”) has been available in almost real time on the PGN site: http://blickv.pandonia-global-network.org/; Bucharest site #111.
Data can be seen also in **Figure 41**.

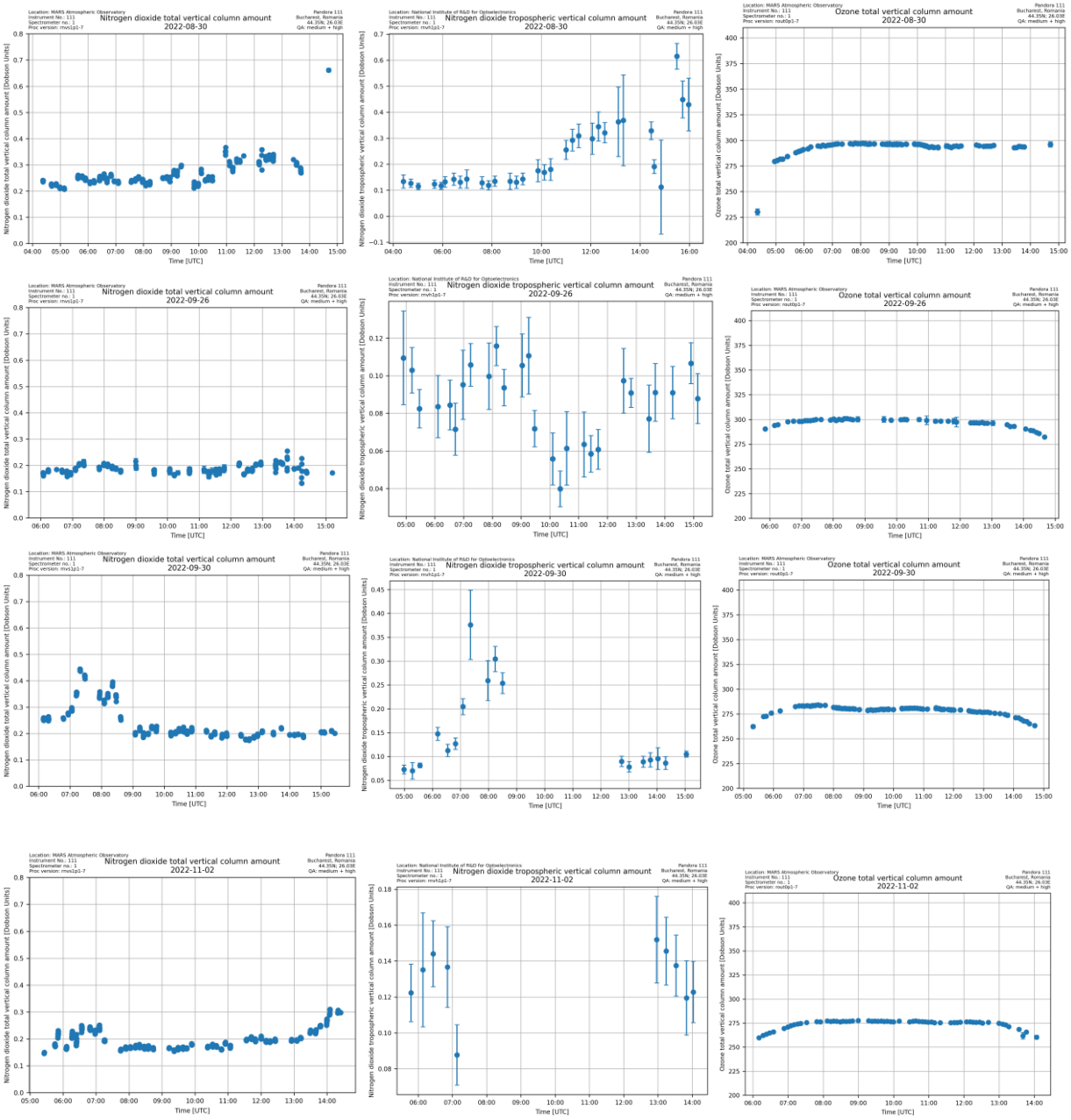

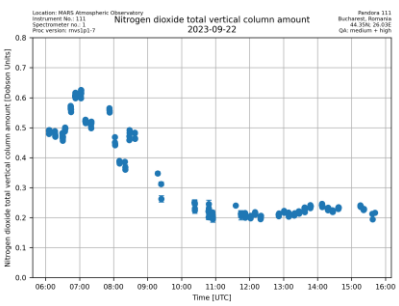
Nitrogen dioxide total vertical column amount
2023-09-22
Time [UTC]

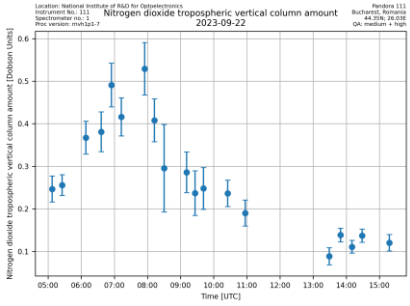
Nitrogen dioxide tropospheric vertical column amount
2023-09-22
Time [UTC]

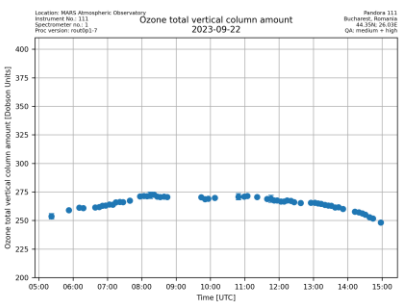
Ozone total vertical column amount
2023-09-22
Time [UTC]

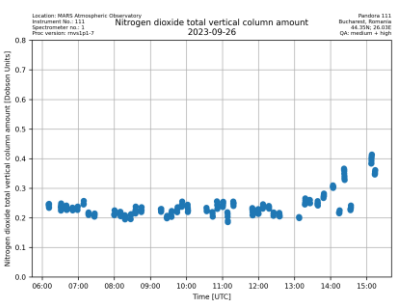
Nitrogen dioxide total vertical column amount
2023-09-26
Time [UTC]

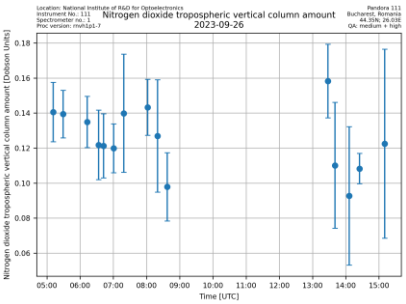
Nitrogen dioxide tropospheric vertical column amount
2023-09-26
Time [UTC]

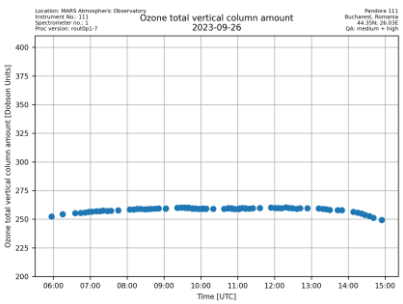
Ozone total vertical column amount
2023-09-26
Time [UTC]

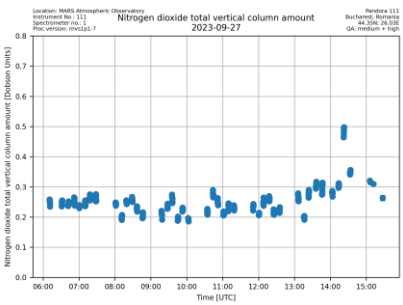
Nitrogen dioxide total vertical column amount
2023-09-27
Time [UTC]

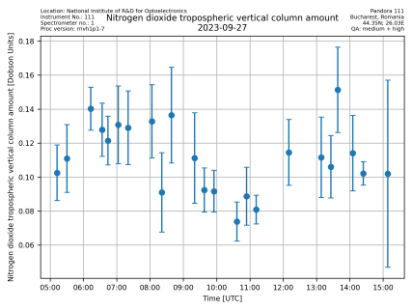
Nitrogen dioxide tropospheric vertical column amount
2023-09-27
Time [UTC]

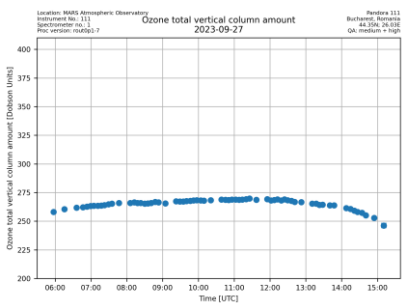
Ozone total vertical column amount
2023-09-27
Time [UTC]

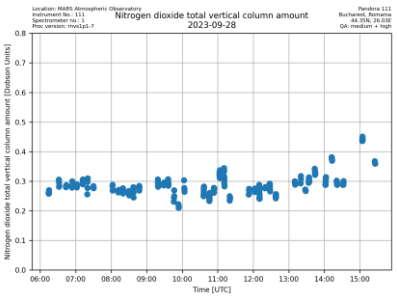
Nitrogen dioxide total vertical column amount
2023-09-28
Time [UTC]

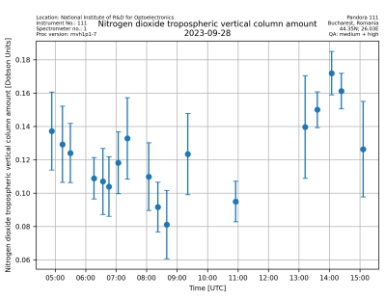
Nitrogen dioxide tropospheric vertical column amount
2023-09-28
Time [UTC]

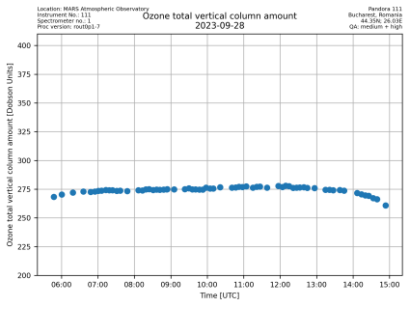
Ozone total vertical column amount
2023-09-28
Time [UTC]

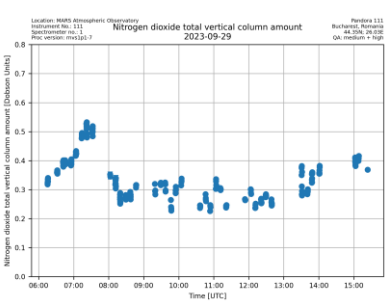
Nitrogen dioxide total vertical column amount
2023-09-29
Time [UTC]

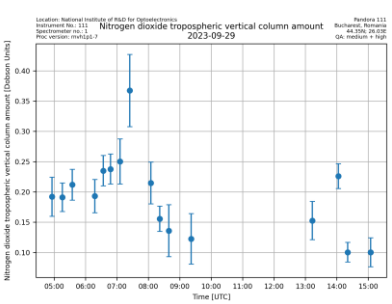
Nitrogen dioxide tropospheric vertical column amount
2023-09-29
Time [UTC]

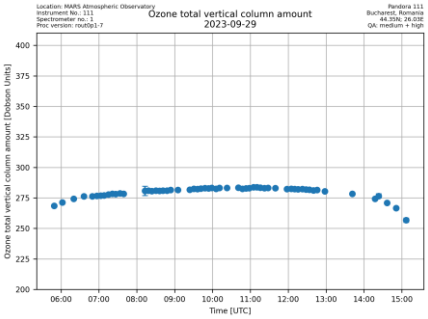
Ozone total vertical column amount
2023-09-29
Time [UTC]

Figure 41 Nitrogen dioxide total vertical column, Nitrogen dioxide tropospheric vertical column and Ozone total vertical column measured over Magurele during QA4EO by PANDORA 2S

FTIR

FTIR data measured in Magurele are available here: https://www.imk-asf.kit.edu/english/3884.php
Diurnal variation of column-averaged dry-air mole fractions of CO2, CO, CH4 and H2O measured over Magurele during QA4EO by FTIR is shown also below in Figure 42.

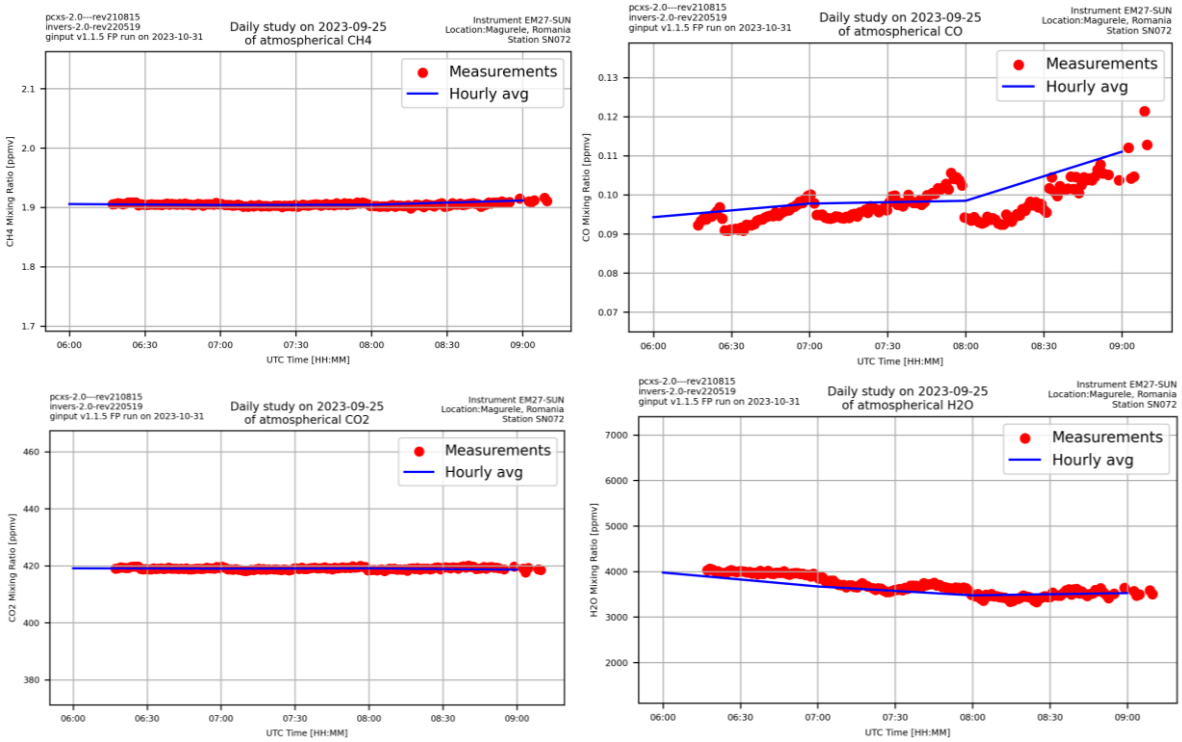

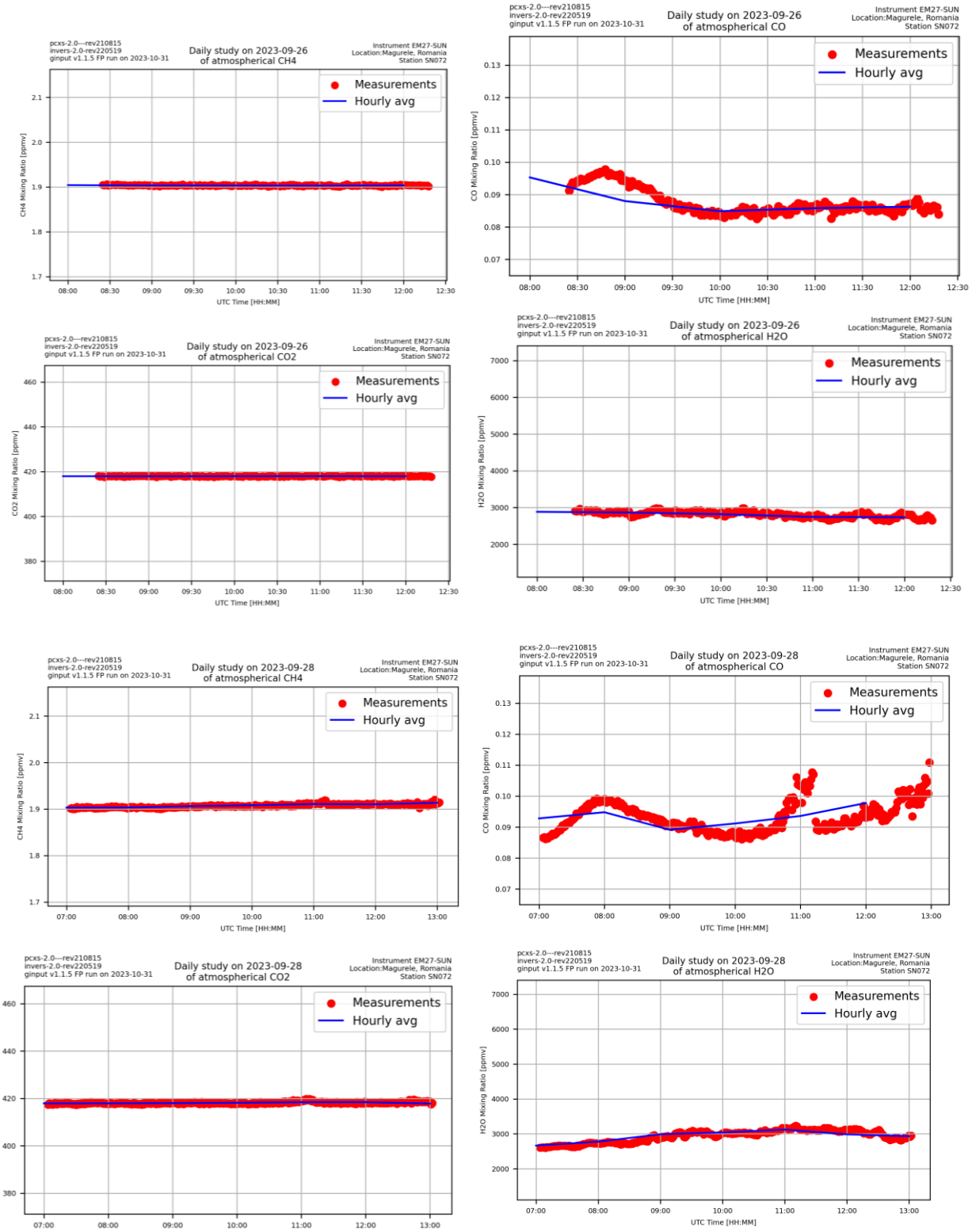

Figure 42 Diurnal variation of column-averaged dry-air mole fractions of CO_2, CO, CH_4 and H_2O measured over Magurele during QA4EO by FTIR

2.2.8.2 ***LIDAR***

2.2.8.3 ***HORIBA gas analyser***

Diurnal variations of CH_4, CO, NMHC, NO, NO_2 , NOx, O_3 , SO_2, THC are represented below, with the green arrows showing the time of S5p overpasses.

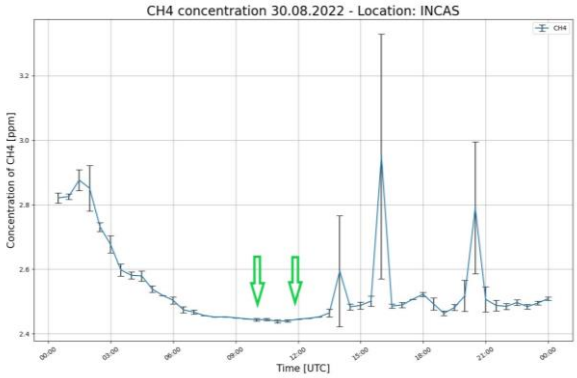

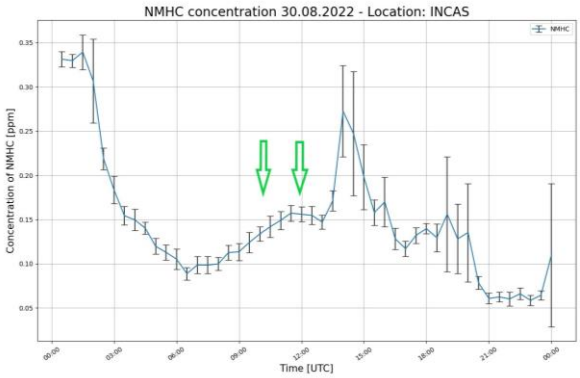

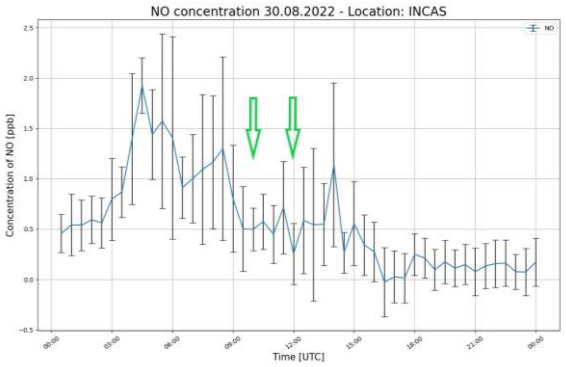

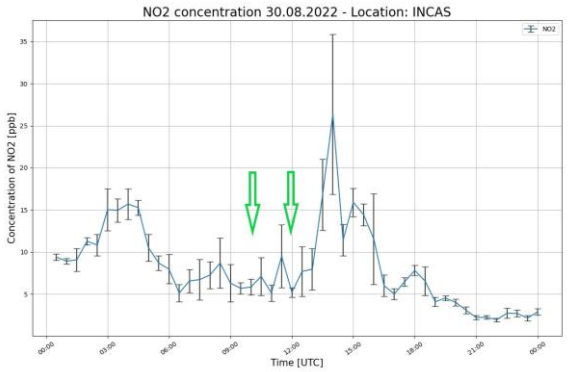

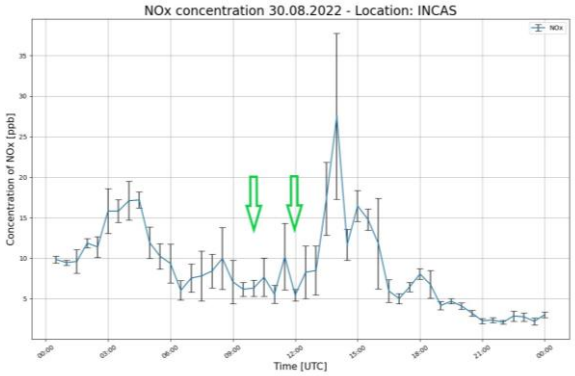

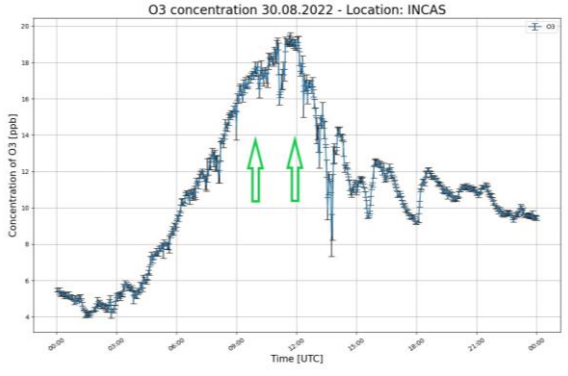

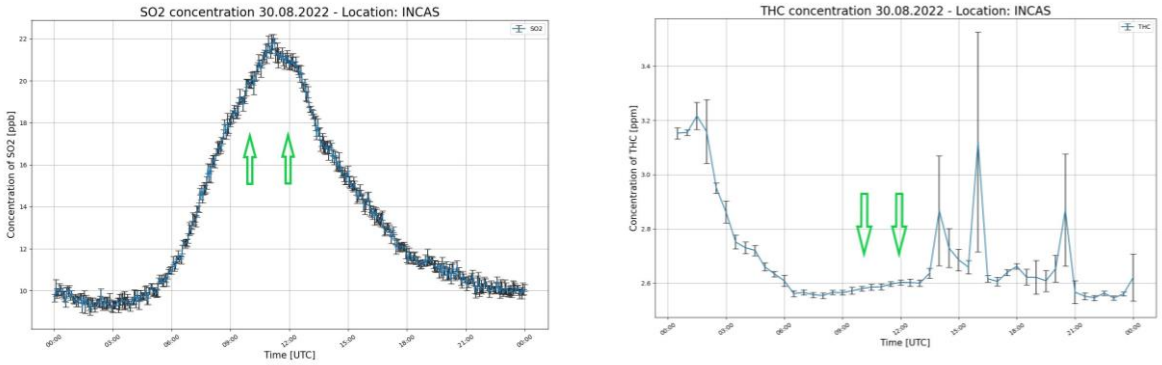

Figure 43 Panel graphs with CH_4, CO, NMHC, NO, NO_2 , NOx, O_3 , SO_2, THC daily variability at INCAS site in Bucharest

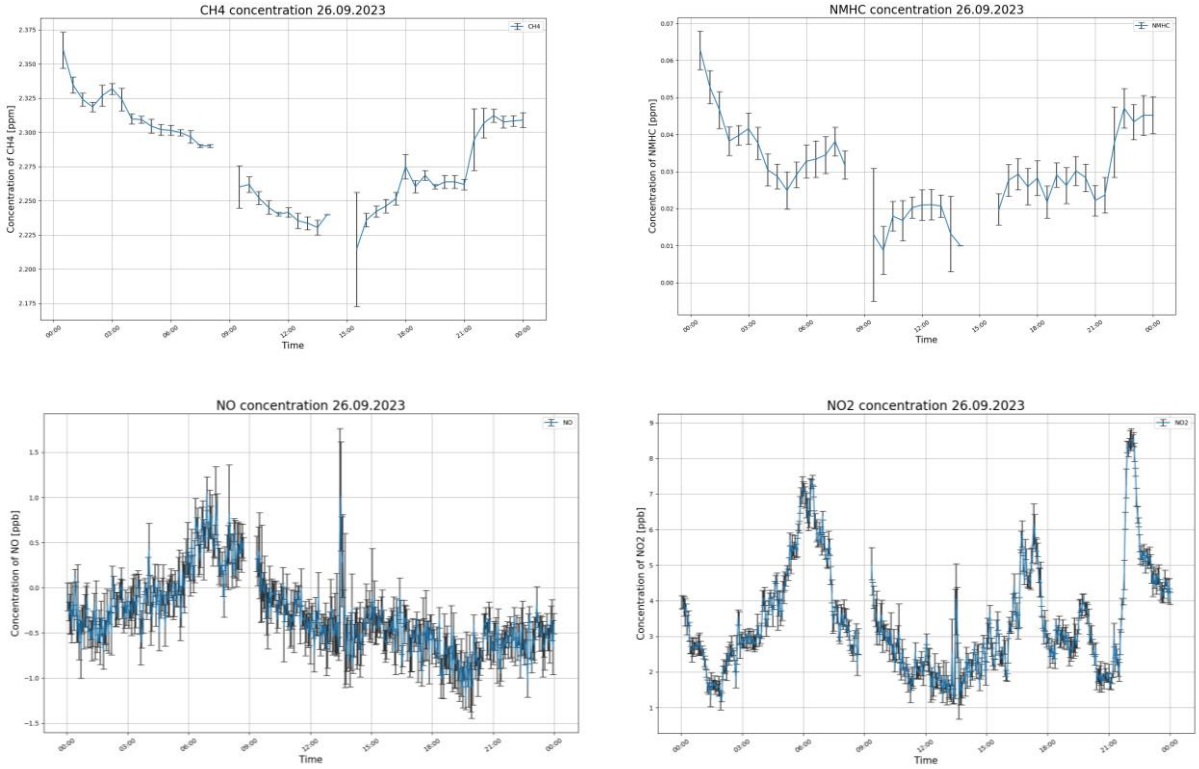

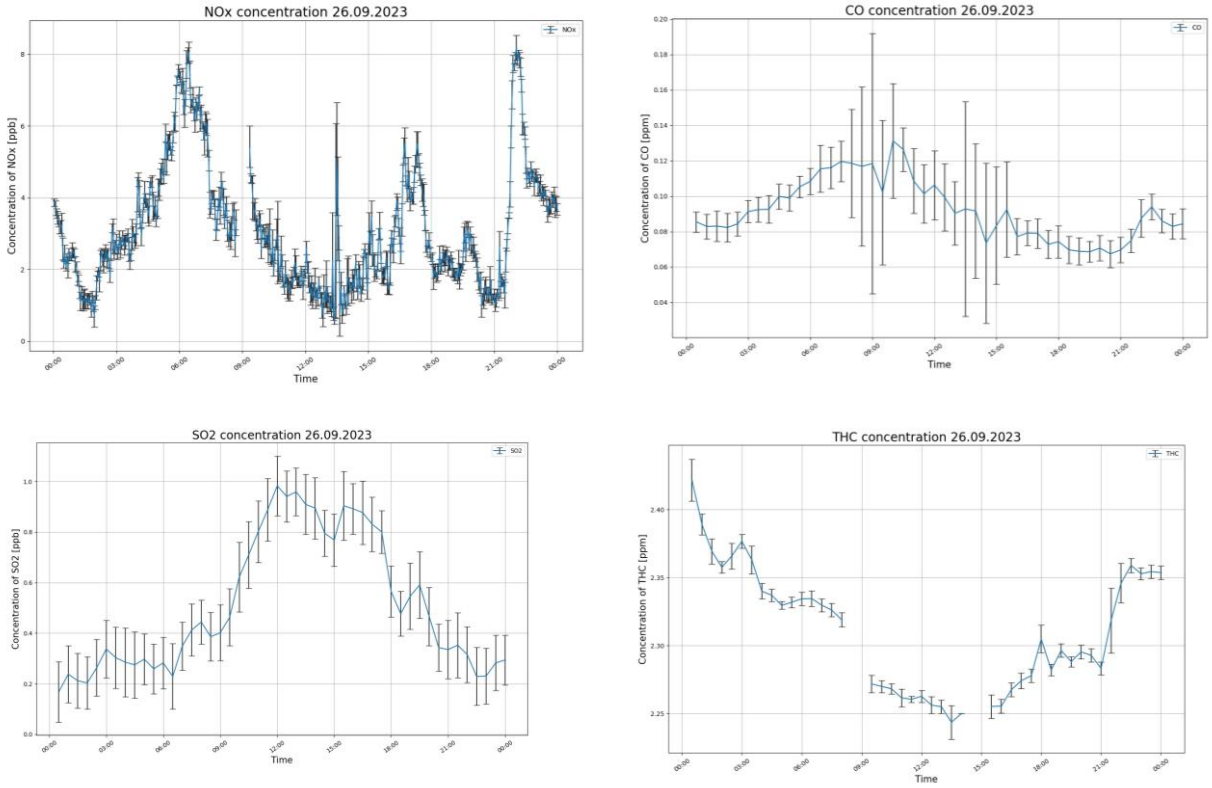

Figure 44 panel graphs with CH_4, CO, NMHC, NO, NO_2, NOx, O_3, SO_2, THC daily variability at MARS site in Magurele- 26.09.2023

Range corrected time series of the lidar measurements are available online at: https://quicklooks.earlinet.org/viewQuicklook.php.

As examples few of the quicklooks are presented below for 25 and 29.09.2023.

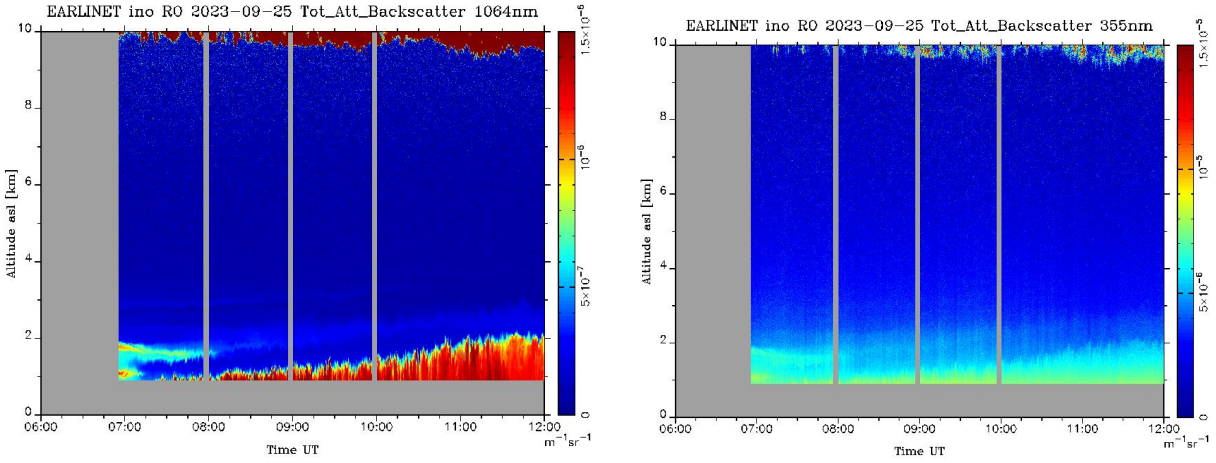

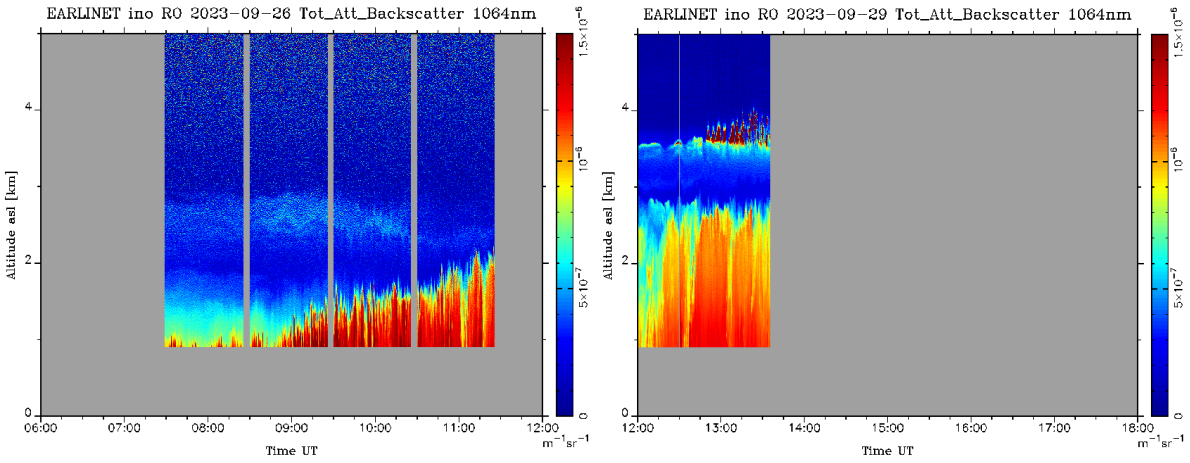

The planetary boundary layer height growth during morning can be noted along with an upper aerosol layer on 29th of September.

One hour averaged backscatter coefficient profiles at 355, 532 and 1064nm along with particles linear depolarization profiles have been derived for each of the campaign dates (shown in the results section Figure 45).

For every campaign date, one-hour averaged profiles of the backscatter coefficient at 355, 532, and 1064 nm as well as linear depolarization profiles of the particles have been determined. Below we are presenting the result for 25-29.09.2023. Several aerosol layers at different altitudes are present during this time and can be easily depicted in the graphs. The PBL (altitudes up cu 2000m) are characterized by depolarization values VLDR-volume linear depolarization ratio between 0.05 up to 0.11, with the highest values during 29.09.2024 when two distinct aerosol layers are present 2-3 km and 3-4km altitude.

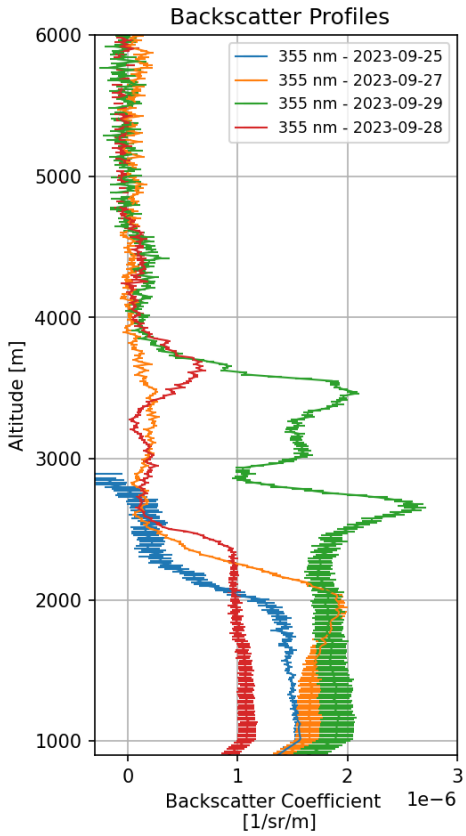
Backscatter Profiles
355 nm - 2023-09-25
355 nm - 2023-09-27
355 nm - 2023-09-29
355 nm - 2023-09-28
Altitude [m]
Backscatter Coefficient [1/sr/m]
1e−6

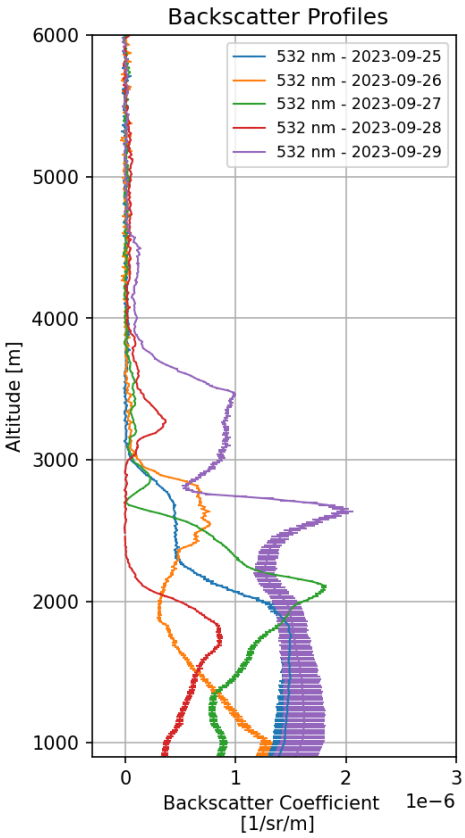
Backscatter Profiles
532 nm - 2023-09-25
532 nm - 2023-09-26
532 nm - 2023-09-27
532 nm - 2023-09-28
532 nm - 2023-09-29
Altitude [m]
Backscatter Coefficient [1/sr/m]
1e−6

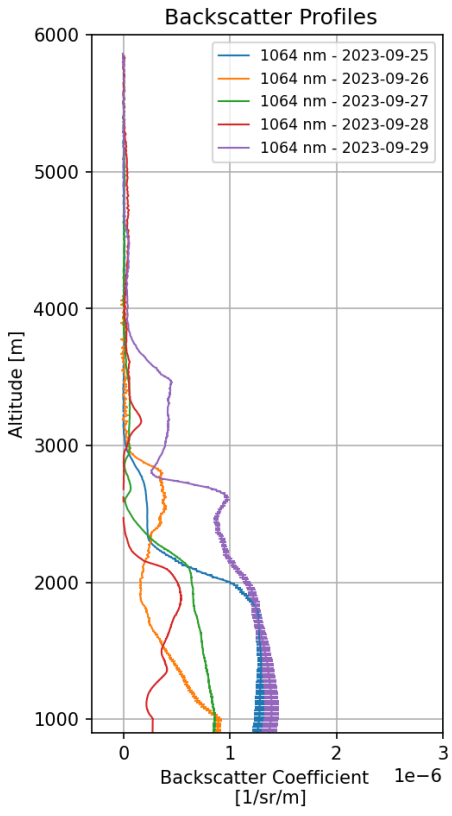
Backscatter Profiles
1064 nm - 2023-09-25
1064 nm - 2023-09-26
1064 nm - 2023-09-27
1064 nm - 2023-09-28
1064 nm - 2023-09-29
Altitude [m]
Backscatter Coefficient [1/sr/m]
1e−6

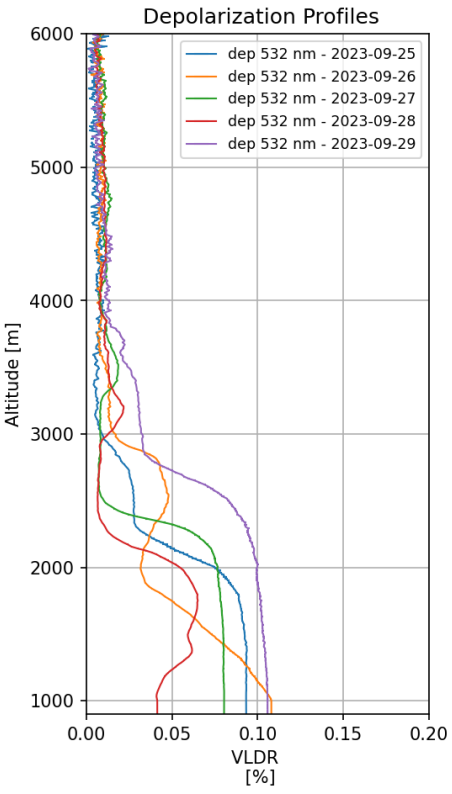
Depolarization Profiles
dep 532 nm - 2023-09-25
dep 532 nm - 2023-09-26
dep 532 nm - 2023-09-27
dep 532 nm - 2023-09-28
dep 532 nm - 2023-09-29
Altitude [m]
VLDR [%]

Figure 45 Lidar measurements; one hour averaged backscatter coefficient profiles at 355, 532 and 1064nm and VDLD at 532nm between 25-29.09.2023

2.2.8.4 *Ground-based data vs. TROPOMI*

Ground-based data collected during QA4EO in Magurele, Romania was compared with level 2 Sentinel 5P data. Only the data from the file description (parameter qa_value) with QA greater than 0.5 were taken into consideration for this analysis. A quality assurance value greater than 0.5 indicates high-quality data, while a qa_value of 1 indicates fully high-quality data. It is advised to disregard data that has a qa_value less than 0.5.

TROPOMI vs. PANDORA

One example of NO_2 data from S5p over Europe and over Romania is presented in Figure 46 overpass is from 26.09.2023.

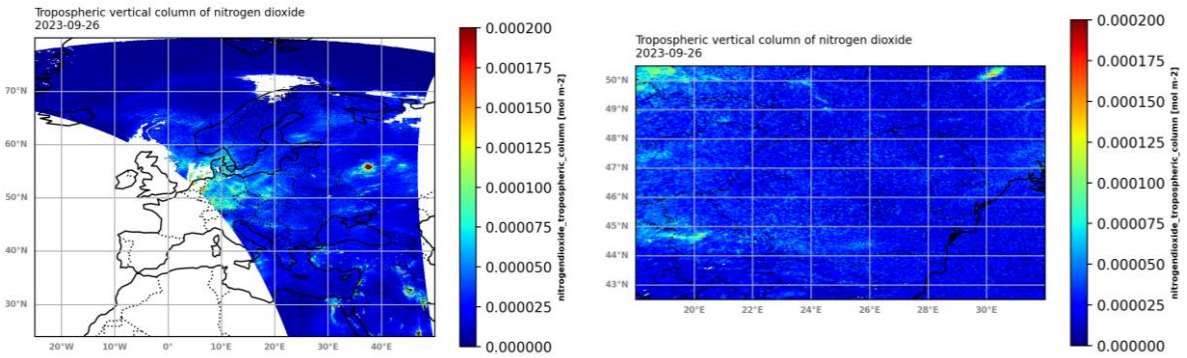

Figure 46 Total column NO_2 from Sentinel 5-Precursor over Europe (left panel) and over Romania (right panel) 26.09.2023

A method for comparison of ground-based PANDORA measurements and S5P data have been developed during RAMOS project and was used to compile the graphs below. Total column, tropospheric and summed NO_2 from Tropomi instrument were compared with the ones derived from ground based measurements of Pandora - 2S over Magurele, Romania (Figure 47).

Short description of the comparison procedure:

Step 1-From every measurement set, only data overpassing the interested area is selected

Step 2-Spatial and temporal dependence is computed from 0.1 degrees to 2.1 degrees radius distance from the ground-based instrument, where 0.1 degree radius represents an average of 10 km (0.1 degree difference in longitude represents 11.11 km while 0.1 degree difference in latitude, represents 9.99 km) and a time difference around the satellite overpass between 0.1 hours and 2.1 hours.

Step 3-The correlation factor, r, is calculated for each of the latter parameters and the results for total column NO_2 from Sentinel 5-Precursor and ground based Pandora - 2S system; the best correlation factor is chosen and the data is plotted against ground based data.

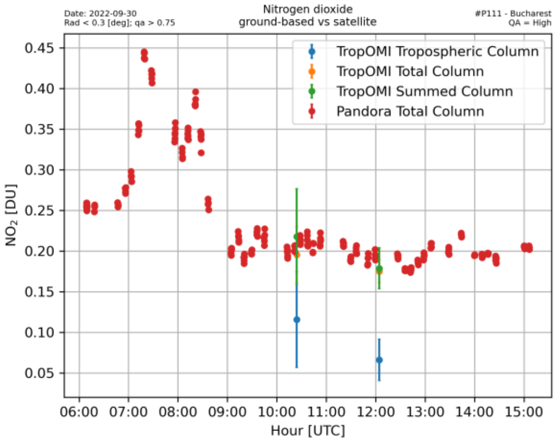

Date: 2022-09-30
Rad < 0.3 [deg]; qa > 0.75
Nitrogen dioxide
ground-based vs satellite
#P111 - Bucharest
QA = High
TropOMI Tropospheric Column
TropOMI Total Column
TropOMI Summed Column
Pandora Total Column
NO2 [DU]
Hour [UTC]

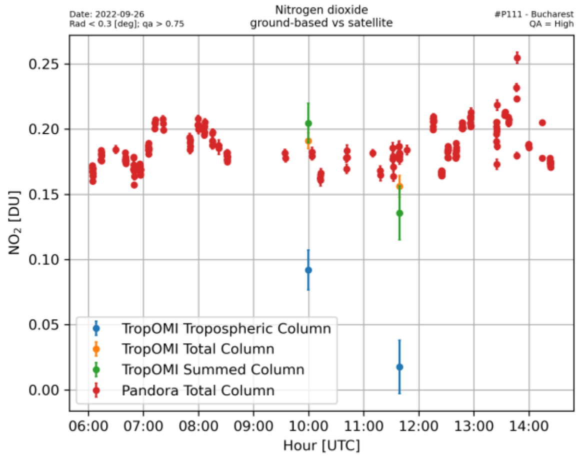

Date: 2022-09-26
Rad < 0.3 [deg]; qa > 0.75
Nitrogen dioxide
ground-based vs satellite
#P111 - Bucharest
QA = High
TropOMI Tropospheric Column
TropOMI Total Column
TropOMI Summed Column
Pandora Total Column
NO2 [DU]
Hour [UTC]

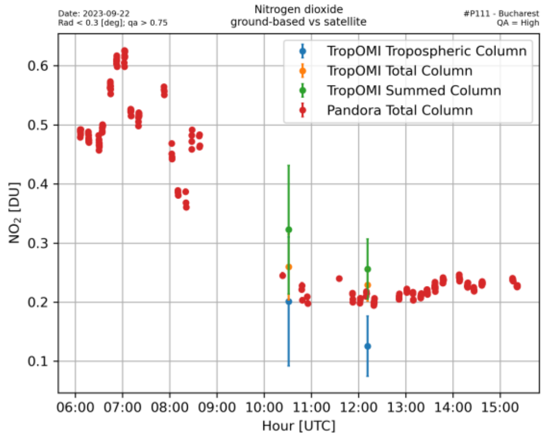

Date: 2023-09-22
Rad < 0.3 [deg]; qa > 0.75
Nitrogen dioxide
ground-based vs satellite
#P111 - Bucharest
QA = High
TropOMI Tropospheric Column
TropOMI Total Column
TropOMI Summed Column
Pandora Total Column
NO2 [DU]
Hour [UTC]

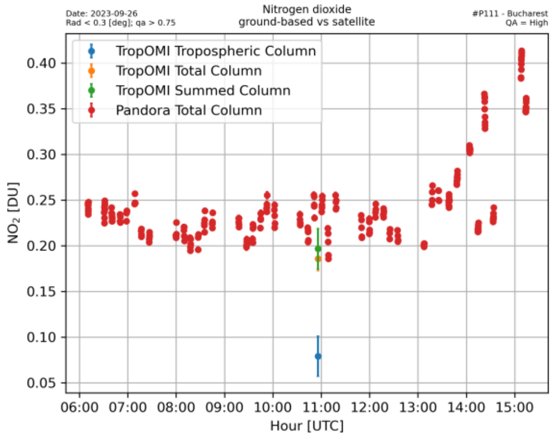

Date: 2023-09-26
Rad < 0.3 [deg]; qa > 0.75
Nitrogen dioxide
ground-based vs satellite
#P111 - Bucharest
QA = High
TropOMI Tropospheric Column
TropOMI Total Column
TropOMI Summed Column
Pandora Total Column
NO2 [DU]
Hour [UTC]

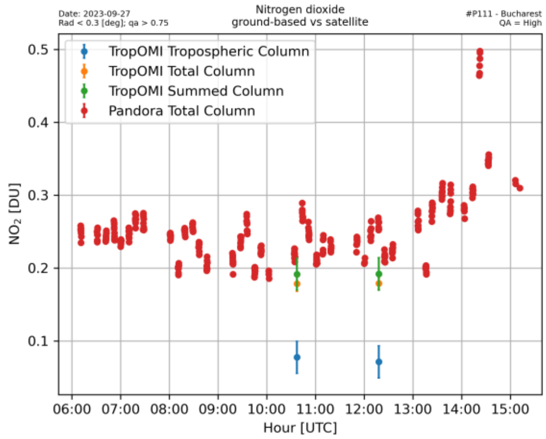

Date: 2023-09-27
Rad < 0.3 [deg]; qa > 0.75
Nitrogen dioxide
ground-based vs satellite
#P111 - Bucharest
QA = High
TropOMI Tropospheric Column
TropOMI Total Column
TropOMI Summed Column
Pandora Total Column
NO2 [DU]
Hour [UTC]

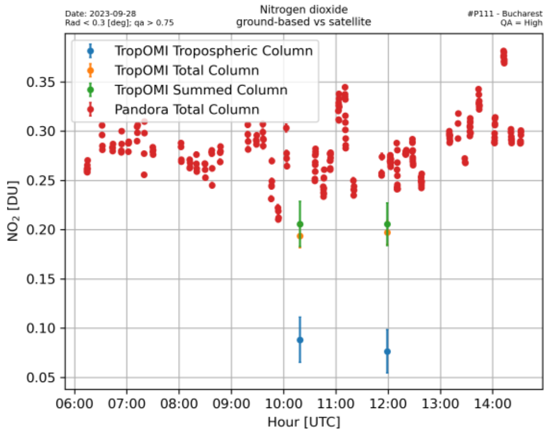

Date: 2023-09-28
Rad < 0.3 [deg]; qa > 0.75
Nitrogen dioxide
ground-based vs satellite
#P111 - Bucharest
QA = High
TropOMI Tropospheric Column
TropOMI Total Column
TropOMI Summed Column
Pandora Total Column
NO2 [DU]
Hour [UTC]

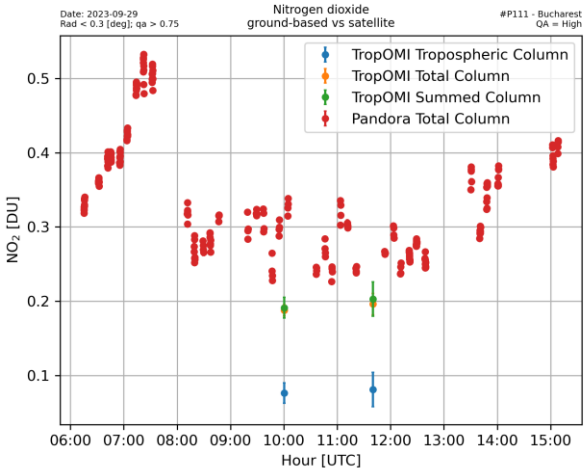

Figure 47 PANDORA data measurements in Magurele vs. TROPOMI

Analyzing the results of comparison between total column, tropospheric and summed NO_2 from Tropomi instrument and the ones derived from ground based measurements of Pandora - 2S over Magurele, Romania we can observe that the derived S5p tropospheric NO_2 is underestimating in all cases. Comparing total column from satellite with the ground base we can see very close values. PANDORA measurements allow us to note the daily variation of the total column for NO_2, while the satellite swap provide a view of the spatial variability in a snap-shot.

TROPOMI vs. FTIR

Total column carbon monoxide and CH_4 densities were derived from the low resolution (0.5 cm^{-1}) FTIR measurements in Magurele, a peri-urban area near Bucharest, Romania during QA4EO campaign and were compared with satellite retrieval from Sentinel-5 Precursor.

To have a good data comparison for both methods satellite and ground-based techniques several criteria were taking into account to reduce the input of punctual spots:

- Time period of FTIR CO and CH_4 retrieval was selected based on average time of ± 1h around sentinel over passing hour in order to diminish the influence of possible local sources like a traffic or local fires, wind directions etc
- Data collection from S5P, to have an appropriate representativeness, was made taking into account the administrative Romanian map. This was a necessary step considering the Bucharest city proximity. The covered area considered was of approximately 1964 km^2 in order to reduce the uncertainty associated with punctual spots like roads or city influences
- The results are represented in Figure 48

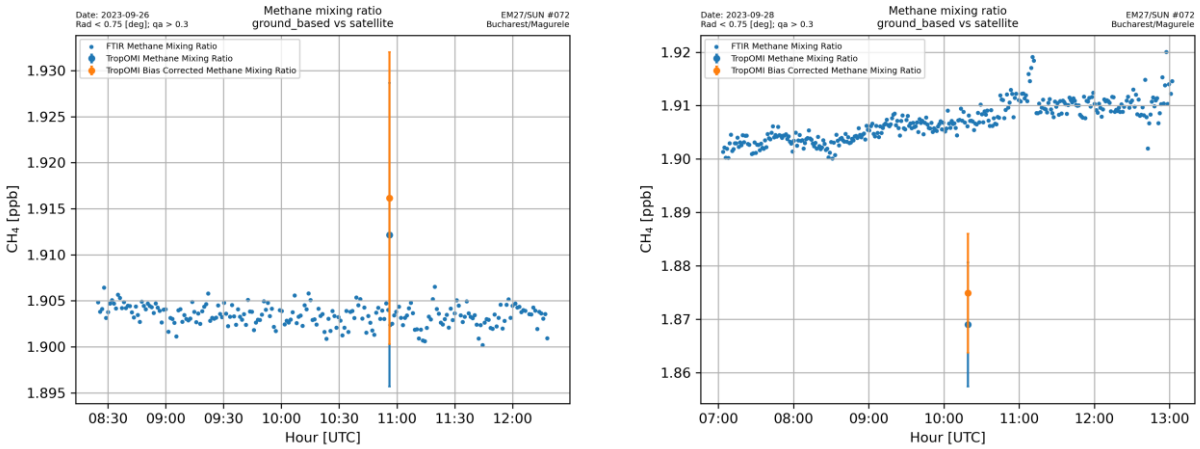

Figure 48 Comparison between TROPOMI and FTIR measurements at MARS site in Magurele- 26 and 28.09.2023

2.2.8.5 *Validation of Aerosol Layer Height product from space-borne instruments using ACTRIS' Aerosol Remote Sensing facilities*

Aerosol Layer Height (ALH) is a new operational Level-2 product retrieved from space-borne instruments including ESA's TROPOMI and under development for Copernicus Sentinel 3. The algorithm is based on hyperspectral measurements of the oxygen A band, assuming that the aerosols are confined to a single layer with a fixed pressure difference between top and bottom of the layer, and constant aerosol volume extinction coefficient. The algorithm features a spectral fit estimation of reflectance across O_2 A band using neural networks and the retrieval method is Optimal Estimation.
This study presents the validation methodology and results of the space-borne Level 2, version 2.2(ALH ATBD, KNMI, ESA, 2022) product of TROPOMI against ACTRIS' Aerosol Remote Sensing Lidar and Ceilometer systems.

Tropomi ALH retrievals from 2018 until 2024 are firstly filtered for quality assurance (qa) values below 0.5 and then spatially averaged around the ground-based stations. Ground-based Range Corrected Signals (RCS) have been used to determine the aerosol layer heights using a modified gradient method with a continuous wavelet function.

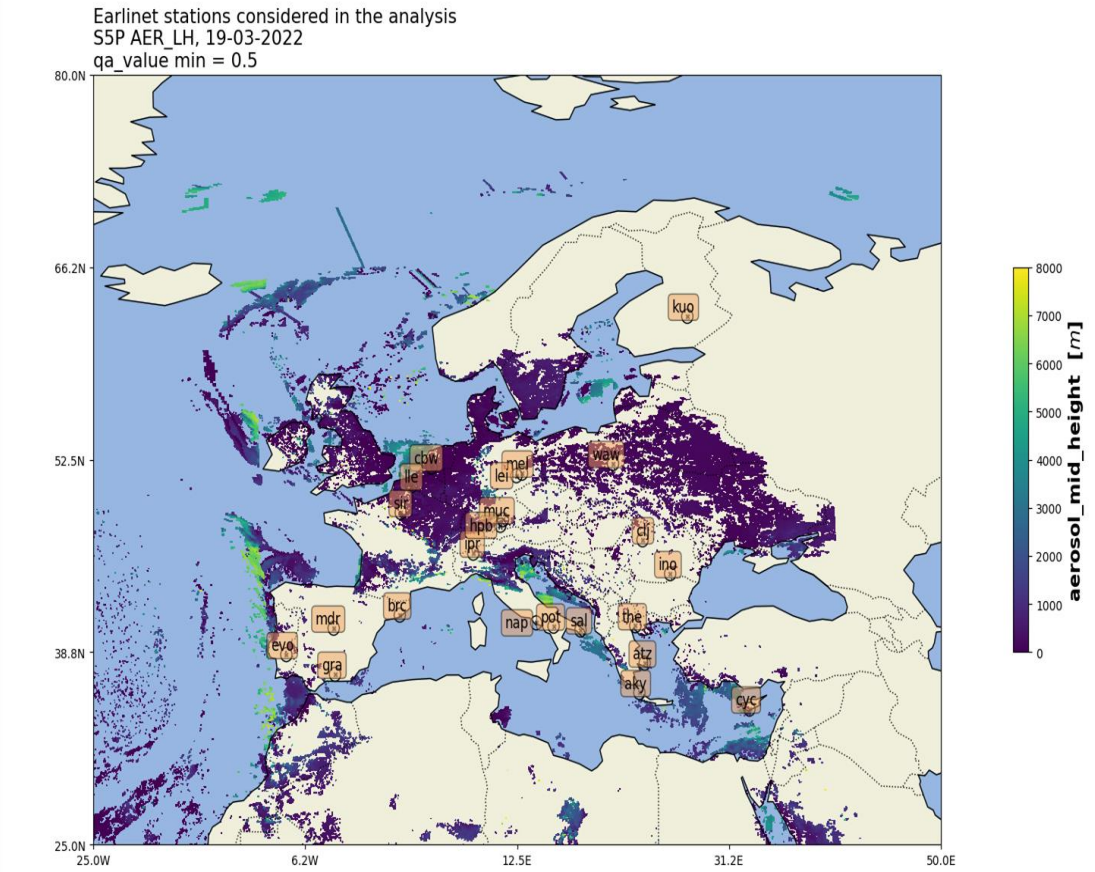

Figure 49 Tropomi ALH product over Europe and selected EARLINET stations, example from 19th March 2022

Experiments over selected lidar stations (Figure 49) have been conducted with NATALI (Nicolae, et. al, 2018) software (Nicolae, et. al, 2018) what has been used to determine the aerosol mid height and the aerosol optical properties. In depth analysis of aerosol optical properties have been made also for cases of long-range transported aerosol cases.

High quality NATALI aerosol type retrieval for all considered stations and correlated with satellite overpass with a time constrain of less than 4 hours and a radius around the ground-based location of 100 km show an overall positive correlation between the two (Figure 50).

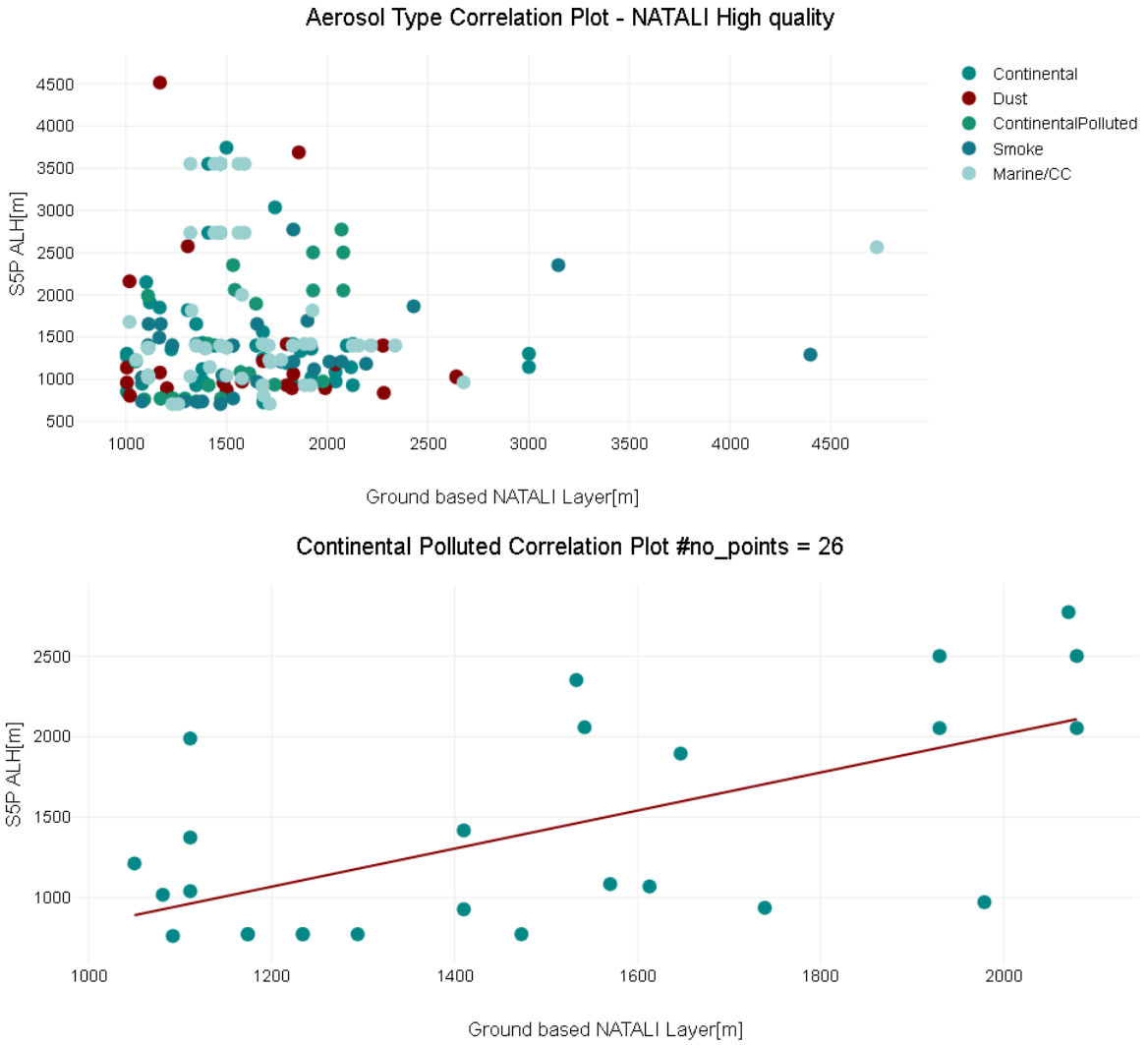

Figure 50 upper graph Ground-based NATALI retrieval of aerosol type height correlation with satellite ALH overpass; lower graph Correlation plot of ground-based elevated layer for Continental Polluted and Tropomi Overpass ALH product

Among the retrieved aerosol types and their related heights, retrieval of Continental Polluted with a Pearson Correlation factor around 0.6.
A different type of comparison between ground-based and satellite borne retrieval of ALH has been conducted. Within this study we calculated Centre of Mass (Mona, et.al., 2012) from Earlinet backscatter signal from 1064 nm channel and compared with satellite retrieval of ALH. Using satellite qa values measurements > 0.7 and a radius of 100 km the Taylor diagram of Pearson correlation, standard deviation and root mean square differences for each station is presented in Figure 51, left and the highest correlation value is found for Leipzig station (Figure 51, lower)

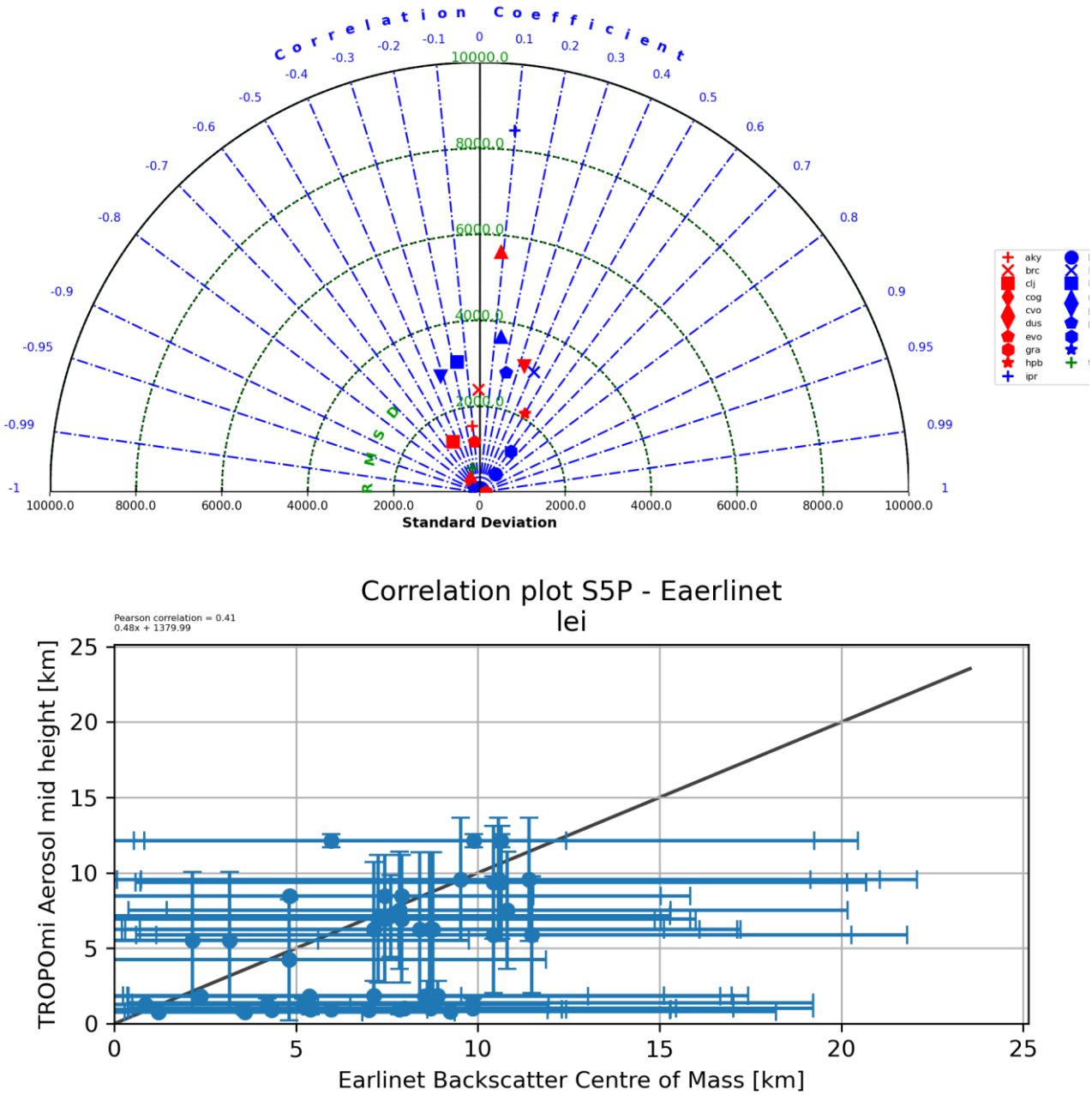

Figure 51 upper graph Taylor diagram of correlation between Earlinet Centre of Mass and Tropomi ALH; lower graph Leipzig Centre of Mass calculated from 1064 nm channel correlation plot with Tropomi ALH

Cloudnet ceilometers' backscatter profiles were also used to determine the ground-based Centre of Mass and compared with the Tropomi ALH product. In this study, a timeframe of ± 1h of data around satellite overpass time and ± 50 km around ground-based locations have been used to compare the two retrievals.

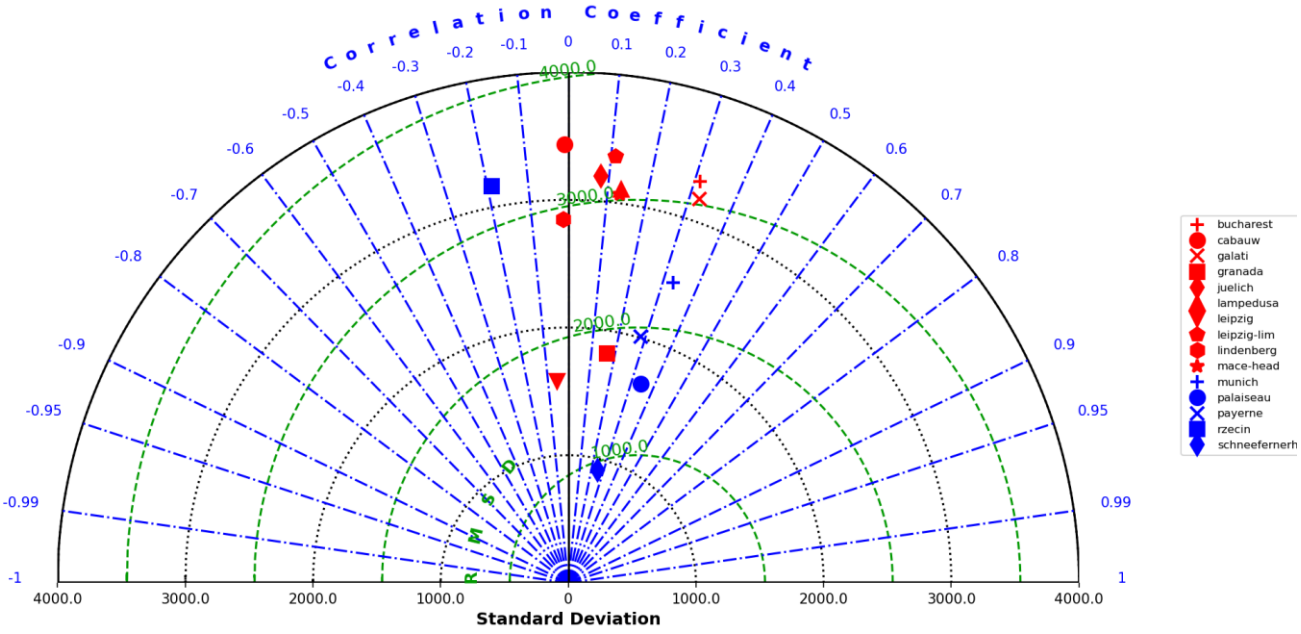

Figure 52 Taylor diagram of correlation plot between ground based Cloudnet centre of mass and Tropomi ALH

Figure 52 shows the Taylor diagram for all considered backscatter profiles' stations used in this study with the highest value of 0.34 for Palaiseu station (Figure 53, right).

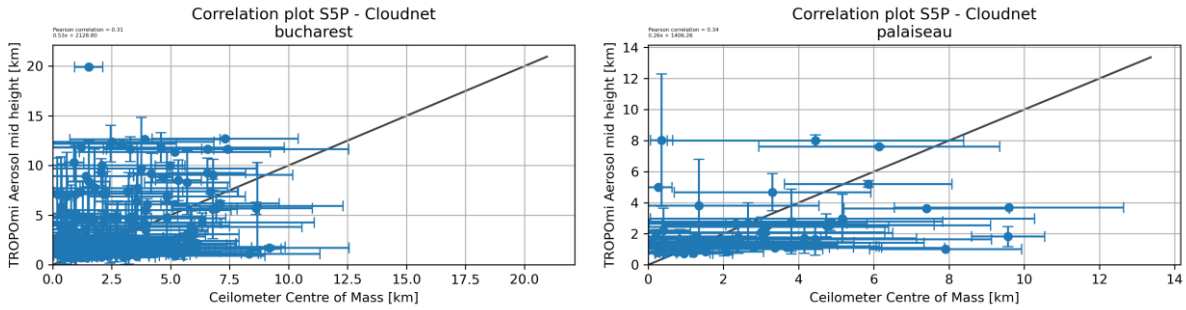

Figure 53 Correlation plot of Cloudnet backscatter centre of mass for Bucharest station (left) and Palaiseau station (right)

EARLINET usage of backscatter, extinction, and depolarisation aerosol profiles have higher quality and confidence level when retrieving the elevated aerosol layer or centre of mass in comparison with the low power lidars from Cloudnet. NATALI high quality retrievals require nighttime measurements therefore there is a relatively high time difference between ground based and satellite observations, Tropomi's mid-latitude overpass being around 13 UTC.
When compared both EARLINET measurements and calculating either NATALI aerosol height or backscatter's centre of mass, positive and negative correlation are found. Overcoming the time differences between the two and using Cloudnet ceilometers and retrieving the centre of mass, the results show good positive correlation for selected stations (e.g., Bucharest, Palaiseau).

Further development will include comparison using all ACTRIS' aerosol remote sensing facilities to retrieve the elevated tropospheric height of aerosols and plume detection and tracking for dust, smoke, etc.

Study presented during ATMOS 2024, 1-5 July 2024 Bologna, Italy; P4.3 Validation of Aerosol Layer Height product from space-borne instruments using ACTRIS' active sensors; Authors: A.M. Dandocsi, S. Nicolae, A. Nemuc, L. Belegante; https://www.atmos2024.org/programme

References

Nicolae, D., Vasilescu, J., Talianu, C., Binietoglou, I., Nicolae, V., Andrei, S., and Antonescu, B.: A neural network aerosol-typing algorithm based on lidar data, Atmos. Chem. Phys., 18, 14511–14537, https://doi.org/10.5194/acp-18-14511-2018, 2018. Mona, L., A. Amodeo, M. Pandolfi, and G. Pappalardo (2006), Saharan dust intrusions in the Mediterranean area: Threeyears of Raman lidar measurements, J. Geophys. Res., 111, D16203, doi:10.1029/2005JD006569 Mona, L., Liu, Z., Müller, D., Omar, A., Papayannis, A., Pappalardo, G., Sugimoto, N., Vaughan, M., Lidar Measurements for Desert Dust Characterization: An Overview, Advances in Meteorology, 2012, 356265, 36 pages, 2012. https://doi.org/10.1155/2012/356265

2.2.8.6 *Evaluation of decadal regional and local NO_2 column densities using space-borne and ground-based instruments and CAMS*

In this study, the main objective is studying the decadal evolution of NO_2 column densities retrieved from OMI and TROPOMI measurements and using a cross-comparison with the CAMS atmospheric modelling product for regional and local scale analyses.

Satellite data are obtained from the *Copernicus Data Space Ecosystem* and *GES-DISC* (Krotkov & Veefkind, 2012) and is re-gridded such that the data from OMI corresponds to a 7 x 7 km^2 grid and TROPOMI data corresponds to a 1 x 1 km^2 grid. For this, we have used a part of ESA's Atmospheric Virtual Lab, *HARP library*, utilizing built-in functions for filtering, re-gridding and temporally averaging the datasets obtained. Furthermore, CAMS data are both temporally averaged and vertically integrated (Douros et al., 2023), such that it can be directly compared to the satellite data.

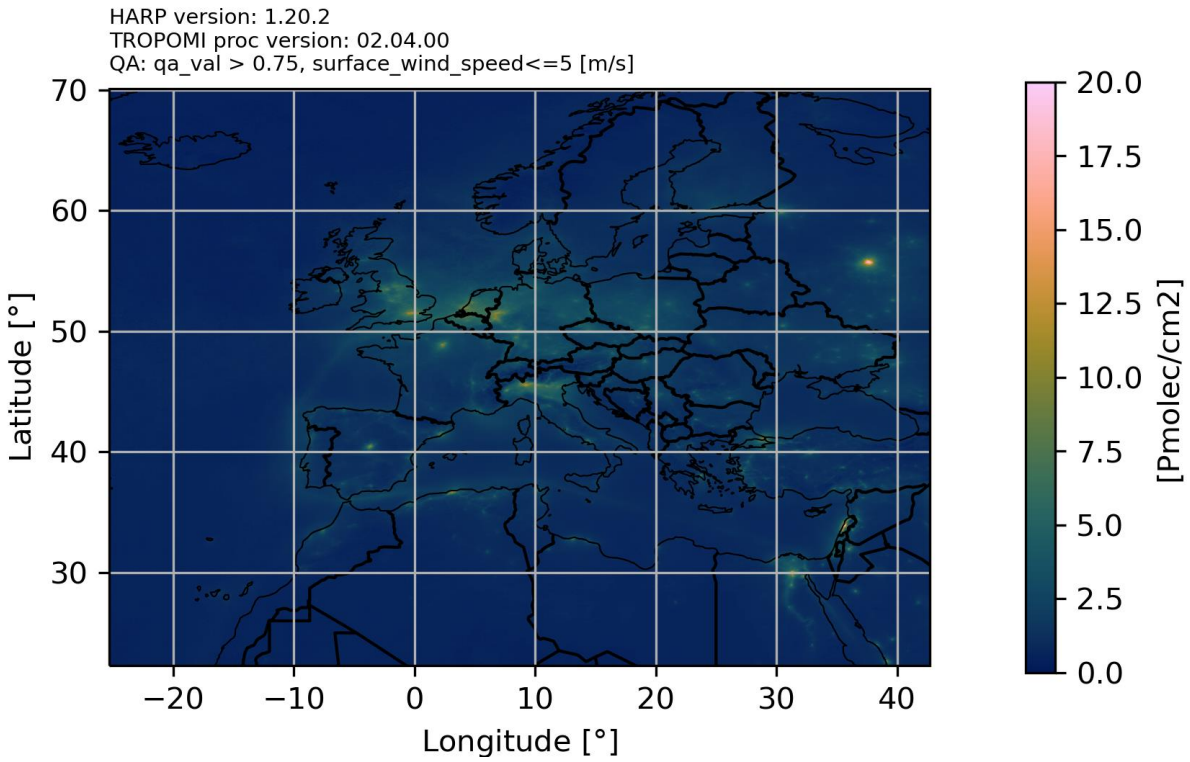

Figure 54 - Yearly 1x1km^2 re-gridded TROPOMI data over Europe

A qualitative analysis present in Figure 54 - **Yearly 1x1km^2 re-gridded TROPOMI data over Europe**Figure 54 reveals elevated values for the tropospheric NO_2 column density measurements in the Netherlands, the north of Italy and south of the UK. Thus, a study of the monthly averaged satellite retrieved values from both the OMI and Sentinel-5P satellites was made, in order to identify the decadal trend in the measurements. The OMI satellite was selected because it offers a decadal timespan (2003-2023), and the Sentinel-5P satellite offers better spatial resolution and more precise measurements.

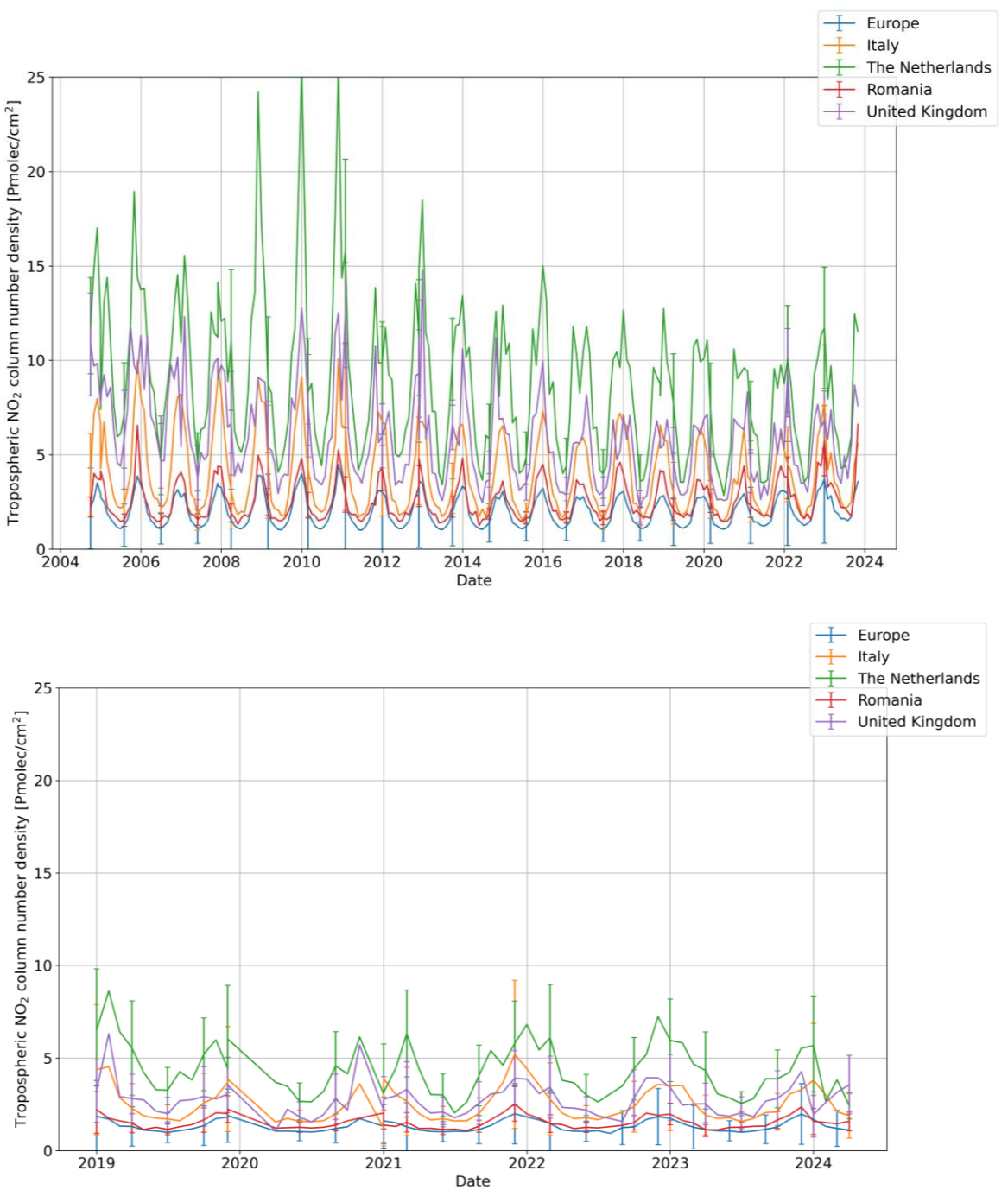

Figure 55, upper graph- Monthly averaged values over the regional hotspots, retrieved from the OMI satellite; lower graph - Monthly averaged values over the regional hotspots, retrieved from the TROPOMI instrument (Sentinel-5P)

Figure 55 showcase the evolution of the tropospheric NO_2 column number densities, as sensed by both instruments used. The absolute values of the parameter show a pronounced seasonal trend, convolved with a descending tendency for the earlier part of the 21st century. However, after the year 2016, there is no longer any decreasing trend in the column number densities studied, as OMI shows. The TROPOMI instrument also supports these findings, illustrating only the seasonal particularities of the trend. However,

the absolute values of the retrieved tropospheric NO_2 column number densities vary significantly between the two instruments (approx. 30%±10%). This discrepancy is due to the different a-priori profiles and algorithms used in retrieving the aforementioned quantities from the satellite data and should be noted, as a quantitative comparison could not be made between the two satellites.

Furthermore, an analysis at a local scale in Romania was made, selecting certain hotspots identified within the country's borders and using satellite measurements to analyse the trend in NO_2 column number density values.

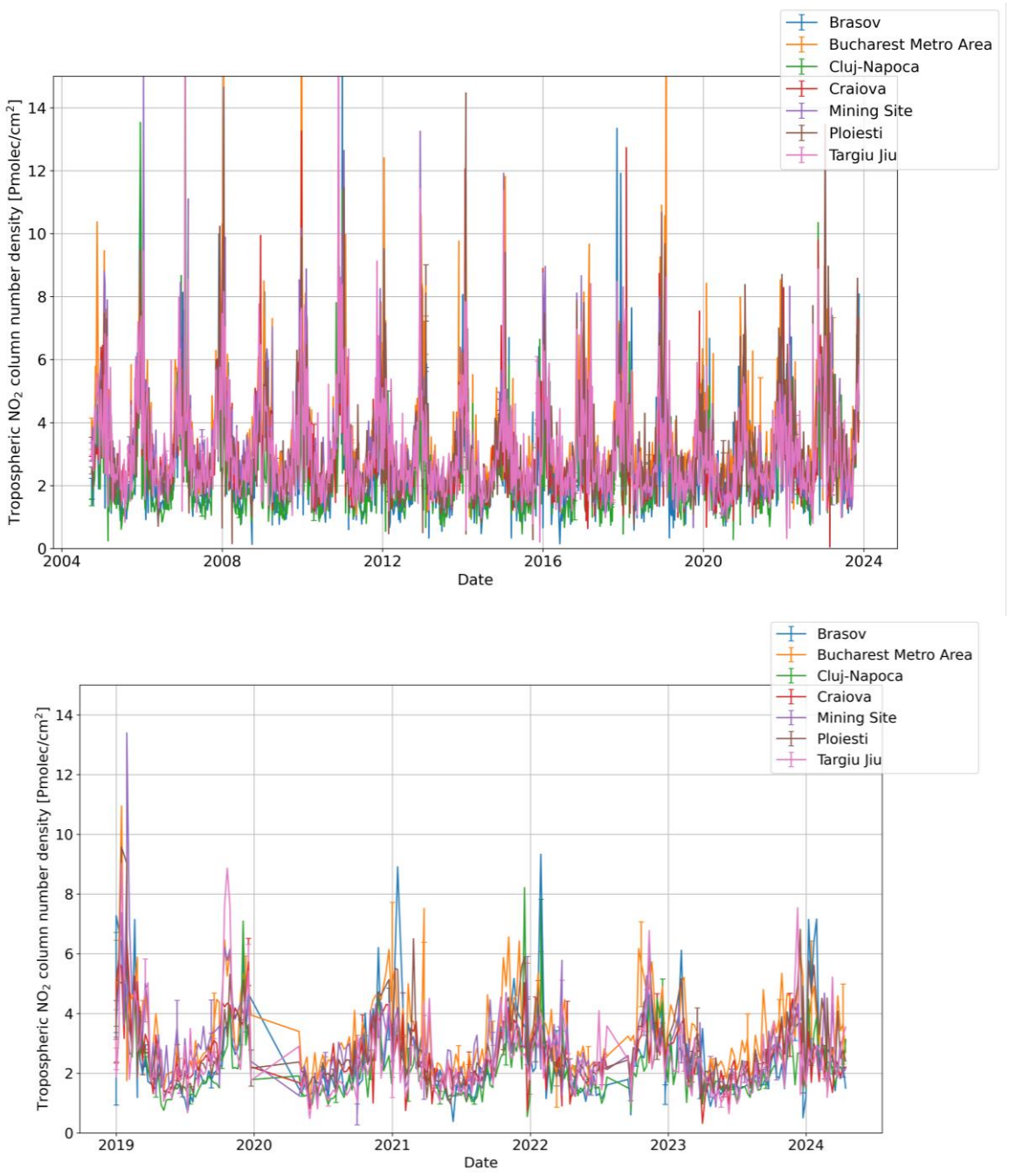

Figure 56, upper graph- Weekly averaged tropospheric NO_2 column number density values for local hotspots in Romania, as retrieved by OMI; lower graph - Weekly averaged tropospheric NO_2 column number density values for local hotspots in Romania, as retrieved by TROPOMI

Figure 56 showcase the aforementioned seasonal trend, but show a lower decreasing tendency than was the case for the regional level hotspots. However, besides the expected urban hotspots located in the major cities in Romania, a mining site was detected and analysed as part of this study.

Finally, a new product simulating a satellite-sensed column density was obtained, using the CAMS European Air Quality Reanalysis Ensemble model. Due to the highest level for

which model data is available (at 5000m above surface level) being usually less than the height of the free troposphere, the new product does not encompass the entire NO_2 present in the free troposphere. However, surface-level emissions are easily detected, as the contrast increases, since they account for most of the tropospheric NO_2 in the polluted hotspots. Therefore, the new product is a good stepping stone for identifying NO_2 hotspots on a surface level, utilising model data and correlating it with Sentinel-5P satellite measurements.

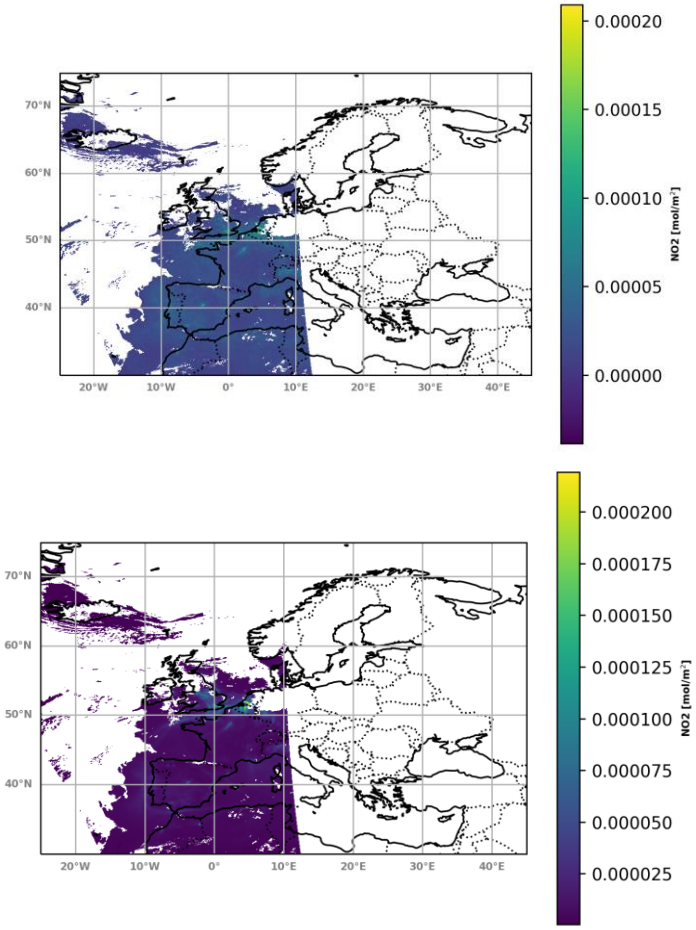

Figure 57 upper graph - TROPOMI retrieved tropospheric NO_2 column number density on orbit no. 24532; lower graph - New product obtained from correlating CAMS European Ensemble Reanalysis model with TROPOMI satellite measurements

Future development ideas for this project are utilising the products obtained from correlating the model with the satellite measurements in order to better detect local NO_2 hotspots, looking for discrepancies between the satellite retrieved tropospheric column and the model simulated one.

This study was presented during ATMOS 2024, 1-5 July 2024 Bologna, Italy; P 3.12 Evaluation of decadal regional and local NO2 column densities using space-borne instruments and CAMS; Authors: ***S.M. Nicolae****, A.M. Dandocsi, A. Ilie, and A. Nemuc*
https://www.atmos2024.org/programme

References:

Douros, J. et al. (2023). Comparing Sentinel-5P TROPOMI NO $_2$ column observations with the CAMS regional air quality ensemble. *Geoscientific Model Development*, *16*(2), 509–534. https://doi.org/10.5194/gmd-16-509-2023

Krotkov, N. A., & Veefkind, P. (2012). *OMI/Aura Nitrogen Dioxide (NO2) Total and Tropospheric Column 1-orbit L2 Swath 13x24 km* [dataset]. NASA Goddard Earth Sciences Data and Information Services Center. https://doi.org/10.5067/AURA/OMI/DATA2017

2.2.9 Airborne results

Each of the flight have been described and the data analysed in details in Annex 1 Annex 1 Flight reports.

Below there is an example for Flight 1: 30 Aug 2022.

2.2.9.1 ***Flight 1: 30 Aug 2022***

Flight overview

- **Altitude:** 500 m
- **Instruments:** IMU, AS32M, Picarro G2041-m, APS
- **Duration:** 1:48
- **Weather summary:** Relatively high-pressure regime over Romania, high cloud-cover close to Bucharest, proper conditions for measurements.

IMU data

Figure 58. Flight path recorded by the IMU on 30 Aug 2022

The flight path recorded by the IMU can be seen in Figure 58. The take-off was from the Băneasa Airport and the mission started in the SW part of Bucharest and ended in the NW, after which the aircraft headed for landing at the Strejnicu Airfield.

AS32M data

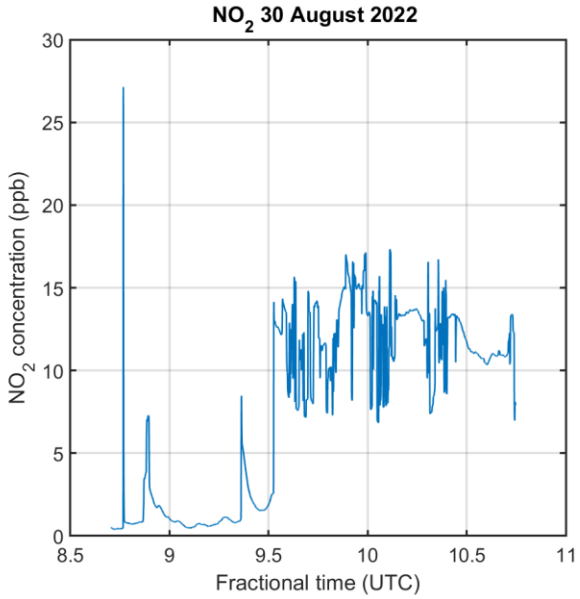

Figure 59. NO_2 concentration time series for the 30 Aug 2022 flight

The NO_2 concentration fluctuates throughout the observed period, showing distinct peaks and troughs. The graph starts with low NO_2 levels, which occasionally spike to moderate levels (around 5 ppb). There is a noticeable peak just before 9.0 UTC, reaching approximately 25 ppb, followed by a sharp drop. Between 9.5 – 10 UTC, the NO_2 levels remain relatively low, with minor fluctuations. From around 10.0 UTC, the NO_2 concentration increases and becomes more variable, frequently oscillating between 5 and 15 ppb, with some peaks nearing 20 ppb. Towards the end of the period, the concentrations slightly stabilize, maintaining around 10 ppb with less fluctuation. The variations in NO_2 levels could be influenced by changes in traffic density, industrial activities, or meteorological conditions. The spikes and variations might also reflect the plane's altitude, speed, or changes in its path, as seen in the IMU data.

Picarro G2401-m data

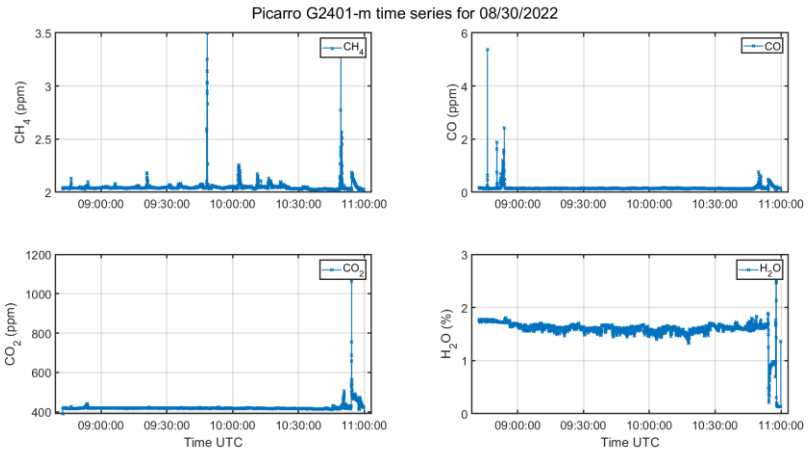

Figure 60. Greenhouse gases concentrations for 30 Aug 2022 (top left: CH_4, top right: CO, bottom left: CO_2, bottom right: H_2O)

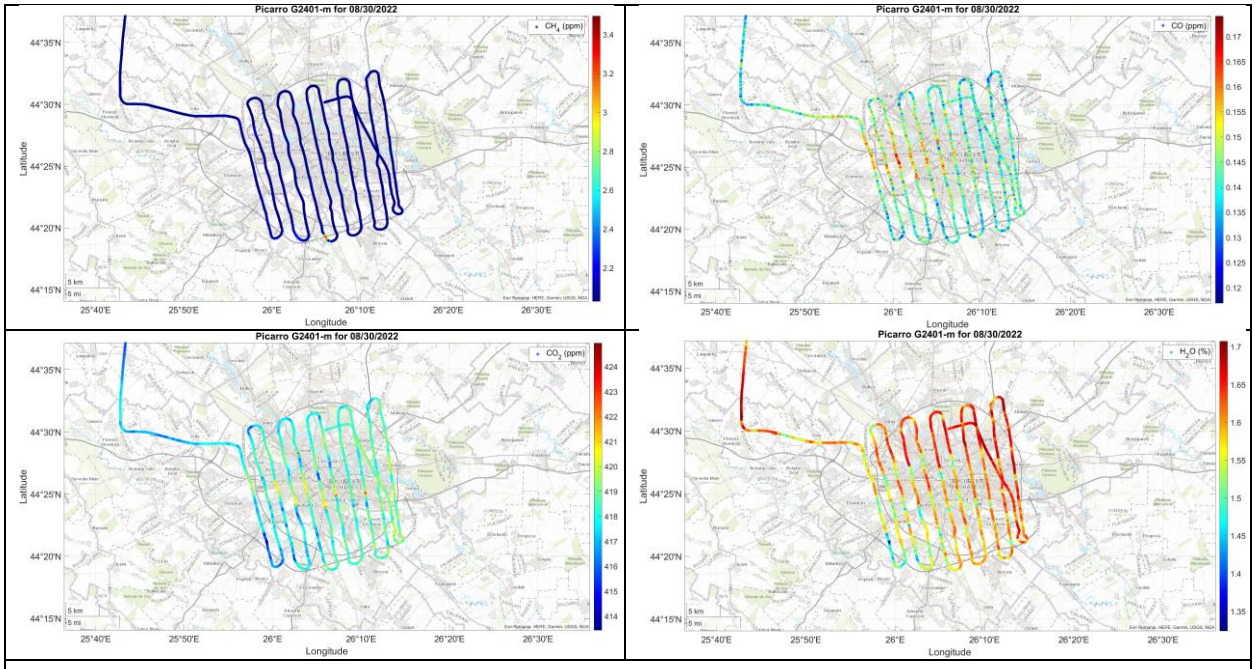

Figure 61. Georeferenced data from the Picarro G2401-m for 30 Aug 2022 (top left: CH_4, top right: CO, bottom left: CO_2, bottom right: H_2O)

Figure 61 shows time series data for greenhouse gases and water vapor concentration levels on August 30, 2022, as recorded by the Picarro G2401-m. The methane levels fluctuate around 2 ppm most of the time. There are several sharp spikes throughout the day, with the highest peak occurring around 10:30 UTC, reaching approximately 3.5 ppm. Smaller peaks are observed at various points, indicating intermittent releases or sources of methane. Carbon monoxide levels are mostly stable around 0.1 – 0.2 ppm, indicating very low baseline concentrations. Several distinct spikes occur, with significant peaks at around 09:30 UTC and another just before 11:00 UTC, reaching up to 5 ppm. These peaks suggest short-term emissions or exposure to CO sources. The CO_2 levels hover around 400 ppm, which is close to the global average atmospheric concentration. There

is a notable increase after 10:30 UTC, with a sharp peak nearing 1200 ppm around 11:00 UTC. This significant spike suggests a substantial localized CO_2 source or an event that caused a sudden release of carbon dioxide. The water vapor content remains relatively stable around 1.5-2% throughout the observed period. A sudden drop in water vapor concentration is seen at the end of the time series, just before 11:00 UTC. This drop could indicate a change in environmental conditions or sensor positioning, such as a move to a drier area or a sudden decrease in relative humidity. The spikes in CH_4, CO, and CO_2 concentrations suggest that the area experienced several episodic emissions of these gases. These could be due to industrial activities, traffic emissions, or natural sources. The general stability in water vapor concentration, with a sudden drop towards the end, might indicate relatively constant ambient conditions with a brief exposure to a different microclimate or environment. The synchronization of some of the spikes across different gases (e.g., CH_4 and CO_2 around 10:30 UTC) could suggest a common source or events causing simultaneous releases of these gases.

Figure 60 displays spatial distributions of methane (CH_4), carbon monoxide (CO), carbon dioxide (CO_2), and water vapor (H_2O) concentrations over Bucharest on 30 Aug 2022. CH_4 concentrations are mostly stable with some elevated levels (around 3 ppm) in the central and southern parts of the flight path. There are localized spikes in CH_4 concentration, consistent with the time series graph that showed several sharp peaks. The highest concentrations (red areas) are observed near the urban centre of Bucharest, indicating potential urban sources of methane emissions. CO concentrations are relatively low across the surveyed area, with occasional higher concentrations in the central urban areas. The highest levels (red spots) are seen in specific areas over Bucharest, suggesting localized sources of CO. The time series graph showed several spikes in CO concentration, which align with the localized higher concentrations seen on the map. CO_2 levels are generally higher in the central and southern regions of Bucharest. There are significant variations in CO_2 concentration along the flight path, with peaks corresponding to urban areas. The time series graph indicated a significant spike in CO_2 concentration towards the end of the period, which is reflected in the higher concentrations observed over the dense urban regions. Water vapor concentrations are relatively higher in the central and eastern parts of the flight path. Lower concentrations are observed at the outskirts and some parts of the western regions. The time series graph showed stable water vapor concentrations with minor fluctuations, which are reflected in the spatial map showing moderate variability.

2.2.9.2 *Issues during airborne campaign*

- Lower data quality has been observed in the data collected with APS, Envea AS32M and nefelometer. Issues such as the presence of negative values (Envea AS32M and nefelometer), high noise levels, and a low number of particles (APS) have been noted. The exact source of these problems remains unidentified. To determine the causes of the decreased data quality, several tests and checks will be conducted:

    - Requests have been made to the technical department to dismantle the instruments from the research aircraft and relocate them to the Strejnicu base for ground tests. This will be performed during the next scheduled maintenance of the aircraft

- The instruments will be tested on a vibrating table. If these tests indicate that vibrations are a problem, vibration sensors will be installed in the instrument rack during a test flight to observe if high vibration levels are causing data degradation.
- The air inlet will be inspected on the ground to ensure that the pipes connected to the instruments are not blocked.

2.2.9.3 *SWING+ vs TROPOMI*

SWING+ vs TROPOMI

Both datasets show a correlation in the spatial distribution of NO_2 levels, with higher concentrations towards the central and northeastern regions (Figure 63. SWING+ vs TROPOMI VCDs for 2 Nov 2022., Figure 63. SWING+ vs TROPOMI VCDs for 2 Nov 2022.) The SWING+ data provides a finer resolution, capturing more localized variations in NO_2 concentrations. TROPOMI data, represented by larger squares, gives a broader regional picture of NO_2 distribution. SWING+ data, represented by smaller dots, offers a more detailed and localized view of NO_2 levels, potentially capturing smaller sources or variations that TROPOMI might not resolve as finely. Both datasets identify similar hotspots of NO_2 concentrations, particularly in the northeastern region. This overlap suggests that these areas are significant sources of NO_2 emissions, which could be industrial zones, high traffic areas, or other pollution sources.

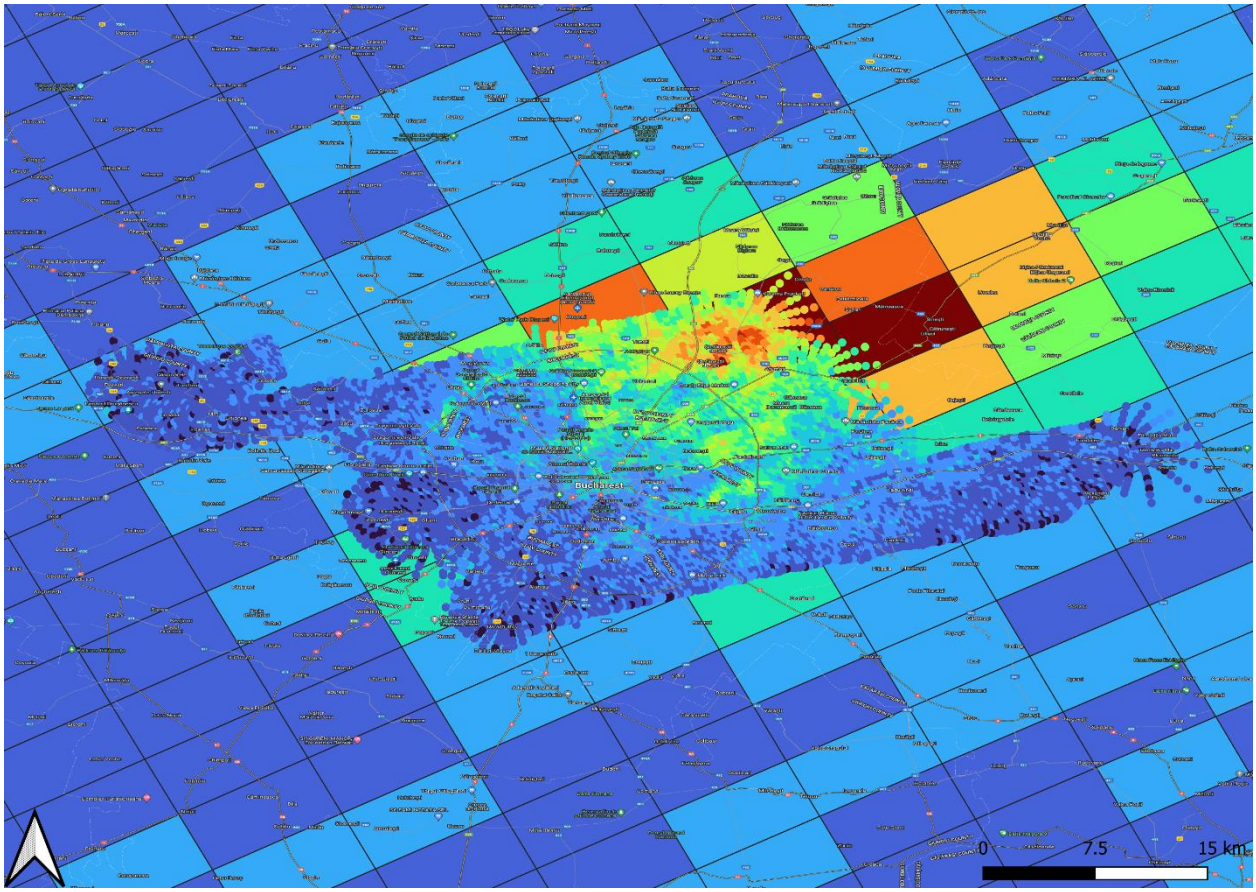

Figure 62. SWING+ vs TROPOMI VCDs for 30 Sept 2022

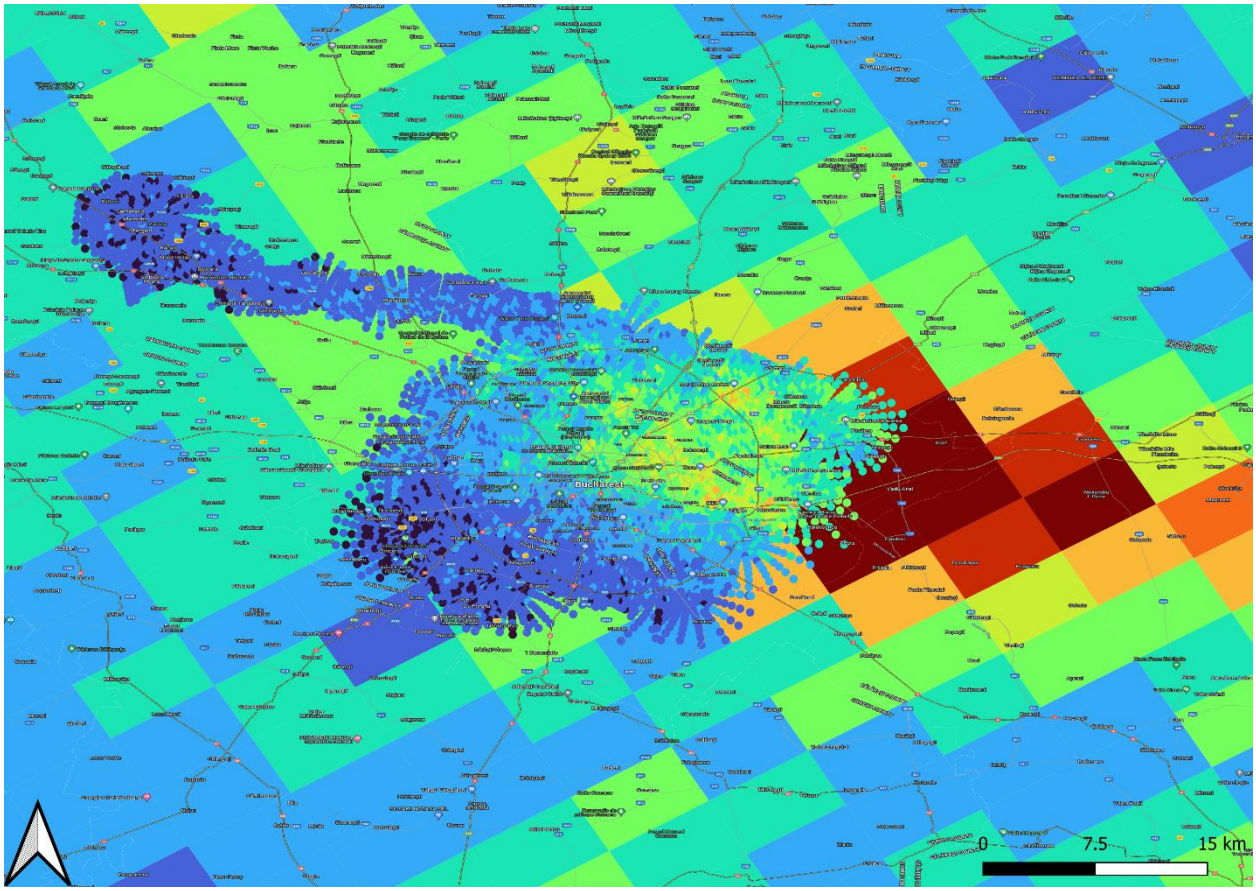

Figure 63. SWING+ vs TROPOMI VCDs for 2 Nov 2022

2.2.10 Dissemination and outreach activities (conference participation, articles, dissertations, etc)

2.2.10.1 *Conference participation:*

No.	Conference title, dates, location	Title of the presentation and authors	Conference website
1	ATMOS 2024, 1-5 July 2024 Bologna, Italy	P 3.12 Evaluation of decadal regional and local NO_2 column densities using space-borne instruments and CAMS Authors: S.M. Nicolae, A.M. Dandocsi, A. Ilie, and A. Nemuc	https://www.atmos2024.org/programme
2		P4.3 Validation of Aerosol Layer Height product from space-borne instruments using ACTRIS' active sensors Authors: A.M. Dandocsi, S. Nicolae, A. Nemuc, L. Belegante	

3	Living Planet Symposium, Bonn, Germany, 27 May 2022	Alpha-lidar: Continuous Daytime Raman Depolarization Lidar for ESA Cal/Val Authors: L. Belegante, D. Nicolae, G. Giorgoussis, D. Ene, A. Dandocsi, C. Radu	https://www.lps22.eu/
4	International Workshop on Greenhouse Gas Measurements from Space - IWGGMS17, United States of America, online, 14 Jun 2021	Using the COllaborative Carbon Column Observing Network for validating space borne GHG sensors Authors: M.K. Sha, B. Langerock, M. Kiel, D. Dubravica, F, Hase, T. Borsdorff, A. Lorente, M. De Mazière, C. Alberti, S. Ars, C.A. Bauer Aquino, B.C. Baier, D. Balis, C. Bes, E. Blandin, T. Blumenstock, H. Boesch, A. Butz, J. Chen, **A. Dandocsi**, A. Dehn, F. Dietrich, J. Franklin, M. Frey, S. Jeong, I. Morino, T. Newberger, O.E. García, E. Gottlieb, M. Grutter, P. Heikkinen, N. Humpage, N. Jacobs, R. Kivi, M. Lopez, E. Marais, M. Mermigkas, **A. Nemuc**, N. Pak, M. Pathakoti, M. Ramonet, S. Roche, A.N. Röhling, H. Ohyama, G.B. Osterman, H. Park, D. Pollard, V.K. Sagar, M.V.R.S. Sai, K.A. da Silva, D. Schuettemeyer, W. Simpson, W. Stremme, N. Taquet, Y. Té, Q. Tu, F. Vogel, D. Wunch;	

2.2.10.2 *Dissertations*

Master thesis

Date: June 2024
Name of the student: Gabriela Ciocan INOE, Romania
Title: Caracterizarea proprietatilor optice și a tipurilor dominante de aerosol atmosferic din Europa/ Characteristics of optical properties and dominant aerosol types for atmospheric aerosol over Europe”
Department "Environmental Physics and Eco-Friendly Materials",
University: Faculty of Physics, University of Bucharest, Bucharest, Romania

Bachelor’s thesis

Date: June 2023
Name of the student: Stefan Nicolae, INOE, Romania
Title: "The FTIR technique in greenhouse gases studies"

University: National University of Science and Technology Politehnica Bucharest, Faculty of Applied Sciences, Bucharest, Romania

2.2.11 Conclusions

During QA4EO, Romanian teams succesfully followed the protocols established during previous campaigns and RAMOS project, coordonating the integrated ground-based and airborne facilities for Cal/Val activities.

2.2.11.1 *Ground based measurements*

The ground-based devices operated effectively, and no significant issues were encountered.
Amethod for comparing S5P data and ground-based PANDORA measurements was created during the RAMOS project and was also applied to data analysis during QA4EO. The values obtained from ground-based observations of Pandora - 2S over Magurele, Romania, are very close to the total column and summed NO_2 values obtained from the Tropomi sensor.
In relation to the Tropomi ALH product, we have been comparing aerosol layer heights from ground-based active remote sensing data using two alternative methodologies. The Tropomi ALH product showed a stronger correlation with the one used to calculate the ground-based Center of Mass of aerosols in a layer using the backscatter profiles obtained from Cloudnet ceilometers, applied for extensive data sets. During QA4EO TROPOMI data did not show any ALH retrieval over Bucharest.

2.2.11.2 *Airborne measurements*

Conclusions

- The dataset spans the entire year, encompassing 10 flights with an average mission time of 2.5 hours per flight. This comprehensive dataset includes detailed profile information from both in-situ and remote sensing sources, which will be used for enhancing the characterization of TROPOMI products over Bucharest. The performance of all instruments was satisfactory, meeting the operational expectations, while the infrastructure supporting these instruments demonstrated reliability and effectiveness throughout the data collection period.
- During the course of the project, many valuable lessons were learned. One significant insight was the detailed revelation of the spatial distribution of pollutants across Bucharest. The data highlighted distinct emission patterns throughout the city, providing a clearer understanding of how pollutants are dispersed in different areas. Additionally, a good correlation was observed between the SWING+ data and TROPOMI data, underscoring the reliability and accuracy of the instruments used in the project. This correlation validates the effectiveness of the measurement techniques and enhances confidence in the findings.
- To ensure optimal performance in future missions, concerted efforts are underway to further improve the stability and precision of the instruments onboard the BN2 aircraft. These efforts are crucial in maintaining and elevating the high standards of data quality required for future research missions. The meticulous process involves refining the calibration procedures, enhancing the robustness of the instrumentation against environmental variables, and implementing advanced data validation techniques.
- Moreover, continuous training and development programs are being instituted for the operational teams to keep up with the latest technological advancements and methodologies. This holistic approach aims not only to ensure the reliability of the current dataset but also to prepare for future missions to achieve even higher levels of accuracy and efficiency. By addressing these aspects comprehensively,

the mission aims to provide robust data that will significantly contribute to the scientific understanding and environmental monitoring capabilities over Bucharest in the context of calibration and validation of current and future Earth observation missions.

2.3 COCCON ground based FTIR deployments

2.3.1 Objectives

Ground-based column averaged measurements of greenhouse gas concentrations are an important data source for validation of space-borne GHG missions. The practical realization of such measurements typically relies on FTIR spectrometers. This is a very well-established technique, which allow broad spectral coverage while achieving sufficient spectral resolution to resolve the molecular bands into individual ro-vibrational lines. The GHG concentrations derived from solar absorption spectra recorded in the NIR from ground offer similar vertical sensitivity characteristics as the space-borne measurements, resulting in comparable observables between ground-based and space-borne sensors, which is an important requirement for a validation data set. In Section 2.3.2, we explain why the data products derived from ground-based measurements achieve the character of a reference point when compared to data retrieved from space-borne observations.

Today, there are two established networks delivering such reference XGAS observations from FTIR observations: the TCCON and COCCON. COCCON offers the advantage over TCCON that it uses portable spectrometers, which can be deployed on campaign basis. COCCON spectrometers can be relocated, while preserving their instrumental characteristics (as the instrumental line shape). COCCON mostly uses the EM27/SUN FTIR spectrometer, which has been developed by KIT in cooperation with the company Bruker, a well-known manufacturer of FTIR spectrometers. Details can be found in the reference documents (Gisi et al., 2012 & Hase et al., 2015). In its final configuration as used today, the EM27/SUN spectrometer measures solar spectra in the spectral range of about 4000 to 10 000 cm^{-1} using a pair of detectors. The main detector covers the 5500 to 10 000 cm^{-1} range, while the auxiliary detector covers the 4000 to 5500 cm^{-1} range. The addition of the auxiliary detector allows to cover the same spectral region as used by TROPOMI and allows the measurement of XCO.

The objective of the COCCON activities from the viewpoint of QA4EO is to provide a reference data set for the validation of TROPOMI XCH4 and XCO data, covering a wide range of different geophysical conditions and ground albedo and using this data set for ensuring that the data provided by the S5P mission meet the mission requirements.

2.3.2 Comprehensive introduction of the context

The ground-based solar absorption approach offers significant advantages: because the spectral intensity of the solar disc is so high, the fraction of scattered photons is negligible

and a pure absorption measurement results. When working in the limit of pure absorption, no proper ordinate calibration of the spectra is required (the amount of atmospheric absorption is derived from the measured local spectral contrast between spectral lines and adjacent continuum), and the radiative transfer problem approaches the simple Lambert-Beer limit. Moreover, the co-observed 1.26 μm oxygen band provides a highly accurate airmass reference (the fluorescence occurring in this band is outshined by the solar disc intensity). Grossly, these characteristics substantiate the reference character of ground based solar absorption FTIR observations.

For the satellite observations, the uncertainty budget is bigger for various reasons: (1) Typically, the available spectral resolution is lower than in the ground-based measurement. (2) The observed terrestrial ground scene is much darker that the solar disc, so a much lower photon flux is available, resulting in lower signal-to-noise ratio. (3) The ground scene can be inhomogeneous within a satellite pixel with respect to topography, atmospheric state and optical behaviour of the ground area. (3) The resulting radiative transfer problem is much more complex, and depends on ground albedo and BDRF, and the presence and vertical structure of aerosol. (4) A mixture of photon path lengths results, and the complete description of scattering even needs to incorporate the polarization state of the photons as well.

2.3.3 Description of timeline and instruments

COCCON has implemented a strict scheme for instrumental characterisation and for common data analysis and data dissemination. We will discuss data analysis and data dissemination in sections 2.3.5 and 2.3.6 below and provide here some further information on the instrumental quality assurance and characterization.

For the quality assurance and quality checks of individual EM27/SUN spectrometers as required by COCCON, laboratory tests and solar-side-by-side measurements are performed on each spectrometer before commissioning. The laboratory tests encompass an evaluation of the optoelectronic and mechanical health status of the spectrometer, and verifies the optical and interferometric alignment. In the next step, laboratory open path and gas cell measurements are performed for pinning down the ILS, for evaluating channeling effects (due to optical resonances), and for revealing undesired double passing of the radiation through the interferometer. If the investigated characteristics do not meet COCCON expectations, the spectrometer under test is revised in cooperation with the manufacturer. The final step of the procedure are solar side-by-side measurements next to the COCCON reference spectrometer which is operated continuously by KIT (SN37) and the TCCON station Karlsruhe. These measurements verify the quality of the solar measurements. Residual discrepancies of derived XGAS amounts between the spectrometer under evaluation and the reference spectrometer are taken into account by empirical instrument- and gas- specific calibration factors, which are listed for all spectrometers. The publications by Frey et al., 2019 and Alberti et al., 2022, provide further details and results for all EM27/SUN spectrometers, they are listed here among the reference documents.

2.3.4 Report on the activities performed

2.3.5 Data analysis

The data analysis chain as required by the COCCON relies on the PROFFAST software suite, which recently has been complemented by the wrapper PYLOT for supporting user-friendly analysis of large observational sets. The complete software suite is publicly available including the sources, which are distributed under GNU public license for ensuring transparency and unrestricted public accessibility of the codes by the scientific community. The PROFFAST code is coded in FORTRAN, supporting FORTRAN 2003 standard, and the PYLOT is coded in Python. The development of PROFFAST is supported by ESA through the projects COCCON-PROCEEDS I-III, COCCON-OPERA, and FRM4GHG I&II.

The PROFFAST work chain is comprised of two steps: (1) the preprocessing, which generates spectra out of raw interferograms, and (2) the subsequent trace gas analysis, which works on the spectra previously generated by the preprocessing.

The preprocessing step also includes a wide range of quality checks (as DC level, variability of DC level as function of OPD, spectral abscissa calibration, absence of out-of-band spectral artefacts), and generates spectra for subsequent trace gas analysis only out of raw interferograms which appear flawless.

The quantitative trace gas analysis uses the spectra generated by the preprocessing and further auxiliary data, specifically ground pressure recorded at the location of the spectrometer and the a-priori trace gas profiles. The latter are retrieved from TCCON in order to maintain a common choice of a-prioris between both networks. Details on the generation of TCCON a-priori profile generation are discussed by Laughner et al, 2023 (see reference documents). The trace gas analysis starts with a tabulation of daily spectral cross-sections for each gas according to the provided meteorological information (ground pressure, temperature and trace gas profiles as provided by TCCON) and afterwards performs least squares fitting on each spectrum measured during the local day. The final step is a post-processing with empirical gas- and instrument- specific empirical corrections, similar to what is done by TCCON.

The proper tying of COCCON data to the TCCON gas scales is achieved by implementation of gas-specific calibration factors. These adjustments bring the data of the COCCON reference spectrometer in agreement with the official TCCON data collected by the collocated TCCON site Karlsruhe. This empirical tying between networks is meanwhile widened by including comparisons involving further COCCON spectrometers and TCCON sites. The level of consistency between TCCON and COCCON reached by this strategy is reviewed in the thesis by Herkommer, 2023 (section 3.2.2, 2023, see reference documents). From this, it can be estimate that the agreement in XCO2 is within 0.1%, the agreement in XCH4 is within 0.2%, and for XCO it is within 1.6%. The evaluation is based on comparisons involving three COCCON spectrometers (the reference SN37 and two additional COCCON spectrometers, SN39 and SN132), and two TCCON stations (Karlsruhe + Sodankyla). Thereby, the errors reported above are fed from both the global bias between the two networks and residual station-to-station

and spectrometer-to-spectrometer biases. When interpreted as a global network bias, the reported numbers should therefore be regarded as upper estimates.

2.3.6 Data format

COCCON data are disseminated in a GEOMS-compatible HDF format via ESA's EVDC data portal (https://evdc.esa.int). For proper citation of the data, a unique DOI is attached to each published data set. The landing page of the COCCON data repository is hosted by KIT (https://www.imk-asf.kit.edu/english/3884.php). The landing page lists all operational sites of COCCON as well as historical campaign activities. The link provided to each list entry directs to the data sets on the EVDC data portal, if data have been made available. As a specific example, the data collected at the permanent COCCON site Magurele near Bucharest is found under entry "Magurele, Romania INOE Spectrometer SN072 Lat = 44.344°, Lon = 26.012°, Alt = 71 m" with two links corresponding to data revisions Version 01 and 02.

The currently available COCCON data also can be found directly by using the search function of the EVDC page. By using EVDC's "Search Cal/Val data" option on the EVDC entry page and then submitting for "data source type" the option "FTIR.COCCON" a list of all data sets collected in a selected time frame (to be set in the "time and location" box) can be generated. EVDC also displays graphically the geographic distribution of COCCON measurement sites. If the time window is set to range 1. 1. 2020 to 11. 12. 2023, all 1959 COCCON data sets collected during this time frame are listed (access: 11. 12. 2023). As a specific example, if in addition the location selection is set to "Magurele" and the time window kept, the 49 measurement days collected at the Magurele site are found and the global station map is redrawn zoomed on the Magurele site region.

2.3.7 Main results achieved, including comparison with S5p data

The dedicated CCN1 activity of deployment of a spectrometer in Brazil was processed successfully only from the formal viewpoint: the spectrometer was calibrated properly according to COCCON requirements before the deployment, and this was redone after the campaign for proving the claimed high level of instrumental stability of COCCON spectrometers. Unfortunately, the deployment occurred during the peak phase of the Covid-19 pandemia, and site operation at the Porto Velho Campus did not happen because the Campus remained permanently closed during 2021. The spectrometer arrived under ATA carnet end of December 2020. Finally, the potential option of compensating for this period of externally enforced inaction by realizing a prolonged deployment of the spectrometer did not work out. Most countries accept ATA carnet extensions of imported goods for a second year (the original carnet offers annual validity), but unfortunately, Brazil decided to abandon the international community of ATA carnet member states in 2021 and refused the further handling and extension of the existing carnet. For this reason, the spectrometer had to be removed before expiration of the carnet in end of October 2021. At least, as described in detail in the previous deliverable D1e-CIP (Porto Velho Campaign Implementation Plan Brazil campaign), the functionality and stability of the spectrometer under the event of transcontinental relocations and

several months storage has been verified. However, the EVDC portal proves that COCCON as an entity remained operational even during the peak phase of Covid-19: 684 measurement days were collected by COCCON sites in the time window from April 2020 until end of 2020.

Several papers using COCCON activities listed in the QA4EO COCCON campaign implementation plan were published, all indicating that TROPOMI XCH4 and XCO meet the requirements. Tu et al. 2020 used boreal COCCON data collected in Kiruna and Sodankyla for TROPOMI validation including the demonstration that TROPOMI is capable of detecting the weak gradients expected in XCH4 fields in that region. Alberti et al, 2022 investigated boreal COCCON data collected in Russia (the field deployment became possible through the H2020 project VERIFY), including a validation of TROPOMI XCH4 and XCO data products, showing excellent agreement for XCH4. For XCO, a high bias of TROPOMI of about 5% is indicated, which, however, is well within the mission's bias requirements of 15%. Mermigkas et al., 2021, used a comprehensive COCCON data set collected at the Thessaloniki site for demonstrating that TROPOMI XCO and XCH4 data products are well within the mission requirements (+3.0% for XCO and -0.07% for XCH4).

2.3.8 Dissemination and outreach activities (conference participation, articles, dissertations, etc)

The previous, current and planned COCCON activities have been presented by F. Hase in the framework of several invited talks: (1) a talk for JPL's "Carbon Club" seminar (Aug 8, 2022), (2) a talk in the framework of the annual meeting of the recently founded Chinese international scientific organization AERSS (Nov 29, 2022) (3) talks on COCCON progress in the framework of breakout sessions of the semi-annual OCO Science Team meetings (in Oct, 2023; Oct 2022; March 2022; Oct 2021). Furthermore, COCCON capabilities were presented in the framework of the MicroCarb and CO2M validation workshop hosted by EUMETSAT (Paris, July 7, 2023).

A highly important publication was the update paper on COCCON calibration activities, including the description of refined experimental and data analysis procedures, a revision of all previous characterization results, and the characterization of many new EM27/SUN spectrometers by the COCCON central facility operated by KIT (reference document 21, Alberti et al., 2022).

Frey et al., 2021 (see reference documents) used COCCON data collected at the Gobabeb site in Namibia (listed as a voluntary activity for QA4EO) for validation of GOSAT XCO2 measurements and for evaluating the influence of the African biosphere on XCO2 measured at the Gobabeb site. Rißmann et al., 2022, used the COCCON observatory operated by TUM for monitoring the Munich region for the validation of OCO-2 target observations. These are important outreach activities, as they demonstrate that COCCON can also support the validation of other sensors as GOSAT, TANSAT, OCO-II/III and related sensors.

2.3.9 Conclusions

We conclude that COCCON has - enabled by continuous ESA support - been developed in a highly useful reference network for the validation of space borne columnar GHG observations. COCCON measurements confirm that the quality of TROPOMI data is well within the mission requirements.

COCCON forms a valuable supplement to the existing TCCON, especially when keeping in mind that upcoming GHG missions strive for quantification of emissions on smaller scales (as CO2M or MicroCarb), the signatures of these sources will be deduced from the observed gradients of GHG columns. As COCCON spectrometers can be arranged to form arrays on relevant scales and detect gradients of GHG columns with reference quality, we expect that COCCON will be a crucial component for the validation of these missions.

2.4 Support to the MAGIC campaign

2.4.1 Objective

Gathering 50 scientists from several French institutions, the **MAGIC campaigns (Monitoring of Atmospheric composition and Greenhouse gases through multi-Instruments Campaigns**) have two main goals:

(i) to better understand the vertical exchange of GHG along the atmospheric column, in connection with atmospheric transport, sources and sinks of the gases at the surface and in the atmosphere;

(ii) (ii) to contribute to the preparation and validation of space missions dedicated to the monitoring of greenhouse gases.

To address these objectives, various instruments are deployed on various platforms: aircraft, balloons, ground. They perform simultaneous observations of GHG concentration: direct in-situ observations at the surface or along the vertical, total and partial weighted columns.
With regards to QA4EO, the main objective of this activity is to contribute to the validation of the column averaged abundances of methane and carbon monoxide derived from Sentinel-5P observations.

2.4.2 Comprehensive introduction of the context

Carbon dioxide (CO_2) and methane (CH_4) are the two main greenhouse gases (GHG) emitted by human activities. To better understand their concentration and vertical distribution in several key regions and to prepare future space missions dedicated to GHG, since 2018, annual campaigns have been organized by CNES and CNRS, with additional support from ESA, EUMETSAT, Ecole polytechnique, CEA, Météo-France and the Universities of Versaille-Saint-Quentin, Lille, Reims and Sorbonne.

MAGIC campaign 2019 took place between 11-21 June 2019. It involved 7 laboratories (LMD, LSCE, GSMA, LOA, LERMA, LPC2E, OPGC), CNES and SAFIRE.

2.4.3 Description of the timeline and instruments

2.4.3.1 *Falcon20 flight objectives and pattern*

All planned flights have been made. Overall, three flights of 3h30 were performed.

June, 13th: first flight of SAFIRE Falcon20
The day was devoted to intensive measurements around ASA: 3h30 flight in a radius of 15 knots around the station, with 4 ascents / descents of the Falcon20 between 0 and 11 km altitude. The objective was to measure the spatiotemporal variability of temperature, humidity, CO_2, CH_4 and CO profiles.
The flight report is:

- 8:50: take-off from Francazal-Toulouse airport.
- 9:11-9:56: first up-down profiling at Aire-sur-l'Adour.
- 9:58-10:42: second up-down profiling at Aire-sur-l'Adour.
- 10:43-11:25: third up-down profiling at Aire-sur-l'Adour.
- 11:44: landing at Francazal-Toulouse airport.

June, 18th: second and third flights of SAFIRE Falcon20
This day is 'the' MAGIC day with all sites connected by the 'Tour de France' flight of SAFIRE Falcon20. In addition to the objectives of the first flight, the objective was to connect each site and give an overview of the overall evolution of greenhouse gases in France, with colocation with satellites. Two successive flights of 3h30 were made by Falcon20:

- First flight:
  - 6:45: take-off from Francazal-Toulouse airport.
  - 7:00-7:40: 20m-11lm profiling at Aire-sur-l'Adour
  - 8:40-9:20: profiling over the Atlantic ocean
  - 9:30-9:45: profiling over Bricy airport, next to Trainou station.
  - 10:10: landing for refueling at Chateauroux airport.
- Second flight:
  - 11:25: take-off from Chateauroux airport.
  - 11:48-12:06: profiling over Bricy airport, next to Trainou station.
  - 12:20-13:08: profiling over Orléans.
  - 13:40-14:25: profiling over Aire-sur-l'Adour.
  - 14:42: landing at Francazal-Toulouse airport

2.4.4 Falcon20 instrument status and data acquisition for individual flights

The three in-situ instruments onboard the Falcon20 work nominally during the flight. However, an issue with CO2 has been detected during first analysis of the data. Only , CH_4, CO and N_2O data from the 2 Picarro G2401-m and SPIRIT can be used.
Overall, 26 dropsondes were released. Two dropsondes were deficient and replaced on-site by a new one. Overall, 24 drospondes are available for exploitation.

2.4.4.1 *Balloon flights*

In addition to Falcon20 flight, meteorological balloons were launched from CNES balloon station at Aire-sur-l'Adour (ASA), Puy-de-Dôme (PDD) and Trainou (TRN). Flights details are given in the following table.

The objectives were to launch balloons at the overpassing time of Falcon20 and IASI, OCO-2 and Sentinel-5P satellites in order to intercompare aircraft-balloon profiles, as well as to validate satellite weighted columns.

Instrument	Station	Date	Launch time	Landing time
AirCore	ASA	13 June	6:20	8:26
			7:44	9:01
			8:52	10:05
		17 June	11:31	13:33
		18 June	5:29	7:35
			9:16	11:18
			12:00	14:01
		19 June	10:52	13:15
			11:59	14:02
	TRN	11 June	10:47	13:36
		17 June	12:29	14:29
		18 June	10:42	12:34
		20 June	7:04	9:13
		21 June	8:13	10:01
	PDD	17 June	11:00	13:25
		18 June	10:00	12:25
		19 June	11:30	13:42
Amulse_CO2	ASA	13 June	10:56	12:54
		18 June	7:41	9:51
		19 June	11:01	13:17
Amulse_CH4	ASA	13 June	8:16	9:35
		17 June	10:29	11:47
		18 June	11:58	13:30

Table 11 List of balloon flights during the MAGIC2019 campaign.

2.4.4.2 *SAFIRE Falcon20*

Based at Toulouse-Francazal airport, the SAFIRE Dassault Falcon 20 f-GBTM is available for scientific operations since 2006. This aircraft is mainly used for multidisciplinary research in the upper troposphere and low stratosphere: remote sensing, chemistry, microphysics. It has been greatly modified in order to be able to board a wide variety of atmospheric and environmental measurement instruments. Nose perch, large

portholes under and over the fuselage, underwater wing stakes, interior fittings including a specific electrical and computer network make it a true flying laboratory.
During the MAGIC2019 campaign, the Falcon 20 ships are equipped with two G2401-m laser diode analyzers developed by the company Picarro and allowing the very precise measurement of the concentration of CO_2, CH_4 and CO. Under the wings, CDP (Cloud Droplet Probe) instruments measure the size of atmospheric particles (water droplets, aerosols). In addition, dropsondes are realeased to make measurements of thermodynamic variables. The crew on board a flight is composed of seven people: 2 pilots, 1 technician, 3 engineers and 1 scientist.

2.4.4.3 *AirCore: An atmospheric sampler for measuring concentration profiles*

The AirCore (Membrive et al., 2017) flown during MAGIC campaigns is an atmospheric sampler developed by the Laboratoire de Météorologie Dynamique (LMD, CNRS / Ecole Polytechnique / ENS Paris / Sorbonne University), flying under a meteorological balloon. It allows the measurement of the vertical profiles (from the surface up to 30 km of altitude) of atmospheric concentration of greenhouse gases (CO_2, CH_4 and CO). Its concept, based on an idea proposed by the NOAA, is extremely simple: it consists of a long tube of stainless steel placed under a meteorological balloon which, in the ascending phase, empties its air by its open end, to fill with air during its downward phase. The captured air column is then interpreted in terms of the vertical gas concentration profile using a Picarro type laser diode analyzer. This system makes it possible to access altitudes not attainable by aircraft flights and to obtain very good vertical resolution. Since 2013, the LMD has developed several versions of this instrument and has deployed them, in partnership with CNES, LSCE (CNRS / CEA / University of Versailles-Saint-Quentin-en -Yvelines) and OPGC (CNRS, Blaise Pascal University), in various places of the globe.

During the MAGIC2019 campaign, AirCore releases were made by the CNES teams at the Aire sur l'Adour site (Landes), by LSCE at the Trainou site (Loiret) and by OPGC at Puy-de-Dôme (Clermont-Ferrand). The preparation of all the instrument and the analysis of the results are carried out by LMD.

2.4.4.4 *Amulse: A laser-diode spectrometer for measuring concentration profiles*

The AMULSE light laser diode spectrometer (Joly et al., 2020) developed by the Group of molecular and atmospheric spectrometry (GSMA, CNRS / University of Reims Champagne-Ardenne) since 2014 allows the measurement of greenhouse gases (CO_2, CH_4 and H_2O) under different types of platforms including weather balloons, captive balloons and drones. The principle of this instrument is based on direct absorption laser spectrometry coupled to Wavelenght Modulation Spectroscopy (WF) spectrometry (2f / 1f) which allows accurate (<1%) and fast (<1s) measurement. In recent years, the instrument still less than 3 kg (limit for legislation under expandable light balloon) has followed several evolutions in terms of the number of detectable gases and better sensitivity limits. Currently, the instrument's performance allows a high spatial resolution (<10 m) with measurements @ 10 Hz and a precision of less than 0.2% on the ground and 3% at 30 km altitude.

During the MAGIC2019 campaign, 4 AMULSE launches were made by the CNES teams at the Aire sur l'Adour site in concomitance with the release of AirCore. The preparation of the instrument, its recovery and the analysis of the results were done by GSMA.

2.4.4.5 *EM27/SUN*

The EM27/SUN is a portable Fourier transform spectrometer. It is equipped with a camera-controlled heliostat that returns solar radiation to the spectrometer with constant direction. The high resolution (of 0.5 cm^{-1}) makes it possible to solve the lines of the minority compounds of the atmosphere. The spectrometer records infrared spectra between 2.5 and 0.8 micrometers with two detectors. A radiative transfer software is then used to determine the total column of the different minority constituents of the Earth's atmosphere from the recorded spectra.

During the MAGIC2019 campaign, three EM27/SUN were deployed at Aire-sur-l'Adour (operated by CNES), Trainou (operated by LSCE), Puy-de-Dôme (operated by LERMA) and Bourges (LSCE instrument operated by LMD).

2.4.5 Data analysis

2.4.5.1 *Transcribing the instrument data from campaign disks to a dedicate campaign archive*

The raw data are collected by the team in charge of each instrument. Picarro data are collected by SAFIRE and downloaded directly to SAFIRE archive after the flight. SPIRIT data are copied to LPC2E archive facility.
Balloon trajectory raw data are collected after payload recovery by each time, put on lab servers and then transferred to a common MAGIC archive.

2.4.5.2 *Consolidating the campaign data acquisition logs (e.g., flight reports).*

Falcon20 flight reports are made available less than 1h after filght by SAFIRE. Details on instrument acquisition and mode changes are detailed.
Balloon flight reports are made during each launch and payload recovery. They are gathered by the PIs, scanned and archived.

2.4.5.3 *SAFIRE Falcon20*

Raw data measured by Falcon20 are provided by SAFIRE team one day after every flight. They are sent to Meteo-France who is in charge of processing them and putting them on the WMO scale. The processing takes about one month. Data are then provided to the scientific team in a NASA-AMES format.

Concerning the measurements of gas dry mixing ratio by the Picarro G2401-m oblard SAFORE, data are sent to LSCE who is in charge of processing and calibrating them, using the reference WMO scale for GHG. Data are then sent back to the scientific team in NASA-AMES format who is in charge of unifying flight data and Picarro data.

2.4.5.4 *AirCore: An atmospheric sampler for measuring concentration profiles*

Processing of air samples acquired by AirCores is described in Membrive et al. (2017). First, each team in charge of balloon launches and payload recovery make an on-ground analyses of the air samples using Picarros G2401 after payload recovery. Calibration to WMO scales in insured by the use of gas targets bottles during the analyses.

The time series of gas mixing ratios are then sent to LMD for a processing that consists in combining flight data (pressure, altitude and time) and mixing ratios time series to produce vertical profiles of mixing ratios of CO_2, CH_4 and CO. Processed data are given in NASA-AMES format. The file header gives all information on the flight (launching and landing times and locations, etc) and potential issues (loss of data, electronic failure, delay in the recovery, etc). The whole processing takes about one month.

2.4.5.5 *Amulse: A laser-diode spectrometer for measuring concentration profiles*

The measurements acquired by Amulse laser-diode spectrometers are performed by GSMA following the procedure discribed in Joly et al. (2020). It is based on semiconductor diode lasers because they offer a continuous-mode emission, are tuneable and have a relatively low noise amplitude. The diodes emit in the near-infrared spectral region (NIR) where most greenhouse gas molecules feature suitable absorption lines. Direct absorption spectroscopy is the simplest application of this technique, and it is well adapted to in situ measurements. It requires that the tuneable laser beam with an intensity of I_0 passes through the gas sample on a distance L and is then measured using a detector. When the frequency of the emitted light is close to a molecular transition v_0 of the gaseous sample, the light is then absorbed and the transmitted intensity $I(v)$ decreases. The concentration of the absorbing species in the gas mixture is then calculated according to Beer's law. The whole processing takes about one month.

2.4.5.6 *EM27/SUN*

A common pre-processing tool PREPROCESS for the recorded interferograms is available (deliverable in the framework of the ESA project COCCON-PROCEEDS) and used, which allows immediate generation of spectra from raw interferograms. The first step along the pre-processing chain is the recognition of observations taken under poor conditions (solar signal too low or too variable during interferogram recording): from such measurements no spectra are generated. Afterwards, the code applies an exhaustive set of quality checks along the subsequent processing chain on each measurement, so that instrumental or operational problems can be uncovered by the operator in a timely

manner. The final output generated by PREPROCESS from each measurement which passed all quality checks is the desired spectrum. This spectrum is derived applying a fast Fourier Transform of a DC-corrected interferogram (which in turn was calculated from the raw interferograms before), making use of a dedicated phase correction scheme for the EM27/SUN spectrometer. The preprocessing code is provided by KIT under Creative Commons license and can be downloaded from the central facility's webpage (https://www.imk-asf.kit.edu/english/COCCON.php).

For the MAGIC2019 campaign, all EM27/SUN data have been processed by LSCE using the tools providing by KIT. Comparisons of code outputs have been made for consistency.

2.4.6 Quicklooks

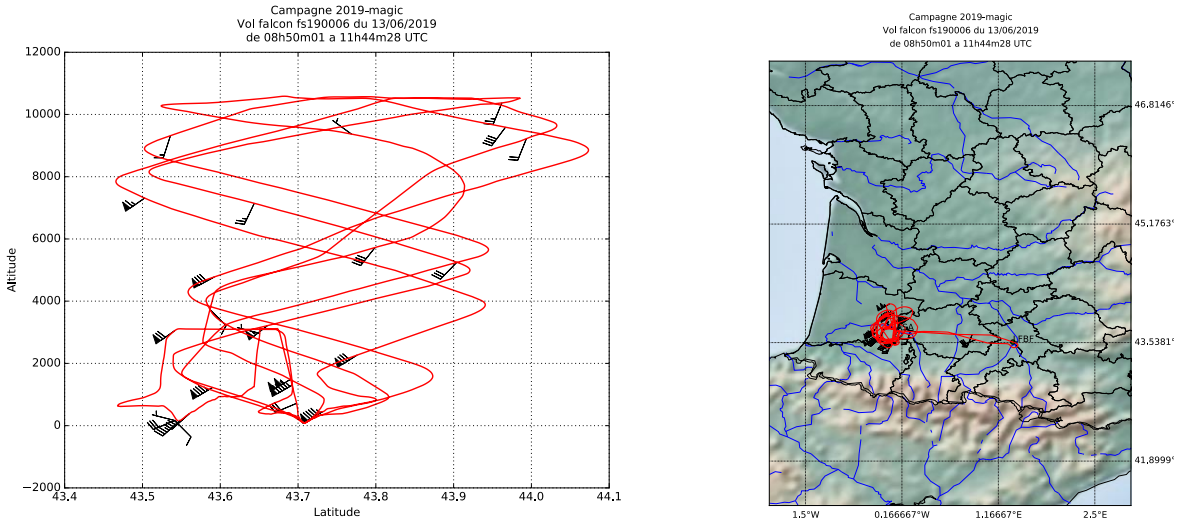

Figure 64 Quicklook of SAFIRE Falcon20 flights on June 13th. (Left) Altitude vs. Latitude of the flight. (Right) Flight track**.**

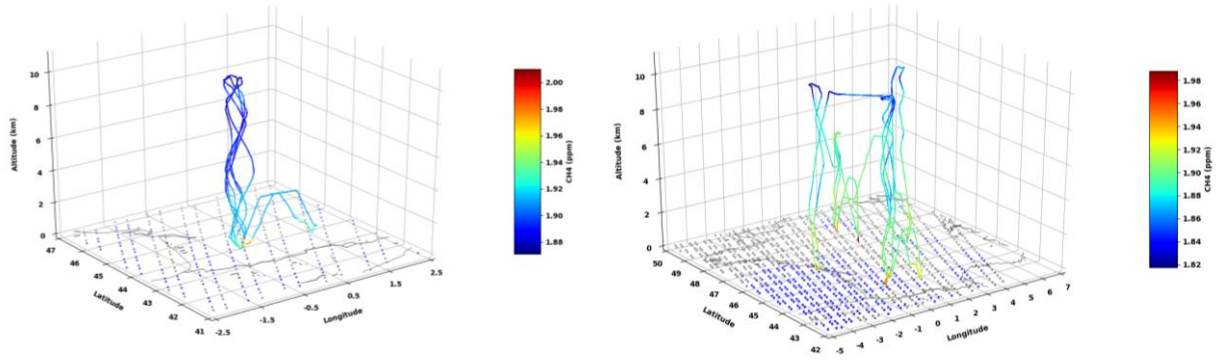

Figure 65 Quicklook of CH_4 mixing ratios measured by one of the G2401-m Picarro analysers on board SAFIRE Falcon20. (Left) On June 13th over Aire-sur-l'Adour (Right) On June 18th over France.

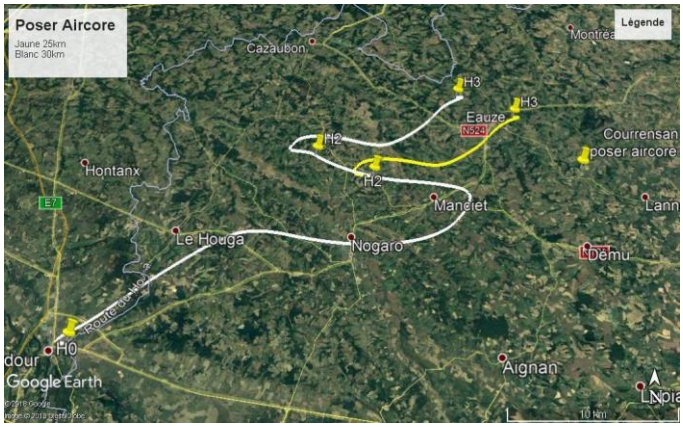

Figure 66 Quicklook of one AirCore flight trajectory from Aire-sur-l'Adour on June, 17th between 11:31 and 13:33 (expected in white and realized in yellow).

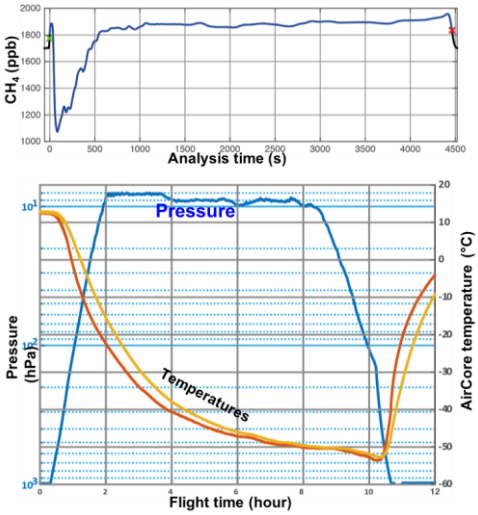

Figure 67 : (Top) Quicklook of CH_4 mixing ratio measured in the air sampler of the AirCore flight shown in Figure 66. (Bottom) Corresponding Pressure and Temperature measured during the flight.

2.4.7 Main results including comparison with S5p data

In the following, we focus on results related to the comparisons between instruments measuring profiles of CH_4, CO_2 and CO mixing ratios and on the validation of space missions operated in the short-wave infrared.

As seen in Figure 68, comparison between CO_2 profiles acquired from balloon-borne AiCrore air samples and Amulse show a very agreement (less than 0.1 ppm) between both instruments at every pressure level, up to 70 hPa. Above, Amulse measurements tend to under-estimate CO_2. This issue has been linked to the combination of an issue with the measurement of stratospheric temperature, combined to an uncertainty in the used spectroscopic parameters. It is currently being corrected by GSMA.

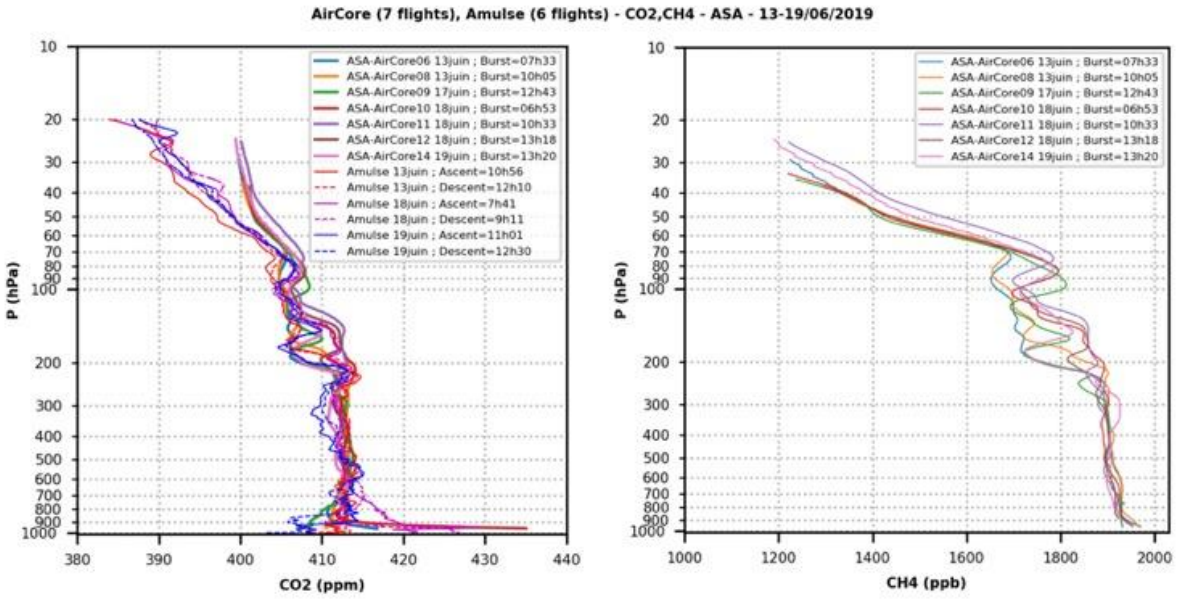

Figure 68: Profiles of CO_2 (left) and CH_4 (right) measured by 7 AirCore and 3 Amulse at Aire-sur-l'Adour.

Figure 69 shows the comparison between CH_4 profiles acquired by AirCores and measured by the Picarro G2401-m analysers on board SAFIRE Falcon20 on June 18th. When comparing the profiles obtained the same day at the same hour, the difference between both instruments is less than 2 pbb on the column. Analysis is being made to inter/extra-prolate each instrument on the same pressure grid and make point-to-point comparison. Overall, the MAGIC2019 campaign confirms that AirCores can be used to compute weighted columns of Ch_4 for validation of satellite retrievals.

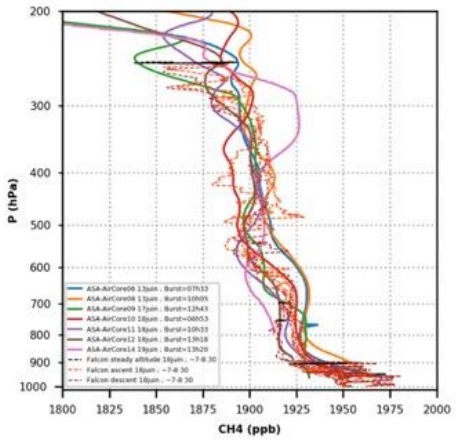

Figure 69 Profiles of CH_4 measured by 7 AirCore and Falcon20 Picarros (3 profiles) at Aire-sur-l'Adour.

Figure 70 shows the comparison between CO profiles acquired by AirCores and measured by the Picarro SPIRIT instrument on board SAFIRE Falcon20 on June 13th and 18th. AirCore CO profiles are much noisier than SPIRIT profiles due to the noise of G2401-

m Picarro analyser for the CO channel. When averaging on broad pressure layers, a small bias of -2.5 ppb up to 400 hPa seem to also exist between both instruments, even if the overall vertical structures as captured by both instruments agree well. This bias needs to be investigated since it could have an impact on the validation of satellite-derived columns of CO.

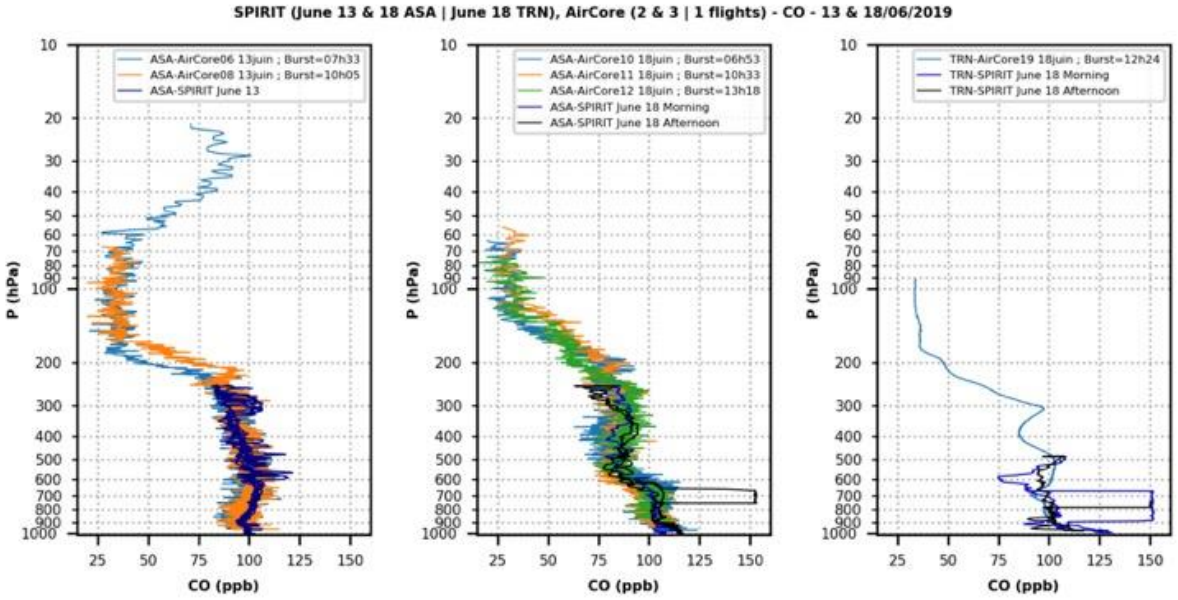

Figure 70 Profiles of CO measured by 6 AirCore and Falcon20 SPIRIT (3 profiles) at Aire-sur-l'Adour and Trainou.

Figure 70 shows the comparison between XCO_2 weighted-columns derived from AirCore/Amulse and retrieved from OCO-2 on June 13th. By applying the averaging kernels associated to retrieved XCO2 and taking into account the a priori profiles used by the ACOS team, it is possible to compare the columns. Overall, the difference between in-situ instruments and OCO-2 is -3.10 ± 1.41 ppm for the official raw XCO_2 columns and -0.39 ± 0.80 ppm for the official bias-corrected XCO_2 column. Their comparison is a direct validation of the bias correction applied to OCO-2 official products.

A similar comparison will be done for Sentinel-5P/TROPOMI XCH_4 data.

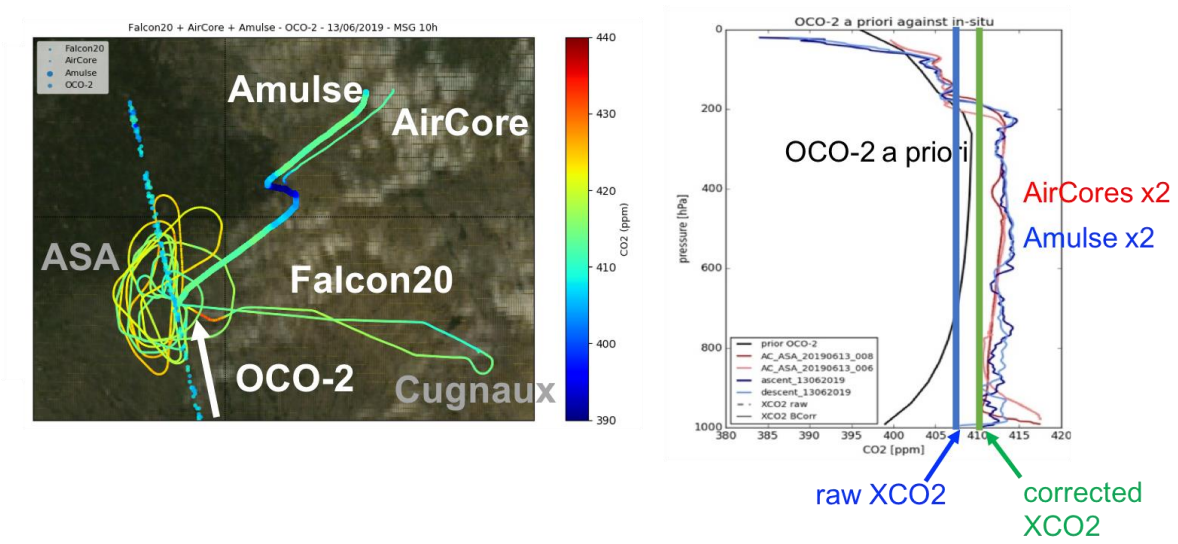

Figure 71 (Left) Map of CO_2 as measured in-situ by Falcon20/G2401-m Picarros analyserx, Amulse and AirCore and as retrieved by OCO-2 on June 13th. (Right) Profiles of CO_2 measured by 2 AirCore (red) and 1 Amulse (blue) and used as an a priori in OCO-2 XCO2 retrieval (black). Also shown are the value of the raw (blue) and bias-corrected (green) XCO2 official Level2 product.

2.4.8 Dissemination and outreach activities (conference participation, articles, dissertations,etc)

- Cyril Crevoisier, Caroline Bes, Lilian Joly, Yao Té, Michel Ramonet, Hervé Herbin, Valéry Catoire, Andreas Fix, Nicolas Cézard, Aurélien Bourdon and the MAGIC team, Overview of the MAGIC initiative for GHG and future plans, *IWGGMS-17*, 15th June 2021 [PDF]

- Yao Té, Pascal Jeseck, Corinne Boursier, Thomas Lesigne, Christof Janssen, Caroline Bès, Denis Jouglet, Cyril Crevoisier, Morgan Lopez, Michel Ramonet, Lilian Joly, A bdelhamid Hamdouni, Bruno Grouiez, Contribution to the validation of GHG space missions by the French COCCON consortium using ground-based FTIR measurements, *IWGGMS-17*, 15th June 2021 [PDF]

- Crevoisier C., Bès C. and the MAGIC team, Characterizing atmospheric vertical distributions of greenhouse gases with combined ground-based and airborne measurements to validate space missions: The MAGIC initiative, *IWGGMS-16,* 5th June 2020 [PDF]

2.4.9 Conclusions

Excellent agreement between AirCore, Amulse and Falcon20 throughout the troposphere. Over the whole MAGIC flights, CH_4 'column' difference AirCore/Amulse - Falcon20 is : -1.58 ± 6.94 ppb.Small discrepancies between AirCore and Amulse in stratospheric structures have been observed. Both AirCore and Amulse highlight overestimation of stratospheric CH_4 by several atmospheric transport models.

Conclusions after the evaluation of the merits of several instruments 'measuring' GHG:
• Successful deployment of portable EM27/SUN and CHRIS to validate various missions on a day-to-day basis: OCO-2 (XCO2), TROPOMI (XCH4), GOSAT-1/2 (XCO2/XCH4) and IASI (MT-CH4).
• Contribution to the validation of IASI during Metop-C commissioning: Temperature, humidity, trace gases.
• Some comparisons with atmospheric transport models … to be continued

2.5 Support for ACCLIP campaign (D5f-- a summary of the measurements performed during the campaign)

ACCLIP stands for Asian Summer Monsoon Chemical & CLimate Impact Project. Two aircraft (the NASA WB-57 and the NCAR G-V), outfitted with state-of-the-art sensors, and approximately 80 scientists from the US and other international research organizations participated in this campaign, middle of July/early September 2022, which started and ended in Houston TX. A total of nine transfer flights were necessary for the two aircraft to go back and forth to Osan US Air Force in South Korea. This was the ground site for 15 research flights around South Korea and above western Pacific.

2.5.1 Objectives

The Asian Summer Monsoon (ASM) is the largest meteorological pattern in the Northern Hemisphere (NH) summer season. Persistent convection and the large anticyclonic flow pattern in the Upper Troposphere and Lower Stratosphere (UTLS) associated with ASM leads to a significant enhancement in the UTLS of trace species from pollution and biomass burning origins. The monsoon convection occurs over South, Southeast, and East Asia, a region of uniquely complex and rapidly changing emissions tied to both its high population density and significant economic growth. The coupling of the most polluted boundary layer on Earth to the largest dynamical system in the summer season through the deep monsoon convection has the potential to create significant chemical and climate impacts. An accurate representation of the ASM transport, chemical and microphysical processes in chemistry-climate models is much needed for characterizing ASM chemistry-climate interactions and for predicting its future impact in a changing climate.
The scientific aim of ACCLIP was to study the Asian Summer Monsoon (ASM) anticyclon, in particular the ASM transport, chemical and microphysical processes in chemistry-climate models, for characterizing ASM chemistry-climate interactions and for predicting its future impact in a changing climate.
Scientific Objectives:
- To investigate the transport pathways of ASM uplifted air from inside of the anticyclone to the global UTLS.
- To sample the chemical content of air processed in the ASM in order to quantify the role of the ASM in transporting chemically active species and short-lived climate forcing agents to the UTLS and determine their impact on stratospheric ozone chemistry and global climate.

- To obtain information on aerosol size, mass and chemical composition necessary for determining the radiative impact of the ASM, for constraining models of aerosol formation and for contrasting the organic-rich ASM UTLS aerosol population with that of the background aerosol population.
- To measure the water vapor distribution associated with the monsoon dynamical structure to evaluate transport across the tropopause, and determine the role of the ASM in water vapor transport into the stratosphere.

2.5.2 Campaign description

This chapter contains general information about the campaign.

2.5.2.1 *The flights objectives and flights patterns*

Before leaving for the campaign, three flights were planned at Ellington Field Airport, one test flight for the integrated instruments (and for the aircraft itself), and two research flights. The first five flights and the last four flights of the campaign were transfer fligths from Ellington Field Airport in Houston TX to Osan Air Base in South Korea and vice versa.
Research flights were planned according to weather conditions and forecasts. Moreover, as one of the goals of the project was the validation of prediction models, some flights were tailored to the verification of specific pollutants distributions, announced by simulations. One flight was devoted to the study of typhoon Hinnamnor, end of august 2022, during its approach to South Korea.

2.5.2.2 *Instrument status and data acquisition during the individual flights*

COLD2 instrument provided useful results all along all the flights.

2.5.2.3 *Raw data*

Raw data from COLD2 instrument consist of two binary files for each flight. One file contains the acquired spectra, already averaged to obtain a 1-second time resolution, plus some data necessary for processing. The other file contains the housekeeping data, in order to verify the proper functioning of all the components of the instrument. These data are saved in the computer of the instrument and, once downloaded, in several computers, or data storage devices, belonging to the group operating the instrument, both on site and in the headquarter in Florence.

Subsequently, the spectral fitting is applied. All the steps of fitting lead to Level-1 (L1) data. Level-2 (L2) data are generated after a post-campaign calibration of the instrument, using a reference mixture.
A dedicated campaign data archive is kept at NASA LaRC Suborbital Science Data for Atmospheric Composition (https://www-air.larc.nasa.gov/missions/acclip/index.html),

where processed data from all instruments are stored. In this archive, each storage of a higher level data automatically erases the previous ones.

The recorded spectra and auxiliary data are sighted and stored on backup external disks immediately after each research flight.
Trace gas retrievals are then performed, and a first evaluation of the data quality is done within one the day from the measurement. The overall performance is checked, such as the time line of the recorded data, plausibility of trace gas amounts, temporal and spatial patterns as well as some first comparisons between instruments.

2.5.2.4 *Instrument acquisition timeline*

During the campaign, instruments may have measured with different time resolution. This is due to the specific detection technique, or simply because of small uncertainties in the instruments clocks. One task of data management is a reconciliation of the time stamps among all the instruments. According to the specific measurement conditions of each instrument, data average or interpolation can be necessary.

2.5.2.5 *Consolidating all available correlative data into a format to be defined by the Contractor to enable data inter-comparison*

The data format is at the moment that requested by NASA for the database in 2.5.2.3. Moreover, upon request of the Royal Belgian Institute for Space Aeronomy, another format has been considered. Data in this format are available at the url: https://spheres.ino.it/index.php/svante-acclip-data-repository/
In case of need, from the final data version, the results will be converted according to ESA requirements.

2.5.3 Description of the CO measurement

2.5.3.1 *Instrument description*

COLD2 is a laser spectrometer, based on a MIR quantum cascade laser, emitting around 4.65 micron, where sufficiently strong CO and N_2O absorptions can be found. The laser beam is splitted into three arms. The main arm is used for the measurement. The interaction between the laser and the atmosphere occurs inside a multipass cell. In this passive optical components the laser beam travels back and forth 192 times between two astigmatic concave mirrors, so reaching a total pathlength of 36 meters, in a volume of about 300 cm^3. The curvature radii of the mirrors, along perpendicular planes, differ by about 3%. With a suitable optical alignment the spots onto the two mirrors fill two rectangles. Entrance and exit occur across one hole only, in the center of one of the mirrors. The absorption profiles of the target gases are obtained by scanning the laser

current. Though the current scan is linear with time, this does not imply that the emitted frequency is linear too, as the laser behavior is not linear. For this reason, inside the instrument there is an optical reference arm. Part of the laser beam crosses a cell containing a very small amount of CO, at reduced pressure, and an optical etalon. This latter component superimposes on the laser emission profile a (roughly sinusoidal) modulation. The combination of the absorption profile of CO in the reference cell and of this modulation allows a frequency linearization of the laser scan, and an absolute assignment of frequency to each acquired point. A third laser arm is used to check the presence of CO inside the box of the analyzer.

2.5.3.2 *Description of the acquired data, processing and data quality analysis*

COLD2 provides point values of mixing ratio of CO and N_2O. This means that the external air is sampled and funneled inside the instrument, where it is probed by a Mid-InfraRed (MIR) laser beam. Due to the time resolution of the instrument (1 s), data are spaced by about 180 meters in the horizontal plane, at the cruise speed of the aircraft. The horizontal/vertical location of each measurement depends on the position of the aircraft along its route. The instrument has a constraint about the minimum sampling altitude. The first 3 km of the atmosphere are the ones where the majority of dust and water can be found. The instrument has no filter at the intake of air, in order to avoid an unwanted pressure drop inside the measurement volume. The only air treatment is heating, to avoid a too strong cooling of the multipass cell. In order to protect the optics inside the measurement volume we operate the circulation pumps for the air only above 3 km. Especially during descent, when the instrument is colder than external air, the coupling of moisture and dust could lead to a permanent stick of particles onto the mirrors, with an unrecoverable decrease of the transmitted laser power.
Moreover, the mixing ratio of CO can be strongly fluctuating in the lowest layer of the atmosphere, which is hardly predictable by the models. The instrument was designed to comply with the models features, for which measuring above 3 km is satisfactory. Because of the combined above reasons we didn't push the measurements below 3 km.
Each absorption spectrum is formed by 2000 points, equally spaced in time. The reference arm described in the previous chapter is used to linearize the laser scan. Then each scan is normalized with respect to laser power. During the scan the laser is shortly driven below threshold, so allowing the record of the zero electric value of the detector amplification chain. By using this region, and the other regions in which the laser beam is unaffected by absorptions it it possible to reconstruct an unperturbed laser emission profile, which is used for power normalization.

2.5.4 Final data validation

After refining the fitting procedure, which led to the step described in 2.5.3.2, we carried out a post-campaign calibration, in order to verify the accuracy, precision and stability of COLD2.

2.5.5 Post-campaign calibration

The instrument was optically aligned in June 2022, immediately before being shipped to Houston. All the optical components in the apparatus are either mounted in a fixed position (laser, multipass cell, detectors), or are kept in their positions, after alignment, by screws or bolts (beam splitters), or are adjustable (mirrors holders). The latter components are provided with a locking feature. At the end of the alignment this locking feature is activated, so that all the components of the optical line are “frozen”. Moreover, the selected mirrors holders (Thorlabs, Polaris Mirror Mounts) were chosen in order to provide an outstanding stability under thermal and mechanical stresses.
The overall result of these precautions is that COLD2 did not need any re-alignment both during the campaign and after coming back in our lab.
This allowed us to calibrate the analyzer after the campaign in the same operating conditions, by using a known mixture of CO in nitrogen and a gas divider.
For CO a calibration mixture should be in the range 100-400 ppbv. Such a low Mixing Ratio (MR) is hard to be found in the market with an accuracy of about 1%. For this reason we adopted a different strategy.
We purchased a mixture, 10 ppmv CO in nitrogen with an accuracy of ±2% (Air Liquide Italia Services, Laboratorio Specialty Gases, Rodano, Italy, Certificate 2023-635 rev.0, tested according to UNI EN ISO 6143). This mixture was diluted down to the required MR by using a gas divider. The diluting gas was nitrogen, namely the exhaust of a large (several cubic meters) liquid nitrogen Dewar. We are aware that, due to the close boiling temperatures (77.4 K for N_2 and 81.7 K for CO), some CO can pollute liquid nitrogen. For this reason, N_2 was purified by using a catalyst, Sofnocat 514.
Another issue is that during calibration, carbon monoxide is diluted in nitrogen only, while measurements are carried out in air. This slightly changes the frequency widths of the absorptions. This is not a problem when Direct Absorption (DA) is used as the detection technique. With DA we need to calculate the integral of the absorbance [absorbance = -log(transmission)], and this calculation is independent from the width of the absorption.
We had to modify the gas flow line. The two pumps inside the instrument, Thomas BL-G 12/085 M, work fine to produce a flow inside the multipass cell of COLD2 (very low pressure difference between gas in and gas out), but are not suitable to reach an absolute pressure of 100 mBar, when at the exit there is atmospheric pressure. So we used an external pumping unit. During flights, the exhaust of one pump is released inside the instrument, after being purged from CO by using Sofnocat 514. The modification in the pumping line implies that the interior of COLD2 was not purged against CO during calibration, contrarily to what occurs in flight. Anyway, this perturbation can be neglected. The free space path of the laser beam is less than half a meter, to be compared with 36 meters inside the multipass cell. Moreover, the pressure difference between the interior of the cell (≤ 450 mBar) and room pressure makes the two absorption contributions very different from each other, so that the fit routine can distinguish them.
We realized a gas divider by using two MKS Mass Flow Controllers (MFC), CMA10A, 1000 scc/min and GE50A, 20.000 scc/min. Table 12 shows the accuracies of the two MFCs, as a function of their set points.

Table 12: Accuracies of the used MFCs

	CMA10A	GE50A

Accuracy	±0.8% of set point for 20 to 100% Full Scale	± 1% of setpoint for > 20 to 100% Full Scale
	±0.16% of Full Scale for <20% of Full Scale	± 0.2% of Full Scale for 2 to 20% Full Scale

The relative errors increase when the set point is below 20% of Full Scale (FS). So we decided to always work at a flow ≥ 20% FS for each MFC.

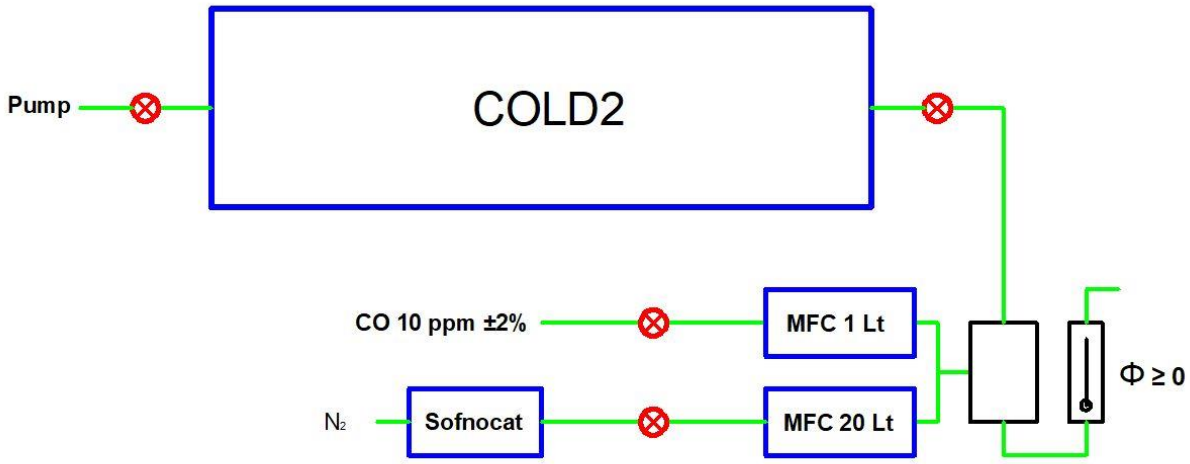

Figure 72: Sketch of the gas divider

The setup of the gas divider is shown in Figure 72. The two MFCs are computer controlled via ethernet. Before starting operations a zero flow procedure was carried out, to properly zero the two instruments. Then, in order to obtain a reasonable number of measurements, we decided to calibrate at five MRs, namely 100, 200, 300, 400, 500 ppbv. Following the above considerations about accuracy, we obtained these MRs by setting the two MFCs as in Table 13.

Table 13: Settings of the two MFCs. Total Flow is the available flow at the exit of the gas divider.

	CMA10A	GE50A	Total Flow
100 ppbv	200 scc/min	19.800 scc/min	20.000 scc/min
200 ppbv	200 scc/min	9.800 scc/min	10.000 scc/min
300 ppbv	200 scc/min	6.467 scc/min	6.667 scc/min
400 ppbv	200 scc/min	4.800 scc/min	5.000 scc/min
500 ppbv	250 scc/min	4.750 scc/min	5.000 scc/min

As for pressure, we selected the values of 138, 190 and 435 mBar. They were obtained by acting on the two valves, at the entrance and at the exit of the instrument. The only constraint was that the ball flowmeter, on the right in Figure 72, had a positive reading. This ensures that no external air is sucked into the measurement cell. So, the flow across COLD2 could never exceed the total flow of the gas divider.
Table 14 shows the results obtained in each measurement. The notation <CO> means the average of CO mixing ratio over the duration of the measurement, 5 minutes, at 1

sec. repetition rate. The reported accuracy is derived from the propagation of the errors in the HITRAN molecular database, in the fitting procedure and in the measured variables (temperature and pressure).

Table 14: Results of the measurements.

	P = 435 ± 4 mbar			P = 190 ± 6 mbar			P = 138 ± 3 mbar		
Set CO	<CO>	1 St. Dev.	Accuracy	<CO>	1 St. Dev.	Accuracy	<CO>	1 St. Dev.	Accuracy
ppb	ppb	ppb	ppb	ppb	ppb	ppb	ppb	ppb	ppb
100±3.8	101.7	0.8	4.1	101.1	3.2	4.0	99.9	1.5	4.0
200±7.6	197.9	0.6	7.9	199.5	2.9	8.0	201.1	0.6	8.0
300±11.4	293.1	2	11.7	295	1.7	11.8	293.6	1.7	11.7
400±15.2	390.1	1.9	15.6	395.1	3.1	15.8	390.9	1.1	15.6
500±19.0	495.9	1.2	19.8	489.2	2.9	19.6	492.6	0.9	19.7

Figure 73, Figure 74 and Figure 75 show the graphs of the measured mixing ratios versus set mixing ratios (red lines) with respect to “measured MR = set MR” (blue lines). In these Figures the error bars along the X axis correspond to the errors in setpoint reported in Table 14, while the error bars along the Y axis are the accuracies, in the same Table. The red lines were obtained by a linear regression of the experimental data with uncorrelated errors. The measured values always agree with the theoretical values, within experimental errors.

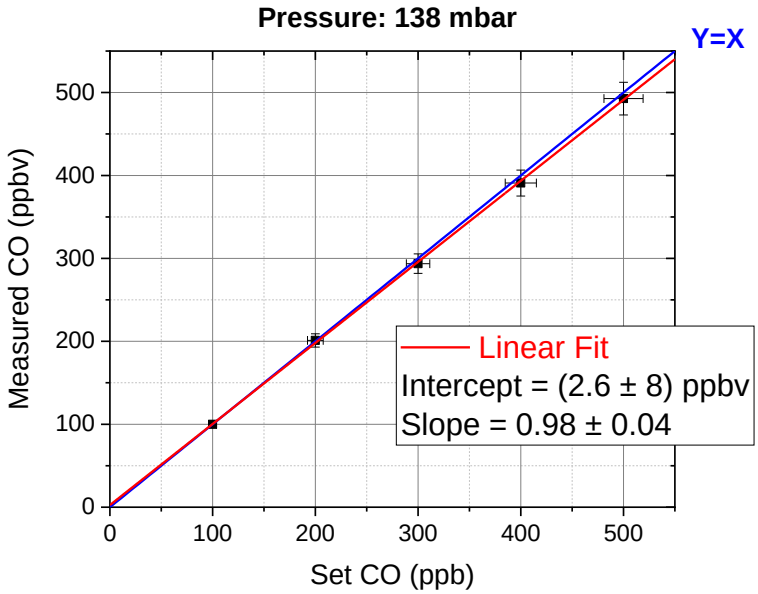

Figure 73: Results vs theory at P = 138 mbar

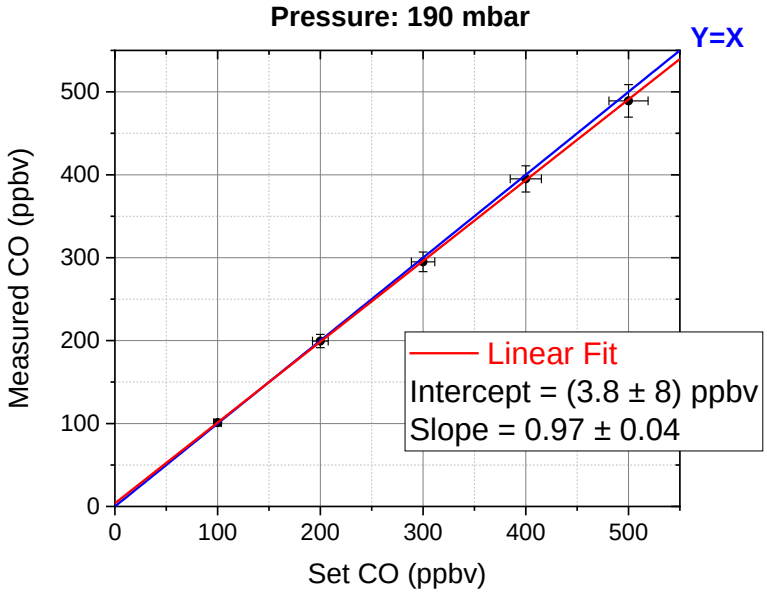

Figure 74: Results vs theory at P = 190 mbar

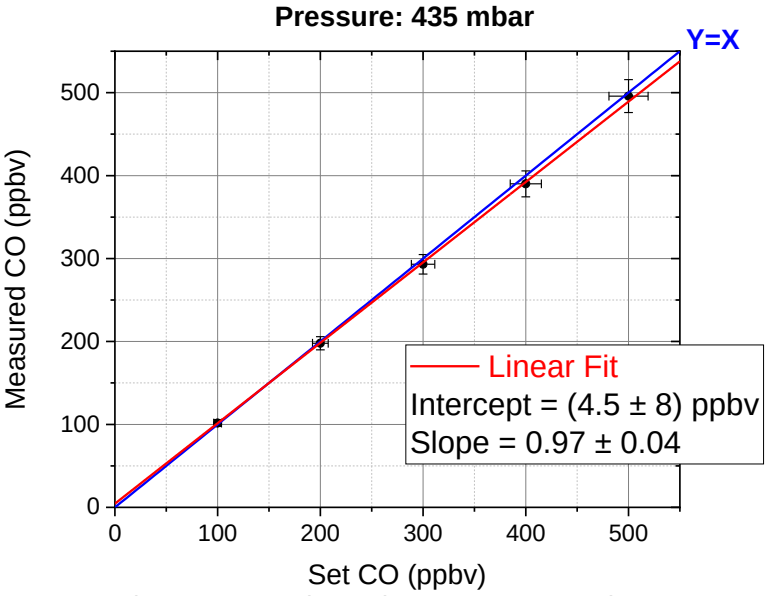

Figure 75: Results vs theory at P = 435 mbar

Table 15: Summary of the calibration results

	Fit: $CO_{meas} = Slope \cdot CO_{set} + Intercept$	
Pressure (mbar)	Slope	Intercept (ppbv)
138	0.98 ± 0.04	2.6 ± 8
190	0.97 ± 0.04	3.8 ± 8
435	0.97 ± 0.04	4.5 ± 8

We expected, within experimental errors, Slope = 1 and intercept = 0. Table 15 shows how the results fit with expectation.

The final test was the Allan-Werle test. This test provides information about the best achievable sensitivity. We set the pressure to 197.3 mBar, CO mixing ratio to 300 ppbv, and the acquisition time to 0.115 s. Figure 76 shows that the best integration time is about

5 s, corresponding to 0.18 ppbv. Due to the speed of the aircraft, the measurement repetition rate was 1 Hz, which raised the Allan-Werle variance to 0.23 ppbv.

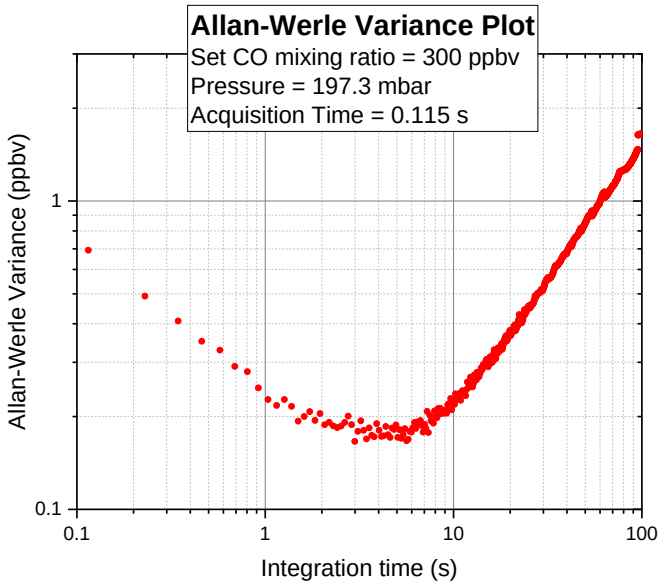

Figure 76: Allan-Werle Variance test for COLD2

Finally, we measured the long-term stability of the analyzer. We measured CO mixing ratio, at a set value of 300 ppbv, for 35 minutes at a frequency of 1 Hz, with P = 200 mBar. Measurement yielded the following results:

- mean CO = 294.8 ppb
- 1σ standard deviation = 3.3 ppb (2% fluctuation @2σ)
- max - min = 12 ppb (maximum fluctuation 4%)

⇒ Long Term Variability ≤ 4%

2.5.6 Conclusions

From the described measurements we can deduce that, within the experimental errors, the accuracy of COLD2 is within ±4%. This value agrees with the estimation coming from direct absorption and errors propagation.
For all the above we confirmed our data, acquired during the ACCLIP Campaign, without changes or rescaling.

2.6 Support for HYTES campaign (D5g)

The Hyperspectral Thermal Emission Spectrometer (HyTES) is a pushbroom airborne imaging spectrometer operating in the thermal infrared with 256 spectral channels between 7.5 and 12 micrometers. NASA/JPL developed this airborne instrument to support the preparation of the Hyperspectral Infrared Imager (HyspIRI) mission. HYTES measures the surface temperature and is able to detect various trace gases (CH_4, H_2S, NH_3, NO2, and SO2) at high spatial resolution (2 m at 1 km altitude). HyTES completed

its first flights in July 2012. Since then, HYTES has flown several science campaigns in the US, first from a Twin Otter and then from the NASA ER-2 aircraft.

In June 2019, HYTES flew for the first time in Europe, onboard the British Antarctic Survey (BAS) Twin Otter, during the NET-Sense campaign, a NASA/ESA collaboration. King's College London (KCL), the Natural Environmental Research Council's (NERC), and the National Centre for Earth Observation (NCEO) led the experiments. The NET-Sense campaign contributed to the planning of the Land Surface Temperature Monitoring (LSTM) mission, a Copernicus high priority candidate mission aiming to provide observations of land-surface temperature, in particular for agricultural and urban planning. Another objective of NET-Sense was to support the development of the Earth Explorer FLEX mission, which aims to map vegetation fluorescence and quantify photosynthetic activity. During NET-Sense, HYTES flew over agricultural and urban areas in the UK and Italy.

BIRA proposed to develop and characterize a new SWING instrument and to install it alongside the HYTES instrument onboard the BAS Twin Otter as the NASA/ESA collaboration planned to perform more of such HYTES flights in Europe. This allows to measure several trace gases at the same in the UV-VIS and the thermal infrared. The SWING instrument was developed in the course of 2021 and has been integrated in the BAS aircraft in spring 2022 and again in spring 2023, in collaboration with KCL. One mission to Saint-Albans took place in 2022 and one mission to Duxford in 2023 to further establish the new collaboration between BIRA and KCL, to perform the integration and to help with first test flights. Two staff members of BIRA performed the necessary courses (first aid course and crew resource management (CRM) course) in order to be able to fly along as an operator in the BAS Twin Otter.

The SWING measurements reveal maps of tropospheric NO_2 VCDs underneath the aircraft. HYTES measures NO_2 as well, but the SWING measurements in the visible range are much more sensitive than in the TIR and can resolve more sources of NOx, including weak ones. HyTES on the other hand is able to measure NH_3 in the thermal infrared with high sensitivity. NO_2 and NH_3 are the main components of the nitrogen cycle. In the context of the NITROCAM project (ESA contract No. 4000133881/21/NL/FF/ab), both instruments were deployed together to identify NO_2 and NH_3 emissions due to farming, industry, transport or urban sources which contribute to the nitrogen cycle. This configuration is seen as an airborne demonstrator for future satellite missions, focusing on monitoring of the global nitrogen cycle at high spatial resolution (0.5-1 km).

At the time of writing the proposal, the exact planning was quite uncertain due to the COVID-19 pandemic. Due to the COVID-19 impact, no HYTES-campaign could be organized in summer 2021 and a foreseen 2022 campaign was cancelled, related to the outbreak of the war in Ukraine. In 2023, the HyTES instrument was moved to Europe and a successful campaign took place over Northern Italy (Po valley + Tuscany) in the June-July 2023 period with a focus on several objectives, such as the LSTM mission, emissions from Volcanoes, and NITROSAT, i.e. an EE11 mission candidate. HyTES was not installed alongside SWING but installed on a Twin Otter from the Canadian company Kenn Borek Air. SWING+ was installed as planned on the BAS Twin Otter, alongside a

large suit of other instruments (see the relevant documents of the SwathSense project (ESA Contract No. 4000134779/20/NL/FF/an) for more details).

Simultaneous flights over NO_2 and NH_3-rich areas with both aircraft and instruments were part of the objectives. However due to the large amount of objectives for the SwathSense campaign they were not a top priority and only a few flights focused effectively on simultaneous mapping of NO_2 and NH_3. For most of the BAS flights, the SWING instrument was switched on but flights were not always performed over NO_2-rich areas due to the other objectives, resulting in a weak NO2 signal most of the time.

The SVANTE project has only foreseen a budget for the SWING development and SWING integration, as described in this section. Dedicated funding for flight hours and data exploitation have been foreseen in the context of the NITROCAM project. For more details on the collected data sets and subsequent data processing we refer to the relevant documents of the SwathSense project (ESA Contract No. 4000134779/20/NL/FF/an) and NITROCAM project (ESA contract No. 4000133881/21/NL/FF/ab).

The developed SWING instrument stays available for future campaigns with the BAS aircraft. It has for example been deployed in Canada in August 2023 in the context of the FIDEX campaign (ESA contract No. 4000136760/21/NL/AI) to measure emissions from wildlife fires and might be deployed in summer 2024 in Brazil.

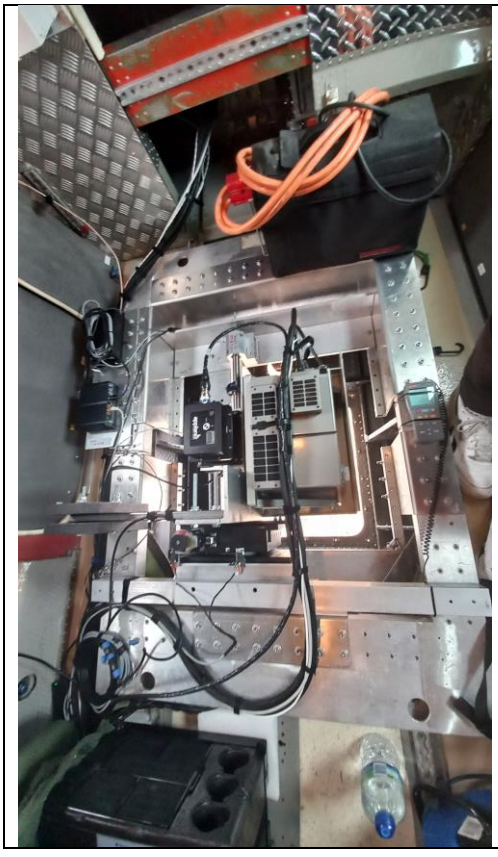

Figure 77 Ongoing instrument integration in the BAS Twin Otter (19/05/2023, Duxford)	Figure 78 HyTES integrated in the Kenn Borek Air Twin Otter (25/05/2023, Siena Aerodrome).

Figure 79 BAS Twin Otter (left) and SWING scanner integrated in the bottom plate alongside the SPECIM OWL spectrometer (right) (25/05/2023, Siena Aerodrome).

3 Summary

The goals of the project were largely achieved.
Essential data for the validation of S5p measurements (aerosols, clouds, methane, and tropospheric reactive trace gases) are being provided by the tasks completed during several field studies:

- Airborne and ground-based campaign 1 and 2 in the German Ruhr area
- Airborne and ground-based campaign in Romania
- COCCON ground based FTIR deployments
- MAGIC campaign 2019
- ACCLIP campaign
- HYTES campaign

The campaigns' outcomes are derived from measurable and documented evaluations of the evidence proving the degree of traceability to agreed reference standards.

References

- Airyx GmbH: SkySpec Compact Instrument v.200, https://airyx.de/wp-content/uploads/2022/05/SkySpec-Compact_v200.pdf, last access: 14 July 2022.
- Alberti, C., Hase, F., Frey, M., Dubravica, D., Blumenstock, T., Dehn, A., Castracane, P., Surawicz, G., Harig, R., Baier, B. C., Bès, C., Bi, J., Boesch, H., Butz, A., Cai, Z., Chen, J., Crowell, S. M., Deutscher, N. M., Ene, D., Franklin, J. E., García, O., Griffith, D., Grouiez, B., Grutter, M., Hamdouni, A., Houweling, S., Humpage, N., Jacobs, N., Jeong, S., Joly, L., Jones, N. B., Jouglet, D., Kivi, R., Kleinschek, R., Lopez, M., Medeiros, D. J., Morino, I., Mostafavipak, N., Müller, A.,

Ohyama, H., Palmer, P. I., Pathakoti, M., Pollard, D. F., Raffalski, U., Ramonet, M., Ramsay, R., Sha, M. K., Shiomi, K., Simpson, W., Stremme, W., Sun, Y., Tanimoto, H., Té, Y., Tsidu, G. M., Velazco, V. A., Vogel, F., Watanabe, M., Wei, C., Wunch, D., Yamasoe, M., Zhang, L., and Orphal, J.: Improved calibration procedures for the EM27/SUN spectrometers of the COllaborative Carbon Column Observing Network (COCCON), Atmos. Meas. Tech., 15, 2433–2463, https://doi.org/10.5194/amt-15-2433-2022, 2022

- Alberti, C., Tu, Q., Hase, F., Makarova, M. V., Gribanov, K., Foka, S. C., Zakharov, V., Blumenstock, T., Buchwitz, M., Diekmann, C., Ertl, B., Frey, M. M., Imhasin, H. Kh., Ionov, D. V., Khosrawi, F., Osipov, S. I., Reuter, M., Schneider, M., and Warneke, T.: Investigation of spaceborne trace gas products over St Petersburg and Yekaterinburg, Russia, by using COllaborative Column Carbon Observing Network (COCCON) observations, Atmos. Meas. Tech., 15, 2199–2229, https://doi.org/10.5194/amt-15-2199-2022, 2022
- Adam et al. EARLINET – Part 1: Data analysis methodology, Atmos. Chem. Phys., 20, 13905–13927, https://doi.org/10.5194/acp-20-13905-2020, 2020
- Adam, M., Fragkos, K., Binietoglou, I., Wang, D., Stachlewska, I.S., Belegante, L., Nicolae, V., Towards Early Detection of Tropospheric Aerosol Layers Using Monitoring with Ceilometer, Photometer, and Air Mass Trajectories, Remote Sens., 14, 1217, https://doi.org/10.3390/rs14051217
- Beirle, S., Dörner, S., Donner, S., Remmers, J., Wang, Y., and Wagner, T.: The Mainz profile algorithm (MAPA), Atmos. Meas. Tech., 12, 1785–1806, https://doi.org/10.5194/amt-12-1785-2019, 2019.
- Belegante L, Nicolae D., Talianu C., Vulturescu V., Performance estimation of Bucharest multiwavelength lidar during the EARLI09 campaign, U.P.B. Sci. Bull., Series A, Vol. 71, Iss. 4, 2009
- Belegante, L., Nicolae, D., Nemuc, A., Talianu, C., and Derognat, C.: Retrieval of the boundary layer height from active and passive remote sensors, Comparison with a NWP model, Acta Geophys., 62, 276–289, https://doi.org/10.2478/s11600-013-0167-4, 2014
- Boldeanu, M., Cucu, H., Burileanu, C., Marmureanu, L., Multi-Input Convolutional Neural Networks for Automatic Pollen Classification, Appl. Sci., 11, 11707. https://doi.org/10.3390/app112411707, 2021
- Bösch, T., Rozanov, V., Richter, A., Peters, E., Rozanov, A., Wittrock, F., Merlaud, A., Lampel, J., Schmitt, S., de Haij, M., Berkhout, S., Henzing, B., Apituley, A., den Hoed, M., Vonk, J., Tiefengraber, M., Müller, M., and Burrows, J. P.: BOREAS – a new MAX-DOAS profile retrieval algorithm for aerosols and trace gases, Atmos. Meas. Tech., 11, 6833–6859, https://doi.org/10.5194/amt-11-6833-2018, 2018.
- Cede, A., Tiefengraber, M., Gebetsberger, M., and Spinei Lind, E.: Pandonia Global NetworkData Products Readme Document, Tech. rep., PGN-DataProducts-Readme, version 1.8-6, 31 December 2022, https://www.pandonia-global-network.org/home/documents/reports (last access: 4 February 2023), 2022.
- Compernolle, S., Argyrouli, A., Lutz, R., Sneep, M., Lambert, J.-C., Fjæraa, A. M., Hubert, D., Keppens, A., Loyola, D., O'Connor, E., Romahn, F., Stammes, P., Verhoelst, T., and Wang, P.: Validation of the Sentinel-5 Precursor TROPOMI cloud data with Cloudnet, Aura OMI O2–O2, MODIS, and Suomi-NPP VIIRS,

Atmos. Meas. Tech., 14, 2451–2476, https://doi.org/10.5194/amt-14-2451-2021, 2021.

- Crippa, M., Guizzardi, D., Muntean, M., Schaaf, E., Dentener, F., van Aardenne, J. A., Monni, S., Doering, U., Olivier, J. G. J., Pagliari, V. and Janssens-Maenhout, G.: Gridded Emissions of Air Pollutants for the period 1970-2012 within EDGAR v4.3.2, Earth Syst. Sci. Data Discuss., 1–40, doi:10.5194/essd-2018-31, 2018.
- D'Amico, G., Amodeo, A., Baars, H., Binietoglou, I., Freudenthaler, V., Mattis, I., Wandinger, U., and Pappalardo, G.: EARLINET Single Calculus Chain – overview on methodology and strategy, Atmos. Meas. Tech., 8, 4891-4916, https://doi.org/10.5194/amt-8-4891-2015, 2015
- D'Amico, G., Amodeo, A., Mattis, I., Freudenthaler, V., and Pappalardo, G.: EARLINET Single Calculus Chain – technical – Part 1: Pre-processing of raw lidar data, Atmos. Meas. Tech., 9, 491-507, https://doi.org/10.5194/amt-9-491-2016, 2016.
- Danckaert, T., Fayt, C., Van Roozendael, M., De Smedt, I., Letocart, V., Merlaud, A., and Pinardi, G.: QDOAS Software user manual Version 3.2, https://uv-vis.aeronomie.be/software/QDOAS/QDOAS_manual.pdf (last access: 14 July 2022), 2017.
- de Graaf, M.: TROPOMI ATBD of the Aerosol Optical Thickness, Tech. rep., S5P-KNMI-L2-0033-RP, Issue 3.0.0, https://data-portal.s5p-pal.com/products/aot.html, last access: 21 December 2022.
- Dee, D. P., Uppala, S. M., Simmons, A. J., Berrisford, P., Poli, P., Kobayashi, S., Andrae, U., Balmaseda, M. A., Balsamo, G., Bauer, P., Bechtold, P., Beljaars, A. C. M., van de Berg, L., Bidlot, J., Bormann, N., Delsol, C., Dragani, R., Fuentes, M., Geer, A. J., Haimberger, L., Healy, S. B., Hersbach, H., Hólm, E. V., Isaksen, L., Kållberg, P., Köhler, M., Matricardi, M., McNally, A. P., Monge-Sanz, B. M., Morcrette, J.-J., Park, B.-K., Peubey, C., de Rosnay, P., Tavolato, C., Thépaut, J.-N. and Vitart, F.: The ERA-Interim reanalysis: configuration and performance of the data assimilation system, Q. J. R. Meteorol. Soc., 137(656), 553–597, doi:10.1002/qj.828, 2011.
- Dubovik, O. and King, M. D.: A flexible inversion algorithm for retrieval of aerosol optical properties from Sun and sky radiance measurements, J. Geophys. Res. Atmos., 105, 20 673–20 696, https://doi.org/10.1029/2000JD900282, 2000.
- European Environment Agency: The European Pollutant Release and Transfer Register (E-PRTR), Member States reporting under Article 7 of Regulation (EC) No 166/2006 — European Environment Agency, [online] Available from: http://www.eea.europa.eu/ds_resolveuid/710e9a407c0e4fecb376ee87ec9515c1 (Accessed 22 March 2017), 2016.
- Fragkos, K., Antonescu, B., Giles, D. M., Ene, D., Boldeanu, M., Efstathiou, G. A., Belegante, L., and Nicolae, D., Assessment of the total precipitable water from a sun photometer, microwave radiometer and radiosondes at a continental site in southeastern Europe, Atmos. Meas. Tech., 12, 1979–1997, https://doi.org/10.5194/amt-12-1979-2019, 2019
- Frey, M., Sha, M. K., Hase, F., Kiel, M., Blumenstock, T., Harig, R., Surawicz, G., Deutscher, N. M., Shiomi, K., Franklin, J. E., Bösch, H., Chen, J., Grutter, M., Ohyama, H., Sun, Y., Butz, A., Mengistu Tsidu, G., Ene, D., Wunch, D., Cao, Z., Garcia, O., Ramonet, M., Vogel, F., and Orphal, J.: Building the COllaborative

Carbon Column Observing Network (COCCON): long-term stability and ensemble performance of the EM27/SUN Fourier transform spectrometer, Atmos. Meas. Tech., 12, 1513-1530, https://doi.org/10.5194/amt-12-1513-2019, 2019

- Frey, M. M., Hase, F., Blumenstock, T., Dubravica, D., Groß, J., Göttsche, F., Handjaba, M., Amadhila, P., Mushi, R., Morino, I., Shiomi, K., Sha, M. K., de Mazière, M., and Pollard, D. F.: Long-term column-averaged greenhouse gas observations using a COCCON spectrometer at the high-surface-albedo site in Gobabeb, Namibia, Atmos. Meas. Tech., 14, 5887–5911, https://doi.org/10.5194/amt-14-5887-2021, 2021
- Friedrich, M. M., Rivera, C., Stremme, W., Ojeda, Z., Arellano, J., Bezanilla, A., García-Reynoso, J. A., and Grutter, M.: NO2 vertical profiles and column densities from MAX-DOAS measurements in Mexico City, Atmos. Meas. Tech., 12, 2545–2565, https://doi.org/10.5194/amt-12-2545-2019, 2019.
- Giles, D. M., Sinyuk, A., Sorokin, M. G., Schafer, J. S., Smirnov, A., Slutsker, I., Eck, T. F., Holben, B. N., Lewis, J. R., Campbell, J. R.,Welton, E. J., Korkin, S. V., and Lyapustin, A. I.: Advancements in the Aerosol Robotic Network (AERONET) Version 3 database- automated near-real-time quality control algorithm with improved cloud screening for Sun photometer aerosol optical depth (AOD) measurements, Atmos. Meas. Tech., 12, 169–209, https://doi.org/10.5194/amt-12-169-2019
- Gisi, M., Hase, F., Dohe, S., and Blumenstock, T.: Camtracker: a new camera controlled high precision solar tracker system for FTIRspectrometers, Atmos. Meas. Tech., 4, 47–54, https://doi.org/10.5194/amt-4-47-2011, 2011.
- Gisi, M., F. Hase, S. Dohe, T. Blumenstock, A. Simon, and A. Keens: XCO2-measurements with a tabletop FTS using solar absorption spectroscopy, Atmos. Meas. Tech., 5, 2969-2980, doi:10.5194/amt-5-2969-2012, 2012
- Gothard, M., Nemuc, A., Radu, C., Dascalu, S., An intensive case of Saharan dust intrusion over South East Romania, Romanian Reports in Physics, 66(2), 509–519, 2014
- Hase, F., M. Frey, T. Blumenstock, J. Groß, M. Kiel, R. Kohlhepp, G. Mengistu Tsidu, K. Schäfer, M. K. Sha, and J. Orphal: Application of portable FTIR spectrometers for detecting greenhouse gas emissions of the major city Berlin, Atmos. Meas. Tech., 8, 3059-3068, doi:10.5194/amt-8-3059-2015, 2015
- Hendrick, F., Pinardi, G., Van Roozendael, M., Apituley, A., Piters, A., Richter, A., Wagner, T., Kreher, K., Friess, U., and Lampel, J.: Fiducial Reference Measurements for Ground-Based DOAS Air-Quality Observations, Deliverable D13 ESA Contract No. 4000118181/16/I-EF, https://frm4doas.aeronomie.be/ProjectDir/Deliverables/FRM4DOAS_D13_Campaign_Planning_Document_20161021_final.pdf (last access: 14 July 2022), 2016.
- Herkommer Benedikt, Dissertation, “Improving the consistency of greenhouse gas measurements from ground-based remote sensing networks using a portable FTIR spectrometer”, KIT (under final revision, will be made accessible via https://publikationen.bibliothek.kit.edu)
- Hersbach, H., Bell, B., Berrisford, P., Biavati, G., Horányi, A., Muñoz Sabater, J., Nicolas, J., Peubey, C., Radu, R., Rozum, I., Schepers, D., Simmons, A., Soci, C., Dee, D., and Thépaut, J.-N.: ERA5 hourly data on single levels from 1959 to

present, Copernicus Climate Change Service (C3S) Climate Data Store (CDS) [data set], https://doi.org/10.24381/cds.adbb2d47, 2018.

- Holben, B., Eck, T., Slutsker, I., Tanré, D., Buis, J., Setzer, A., Vermote, E., Reagan, J., Kaufman, Y., Nakajima, T., Lavenu, F., Jankowiak, I., and Smirnov, A.: AERONET—A Federated Instrument Network and Data Archive for Aerosol Characterization, Remote Sens. Environ., 66, 1 – 16, https://doi.org/10.1016/S0034-4257(98)00031-5, 1998.
- Hoffer, A., Tóth, Á., Jancsek-Turóczi, B., Machon, A., Meiramova, A., Nagy, A., Marmureanu, L., Gelencsér, A., Potential new tracers and their mass fraction in the emitted PM10 from the burning of household waste in stoves, Atmos. Chem. Phys., 21, 17855–17864, https://doi.org/10.5194/acp-21-17855-2021, 2021
- Ibrahim, O., Shaiganfar, R., Sinreich, R., Stein, T., Platt, U., and Wagner, T.: Car MAXDOAS measurements around entire cities: quantification of NOx emissions from the cities of Mannheim and Ludwigshafen (Germany), Atmospheric Measurement Techniques, 3, 709–721, https://doi.org/10.5194/amt-3-709-2010, 2010.
- Judd, L. M., Al-Saadi, J. A., Szykman, J. J., Valin, L. C., Janz, SJ., Kowalewski, M. G., Eskes, H. J., Veefkind, J. P., Cede, A., Mueller, M., Gebetsberger, M., Swap, R., Pierce, R. B., Nowlan, C. R., Abad, G. G., Nehrir, A., and Williams, D.: Evaluating Sentinel-5P TROPOMI tropospheric NO2 column densities with airborne and Pandora spectrometers near New York City and Long Island Sound, Atmos. Meas. Tech., 13, 6113–6140, https://doi.org/10.5194/amt-13-6113-2020, 2020.
- Kreher, K., et al.: Intercomparison of NO2, O4, O3 and HCHO slant column measurements by MAX-DOAS and zenith-sky UV–visible spectrometers during CINDI-2, Atmos. Meas. Tech., 13, 2169–2208, https://doi.org/10.5194/amt-13-2169-2020, 2020.
- Krings, T., Neininger, B., Gerilowski, K., Krautwurst, S., Buchwitz, M., Burrows, J. P., Lindemann, C., Ruhtz, T., Schüttemeyer, D. and Bovensmann, H.: Airborne remote sensing and in situ measurements of atmospheric CO2 to quantify point source emissions, Atmospheric Meas. Tech., 11(2), 721–739, doi:10.5194/amt-11-721-2018, 2018.
- Lange, Kezia: Investigating NO2 distributions from satellite, airborne and ground-based measurements: spatiotemporal variability of NOx emissions and validation of the TROPOMI NO2 product, PhD Thesis, University of Bremen, 2023.
- Lange, K., Richter, A., Schönhardt, A., Meier, A. C., Bösch, T., Seyler, A., Krause, K., Behrens, L. K., Wittrock, F., Merlaud, A., Tack, F., Fayt, C., Friedrich, M. M., Dimitropoulou, E., Van Roozendael, M., Kumar, V., Donner, S., Dörner, S., Lauster, B., Razi, M., Borger, C., Uhlmannsiek, K., Wagner, T., Ruhtz, T., Eskes, H., Bohn, B., Santana Diaz, D., Abuhassan, N., Schüttemeyer, D., and Burrows, J. P.: Validation of Sentinel-5P TROPOMI tropospheric NO2 products by comparison with NO2 measurements from airborne imaging DOAS, ground-based stationary DOAS, and mobile car DOAS measurements during the S5P-VAL-DE-Ruhr campaign, Atmos. Meas. Tech., 16, 1357–1389, https://doi.org/10.5194/amt-16-1357-2023, 2023.
- Laughner, J. L., Roche, S., Kiel, M., Toon, G. C., Wunch, D., Baier, B. C., Biraud, S., Chen, H., Kivi, R., Laemmel, T., McKain, K., Quéhé, P.-Y., Rousogenous, C.,

Stephens, B. B., Walker, K., and Wennberg, P. O.: A new algorithm to generate a priori trace gas profiles for the GGG2020 retrieval algorithm, Atmos. Meas. Tech., 16, 1121–1146, https://doi.org/10.5194/amt-16-1121-2023, 2023

- Löhnert, U., Schween, J. H., Acquistapace, C., Ebell, K., Maahn, M., Barrera-Verdejo, M., Hirsikko, A., Bohn, B., Knaps, A., O'Connor, E., Simmer, C., Wahner, A., and Crewell, S.: JOYCE: Jülich Observatory for Cloud Evolution, B. Am. Meteorol. Soc., 96, 1157–1174, https://doi.org/10.1175/BAMS-D-14-00105.1, 2015.
- Marmureanu, L., Marin, C.A., Andrei, S., Antonescu, B., Ene, D., Boldeanu, M., Vasilescu, J., Viţelaru, C., Cadar, O., Levei, E., Orange Snow—A Saharan Dust Intrusion over Romania During Winter Conditions, Remote Sens., 11, 2466. https://doi.org/10.3390/rs11212466, 2019
- Marmureanu, L., Vasilescu, J., Slowik, J., Prévôt, A.S.H., Marin, C.A., Antonescu, B., Vlachou, A., Nemuc, A., Dandocsi, A., Szidat, S., Online Chemical Characterization and Source Identification of Summer and Winter Aerosols in Măgurele, Romania, Atmosphere, 11, 385. https://doi.org/10.3390/atmos11040385, 2020
- Mattis, I., D'Amico, G., Baars, H., Amodeo, A., Madonna, F., and Iarlori, M.: EARLINET Single Calculus Chain – technical – Part 2: Calculation of optical products, Atmos. Meas. Tech., 9, 3009-3029, https://doi.org/10.5194/amt-9-3009-2016, 2016.
- Meier, A. C., Schönhardt, A., Bösch, T., Richter, A., Seyler, A., Ruhtz, T., Constantin, D.-E., Shaiganfar, R., Wagner, T., Merlaud, A., Van Roozendael, M., Belegante, L., Nicolae, D., Georgescu, L. and Burrows, J. P.: High-resolution airborne imaging DOAS measurements of NO2 above Bucharest during AROMAT, Atmos Meas Tech, 10(5), 1831–1857, doi:10.5194/amt-10-1831-2017, 2017.
- Merlaud, Alexis: Development and use of compact instruments for tropospheric investigations based on optical spectroscopy from mobile platforms, Phd Thesis, 2013.
- Merlaud, A., Belegante, L., Constantin, D.-E., Den Hoed, M., Meier, A. C., Allaart, M., Ardelean, M., Arseni, M., Bösch, T., Brenot, H., Calcan, A., Dekemper, E., Donner, S., Dörner, S., Balanica Dragomir, M. C., Georgescu, L., Nemuc, A., Nicolae, D., Pinardi, G., Richter, A., Rosu, A., Ruhtz, T., Schönhardt, A., Schuettemeyer, D., Shaiganfar, R., Stebel, K., Tack, F., Nicolae Vâjâiac, S., Vasilescu, J., Vanhamel, J., Wagner, T., and Van Roozendael, M.: Satellite validation strategy assessments based on the AROMAT campaigns, Atmos. Meas. Tech., 13, 5513–5535, https://doi.org/10.5194/amt-13-5513-2020, 2020.
- Mermigkas, M.; Topaloglou, C.; Balis, D.; Koukouli, M.E.; Hase, F.; Dubravica, D.; Borsdorff, T.; Lorente, A. FTIR Measurements of Greenhouse Gases over Thessaloniki, Greece in the Framework of COCCON and Comparison with S5P/TROPOMI Observations. Remote Sens. 2021, 13, 3395. https://doi.org/10.3390/rs13173395
- Nicolae, D., Vasilescu, J., Talianu, C., Binietoglou, I., Nicolae, V., Andrei, S., and Antonescu, B., A Neural Network Aerosol Typing Algorithm Based on Lidar Data, Atmos. Chem. Phys., 18, 14511–14537, https://doi.org/10.5194/acp-18-14511-2018, 2018

- Nemuc, A., Vasilescu, J., Talianu, C., Belegante, L., and Nicolae, D.: Assessment of aerosol's mass concentrations from measured linear particle depolarization ratio (vertically resolved) and simulations, Atmos. Meas. Tech., 6, 3243–3255, https://doi.org/10.5194/amt-6-3243-2013, 2013.
- Pan, L.L., Kinnison, D., Liang, Q., Chin, M., Santee, M.L., Flemming, J., et al. (2022). A multimodel investigation of Asian summer monsoon UTLS transport over the Western Pacific. Journal of Geophysical Research: Atmospheres, 127, e2022JD037511. https://doi.org/10.1029/2022JD037511.
- Piters, A. J. M., Boersma, K. F., Kroon, M., Hains, J. C., Van Roozendael, M., Wittrock, F., Abuhassan, N., Adams, C., Akrami, M., Allaart, M. A. F., Apituley, A., Beirle, S., Bergwerff, J. B., Berkhout, A. J. C., Brunner, D., Cede, A., Chong, J., Clémer, K., Fayt, C., Frieß, U., Gast, L. F. L., Gil-Ojeda, M., Goutail, F., Graves, R., Griesfeller, A., Großmann, K., Hemerijckx, G., Hendrick, F., Henzing, B., Herman, J., Hermans, C., Hoexum, M., van der Hoff, G. R., Irie, H., Johnston, P. V., Kanaya, Y., Kim, Y. J., Klein Baltink, H., Kreher, K., de Leeuw, G., Leigh, R., Merlaud, A., Moerman, M. M., Monks, P. S., Mount, G. H., Navarro-Comas, M., Oetjen, H., Pazmino, A., Perez-Camacho, M., Peters, E., du Piesanie, A., Pinardi, G., Puentedura, O., Richter, A., Roscoe, H. K., Schönhardt, A., Schwarzenbach, B., Shaiganfar, R., Sluis, W., Spinei, E., Stolk, A. P., Strong, K., Swart, D. P. J., Takashima, H., Vlemmix, T., Vrekoussis, M., Wagner, T., Whyte, C., Wilson, K. M., Yela, M., Yilmaz, S., Zieger, P., and Zhou, Y.: The Cabauw Intercomparison campaign for Nitrogen Dioxide measuring Instruments (CINDI): design, execution, and early results, Atmos. Meas. Tech., 5, 457–485, doi:10.5194/amt-5-457-2012, 2012.
- Prunet, P., Bacour, C., Price, I., Muller, J. P., Lewis, P., Vountas, M., von Hoyningen-Huene, W., Burrows, J. P., Schlundt, C., Bréon, F. M., Gonzales, L., North, P., Fischer, J., and Domenech, C.: A Surface Reflectance DAtabase for ESA's Earth Observation Missions (ADAM), ESA Final Report NOV-3895-NT-12403, Noveltis, https://nebula.esa.int/sites/default/files/neb_study/1089/C4000102979ExS.pdf (last access: 9 February 2023), 2013.
- Rißmann, M., Chen, J., Osterman, G., Zhao, X., Dietrich, F., Makowski, M., Hase, F., and Kiel, M.: Comparison of OCO-2 target observations to MUCCnet – is it possible to capture urban XCO2 gradients from space?, Atmos. Meas. Tech., 15, 6605–6623, https://doi.org/10.5194/amt-15-6605-2022, 2022
- Schönhardt, A., Altube, P., Gerilowski, K., Krautwurst, S., Hartmann, J., Meier, A. C., Richter, A. and Burrows, J. P.: A wide field-of-view imaging DOAS instrument for two-dimensional trace gas mapping from aircraft, Atmos Meas Tech, 8(12), 5113–5131, doi:10.5194/amt-8-5113-2015, 2015.
- Sentinel-5P-TROPOMI-ATBD, accessed on http://www.tropomi.eu/documents/atbd
- Seyler, A., Meier, A. C., Wittrock, F., Kattner, L., Mathieu-Üffing, B., Peters, E., Richter, A., Ruhtz, T., Schönhardt, A., Schmolke, S. and Burrows, J. P.: Studies of the horizontal inhomogeneities in NO2 concentrations above a shipping lane using ground-based multi-axis differential optical absorption spectroscopy (MAX-DOAS) measurements and validation with airborne imaging DOAS measurements, Atmospheric Meas. Tech., 12(11), 5959–5977, doi:https://doi.org/10.5194/amt-12-5959-2019, 2019.

- Shaiganfar, R., Beirle, S., Petetin, H., Zhang, Q., Beekmann, M. and Wagner, T.: New concepts for the comparison of tropospheric NO2 column densities derived from car-MAX-DOAS observations, OMI satellite observations and the regional model CHIMERE during two MEGAPOLI campaigns in Paris 2009/10, Atmos. Meas. Tech., 8(7), 2827–2852, doi:10.5194/amt-8-2827-2015, 2015.
- Tack, F., Merlaud, A., Meier, A. C., Vlemmix, T., Ruhtz, T., Iordache, M.-D., Ge, X., Wal, L. van der, Schuettemeyer, D., Ardelean, M., Calcan, A., Constantin, D., Schönhardt, A., Meuleman, K., Richter, A. and Roozendael, M. V.: Intercomparison of four airborne imaging DOAS systems for tropospheric NO2 mapping – the AROMAPEX campaign, Atmospheric Meas. Tech., 12(1), 211–236, doi:https://doi.org/10.5194/amt-12-211-2019, 2019.
- Tack, F., Merlaud, A Intercomparison of four airborne imaging DOAS systems for tropospheric NO2 mapping – the AROMAPEX campaign, Atmos. Meas. Tech., 12, 211–236, https://doi.org/10.5194/amt-12-211-2019, 2019.
- Tack, F., Merlaud, A., Iordache, M.-D., Pinardi, G., Dimitropoulou, E., Eskes, H., Bomans, B., Veefkind, P., and Van Roozendael, M.: Assessment of the TROPOMI tropospheric NO2 product based on airborne APEX observations, Atmos. Meas. Tech., 14, 615–646, https://doi.org/10.5194/amt-14-615-2021, 2021.
- Tilstra, L.: TROPOMI ATBD of the directionally dependent surface Lambertian-equivalent reflectivity, Tech. rep., KNMI Report S5P-KNMI-L3-0301-RP, Issue 1.2.0, https://www.temis.nl/surface/albedo/tropomi_ler.php, last access: 13 September 2022.
- Thyng, K.M., C.A. Greene, R.D. Hetland, H.M. Zimmerle, and S.F. DiMarco. 2016. True colors of oceanography: Guidelines for effective and accurate colormap selection. Oceanography 29(3):9–13, http://dx.doi.org/10.5670/oceanog.2016.66;
- Torres, B., Toledano, C., Berjón, A., Fuertes, D., Molina, V., Gonzalez, R., Canini, M., Cachorro, V. E., Goloub, P., Podvin, T., Blarel, L., Dubovik, O., Bennouna, Y., and de Frutos, A. M.: Measurements on pointing error and field of view of Cimel-318 Sun photometers in the scope of AERONET, Atmos. Meas. Tech., 6, 2207–2220, https://doi.org/10.5194/amt-6-2207-2013, 2013
- Tu, Q., Hase, F., Blumenstock, T., Kivi, R., Heikkinen, P., Sha, M. K., Raffalski, U., Landgraf, J., Lorente, A., Borsdorff, T., Chen, H., Dietrich, F., and Chen, J.: Intercomparison of atmospheric CO2 and CH4 abundances on regional scales in boreal areas using Copernicus Atmosphere Monitoring Service (CAMS) analysis, COllaborative Carbon Column Observing Network (COCCON) spectrometers, and Sentinel-5 Precursor satellite observations, Atmos. Meas. Tech., 13, 4751–4771, https://doi.org/10.5194/amt-13-4751-2020, 2020
- van Geffen, J., Eskes, H., Compernolle, S., Pinardi, G., Verhoelst, T., Lambert, J.-C., Sneep, M., ter Linden, M., Ludewig, A., Boersma, K. F., and Veefkind, J. P.: Sentinel-5P TROPOMI NO2 retrieval: impact of version v2.2 improvements and comparisons with OMI and ground-based data, Atmos. Meas. Tech., 15, 2037–2060, https://doi.org/10.5194/amt-15-2037-2022, 2022.
- Viciani, S., D'Amato, F., Mazzinghi, P., Castagnoli, F., Toci, G., Werle, P.W.: "A cryogenically operated laser diode spectrometer for airborne measurement of stratospheric trace gases", Appl. Phys. B 90, pp. 581-592 (2008), doi: 10.1007/s00340-007-2885-2.

- Viciani, S., Montori, A., Chiarugi, A., and D'Amato, F.: "A Portable Quantum Cascade Laser Spectrometer for Atmospheric Measurements of Carbon Monoxide", Sensors 18, 2380 (2018), doi:10.3390/s18072380.
- Vlemmix, T., Ge, X., de Goeij, B. T. G., van der Wal, L. F., Otter, G. C. J., Stammes, P., Wang, P., Merlaud, A., Schüttemeyer, D., Meier, A. C., Veefkind, J. P. and Levelt, P. F.: Retrieval of tropospheric NO2 columns over Berlin from high-resolution airborne observations with the spectrolite breadboard instrument, Atmos Meas Tech Discuss, 2017, 1–34, doi:10.5194/amt-2017-257, 2017.
- Wagner, T., Ibrahim, O., Shaiganfar, R., and Platt, U.: Mobile MAX-DOAS observations of tropospheric trace gases, Atmos. Meas. Tech., 3, 129-140, 10.5194/amt-3-129-2010, 2010.
- Zhao, X., Griffin, D., Fioletov, V., McLinden, C., Davies, J., Ogyu, A., Lee, S. C., Lupu, A., Moran, M. D., Cede, A., Tiefengraber, M., and Müller, M.: Retrieval of total column and surface NO2 from Pandora zenith-sky measurements, Atmos. Chem. Phys., 19, 10619–10642, https://doi.org/10.5194/acp-19-10619-2019, 2019.
- https://climate.copernicus.eu/climate-bulletins
- https://cds.climate.copernicus.eu/cdsapp#!/home

Annex 1

Annex 1 Flight reports campaign in Romania

Flight 2: 26 Sept 2022

Flight overview

- Altitude: 500 m
- Instruments: IMU, AS32M, Picarro G2041-m, APS
- Duration: 2:12
- Weather summary: Low pressure regime over Romania with decreasing tendency, overcast, inappropriate conditions for measurements.

IMU data

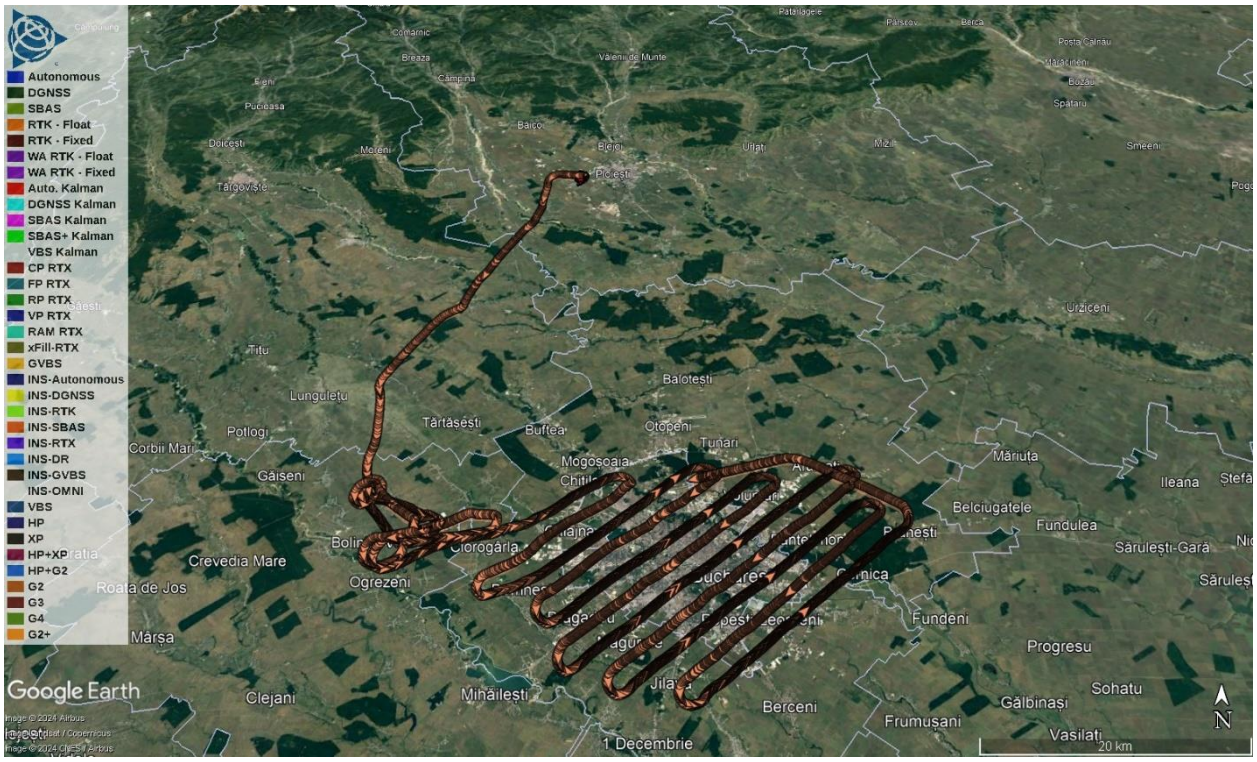

Figure 80. Flight path recorded by the IMU on 26 Sept 2022

Picarro G2041-m data

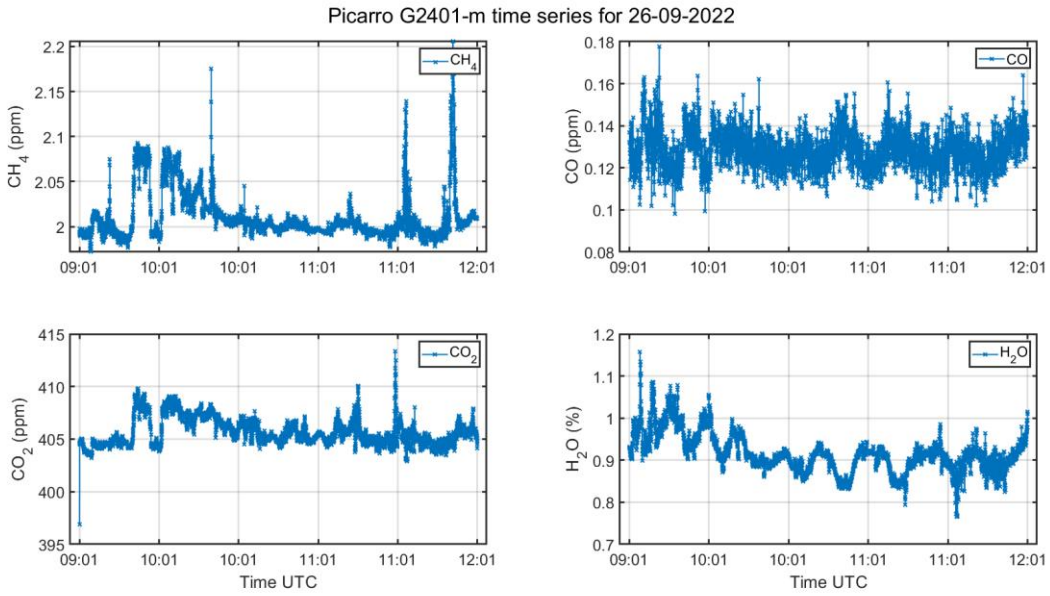

Figure 81. Greenhouse gases concentrations for 26 Sept 2022 (top left: CH_4, top right: CO, bottom left: CO_2, bottom right: H_2O)

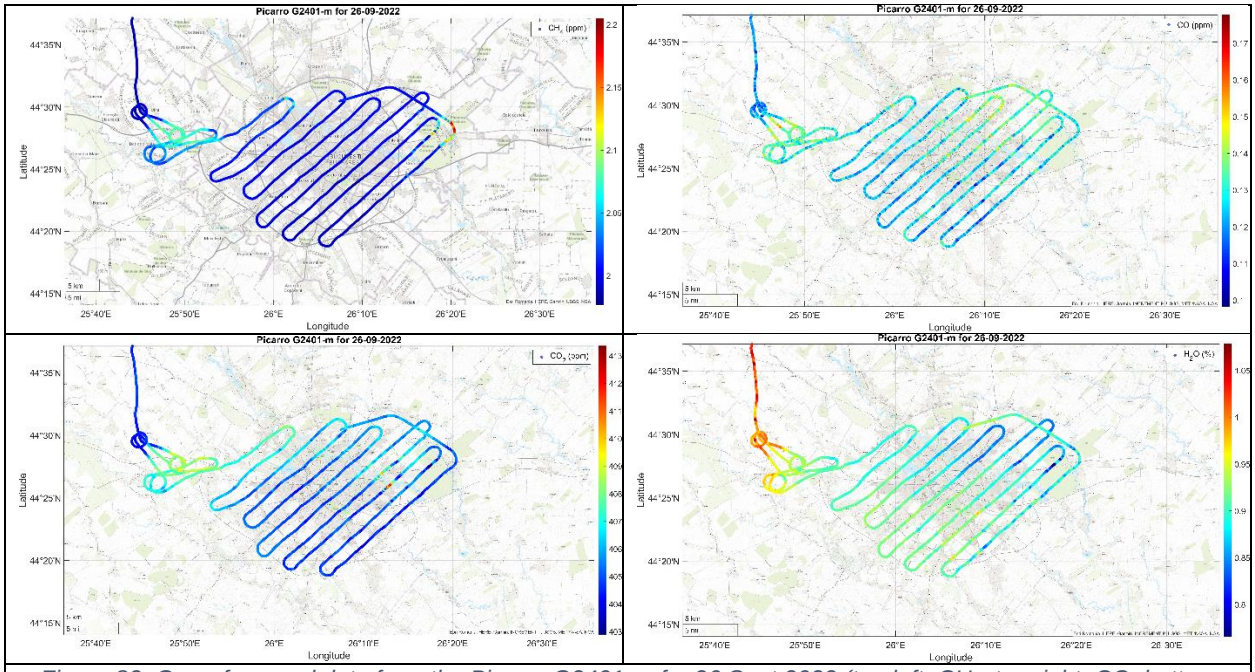

Figure 82. Georeferenced data from the Picarro G2401-m for 26 Sept 2022 (top left: CH_4, top right: CO, bottom left: CO_2, bottom right: H_2O)

Figure 2 shows time series data for greenhouse gases and water vapor concentration levels on 26 Sept 2022, as recorded by the Picarro G2401-m. The concentration of CH_4 is around 2.00-2.15 ppm. There are several peaks observed around 10:00 and 11:00

UTC, indicating higher emissions or localized sources of methane during these times. General trend shows fluctuations with significant short-term increases. The concentration of CO varies between 0.1 and 0.18 ppm. There is a noticeable variation with peaks and troughs, suggesting variable emission sources or atmospheric conditions affecting CO levels. The concentration of CO_2 ranges from approximately 395 to 415 ppm. Several peaks are visible around 10:00 and 11:00 UTC, similar to methane, indicating possible concurrent sources or activities affecting both gases. The percentage of H_2O ranges from 0.7 to 1.2%. The data shows fluctuations, with notable peaks around 11:30 UTC.

Figure 19 displays spatial distributions of methane (CH_4), carbon monoxide (CO), carbon dioxide (CO_2), and water vapor (H_2O) concentrations over Bucharest on 26 Sept 2022. Methane concentrations vary from 2.00 to 2.15 ppm. Higher concentrations (red and yellow areas) are visible in specific locations, indicating potential emission hotspots. The paths show higher CH_4 levels along certain routes, suggesting sources or areas with higher emissions. CO concentrations range from 0.1 to 0.17 ppm. Similar to methane, there are areas with higher CO concentrations. The spatial distribution shows variability, with certain paths having higher CO levels, indicating possible emission sources. CO_2 levels range from 403 to 413 ppm. There are distinct areas with higher CO_2 concentrations, similar to methane and CO maps. The spatial pattern suggests emission sources affecting CO_2 levels along certain paths. Water vapor concentration varies from 0.8 to 1.05%. Higher concentrations are seen along specific paths, suggesting areas with higher humidity or water vapor sources.

Flight 3: 30 Sept 2022

Flight overview

- **Altitude:** 3300 m.
- **Instruments:** IMU, SWING+, AS32M, APS.
- **Duration:** 3:13.
- **Weather summary:** Low pressure regime over Romania with an increasing tendency, clear sky over Bucharest, good conditions for measurements.

IMU data

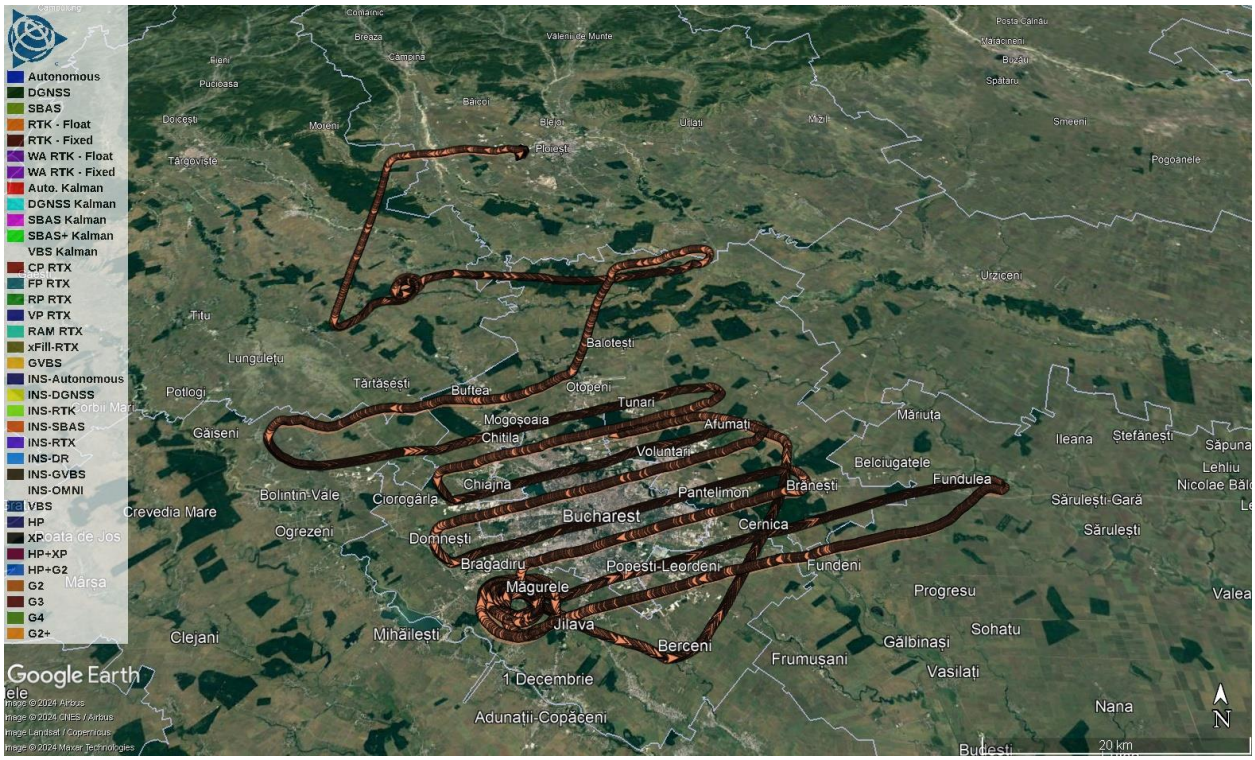

Figure 83. Flight path recorded by the IMU on 30 Sept 2022

The flight path recorded by the IMU can be seen in Figure 20. The take-off was from the Strejnicu Airfield and the mission started in the NW part of Bucharest and ended in the SW, after which the aircraft headed for landing at the Băneasa Airport. In addition to the lines above the city, a vertical sounding was also performed above Măgurele.

SWING+ data

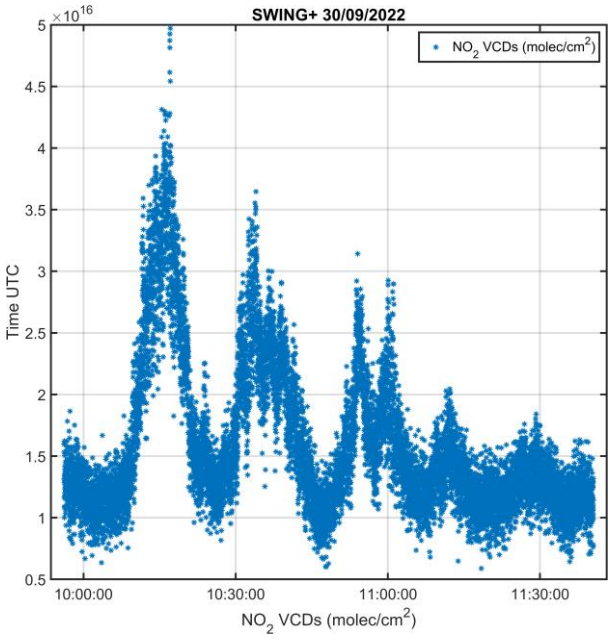

Figure 84. NO_2 vertical column densities as recorded by the SWING+ on 30 Sept 2022

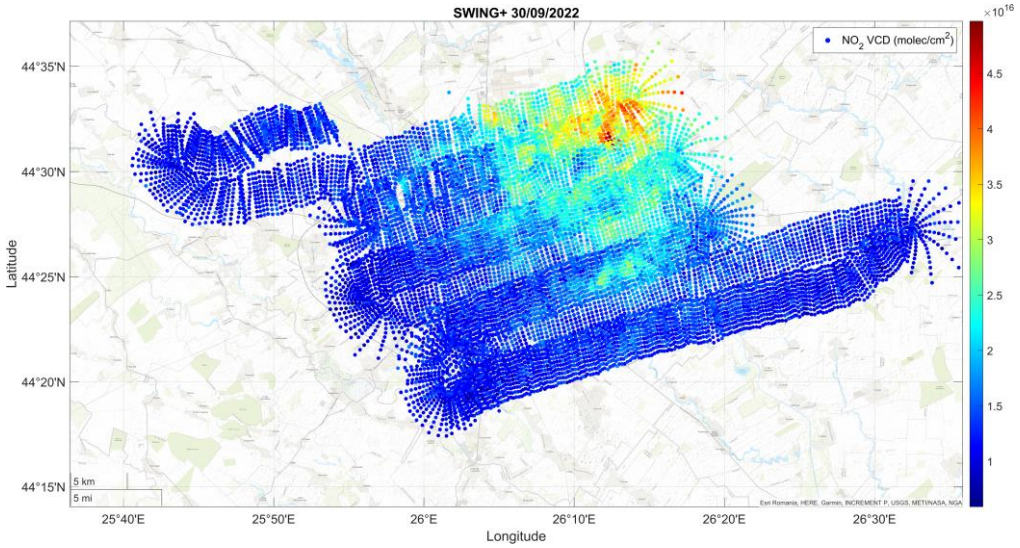

Figure 85. Georeferenced NO_2 VCDs as recorded by the SWING+ on 30 Sept 2022

The time series in Figure 21 shows significant variability in NO_2 concentrations, with several peaks and troughs. Peaks in NO_2 levels are observed around 10:10, 10:30, 10:50, and 11:10 UTC, with the highest concentration reaching close to 5 × 10¹⁶ molec/cm². The lowest concentrations are observed around 10:20 and 11:20 UTC, with values around 1 × 10¹⁶ molec/cm². Higher NO_2 concentrations are observed in the northeastern part of the surveyed area, with concentrations reaching up to 4.5 × 10¹⁶ molec/cm². There is a gradient from high to low NO_2 levels, with the southwestern part showing lower concentrations (around 1 × 10¹⁶ molec/cm²).

APS data

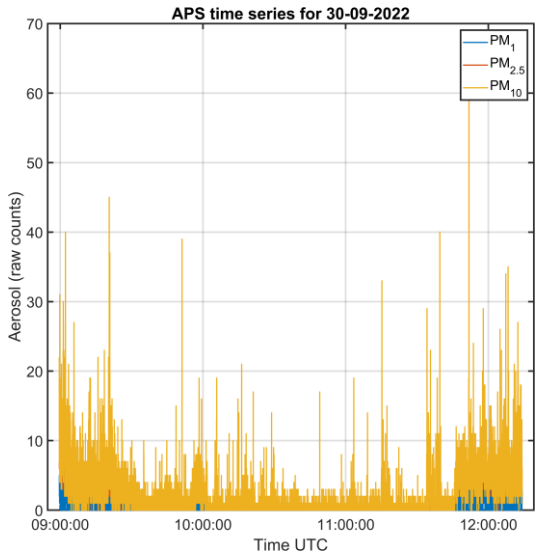

Figure 86. Aerosol data as recorded by the APS on 30 Aug 2022

PM_{10} dominates the aerosol counts throughout the day, with the highest counts reaching around 70. $PM_{2.5}$ and PM_1 are present in much lower counts compared to PM_{10}. Between

9 – 10 UTC, aerosol counts are relatively high in the early morning, with multiple peaks observed for PM_{10}, reaching up to 40 counts. $PM_{2.5}$ and PM_1 also show some activity but are significantly lower in comparison to PM_{10}. Between 10 – 11 UTC, there is a decrease in aerosol counts, with fewer peaks observed for PM_{10}. The counts mostly stay below 10. $PM_{2.5}$ and PM_1 remain at low levels, with minimal spikes. Between 11 – 12 UTC, Aerosol counts start to rise again, particularly for PM_{10}, with several peaks reaching up to 70 counts. $PM_{2.5}$ and PM_1 continue to show lower counts but with a slight increase in activity towards the end of the period. After 12 UTC, The aerosol counts, especially for PM_{10}, increase significantly with multiple peaks. $PM_{2.5}$ and PM_1 show more frequent spikes compared to earlier periods, indicating an overall rise in aerosol concentrations.

Flight 4: 2 Nov 2022

Flight overview

- **Altitude:** 3500 m.
- **Instruments:** IMU, SWING+, AS32M, APS.
- **Duration:** 2:35.
- **Weather summary:** High pressure regime over Romania, clear sky over Bucharest, good conditions for measurements.

IMU data

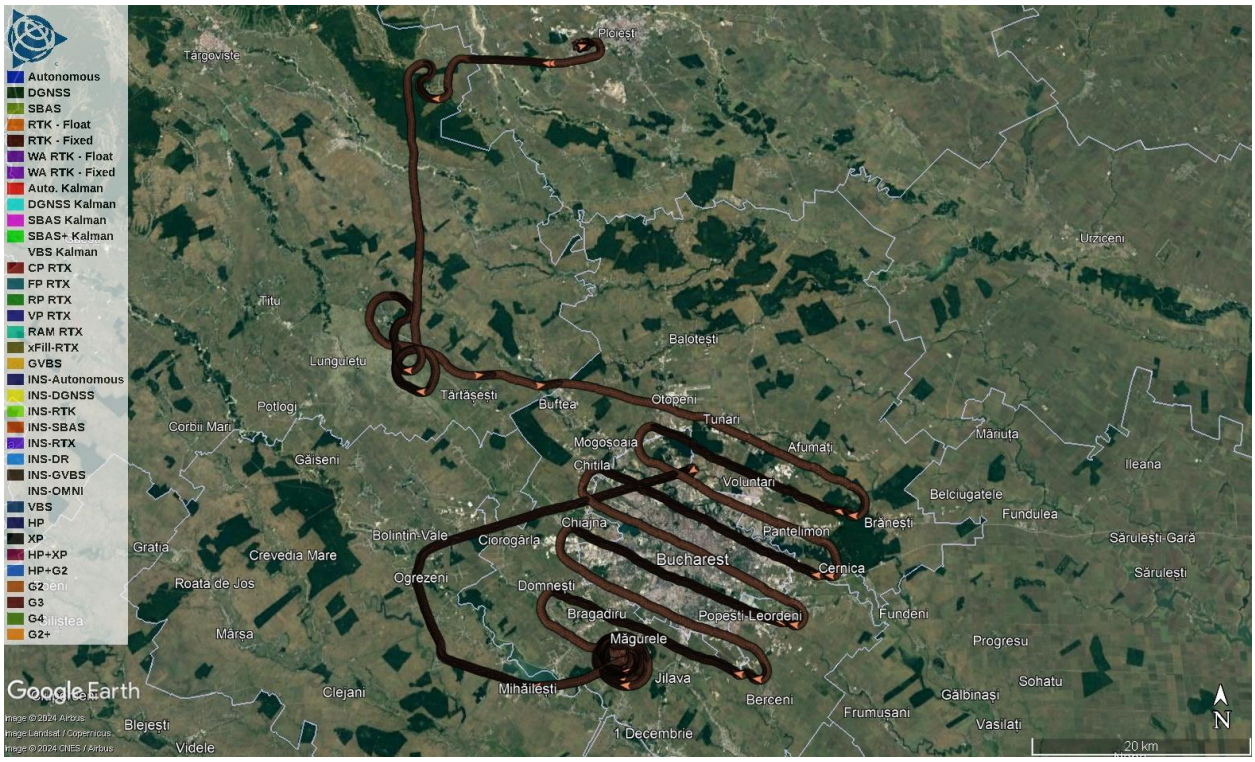

Figure 87. Flight path recorded by the IMU on 2 Nov 2022

The flight path recorded by the IMU can be seen in Figure 24. The take-off was from the Strejnicu Airfield and the mission started in the NE part of Bucharest and ended in the

SW, after which the aircraft headed for landing at the Băneasa Airport. In addition to the lines above the city, a vertical sounding was also performed above Măgurele.

SWING+ data

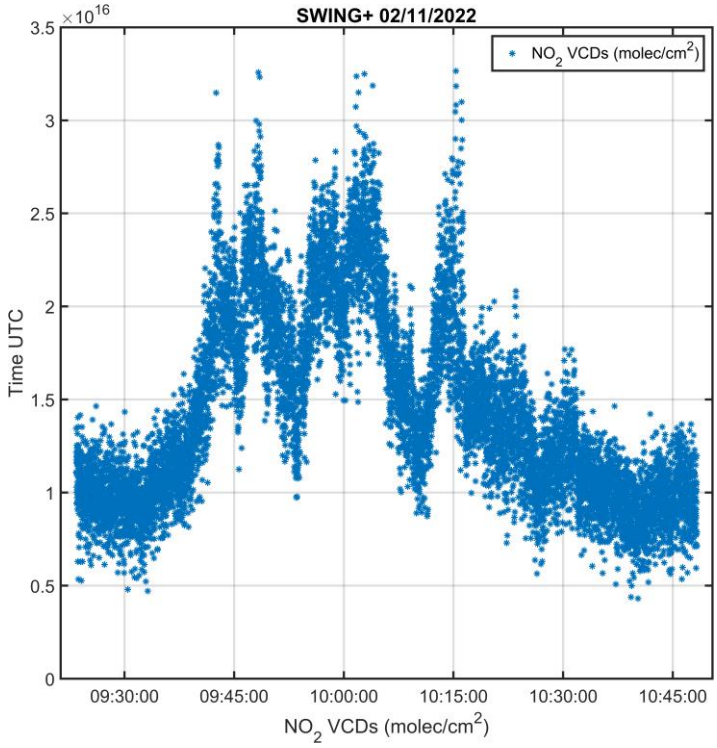

Figure 88. NO_2 vertical column densities as recorded by the SWING+ on 2 Nov 2022

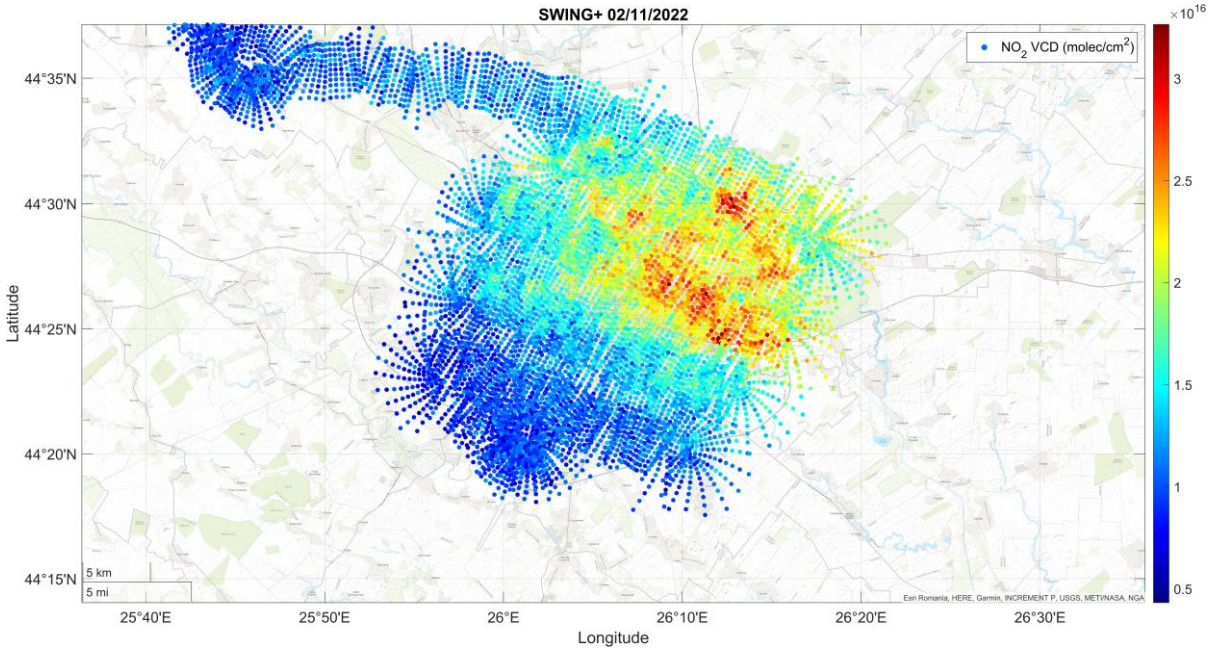

Figure 89. Georeferenced NO_2 VCDs as recorded by the SWING+ on 2 Nov 2022

The time series in Figure 25 shows significant variability in NO_2 concentrations, with several peaks and troughs. Peaks in NO_2 levels are observed around 09:45, 10:00, and 10:15 UTC, with the highest concentration reaching close to 3.5 × 10¹⁶ molec/cm². The lowest concentrations are observed around 09:30 and 10:45 UTC, with values around 0.5 × 10¹⁶ molec/cm². Figure 26 shows higher NO_2 concentrations in the central to eastern part of the surveyed area, with concentrations reaching up to 3.0 × 10¹⁶ molec/cm². The southwestern and northern parts show lower concentrations (around 0.5 × 10¹⁶ to 1.5 × 10¹⁶ molec/cm²).

APS data

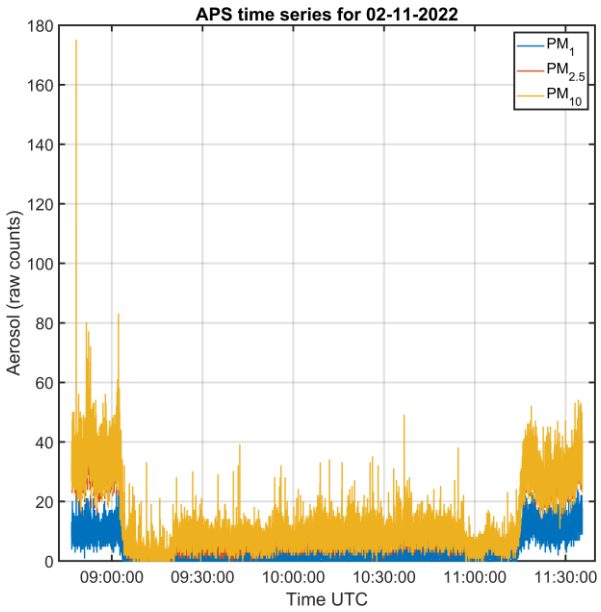

Figure 90. Aerosol data as recorded by the APS on 2 Nov 2022

PM_{10} dominates the aerosol counts throughout the day, with the highest counts reaching around 180. $PM_{2.5}$ and PM_1 are present in much lower counts compared to PM_{10}. Between 9 – 9.30 UTC, Aerosol counts are relatively high initially, with multiple peaks observed for PM_{10}, reaching up to 80 counts. $PM_{2.5}$ and PM_1 also show some activity but are significantly lower in comparison to PM_{10}. This part corresponds to the take-off and the ascending part of the flight, moving through air masses located at lower altitudes. Between 9.30 – 10.30 UTC, there is a decrease in aerosol counts, with fewer peaks observed for PM_{10}. The counts mostly stay below 20. $PM_{2.5}$ and PM_1 remain at low levels, with minimal spikes. This part corresponds to the cruising altitude of 3500 m. Between 10.30 – 11.30 UTC, Aerosol counts start to rise again, particularly for PM_{10}, with several peaks reaching up to 40 counts. $PM_{2.5}$ and PM_1 show more frequent spikes compared to earlier periods, indicating an overall rise in aerosol concentrations. This part corresponds to the descending and landing part of the flight. The higher aerosol counts close to the beginning and the end of the flight might indicate typical urban activities such as commuting traffic, construction, and other industrial activities contributing to the aerosol load at lower altitudes.

Flight 5: 22 Sept 2023

Flight overview

- **Altitude:** 3500 m.
- **Instruments:** IMU, SWING+, AS32M, APS, Picarro G2401-m, APS.
- **Duration:** 1:48.
- **Weather summary:** Low pressure regime over Romania with increasing tendency, clear sky over Bucharest, good conditions for measurements.

IMU data

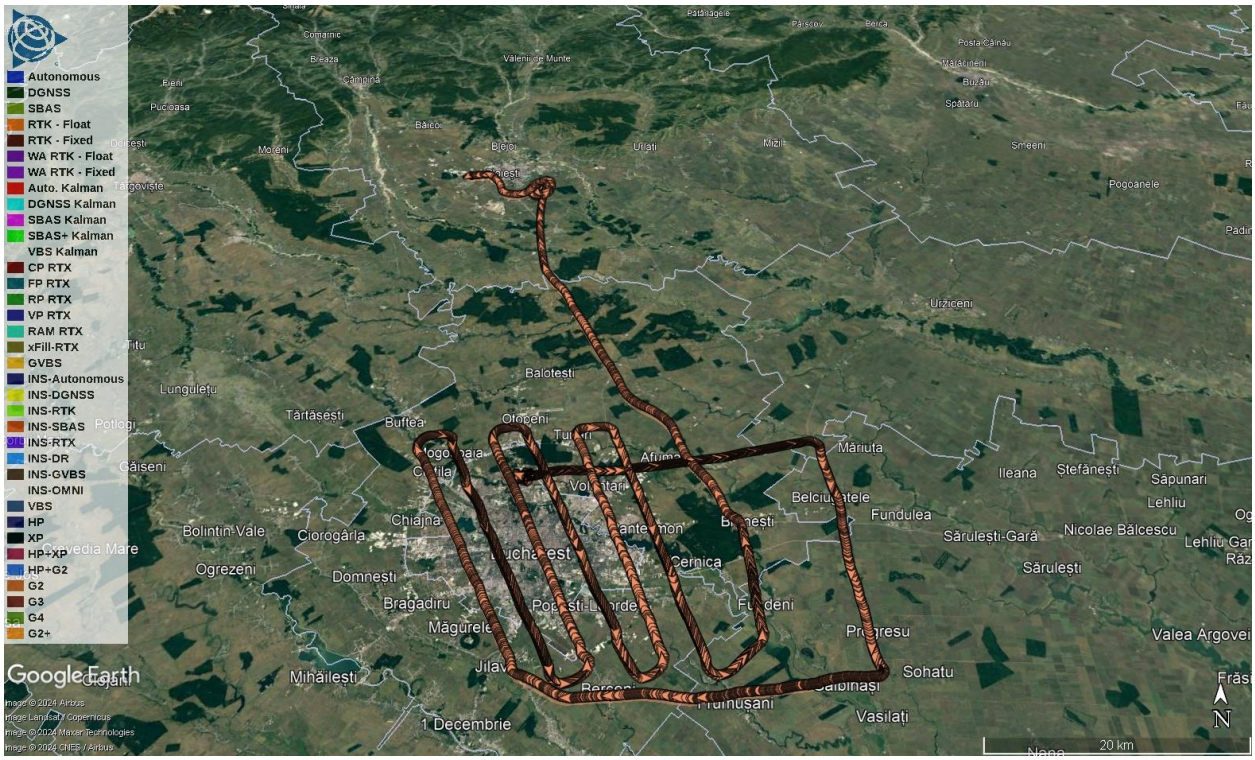

Figure 91. Flight path recorded by the IMU on 22 Sept 2023

The flight path recorded by the IMU can be seen in Figure 28. The take-off was from the Strejnicu Airfield and the mission started in the SE part of Bucharest and ended in the SW, after which the aircraft headed for landing at the Băneasa Airport.

SWING+ data

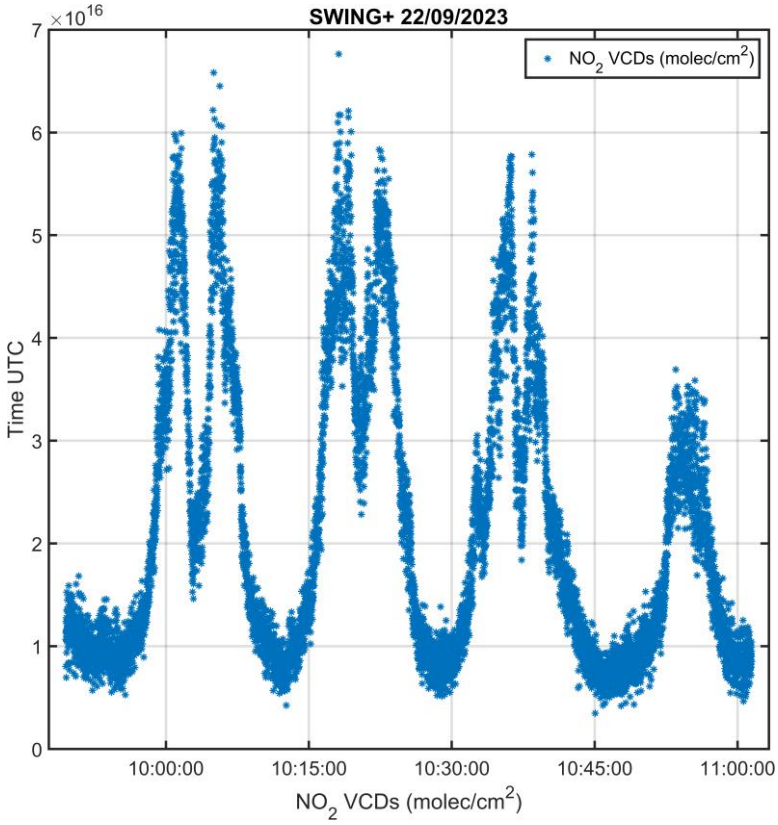

Figure 92. NO2 vertical column densities as recorded by the SWING+ on 22 Sept 2023

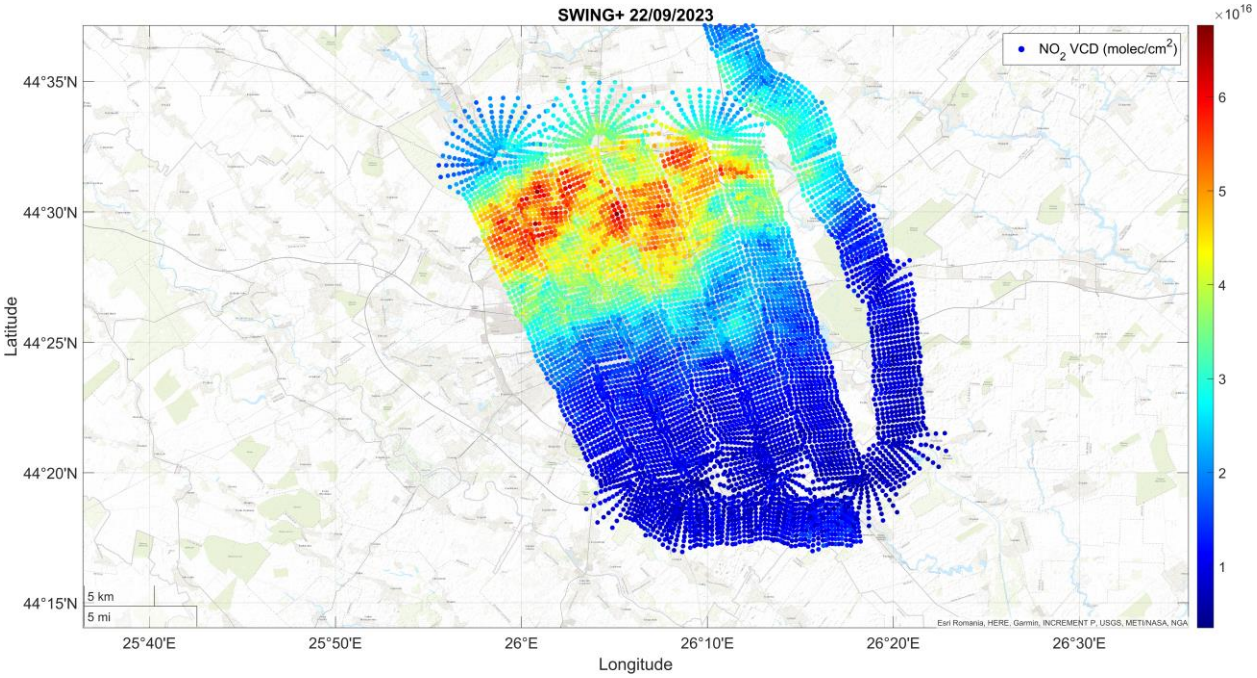

Figure 93. Georeferenced NO2 VCDs as recorded by the SWING+ on 22 Sept 2023

The time series in Figure 29 shows significant variability in NO_2 concentrations, with several peaks and troughs. Peaks in NO_2 levels are observed around 10:00, 10:15, 10:30, and 10:45 UTC, with the highest concentration reaching close to 7 × 10^{16} molec/cm². The lowest concentrations are observed around 10:10, 10:25, and 10:40 UTC, with values around 1 × 10^{16} molec/cm². In Figure 30 higher NO_2 concentrations are observed in the central part of the surveyed area, with concentrations reaching up to 6 × 10^{16} molec/cm². The northeastern part shows moderate concentrations (around 3 × 10^{16} to 5 × 10^{16} molec/cm²). The southeastern part shows lower concentrations (around 1 × 10^{16} to 3 × 10^{16} molec/cm²). The map shows higher NO_2 concentrations in the central region, which correlates with the peaks observed in the time series around 10:00, 10:15, 10:30, and 10:45 UTC. Lower NO_2 concentrations in the southeastern part of the map align with the troughs in the time series, such as the dips around 10:10, 10:25, and 10:40 UTC. The higher concentrations in the central region might be due to local emission sources such as industrial activities, traffic, or other urban factors.

AS32M data

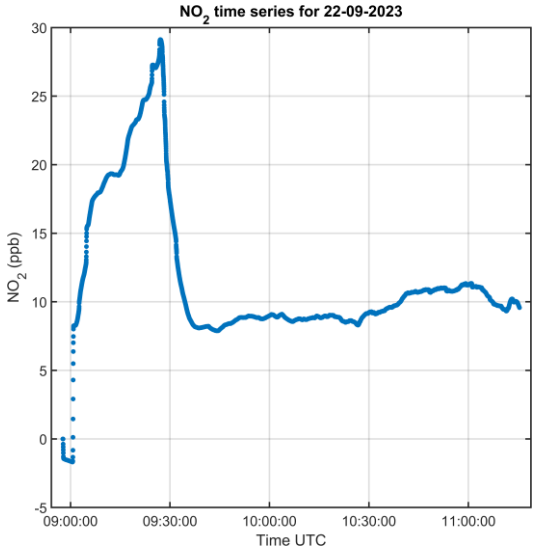

Figure 94. NO2 time series recorded by the AS32M on 22 Sept 2023

The NO_2 concentration starts at a low value and shows a significant increase from around 09:00 to 09:20 UTC, reaching a peak of approximately 30 ppb. After reaching the peak, the concentration drops sharply and stabilizes around 10 ppb from 09:30 to 10:00 UTC. From 10:00 to 11:00 UTC, the concentration shows minor fluctuations but remains relatively stable around 10-12 ppb. The rapid increase in NO_2 concentration suggests a strong emission source or a sudden influx of NO_2-rich air. This could be due to traffic rush hour, industrial emissions, or other localized pollution sources, as this was recorded at lower altitudes, during the take-off and the ascending part of the flight. The concentration peaks at approximately 30 ppb, indicating a significant pollution event. This peak could correspond to a period of intense emissions or a short-term atmospheric phenomenon concentrating NO_2 in the area. The sharp drop in NO_2 levels suggests a cessation of the emission source or a change in atmospheric conditions such as wind direction or speed dispersing the NO_2. The concentration stabilizes around 10-12 ppb with minor fluctuations, indicating a return to typical background levels or a steady-state emission rate.

Picarro G2401-m data

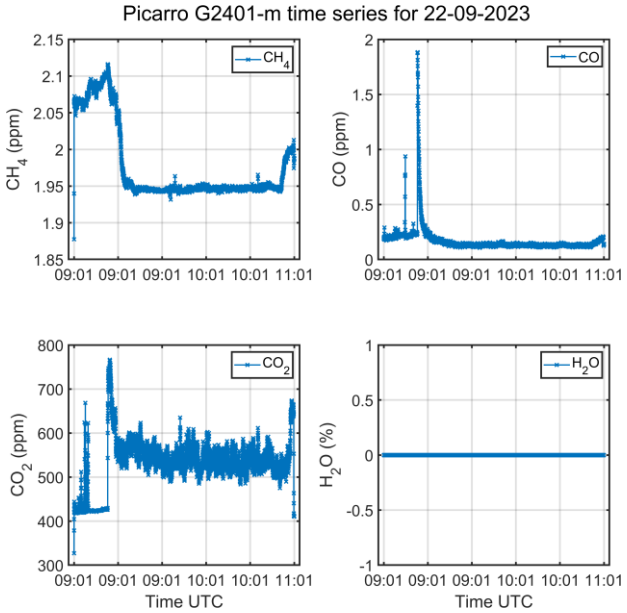

Figure 95. Greenhouse gases concentrations for 22 Sept 2023 (top left: CH_4, top right: CO, bottom left: CO_2, bottom right: H_2O)

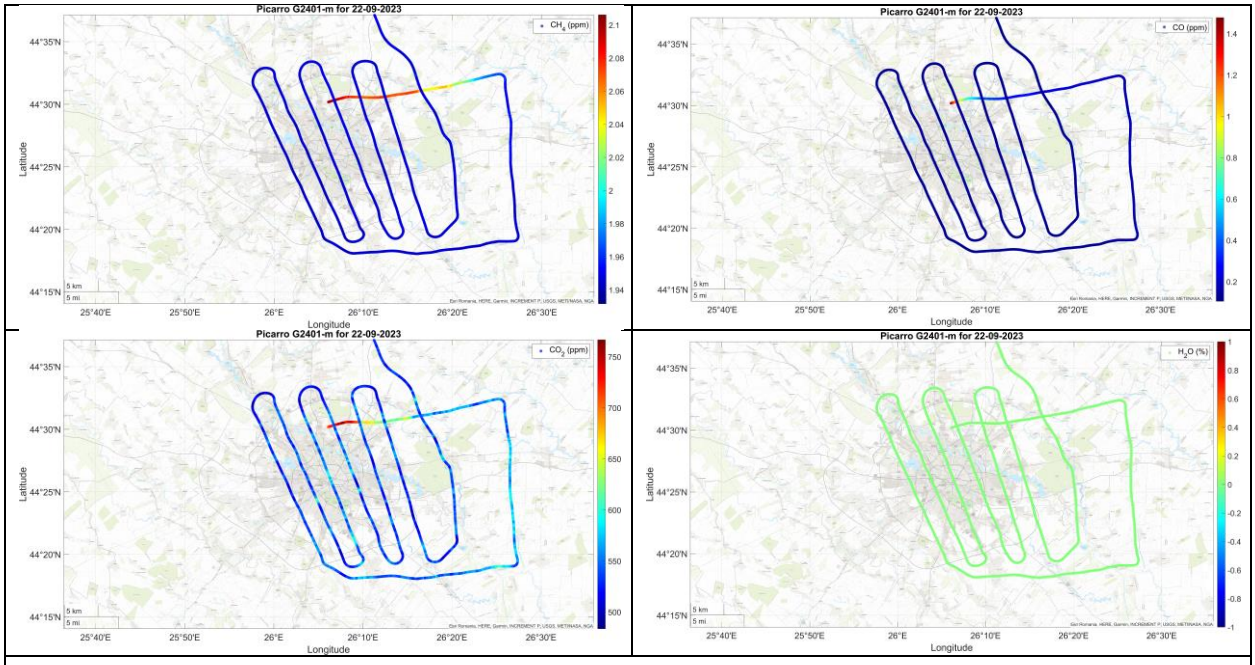

Figure 96. Georeferenced data from the Picarro G2401-m for 22 Sept 2023 (top left: CH_4, top right: CO, bottom left: CO_2, bottom right: H_2O)

Figure 32 shows time series data for greenhouse gases and water vapor concentration levels on 22 Sept 2023, as recorded by the Picarro G2401-m. The CH_4 concentration starts at around 1.95 ppm, rises sharply to 2.05 ppm by 09:15 UTC, and then drops to around 1.98 ppm by 09:30 UTC. After 09:30 UTC, the concentration remains stable around 1.98 ppm until it rises again to about 2.03 ppm towards 11:00 UTC. CO concentration peaks at around 1.8 ppm at 09:10 UTC and then drops sharply to about 0.5 ppm by 09:20 UTC. After the peak, the CO concentration remains relatively stable,

fluctuating between 0.3 and 0.6 ppm. The CO_2 concentration starts at around 400 ppm, rises sharply to about 700 ppm by 09:15 UTC, and then drops to around 600 ppm by 09:30 UTC. After 09:30 UTC, the CO_2 concentration remains stable around 600-650 ppm.

Figure 33 displays spatial distributions of methane (CH_4), carbon monoxide (CO), carbon dioxide (CO_2), and water vapor (H_2O) concentrations over Bucharest on 22 Sept 2023. Higher CH_4 concentrations (around 2.1 ppm) are observed along the flight path in the central part of the surveyed area. Lower concentrations (around 1.94 ppm) are observed towards the edges of the flight path. Higher CO concentrations (around 1.4 ppm) are observed in the central part of the flight path, correlating with the time series peak around 09:10 UTC. Lower concentrations (around 0.2 ppm) are observed along the edges. Higher CO_2 concentrations (around 750 ppm) are observed along the central part of the flight path. Lower concentrations (around 500 ppm) are observed towards the edges.

The time series peaks in CH_4, CO, and CO_2 correlate well with the higher concentrations observed in the central part of the flight path on the maps, indicating localized emission sources or specific atmospheric conditions affecting these regions. The time series shows peaks in CH_4 concentration around 09:15 and 11:00 UTC, which correspond to higher concentrations observed in the central part of the flight path on the map. The sharp peak in CO concentration at 09:10 UTC in the time series correlates with the higher concentrations observed in the central part of the map. The subsequent stabilization is reflected in the lower concentrations along the edges. The time series peak around 09:15 UTC correlates with the high CO_2 concentrations observed in the central part of the flight path on the map. The stable concentrations around 600-650 ppm after 09:30 UTC are reflected in the moderate concentrations across the map.

Flight 6: 25 Sept 2023

Flight overview

- **Altitude:** 3500 m.
- **Instruments:** IMU, SWING+, AS32M, APS, Picarro G2401-m, APS.
- **Duration:** 2:29.
- **Weather summary:** High pressure regime over the lower levels with an upper-level cut-off low centred over the eastern Mediterranean basin, cirrocumulus clouds over Bucharest (at approx. 10-12 km altitude), good conditions for lower-level measurements.

IMU data

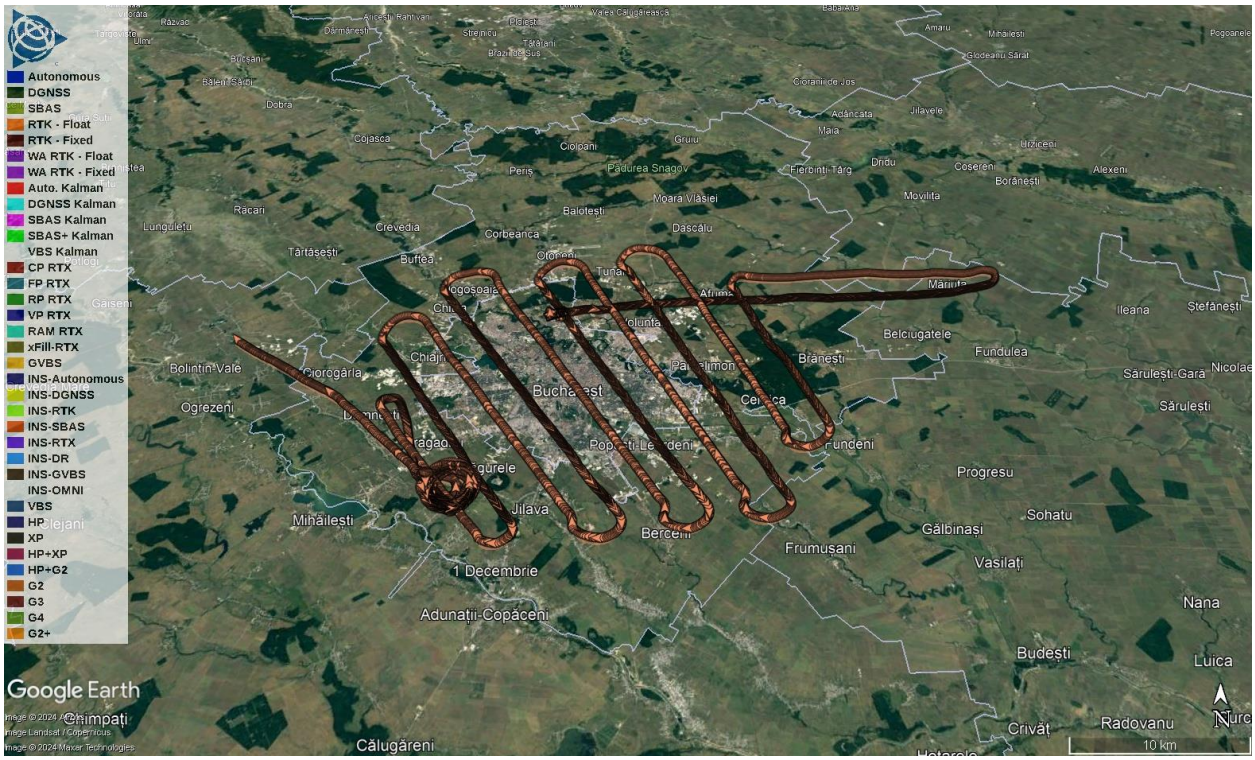

Figure 97. Flight path recorded by the IMU on 25 Sept 2023

The flight path recorded by the IMU can be seen in Figure 31. The take-off was from the Băneasa Airport and the mission started in the SE part of Bucharest and ended in the SW, after which the aircraft headed for landing at the Strejnicu Airfield. In addition to the lines above the city, a vertical sounding was also performed above Măgurele.

SWING+ data

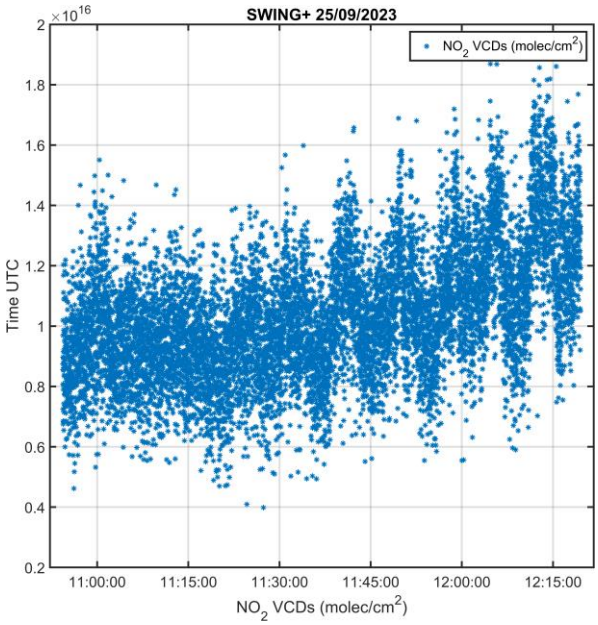

Figure 98. NO2 vertical column densities as recorded by the SWING+ on 25 Sept 2023

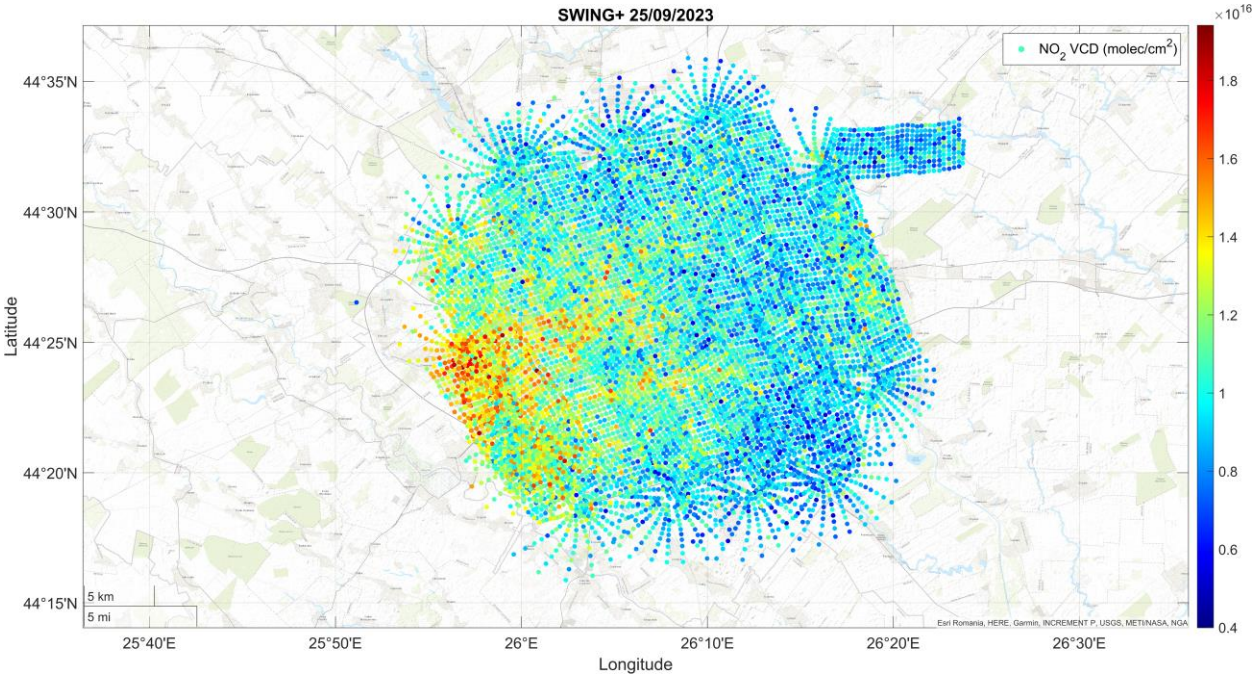

Figure 99. Georeferenced NO2 VCDs as recorded by the SWING+ on 25 Sept 2023

The time series in Figure 32 shows significant variability in NO_2 concentrations, with several peaks and troughs. The NO_2 levels gradually increase over time, starting from around 0.4×10^{16} and reaching up to 1.8×10^{16} molec/cm² by the end of the period. Peaks in NO_2 levels are observed intermittently, indicating fluctuating NO_2 concentrations during the flight. In Figure 33, higher NO_2 concentrations are observed in the central to southwestern part of the surveyed area, with concentrations reaching up to 1.8×10^{16} molec/cm². The northeastern part shows moderate concentrations (around 1.0×10^{16} to 1.4×10^{16} molec/cm²). The southeastern and northern parts show lower concentrations (around 0.4×10^{16} to 0.8×10^{16} molec/cm²). The map shows higher NO_2 concentrations in the central to southwestern regions, which correlate with the peaks observed in the time series towards the end of the period (12:00 to 12:15 UTC). Lower NO_2 concentrations in the southeastern and northern parts of the map align with the troughs in the time series, such as the dips observed around 11:15 and 11:30 UTC. The higher concentrations in the central to southwestern regions might be due to local emission sources such as industrial activities, traffic, or other urban factors.

AS32M data

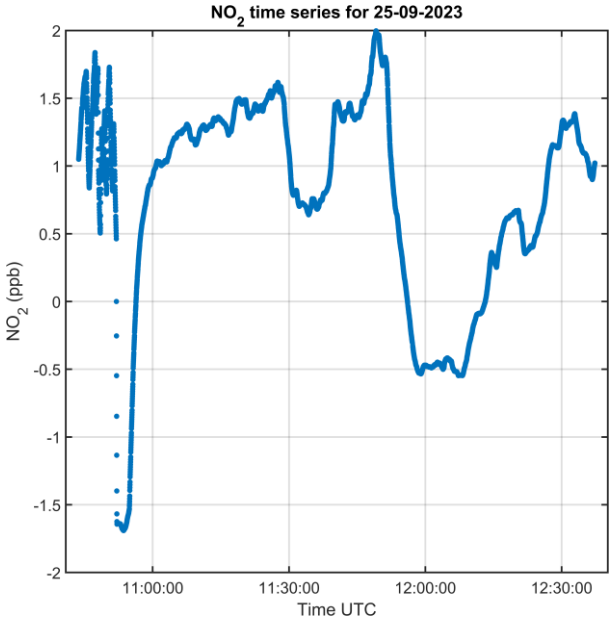

Figure 100. NO2 time series recorded by the AS32M on 25 Sept 2023

The NO_2 concentration starts slightly below 0 ppb, then shows an initial rise to about 1.5 ppb. After 11:10 UTC, the NO_2 concentration shows a gradual increase, stabilizing around 1.0 ppb with fluctuations. A peak of nearly 2.0 ppb is observed around 11:30 UTC. Following the peak, there's a notable dip, reaching a minimum around -1.5 ppb at 12:00 UTC. After 12:00 UTC, the concentration rises sharply back to around 1.0 ppb and shows another peak before stabilizing again towards the end of the period. The initial rise and subsequent fluctuations in NO_2 concentration may indicate the aircraft moving through regions with variable NO_2 sources, such as urban areas with vehicular emissions or industrial areas. The peak around 11:30 UTC suggests the presence of a significant NO_2 source, likely from traffic or industrial emissions. This peak corresponds with the highest observed concentration near 2.0 ppb. The sharp dip to -1.5 ppb at around 12:00 UTC could be due to a sudden change in flight path, altitude, or entering a cleaner air mass. Negative values may indicate sensor calibration issues or rapid changes in atmospheric conditions. The rapid increase after the dip and the subsequent stabilization reflect the aircraft re-entering regions with more consistent NO_2 levels, possibly influenced by urban areas or steady emission sources. The observed peaks likely correlate with the aircraft flying over or near urban and industrial areas, known for higher NO_2 emissions. The fluctuations and sharp changes can also be influenced by atmospheric conditions such as wind direction, temperature inversions, and vertical mixing, which can disperse or concentrate pollutants.

Picarro G2401-m data

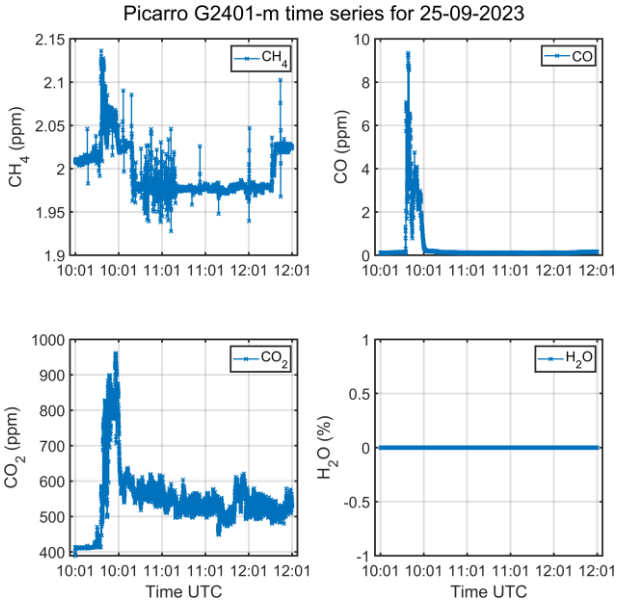

Figure 101. Greenhouse gases concentrations for 25 Sept 2023 (top left: CH_4, top right: CO, bottom left: CO_2, bottom right: H_2O)

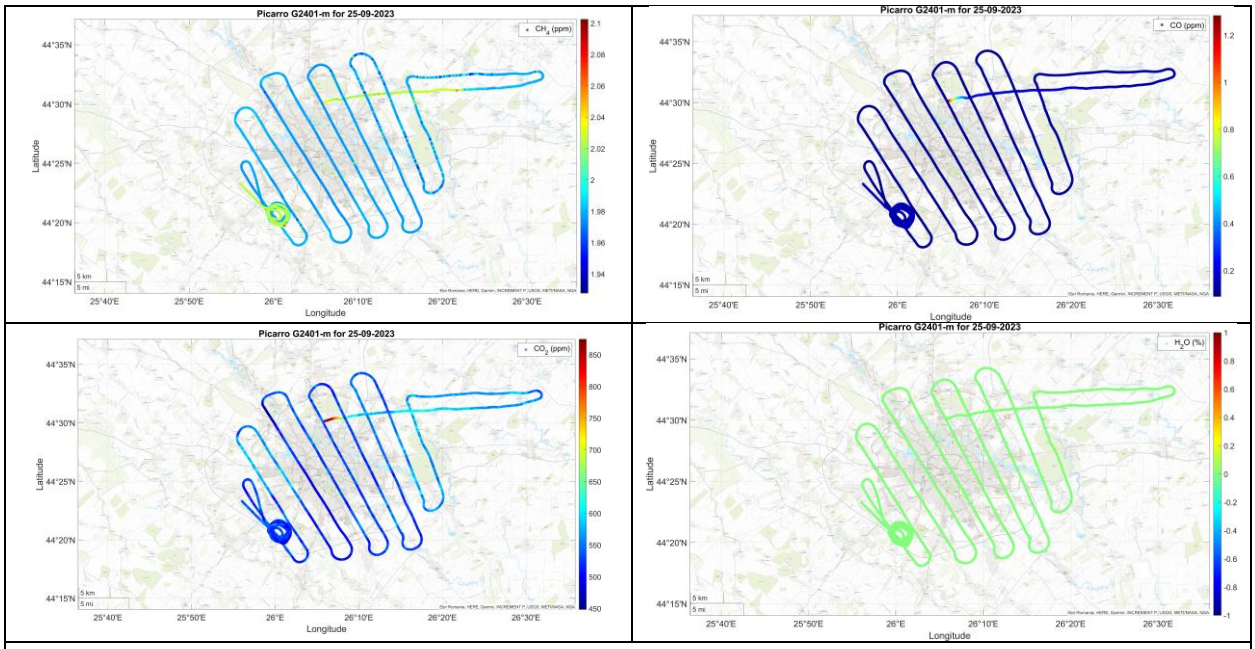

Figure 102. Georeferenced data from the Picarro G2401-m for 25 Sept 2023 (top left: CH_4, top right: CO, bottom left: CO_2, bottom right: H_2O)

Figure 38 shows time series data for greenhouse gases and water vapor concentration levels on 25 Sept 2023, as recorded by the Picarro G2401-m. The CH_4 concentration starts around 2.05 ppm at 10:00 UTC, drops to approximately 1.95 ppm by 11:00 UTC, and remains relatively stable until 12:00 UTC with slight fluctuations. A noticeable rise back to around 2.05 ppm occurs near the end of the period. A sharp peak in CO concentration is observed at around 10:00 UTC, reaching nearly 8 ppm, then drops quickly to around 0.5 ppm by 10:15 UTC. After the initial peak, CO levels remain low and stable. The CO_2 concentration shows a peak around 10:00 UTC at about 900 ppm, which

then drops to around 500 ppm by 10:15 UTC. Post-drop, the concentration fluctuates between 500-600 ppm for the rest of the period.

Figure 39 displays spatial distributions of methane (CH_4), carbon monoxide (CO), carbon dioxide (CO_2), and water vapor (H_2O) concentrations over Bucharest on 25 Sept 2023. Higher CH_4 concentrations (around 2.1 ppm) are observed along the flight path, especially in the southern loop area. Lower concentrations (around 1.94 ppm) are observed towards the western and eastern edges. Higher CO concentrations are localized in the central part of the flight path, correlating with the time series peak at the beginning of the flight. Lower concentrations are found towards the peripheries of the flight path. The highest CO_2 concentrations are observed in the central and northern parts of the flight path, reflecting the initial peak in the time series. Lower concentrations are seen towards the edges.

The time series shows a drop and subsequent rise in CH_4 concentration, which correlates with higher concentrations in the southern loop area and lower concentrations in the western and eastern parts of the flight path. The sharp peak at the beginning of the time series matches the high CO concentrations observed in the central part of the flight path. The stable low levels afterward are consistent with the lower concentrations found towards the edges. The initial peak in the time series is reflected in the higher concentrations observed in the central and northern parts of the flight path. The fluctuations in the time series correlate with the moderate concentrations seen across the map.

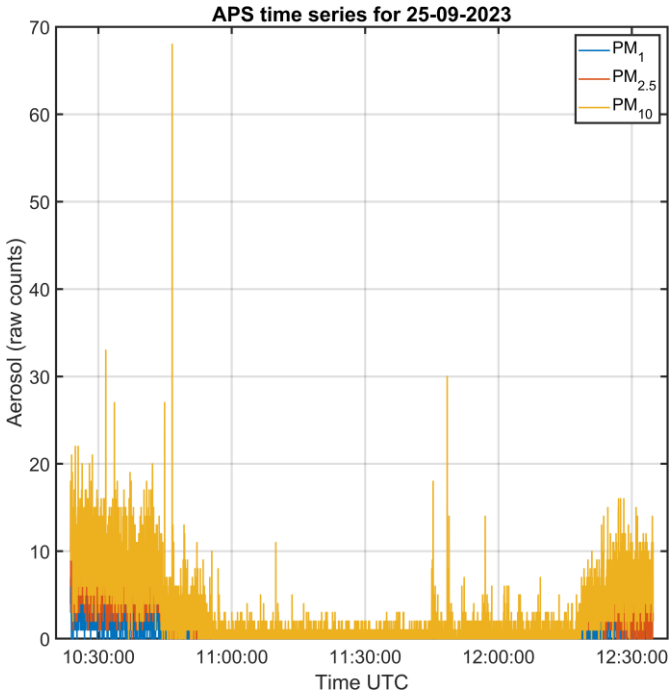

Figure 103. Aerosol data as recorded by the APS on 25 Sept 2023

A significant spike in PM_{10} concentration suggests the presence of a high emission source or passing through an area with high particulate matter. This peak corresponds to

increased human activity, industrial processes, or localized pollution sources. Following the initial peak, there is a sharp drop in PM_{10} counts, with levels stabilizing at lower counts. This could indicate moving away from the initial emission source or changes in atmospheric conditions. PM_{10}, $PM_{2.5}$, and PM_1 levels remain relatively low and stable during this period, suggesting the aircraft was flying through cleaner air masses or areas with lower particulate emissions. Another significant increase in PM_{10} counts is observed, though not as high as the initial peak. This indicates encountering another emission source or re-entering areas with higher particulate matter concentrations. PM_1 and $PM_{2.5}$ also show a slight increase towards the end of the period.

Flight 7: 26 Sept 2023

Flight overview

- **Altitude:** 3500 m.
- **Instruments:** IMU, SWING+, AS32M, APS, Picarro G2401-m, APS.
- **Duration:** 2:02.
- **Weather summary:** High pressure regime over Romania, clear sky over Bucharest, good condition for measurements.

IMU data

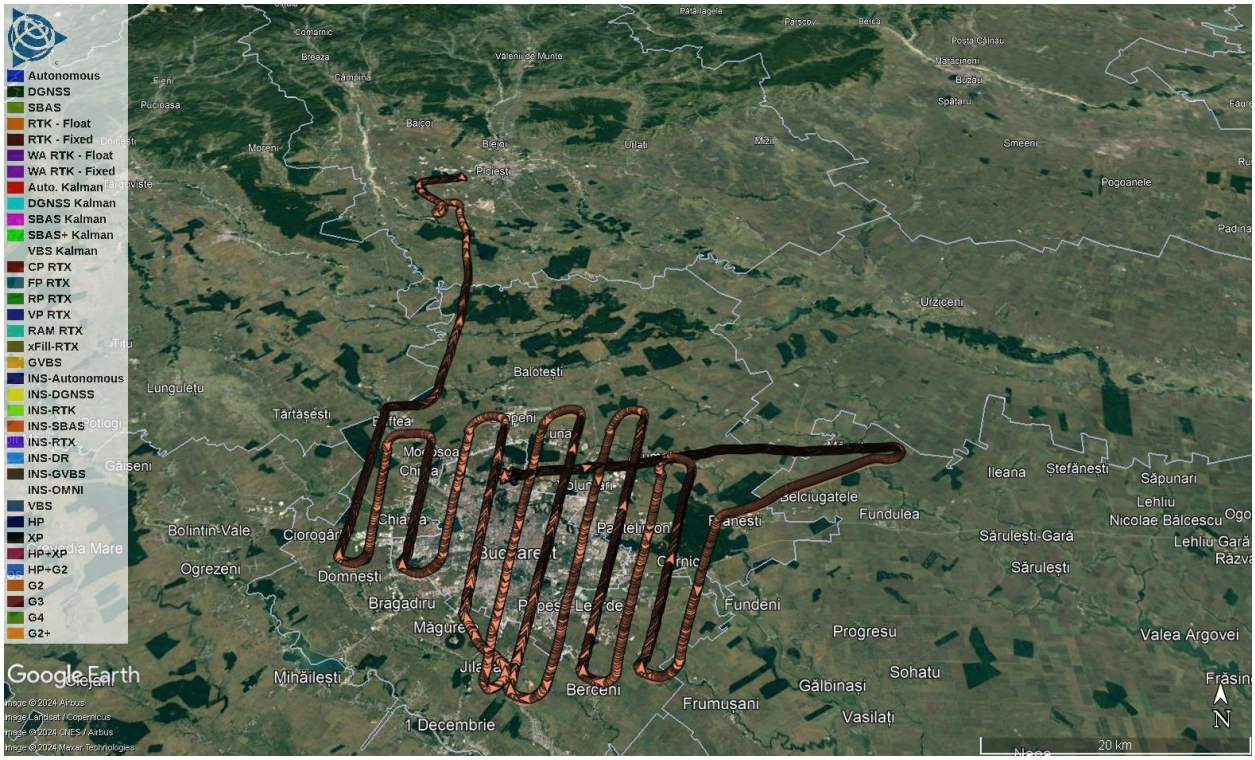

Figure 104. Flight path recorded by the IMU on 26 Sept 2023

The flight path recorded by the IMU can be seen in Figure 41. The take-off was from the Băneasa Airport and the mission started in the SE part of Bucharest and ended in the

SW, after which the aircraft headed for landing at the Strejnicu Airfield. In addition to the lines above the city, a vertical sounding was also performed above Măgurele.

SWING+ data

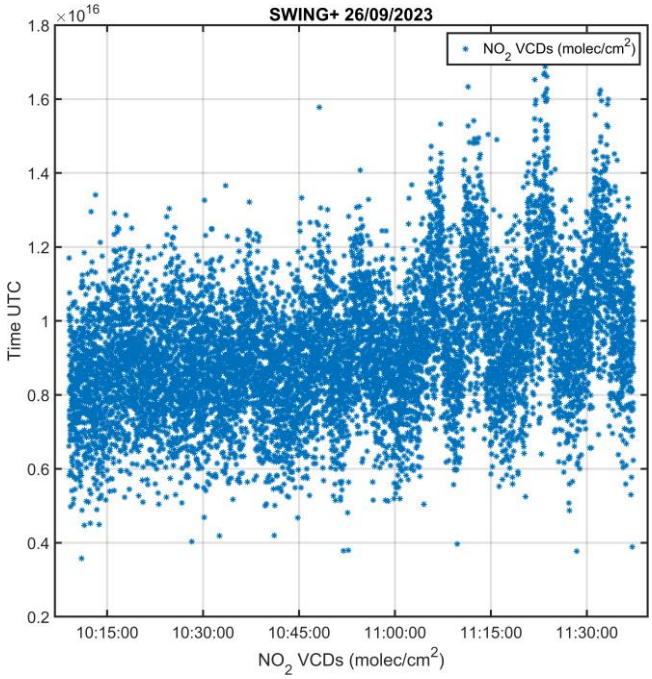

Figure 105. NO_2 vertical column densities as recorded by the SWING+ on 26 Sept 2023

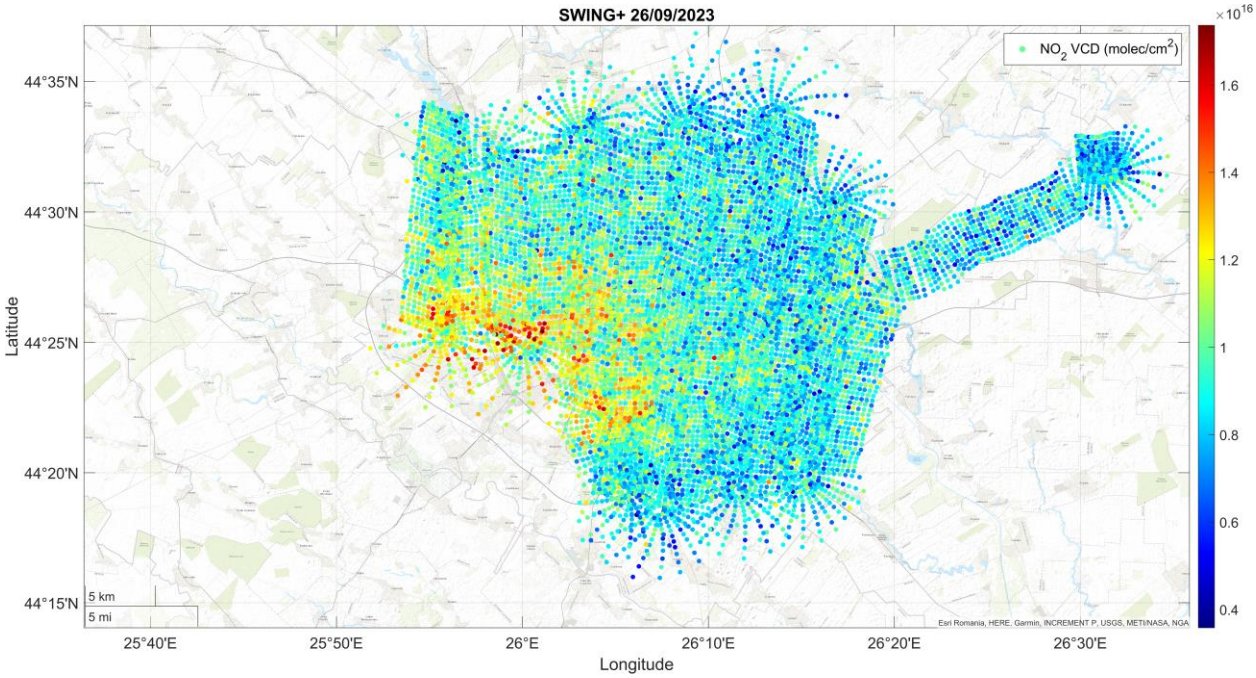

Figure 106. Georeferenced NO_2 VCDs as recorded by the SWING+ on 26 Sept 2023

The map shows high NO_2 concentrations predominantly in the central and southwestern parts of Bucharest. Yellow and green areas indicate moderate NO_2 levels, which are more dispersed but still central and southern parts. Blue areas represent lower NO_2 levels, mainly found in the outskirts and northern parts of the city. The highest NO_2 concentrations are around 1.6×10^{16} molecules/cm², while the lowest are around 0.4×10^{16} molecules/cm².

AS32M data

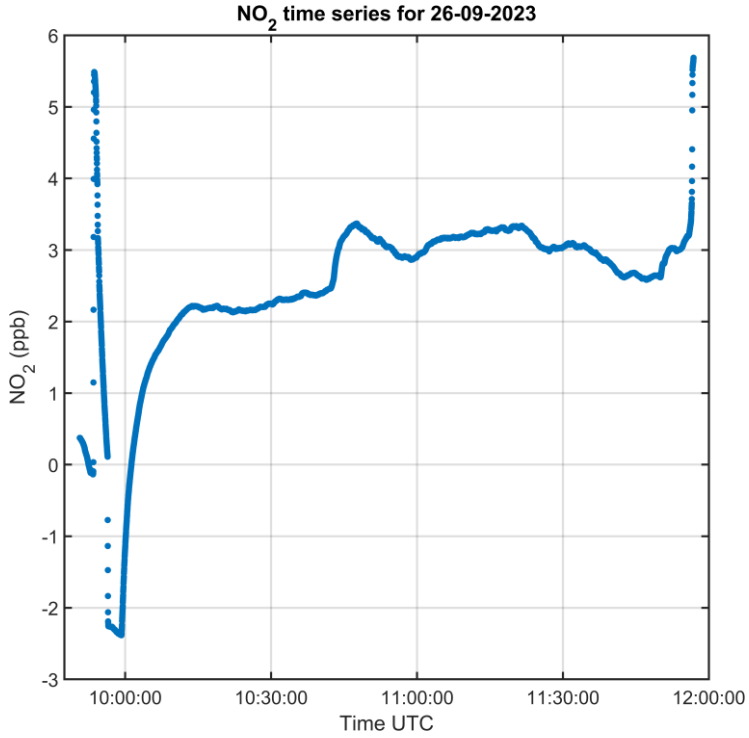

Figure 107. NO2 time series recorded by the AS32M on 26 Sept 2023

The time series in Figure 44 displays NO_2 concentrations in parts per billion (ppb) over the course of the flight from 10:00 UTC to 12:00 UTC. The NO_2 concentrations start below 0 ppb, indicating negative readings or possibly calibration errors at the beginning. At around 10:00 UTC, there is a sharp increase in NO_2 concentration, peaking just above 5 ppb. After the initial peak, the concentration drops and stabilizes between 2 and 3 ppb, with minor fluctuations throughout the remaining duration of the flight. Towards the end of the flight, around 11:45 UTC, there is another noticeable increase, with concentrations reaching around 4 ppb. The sharp initial peak and the subsequent stabilization could suggest flying over or near a major NO_2 source, such as an industrial zone or a densely populated urban area. The minor fluctuations between 2 and 3 ppb indicate relatively consistent exposure to NO_2 throughout the flight, possibly from background levels or minor sources scattered along the path. The secondary increase towards the end of the flight may indicate another significant NO_2 source or a change in flight altitude affecting measurements.

APS data

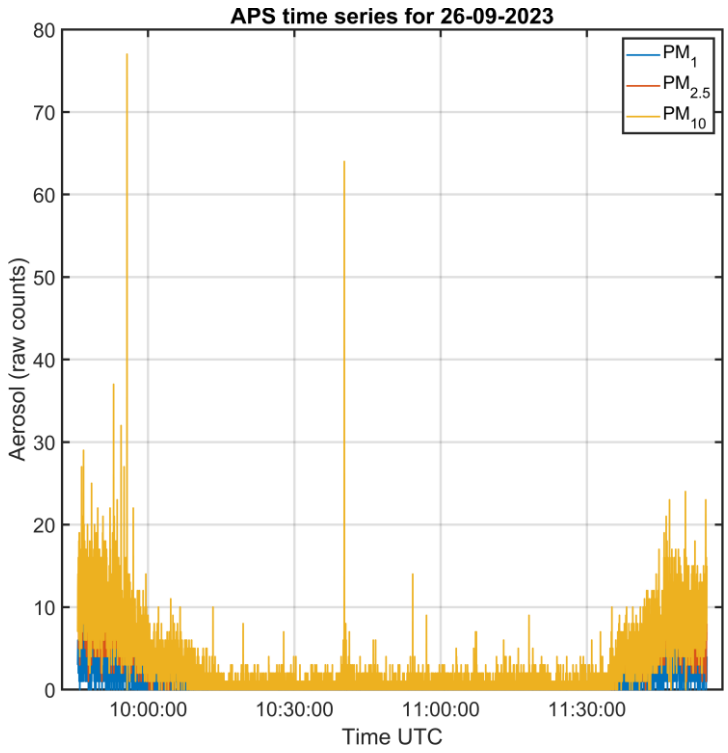

Figure 108. Aerosol data as recorded by the APS on 26 Sept 2023

Initial high counts for PM10, which decrease over time. PM2.5 and PM1 remain relatively low and stable. PM10 counts decrease significantly after the initial spike, showing a relatively stable pattern with occasional minor peaks. PM2.5 and PM1 maintain their stable trends. This period is characterized by lower and more stable counts across all particle sizes, with PM10 showing a noticeable decrease in variability. A slight increase in counts for PM10 is observed towards the end of the period, while PM2.5 and PM1 also show a minor upward trend. The significant spikes in PM10 around 10:00 and 10:30 UTC could indicate short-term events such as construction activities, traffic surges, or other localized pollution sources.

Flight 8: 27 Sept 2023

Flight overview

- **Altitude:** 3500 m.
- **Instruments:** IMU, SWING+, AS32M, APS.
- **Duration:** 1:59.

- **Weather summary:** High pressure regime over Romania, broken clouds over Bucharest, good condition for measurements.

IMU data

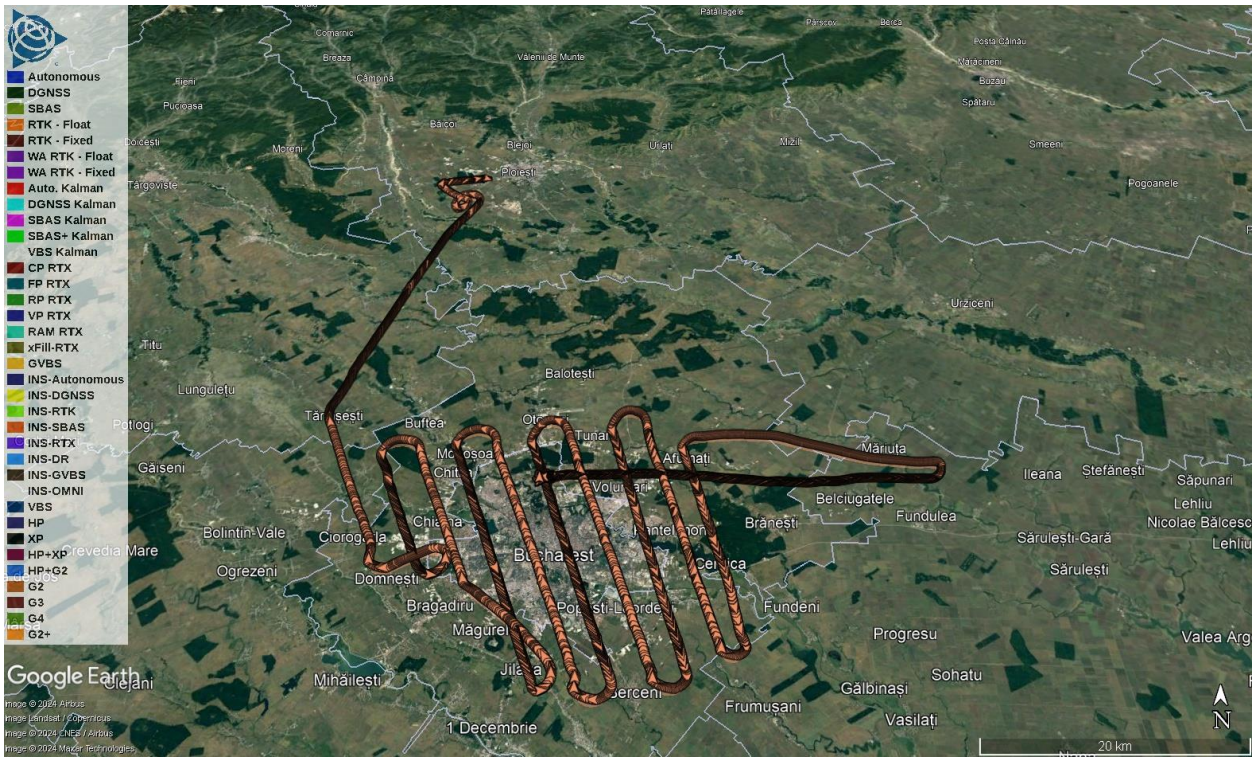

Figure 109. Flight path recorded by the IMU on 27 Sept 2023

The flight path recorded by the IMU can be seen in Figure 46. The take-off was from the Băneasa Airport and the mission started in the SE part of Bucharest and ended in the NW, after which the aircraft headed for landing at the Strejnicu Airfield.

SWING+ data

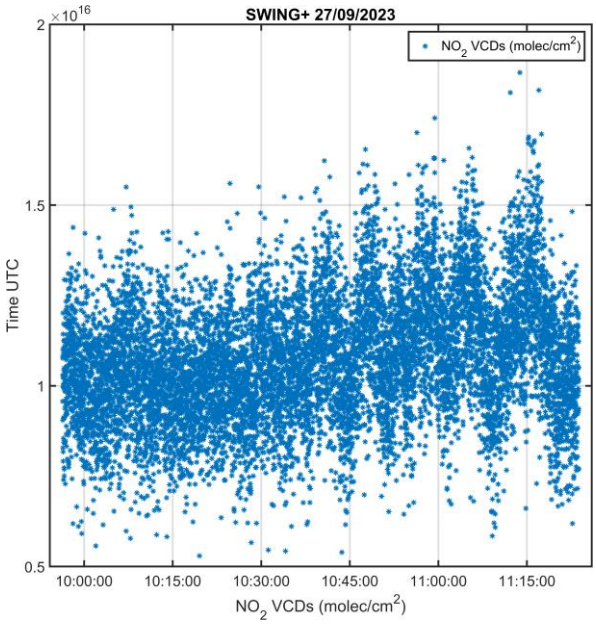

Figure 110. NO2 vertical column densities as recorded by the SWING+ on 27 Sept 2023

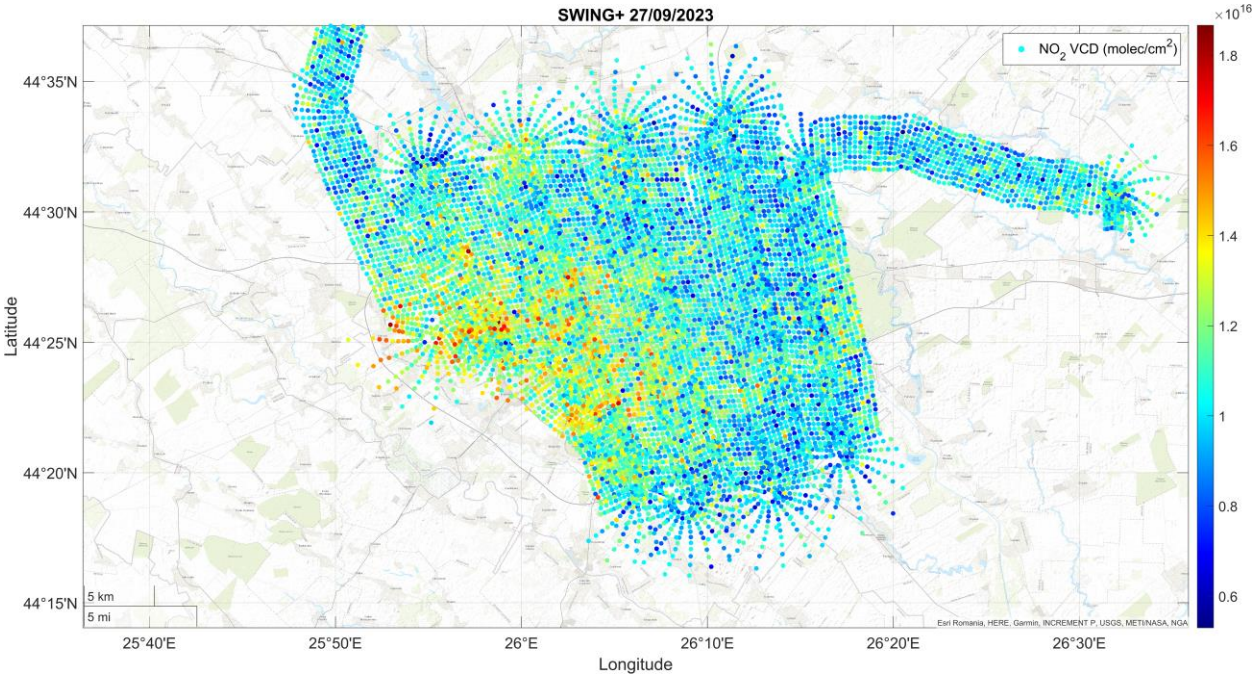

Figure 111. Georeferenced NO2 VCDs as recorded by the SWING+ on 27 Sept 2023

In Figure 47, the NO_2 VCD values fluctuate primarily between 1.0×10^{16} and 1.5×10^{16} molec/cm², with occasional higher values approaching 2.0×10^{16} molec/cm². The plot

shows a relatively consistent spread of NO_2 VCDs over time, indicating stable or gradually varying emission sources during the observed period. There are a few outliers with significantly higher NO_2 VCDs. These could be due to transient emission events, such as traffic spikes, industrial releases, or other localized sources of NO_2.

In Figure 48, areas with the highest concentrations of NO_2 are scattered but more concentrated in the southern and central parts of the map. The lowest concentrations are more widespread but notably present in the northern and northeastern parts of the map. The distribution pattern may indicate urban or industrial activity in the southern and central regions, causing higher NO_2 emissions. In contrast, the northern regions may be more rural or have less pollution sources.

APS data

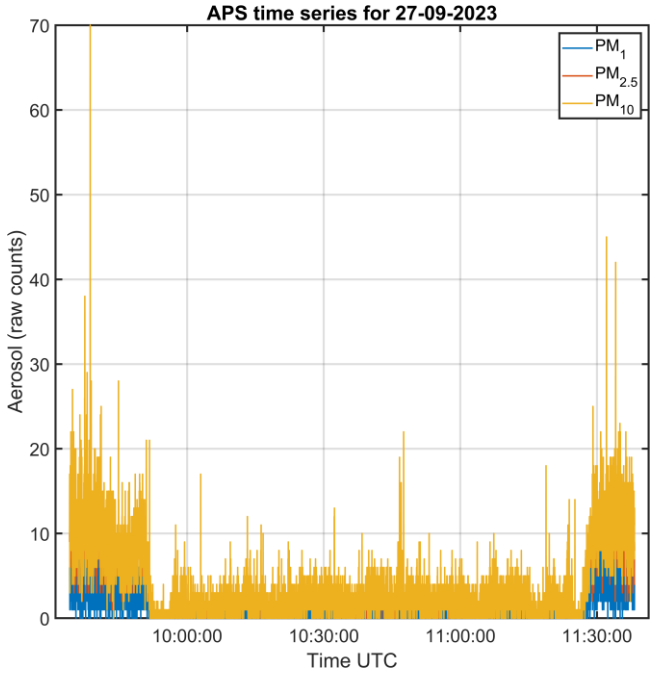

Figure 112. Aerosol data as recorded by the APS on 27 Sept 2023

There is a significant spike in aerosol counts at the beginning of the time period for all three particle sizes, with PM_{10} showing the highest counts, reaching up to 70 raw counts. After the initial spike, the counts for all particle sizes decrease significantly and remain relatively low and stable throughout the majority of the observed period. Towards the end of the period (around 11:30:00), there is another noticeable increase in counts, similar to the initial spike. PM_{10}: Consistently shows higher counts compared to $PM_{2.5}$ and PM_1. The spikes at the beginning and end of the period are particularly pronounced for PM_{10}. $PM_{2.5}$: Shows moderate counts with visible spikes at the same times as PM_{10}, but the counts are significantly lower. PM_1: The counts are the lowest among the three, with minor fluctuations throughout the period and smaller spikes compared to $PM_{2.5}$ and PM_{10}. The spikes at the beginning and end of the period could indicate specific events or activities that released a large amount of particulate matter into the air, such as traffic, industrial processes, or construction activities that are more easily measured at lower altitudes.

Flight 9: 28 Sept 2023

Flight overview

- **Altitude:** 3500 m.
- **Instruments:** IMU, SWING+, AS32M, APS.
- **Duration:** 2:17.
- **Weather summary:** High pressure regime over Romania, broken clouds over Bucharest, good condition for measurements.

IMU data

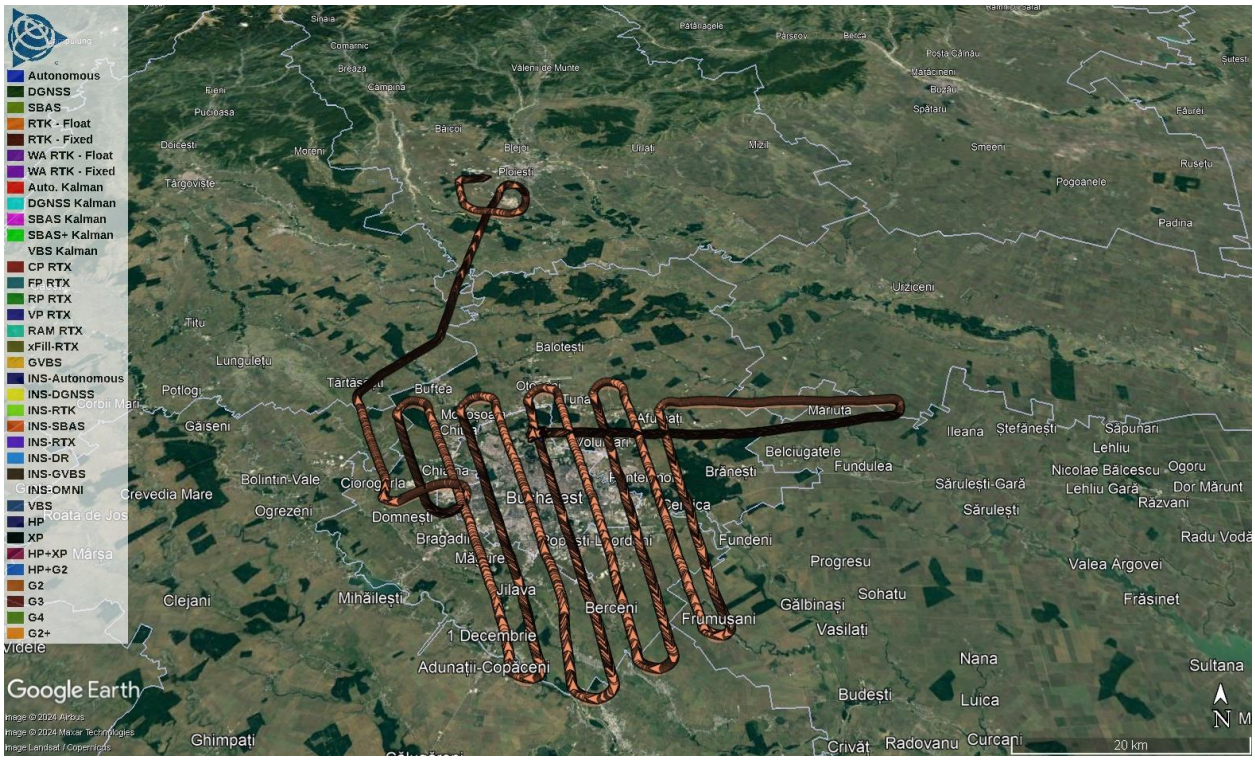

Figure 113. Flight path recorded by the IMU on 28 Sept 2023

The flight path recorded by the IMU can be seen in Figure 50. The take-off was from the Băneasa Airport and the mission started in the NE part of Bucharest and ended in the NW, after which the aircraft headed for landing at the Strejnicu Airfield.

SWING+ data

The NO_2 VCD values range primarily between 0.6×10^{16} and 1.6×10^{16} molec/cm², with occasional higher values approaching 2.0×10^{16} molec/cm². The plot in Figure 51 shows several peaks in NO_2 VCDs, indicating fluctuating emission sources during the observed period. The data shows distinct peaks around 10:45:00 and 11:15:00, suggesting periodic increases in NO_2 emissions, possibly related to traffic patterns or industrial processes.

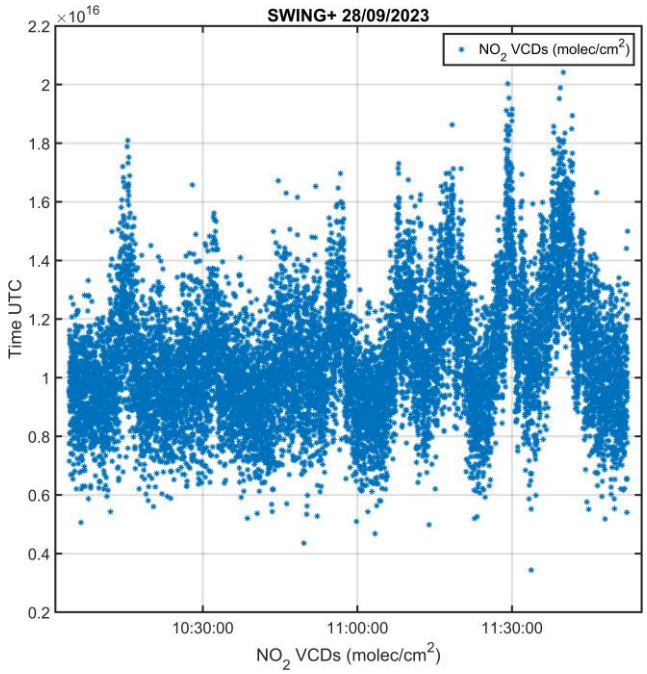

Figure 114. NO2 vertical column densities as recorded by the SWING+ on 28 Sept 2023

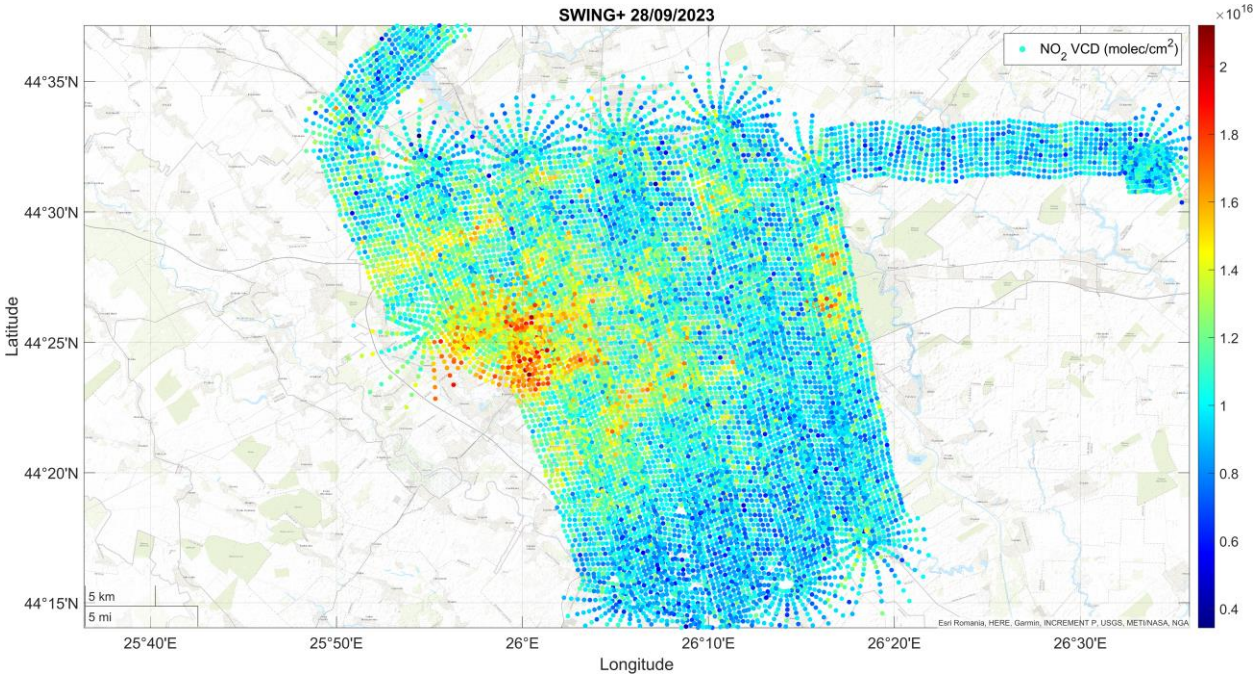

Figure 115. Georeferenced NO2 VCDs as recorded by the SWING+ on 28 Sept 2023

In Figure 52, the highest NO_2 concentrations are concentrated in the central part of the map, indicating significant emission sources in that area. Areas with moderate concentrations surround the central high-concentration region, gradually decreasing towards the edges of the map. The distribution pattern suggests urban or industrial activities in the central area causing high NO_2 emissions, while the peripheral regions have lower emissions, potentially due to less urbanization or industrial activity.

Flight 10: 29 Sept 2023

Flight overview

- **Altitude:** 3500 m.
- **Instruments:** IMU, SWING+, AS32M, APS, Picarro G2401-m.
- **Duration:** 2:26.
- **Weather summary:** High pressure regime over Romania with a decreasing tendency, broken clouds over Bucharest, good condition for measurements.

IMU data

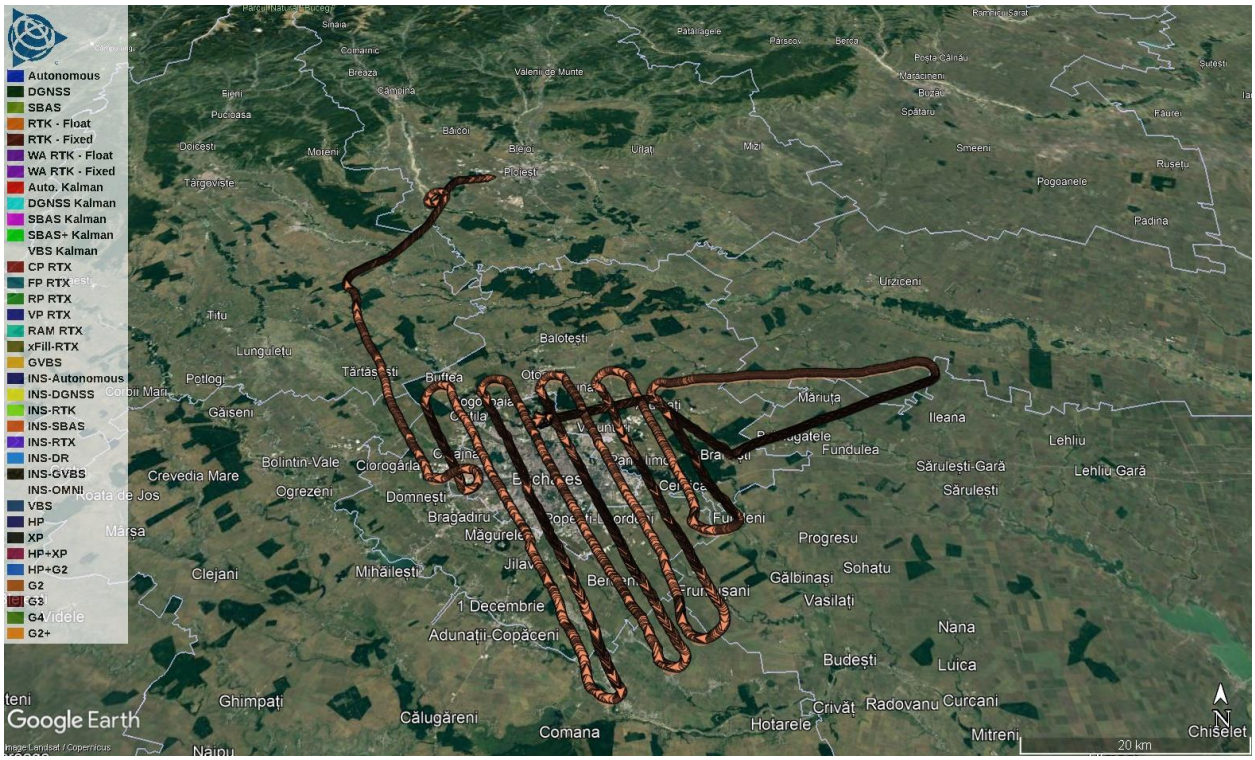

Figure 116. Flight path recorded by the IMU on 29 Sept 2023

The flight path recorded by the IMU can be seen in Figure 50. The take-off was from the Băneasa Airport and the mission started in the NE part of Bucharest and ended in the NW, after which the aircraft headed for landing at the Strejnicu Airfield.

SWING+ data

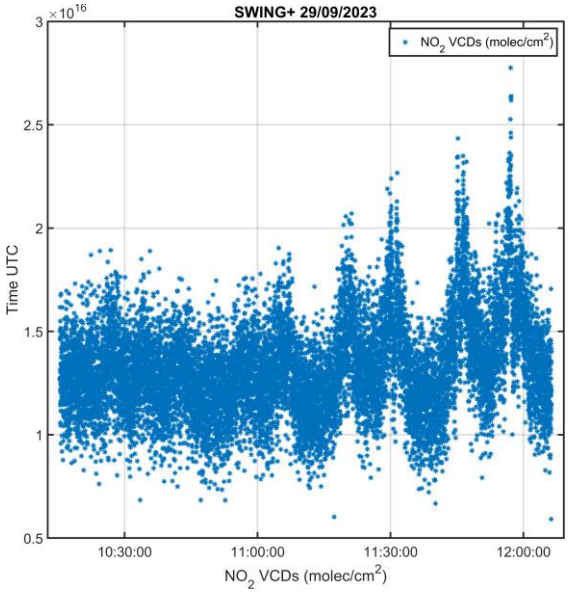

Figure 117. NO2 vertical column densities as recorded by the SWING+ on 29 Sept 2023

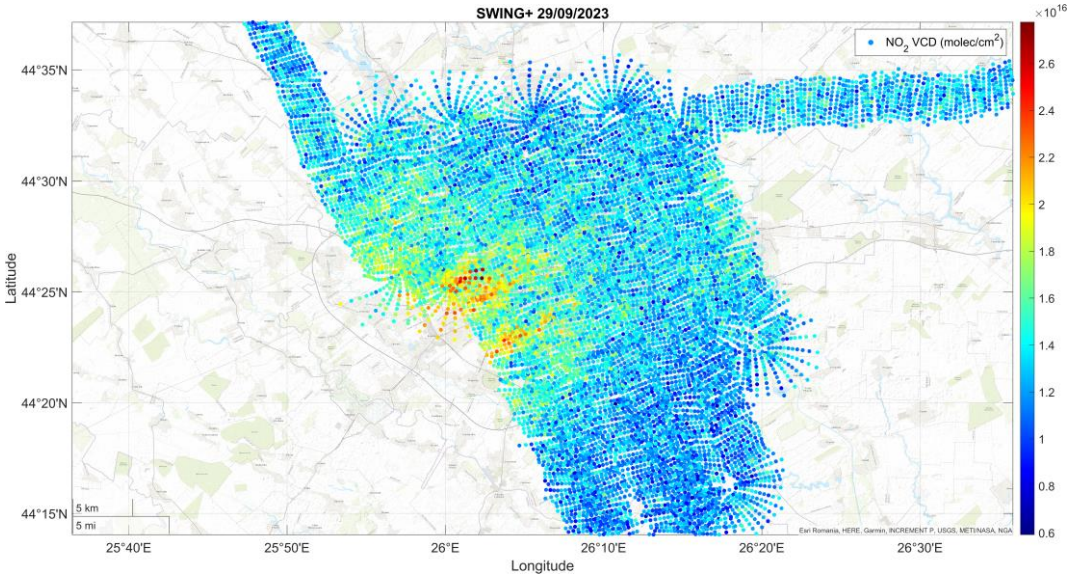

Figure 118. Georeferenced NO2 VCDs as recorded by the SWING+ on 29 Sept 2023

In Figure 54, The NO_2 VCD values fluctuate primarily between 1.0×10^{16} and 1.5×10^{16} molec/cm², with occasional spikes reaching up to 3.0×10^{16} molec/cm². The plot shows a series of peaks, indicating periodic increases in NO_2 emissions during the observed period. Distinct peaks are observed around 10:45:00, 11:15:00, and 11:45:00, suggesting cyclical or episodic emission events, possibly related to traffic patterns, industrial processes, or other urban activities.

In Figure 55, the highest NO_2 concentrations are clustered in the central part of the map, suggesting significant sources of NO_2 emissions in this area. Surrounding the central high-concentration area are regions with moderate concentrations, gradually decreasing to low concentrations as you move away from the centre. This pattern indicates a likely urban or industrial area in the centre, contributing heavily to NO_2 emissions. The lower concentrations in the surrounding areas suggest less urbanization or fewer sources of pollution.

Picarro G2401-m data

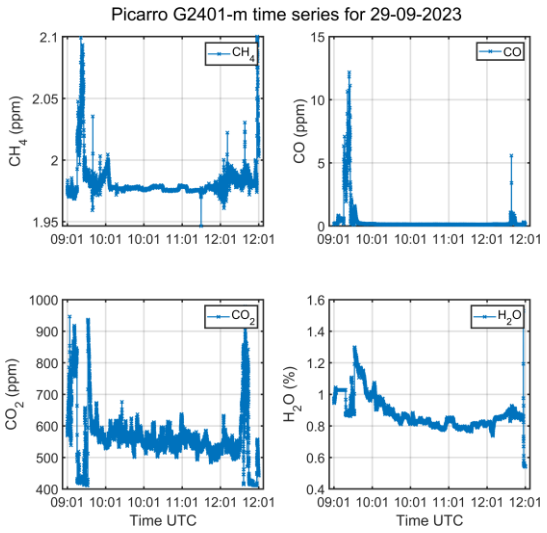

Figure 119. Greenhouse gases concentrations for 29 Sept 2023 (top left: CH4, top right: CO, bottom left: CO2, bottom right: H2O)

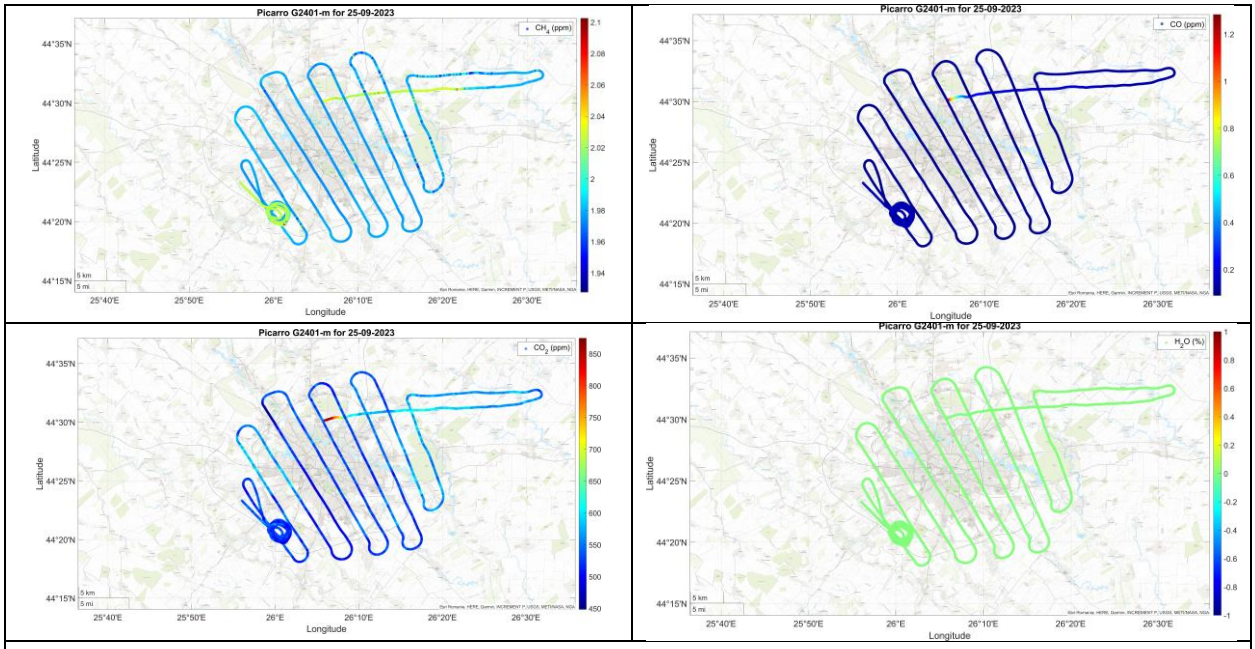

Figure 120. Georeferenced data from the Picarro G2401-m for 29 Sept 2023 (top left: CH_4, top right: CO, bottom left: CO_2, bottom right: H_2O)

Figure 56 shows time series data for greenhouse gases and water vapor concentration levels on 29 Sept 2023, as recorded by the Picarro G2401-m. he CH_4 concentration shows an initial spike around 09:01, peaking at about 2.1 ppm. After the initial spike, the concentration stabilizes around 2.0 ppm with minor fluctuations. A slight increase is observed towards the end of the period, around 12:01. The CO concentration spikes dramatically at 09:01, reaching up to 12 ppm. Following the spike, the concentration drops rapidly to near zero and remains low with minor fluctuations for the rest of the period. There are small spikes observed sporadically throughout the period. The CO_2 concentration is high at the beginning, peaking around 1000 ppm. The concentration drops to around 500-600 ppm and stabilizes with minor fluctuations. A significant increase is observed towards the end, around 12:01, peaking around 900 ppm. The H_2O concentration starts high at about 1.2%. The concentration gradually decreases to around 0.8-0.9% over the observed period. Minor fluctuations are observed throughout the period.

Figure 19 displays spatial distributions of methane (CH_4), carbon monoxide (CO), carbon dioxide (CO_2), and water vapor (H_2O) concentrations over Bucharest on 29 Sept 2023. The concentration of methane ranges from 1.95 ppm to 2.03 ppm. Higher concentrations are seen in a few localized areas, with most areas showing moderate concentrations. The CO concentration ranges from 0.1 ppm to 1.1 ppm. Higher concentrations are localized, with most areas showing lower concentrations. The CO_2 concentration ranges from 500 ppm to 850 ppm. Higher concentrations are seen in specific areas, with most areas showing moderate concentrations. The H_2O concentration ranges from 0.75% to 1.25%. Higher concentrations are seen in some areas, with most areas showing moderate concentrations.

The initial spikes observed in the time series plots for CH_4, CO, and CO_2 around 09:01 could be due to specific emission events, such as industrial activities, traffic peaks, or other localized sources of pollution. The stabilization of concentrations after the initial spikes indicates a return to more typical background levels after the initial event. The increase in concentrations towards the end of the period suggests another emission event or change in environmental conditions. The maps show that the higher concentrations of gases are localized, suggesting specific areas with higher emissions.